BIMODAL DYNAMIC IMAGING SYSTEM FOR TUMOR CHARACTERIZATION USING HYBRID HIERARCHICAL STATISTICAL CONTROL

A Dissertation
Submitted to
the Temple University Graduate Board

---

in Partial Fulfillment
of the Requirements for the Degree of
DOCTOR OF PHILOSOPHY

---

by
Firdous Saleheen
August, 2017

Examining Committee Members:

Dr. Chang-Hee Won, Advisory Chair, Dept. of Electrical and Computer Engineering
Dr. Saroj Biswas, Dept. of Electrical and Computer Engineering
Dr. Li Bai, Dept. of Electrical and Computer Engineering
Dr. Nancy Pleshko, Dept. of Bioengineering
Dr. Bo Ji, External Member, Dept. of Computer and Information Sciences

ABSTRACT

Conventional medical imaging technologies for cancer diagnosis utilize fixed geometric configuration of the source and the detector to image the target. In this dissertation, we hypothesize that dynamic utilization of source and detector geometry will lead to better performance of medical imaging devices. Interrogating a target in a three dimensional space requires cooperation and coordination between the source and detector positions. The goal of this dissertation is to develop a dynamic imaging method, which will improve the tumor characterization performance, and provide a control scheme appropriate for the dynamic interrogation. This dissertation proposes a bimodal dynamic imaging (BDI) method for improving tumor characterization and a hybrid hierarchical statistical control scheme for the autonomous control of the sources and detectors.

The tactile imaging sensor has high specificity but low sensitivity in tumor characterization. The spectral sensor has high sensitivity but low specificity. The BDI system integrates the tactile sensing and the spectral sensing modalities with the capability of dynamic positioning of the source and detector to determine the mechanical and spectral properties of a tumor. The tactile sensing can estimate the mechanical properties of the tumor, such as size, depth, and elastic modulus, while the spectral sensing can determine the absorption coefficient of the tumor through diffuse optical imaging. These properties help us characterize the tumor, and differentiate cancerous tissues from healthy tissues. We designed and experimentally evaluated the BDI system for estimating the size, depth, elastic modulus, and absorption coefficient of embedded inclusions. The system performance in characterizing mechanical properties was then compared to that of the tactile imaging sensor. The proposed BDI method was experimentally validated using fabricated bimodal phantom. The experimental results showed that the tactile imaging system (TIS) estimated the tumor phantom size with 7.23% error; BDI measured the size with 0.8% error. The TIS depth estimation error was 41.83%; BDI reduced the depth measurement error to 20.00%. The TIS elastic modulus estimation error was 96.80%; the BDI method showed 74.79% error. Additionally, BDI estimated the absorption coefficient with 14%-25% estimation error.

For further improvement the system performance, this bimodal imaging system is im-

plemented on a dual-arm robot, Baxter, where the laser source and the tactile imaging sensors were mounted on the end-effectors. Each arm of Baxter robot has seven Degree-of-Freedom. This provides more flexibility in terms of interrogating the target compared to the fixed geometric configuration. We devised a hybrid statistical controller for maneuvering the source and the detector of the system. In this control architecture, a high-level supervisory controller was used for the functions at a higher level for coordinating two arms. At lower level, a full-state feedback statistical controller was used to facilitate the minimum position variation. A linear model for the dual-arm Baxter robot was derived for testing the proposed architecture. We performed the simulations of hybrid hierarchical statistical controller on the Baxter model for trajectory tracking. The simulation studies demonstrated accurate sequential task execution for the bimodal dynamic imaging system using a hybrid hierarchical statistical control.

To my parents and wife

ACKNOWLEDGMENTS

This journey started seven years ago when I ran across the research activities of Dr. Chang-Hee Won through the CSNAP (Control, Sensor Network, and Perception) Laboratory website. The tactile imaging sensor research caught my attention because of its multidisciplinary aspects and clinical applicability. The statistical control research has its own charm because of the theoretical rigor. As any other prospective student, I wrote to Dr. Won about my interest, and he was kind enough to provide me an opportunity to work in his lab.

I thank my advisor Dr. Won, who has been a constant source of energy for my PhD academic career. He has guided me through the perilous journey towards being an independent researcher. He has taught me to think critically about scientific problems, to write for the scientific world, to present my research in front of my peers. His door has been always open for me, of which I took the opportunities numerous times. I am truly grateful for his patience, trust, advice, mentorship and encouragement.

I thank my PhD dissertation committee members, Dr. Saroj Biswas, Dr. Nancy Pleshko, Dr. Li Bai, and Dr. Bo Ji for their invaluable time and suggestions on my PhD work. I also thank Dr. Iyad Obeid for serving on my PhD proposal committee. I thank Dr. Biswas specially, who kept his door open for me for any issue, be it mathematical, be it personal.

In CSNAP laboratory, I came across some wonderful research minds. Without the support of my labmates, this journey would be intolerable. Among the labmates, I would single out Vira Oleksyuk and Salvatore Giorgi. I value their friendship. Vira amazed me with her ability to keep the balance between work and personal life. She has active contribution in this dissertation in preparing the bimodal phantom used for the experiment. Another such friend is Salvatore, who has this amazing ability to cruise through difficult mathematical problems. Vira, Salvatore, and I had lunch together on most occasions, talked about various ‘critical’ topics!

I thank all my friends who were there for me throughout my graduate years. Among many friends, I fondly remember the friendship of Oishi Anam, Dennis Roshan, Rahul Dharaiya, and Amrita Anam. The doors to their homes have been always open for me with all the hospitality and support. I also thank Ashique Mahmood and Tanjima Ferdous for

their friendship. Fariha Hasan has been a good friend throughout my PhD years, who is also a cousin of mine. I thank Shoumik Roychoudhury for being an awesome roommate for five years and a friend.

I cannot thank my parents, Ayesha Begum Irani and Md. Alamgir Hussain, enough for loving me and believing in me. They provided me with all my needs from the first second of my life, and brought me to the gateway of higher education sacrificing their own happiness. My younger brothers Faisal Hussain and Raihan Hussain have always supported me with love. I remember my relatives who encouraged me in my childhood. I love them all.

Most of all, I thank my wife Nancy Dutta for her unconditional love and support. We have known each other for fourteen years. She has been a great partner to me, who supported me with her love, patience, and encouragement. She is the one who understands me the most, always stands beside me. Despite being a PhD student in another school, she always finds time for me. The development of my dissertation work would not be possible without her support and sacrifice. I cannot love her enough.

I thank all the funding agencies, the National Science Foundation, the Department of Defense, Pennsylvania Department of Health, and the Department of Energy for supporting my research works throughout these years. I also thank Electrical and Computer Engineering Department of Temple University for their financial support.

All in all, this dissertation work stands on contributions and sacrifices of many known-unknown personnel. I thank all of them. I am specially grateful to my beautiful country, Bangladesh, who nourished my education career all the way to my Bachelors' degree, and made this journey possible.

TABLE OF CONTENTS

LIST OF FIGURES

LIST OF TABLES

CHAPTER 1

INTRODUCTION

1.1 Motivations

Overdiagnosis has been gaining attention among cancer researchers in recent years [4], [5], [6]. Overdiagnosis is the diagnosis of a disease, which never becomes fatal during the patient's life-span. Because of overdiagnosis, patients go through treatments with harmful side-effects; eventually becoming a psychological and economic burden for the patients. Compelling evidence of overdiagnosis comes from studies of screening detected breast cancer. There is a widespread overdiagnosis in the USA according to a study on 16 million women across 547 US counties [7]. Previously, a 2007 study in *Lancet Oncology* showed 1.7% to 54% overdiagnosis in case of invasive breast cancer among woman over 50 [8]. An Australian study suggested a minimum 30% occurrence of overdiagnosis [9]. A Norwegian study determined the proportion as 15-25% [10]. Another study in *BMJ* showed that up to 33% of all screening detected cancer may overdiagnosed [11]. Therefore, physicians need to identify consequential cancer, which is likely to progress within the patient's lifetime to cause harm; at the same time the inconsequential cancer should undergo 'watchful waiting' [12], [13]. Improving accuracy in tumor characterization can help in making the predictions about consequential and inconsequential cancers.

Breast cancer occurs when the cells in the breast begin to grow uncontrollably. These cells usually form a lump called a tumor or a growth. The tumor is considered cancer if the cells invade the surrounding tissues, and spread (metastasize) to distant body parts. Early detection of breast cancer is an important strategy in the breast cancer management. For that, screening tests (such as yearly mammogram) are conducted to find the breast cancer before it causes symptoms. If the screening test shows the doctors a suspicious lump or the symptoms start to appear, more tests are required to diagnose whether it is cancer. Diagnostic tests (such as mammogram, breast ultrasound, biopsy) are used to find the presence of cancer, how far it spreads, and gather more information for treatment plan. In other

words, the tests for breast cancer diagnosis characterize tumor, and find out whether the tumor is cancer. Once the breast cancer is diagnosed, further tests and exams are performed for staging the breast cancer. Eventually, a patient goes through treatment, therapies, and monitoring.

Imaging is an indispensable tool in breast cancer screening, diagnosis, staging, treatment, and monitoring. It allows the doctors to observe the inside of breast tissues non-invasively. This dissertation specifically focuses on the imaging techniques used for breast cancer diagnosis. Currently, various imaging modalities are utilized for diagnosis, such as mammography, breast ultrasound (US), and breast magnetic resonance imaging (MRI). Mammography uses X-ray radiation to detect abnormality in tissue. Ultrasound imaging utilizes high frequency sound wave to probe the tissue. Magnetic resonance imaging (MRI) use high frequency radio waves on tissue under strong magnetic field. All these imaging modalities are not without their limitations. Mammography sensitivity deteriorates for the high grandular tissues, which is relevant to younger women. Mammography uses ionized radiation for imaging. Ultrasound is used with mammography if further investigation on cancer is required. Ultrasound has higher sensitivity and lower specificity than mammography. MRI is highly sensitive among the imaging modalities. However, it has limited specificity. Moreover, MRI is limited in use because of its high cost. Thus, there is still a need for imaging modalities with higher sensitivity and specificity using non-ionized radiation.

The conventional imaging modalities utilize stationary or fixed geometric configurations of the source and detectors. In those cases, the source-detector setup is maneuvered manually or using a gantry. For example, mammography is a two dimensional representation of a three dimensional structure. Depending on the patients' conditions, the radiologists have to take multiple views of the breast (standard and additional). The manual handling affects the accuracy. Computed tomography uses different geometric configuration, translations, and rotations of the source and the detector for improving imaging performance. All of those configurations have fixed geometry for the source and the detectors. A dynamic positioning of the source and the detectors with six degree of freedom movement can improve the characterization accuracy. Magnetic resonance imaging also

utilize fixed geometric configuration and rotations of the magnets and radio frequency coil. The patients often feel claustrophobic because of MRI scanner construction. The dynamic positioning of source-detector configuration using six-degree of freedom manipulators can improve the convenience of imaging.

The tumor characterization is an important aspect in breast cancer diagnosis. The conventional imaging modalities are sensitive to various types of biological contrast. Therefore, a single imaging modality does not give a complete picture of breast tumor properties, specially mechanical and spectral properties. The mechanical properties of a tumor, such as size, depth, elastic modulus indicate the malignancy level, while the spectral properties, absorption and reduced scattering coefficients give access to the physiological information, such as concentration of total hemoglobin, blood oxygen saturation, lipid, and water. Researchers have been working on two emerging modalities, tactile sensing imaging and diffuse optical tomography, in order to estimate mechanical and spectral properties. The advantages of these two modalities are use of non-ionized radiation and relatively low cost (compared to MRI). Integrating these two approaches on a single dynamic positioning system has yet to be explored. This dynamic and multimodal approach of imaging may enhance the tumor characterization accuracy.

1.2 Background and Literature Review

In this section, we present literature review on several imaging techniques, dynamic positioning, statistical game control, tactile sensing, and diffuse optical imaging.

1.2.1 Imaging Techniques used in Breast Cancer Diagnosis

Over the past few decades, various imaging techniques have been aiding the physicians for breast cancer diagnosis. Each of the conventional imaging techniques has its advantages and limitations. This section reviews some of the modern imaging techniques used for breast cancer diagnosis.

1.2.1.1 Mammography

Mammography is the imaging technique that uses a low-dose X-ray to image the breast. Mammography creates the X-ray image of the breast, which is called mammogram. Depending on the density, different parts of the breast attenuate X-ray radiation differently. Based on that fact, the mammogram is generated. There are two types mammography: screening mammography and diagnostic mammography [1]. The screening mammography is targeted to the patients with no cancer symptoms. In this type of mammography, X-ray images of each breast are taken from two different angles (four views in total). On the other hand, in diagnostic mammography, additional views of breast are captured from different vantage points along with four standard views. The diagnostic mammography is targeted to the patients after suspicious results from the screening mammography. Also, the diagnostic mammography is used for the patients who are treated before for cancer. Fig. 1.1 shows the mammography procedure. During the procedure, the breast is placed between two glass plates and compressed. Then the X-ray image is captured. When the captured image is stored on a film, it is called film mammography. When the captured image is stored on a computer, it is called digital mammography. Film and digital mammography are similar in finding cancer [14], [15], [16].

In detecting all types of invasive breast carcinomas, the sensitivity of mammography ranges from 63% to 98% [17], [18]. For invasive lobular carcinoma, the sensitivity ranges from 57% to 81% [19], [20], [21]. The mammographic sensitivity is inversely correlated with the degree of fibrograndular tissue density. Therefore, false positive results are more common for younger women due to high glandular tissues [22]. Note that false positive results occur when mammograms appear abnormal even though there is no cancer. In the presence of dense breast tissue, the mammographic sensitivity for the detection of invasive tumor can be as low as 30% to 48% [23], [24]. Screening mammography is a fast procedure (about 20 minutes) and exposes the patient to a small dose of radiation. On the other hand, diagnostic mammography takes longer than screening mammography and the total dose of radiation is higher than that of screening mammography [1].

Conventional film and digital mammography have some limitations. They are painful

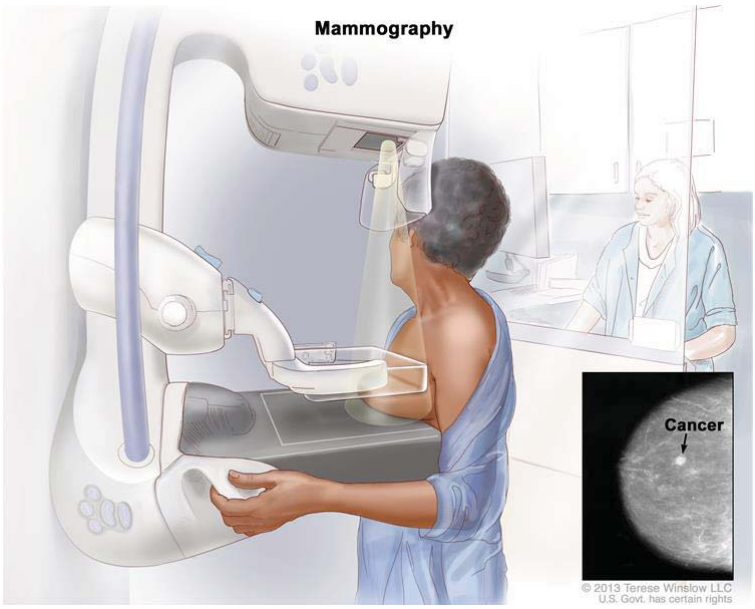

Figure 1.1: The breast is pressed between two plates while taking x-ray image [1].

for some women. Under compression the breast tissue may overlap and obscure the cancerous tumor during mammography. Also, a mammogram is a two-dimensional image, which may not give the full picture of the tumor. Three-dimensional mammography, also known as digital breast tomosynthesis, overcomes the above limitation of two-dimensional mammography. In tomosynthesis, multiple X-ray images are taken from different angles typically between $\pm 30^{\circ}$ [25]. Then, the images are assembled to construct a three-dimensional image of the breast. Digital breast tomosynthesis with digital mammography has been shown to detect more breast lesions, better classify those lesions, and generates lower callback rates than mammography alone. The combination of tomosynthesis and digital mammography can reduce false negatives and increase true positive rates. However, the radiation dose in this combination is higher than standard mammography.

Another emerging mammography technique is contrast-enhanced mammography, which uses iodine contrast agents. This technique is based on the fact that rapidly growing tumors need increased blood supply through angiogenesis for supporting tumor growth. Equipped with tomosynthesis, it provides a method of imaging contrast distribution in breast. The contrast agents are administered before compression. After tomosynthesis, the images are evaluated based on the concentrations of iodine. The hight uptake region indicates the

active tissue growth [26].

1.2.1.2 Ultrasound

Ultrasound is one of the most commonly used diagnostic imaging methods in breast cancer. This is also known as ultrasonography, sonography, and sonogram. This technique helps doctors for further investigation of a tumor after mammography. It uses high frequency sound wave to image the inside of the body from echo [1]. This method is fast (20 to 30 minutes) and does not use ionized radiation. Ultrasound is good in imaging some soft tissues that do not show up well on X-rays. Also based on different echo pattern, it can differentiate fluid-filled cyst and solid tumor.

An ultrasound machine uses a microphone or computer mouse shaped transducer. It sends out the sound wave to the scanning area and picks up the echoes. These echoes are analyzed and displayed on the screen. The newer forms of ultrasound can provide three-dimensional images. The overall sensitivity of ultrasound in detecting invasive lobular carcinoma is found to be 68% to 98% [27], [28], [29]. This sensitivity range cannot be compared directly with the sensitivity of mammography, because the sensitivity study of mammography typically includes both screening and diagnostic exams. The lower end of the sensitivity range of ultrasound was reported in the earliest study. With the advancement of ultrasound technology, the sensitivity improved significantly.

1.2.1.3 Breast Magnetic Resonance Imaging

Magnetic resonance imaging (MRI) is the most sensitive imaging modality compared to mammography and ultrasound. It is utilized for cancer detection, staging, therapy response monitoring, and biopsy guidance. It uses radio waves in the presence of strong magnetic field for scanning the patient and then images the radio waves emitted by tissue [1]. Different types of tissue emit different amount of signal intensity, which helps image the areas inside the body.

The sensitivity of breast MRI are reported from 86% to 100% [30]. However, the high sensitivity comes at the cost of reduced specificity. Also, breast MRI can cost a lot and can be uncomfortable for the claustrophobic patients, and inconvenient for overweight

patients [1]. It does not expose the patient to ionized radiation. Fig. 1.2 shows the MRI scanning procedure of a patient.

Figure 1.2: The patient lies on a table that slides into MRI machine [1].

1.2.2 Dynamic Positioning

Most of the medical imaging technology consists of either stationary source-detector setup (Mammography) or translation and rotation of a fixed geometric source-detector setup (CT, MRI). In surgical imaging, we found another type of dynamic positioning implemented in mobile C-arms. Mobile C-arms are medical imaging devices based on X-ray technology and can be used flexibly in operating rooms. The name “C-arms" is derived from the C-shape of arm that connect X-ray source and X-ray detector as shown in Fig. 1.3. The C-arm allows the elements connected to it move horizontally, vertically, and around the swivel axis. This permits the imaging of the patient almost from any angle. Researchers attempted to make C-arms a six-degree of freedom imaging system by introducing the translational motion to the operating table [31]. As far as the author is aware, the positioning of the source and the detectors with six degree of freedom motion is not available in the medical imaging technology literature.

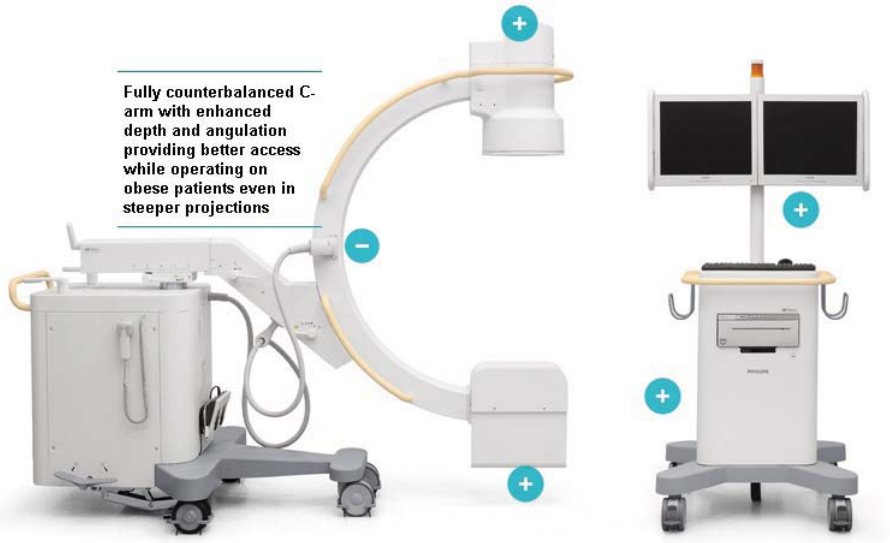

Figure 1.3: C-arms capable of x-ray imaging used during surgery [2].

1.2.3 Statistical Game Control and Hybrid Statistical Control

The dynamic positioning of sources and detectors require coordinated control schemes. The statistical game control is an ideal choice for this scenario because sources and detectors can be viewed as multiple players. The statistical game control deals with the statistical control of multiple players under game theoretic framework.

1.2.3.1 Game Theory

Osborne and Rubinstein defines *game* in [32] as, “A game is a description of strategic interaction that includes the constraints on the actions that the players can take and the players’ interests, but does not specify the actions that the players do take." Game theory provides reasonable solutions to classes of games and studies their properties. Game theory has applications in different fields of research such as, economics, biology, management, communication networks, power systems, and control systems. The notion of games of strategies are first found in Borel’s works in the early 1920s. Later, the modern game theory was developed by Von Neumann and Morgenstern and published in “Theory of Games and

Economic Behavior" in 1944 [33]. In the early 50s, differential games were developed by Isaacs [34]. In differential games, the states of the players evolve with the change of time. Differential games are also termed as dynamics games.

Differential games can be broadly classified into two categories: cooperative game and non-cooperative game. In cooperative games, the players can make binding agreements about the distribution of payoffs or about the selection of strategies, even if these agreements are not specified or implied by the rules of the game [32]. Thus the players form coalitions, and the coalitions compete with each other. Inside a coalition, the players behave cooperatively. On the other hand, in non-cooperative differential games, each player acts independently, without collaboration or communication with any of the others.

In 1950 Nash proved the existence of a strategic equilibrium for non-cooperative games which is called the “Nash equilibrium" [35]. Nash equilibrium solution is optimal to all the players in the game, because deviations from the Nash equilibrium strategy is not profitable for any player, while others are maintaining their equilibrium strategies. Thus, in Nash equilibrium solution or *Nash game*, no single player dominates the decision making.

In some non-cooperative decision problems, one of the players has the ability to enforce his strategy on other players. The player who possesses the powerful position is called leader, and the other players who react rationally to the leader’s decision are called the followers. Such games are referred to as *Stackelberg games* [36]. The Stackelberg equilibrium solution was first introduced by H. Von Stackelberg [37].

1.2.3.2 Statistical Control

Stochastic differential game results from strategic interactions among players in random dynamic system. The stochastic optimal control can be viewed as a differential game, where a single player strives to optimize a single cost function. In stochastic differential game, there are multiple players, each with a separate cost function to optimize.

The statistical control is a type of stochastic optimal control, where the cumulants of the cost function are minimized. In other words, the statistical control shapes the probability density function of the cost the cost cumulants. The statistical control has been initiated by Sain [38–40] through the minimization of cost variance. This was later extended by Won *et*

al. for higher order cumulants for a nonlinear system with nonquadratic cost functions [41]. Won and Aduba investigated the statistical control under Nash game theoretic framework, which deals with the simultaneous optimization of cost cumulants of multiple players [42].

1.2.3.3 Stackelberg Game in Dynamic Positioning

Stackelberg equilibrium solution comes into control systems literature through the works of Chen, Cruz, and Simaan [43–45]. For the dynamic positioning, the source can act as a leader and the detector can act as a follower. The source optimizes the cost variance of the target position while the detector minimizes the mean. Bagchi and Basar worked on the minimization of cost mean for both the leader and the follower for a linear system [46]. The minimization of leader cost variance has not been explored yet. So, we choose the Stackelberg solution concept with statistical control theory for coordinated control of sources and detectors in our dynamic positioning scenario.

1.2.3.4 Hierarchical Hybrid Systems and Control

Hierarchical and Hybrid systems are two different concepts, both of which are relevant for the modern day complex systems. Hierarchical systems view the complex system as a group of tier with different functions within and between tiers. In this way, a large, complex system can be divided into several smaller subsystems, and become easier to be organized and controlled. Multi-agent systems and sensor networks are examples of hierarchical systems. On the other hand, hybrid systems have both continuous and discrete dynamics. The combination of hierarchical and hybrid systems concept can offer an effective control approach on a complex system compared to the stand-alone statistical control approach.

The statistical control can be applied directly to control the continuous dynamics of the hybrid system, which may not be applicable for controlling the discrete events. The discrete event system model is appropriate for modeling the discrete dynamics. In discrete event systems, the state-space of a system is described by a discrete set, and state transitions are observed at discrete points in time. An event may be viewed as a spontaneous occurrence, which causes a transition of system from one node to another. For a detailed description on discrete event systems, see [47].

The hierarchical system concept has been used in discrete-time sensor based control of robotic systems [48], flexible task execution in human-robot interaction [49], action-intention-based grasp control [50], multiple satellite systems control [51] , and sensor networks [52]. The bimodal dynamic imaging system consists of continuous and discrete dynamics. For a given reference trajectory, the low-level statistical control is sufficient for controlling the source-detector manipulator of the system. Scanning a target in three dimensional space using two six-degree-of-freedom manipulators will create a complex task scenario. In that scenario, cooperation and coordination of the manipulators will be necessary. Under that circumstances, a high-level supervisory controller with a low-level statistical controller is more appropriate for the bimodal imaging system applications. In this dissertation, we explore the combination of hierarchical system and hybrid system to form a hybrid statistical controller for controlling the source-detector manipulator of the bimodal imaging system.

1.2.4 Tactile Sensing

Now, we discuss one of the proposed imaging modalities, tactile sensing imaging. The tactile sensing uses the fact that the cancerous tumor is stiffer than the healthy tissues [53], [54]. The benign and malignant tumors exhibit different elastic modulus [55]. Also, the TNM classification system, which is used to describe the stage cancer in a person, considers the size information of tumor (T) as an important characterizing factor [56]. Therefore, the accurate mechanical characterization of tumor is important for the cancer detection and treatment. The breast self examination (BSE) and clinical breast examination (CBE) are two widely used methods for the early breast cancer detection. BSE is recommended for early detection of breast tumor, while CBE is performed by physicians or health care providers. These two methods utilize the human palpation or tactile sensation to obtain the qualitative interpretation of mechanical properties of the tumor. The major drawbacks of the methods are that they are subjective and the efficiency of the methods relies on the individual experience. Moreover, study shows that the overall sensitivity of CBE is 58.8% and the overall specificity is 93.4% [57]. Therefore, the artificial tactile sensors, which can give quantitative information on the mechanical properties of an object, play an important

role for early detection of breast cancer.

The imaging technique that deals with the mechanical properties of an object is known as mechanical imaging. They are also known as elasticity imaging or tactile sensation imaging. The tactile sensation imaging provides important tumor information such as size, depth, and elastic modulus. For the last two decades, various groups from Harvard University [58–60], Artann Laboratory [61], Temple University [62–64] have been working on the development of tactile sensation imaging.

Harvard University researchers developed a handheld scanner consisting of distributed pressure sensor and magnetic tracker for documenting the mechanical properties of the palpable lumps. Wellman formulated an algorithm to create a composite tactile map and estimated the size of the lump within 13% mean absolute error and 7.5% repeatability [59]. Galea developed an algorithm for estimating lesion modulus using finite element model, which gave 5.4% error for physical models [60].

Artann laboratories developed a breast mechanical imaging system consisting of a probe with a pressure sensor array, an electronic unit, and a laptop. This system was commercialized under the trade name of SureTouch by a company Medical Tactile, Inc., Los Angeles, CA. The system is shown in Fig. 1.4. The system estimated the size with a typical relative error of 5%. The smallest inclusion it detected was of 5 mm in diameter. However, the accuracy of the result is affected by the inclusion depth inside the phantom. The inclusion's Young's modulus estimation showed a relative error of 10% [61]. With this mechanical imaging system, they performed a statistical analysis of differentiation capability for 147 benign and 32 malignant lesions from human patients, which revealed an average sensitivity of 91.4% and specificity of 86.8% with a standard deviation of $\pm$6.1% [55].

Temple University researchers have been utilizing high resolution CCD sensors to capture the tactile information. Lee and Won developed a tactile imaging system with non-rigid pattern matching algorithm for elastic modulus estimation. The estimation error was 5.38%. This tactile imaging sensor exhibits a relatively low sensitivity (67%) for differentiating malignant and benign tumours [64]. Therefore, we require to improve the tactile imaging sensor performance. Integrating diffuse optical imaging approach with tactile imaging and dynamic positioning can be key factors to improve the tactile imaging sensor

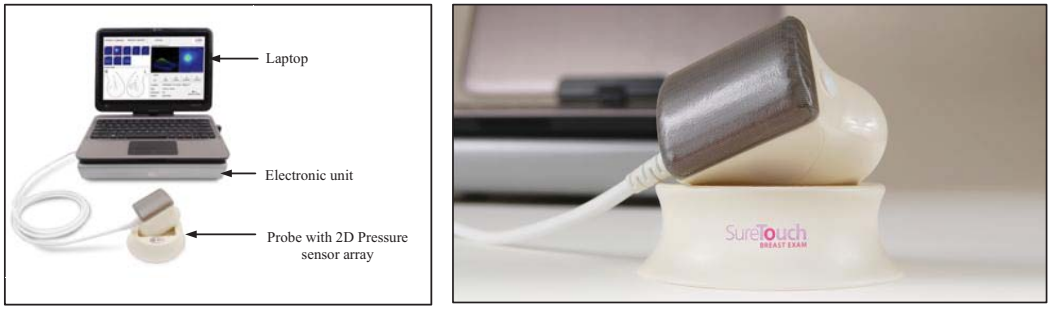

(a) Breast mechanical imager system (b) Breast mechanical imager probe

Figure 1.4: Breast Mechanical Imager (Trade name “SureTouch")

performance.

1.2.5 Diffuse Optical Imaging and Its Use in Multimodal Imaging

In order to improve the mechanical property estimation, we explored another imaging modality called “diffuse optical imaging". Near infra-red diffuse optical imaging uses near infra-red light source to probe tumor and captures diffuse optical information using photo detectors. In diffuse optical tomography, the diffused light is measured to reconstruct three-dimensional absorption and reduced scattering coefficient maps of tissue. Depending on the wavelength range of infra red light source, these coefficients vary differently. From the absorption and reduced scattering coefficients, it is possible to reconstruct the physiological information map of tissue such as, blood dynamics, total hemoglobin concentration, blood oxygen saturation, concentrations of water and lipid using the well-known spectral window shown in Fig. 1.5 [65, 66]. Cancerous tissues show increased vascularity, altered oxygen content, and altered cellular structures at the microscopic scale [67–69]. The diffuse optical imaging can be adapted further to measure exogenous contrast agents such as dye for improved tumor contrast [70]. This imaging modality has a potential to be instrumental in breast cancer detection, diagnosis, and therapy monitoring [71, 72].

The diffuse optical community already explored MRI, CT, PET, and US imaging modalities to combine them with diffuse optical tomography. This type of multi-modality imaging improves the parameter reconstruction spatially and quantitatively.

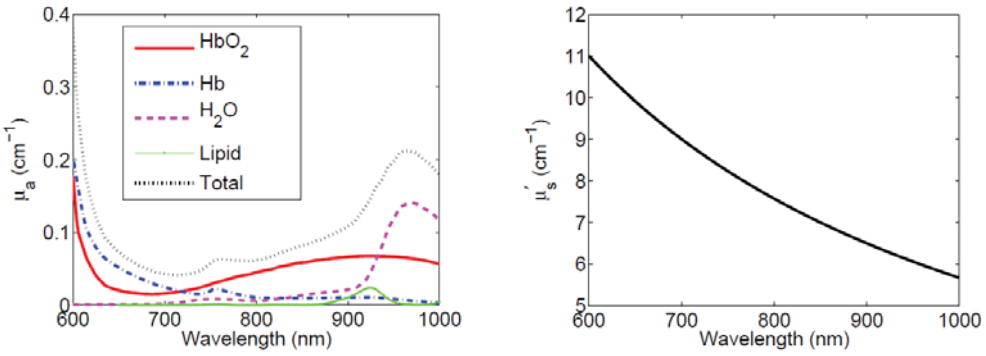

(a) Absorption spectra of tissue chromophores (b) Reduced scattering coefficient assuming simplified Mie scattering law

Figure 1.5: Spectral window for tissue chromophores

Fusion of diffuse optical imaging with MRI is an active research field. MRI can achieve high resolution, but suffers from low specificity [73]. Because of high resolution, this modality is the first natural choice for combining with diffuse optical tomography. Chang *et al.* used volumetric breast MRI data as a priori information for simulating a realistic anatomical medium for diffuse optical probe [74]. He showed that in the case of limited multiply-scattered photons, sufficient information can be gained from MRI to permit accurate reconstruction of absorption coefficient map. Later, Pogue showed on two simulated pathologies, magnetic resonance and optical measurement scheme can reconstruct the absorption coefficient map within 10% error. Also, he showed that the MRI guided diffuse optical scheme produced absorption coefficient maps with a good contrast compared to diffuse optical tomography alone [75]. Ntziachristos developed a MRI-guided diffuse optical spectroscopy for in vivo study of breast cancer [76]. With this system, he quantified the oxy- and deoxyhemoglobin of five malignant and nine benign breast lesions and found decreased oxygen saturation and higher blood concentration in malignant lesions than most benign lesions. Brooksby investigated the optical heterogeneity reconstruction based on MRI infra-red data [77, 78]. Brooksby showed that when prior information of the structure is used to guide NIR property estimation, root mean square (rms) image error decreases from 58% to 26%. Thus, MRI is used to provide *a priori* information to diffuse optical tomography. However, the high magnetic field in MRI causes challenging situation to collect

diffuse optical imaging data without interference.

Li [79] and Zhang [80] described the co-registration of the high resolution tomographic X-ray (CT) with low resolution diffuse optical tomography. The tomographic X-ray help labelling the tissue for diffuse optical tomography inverse problem solution. PET is another imaging modality that can be combined with diffuse optical tomography. A non-concurrent implementation was found in [81].

Zhu proposed the concurrent probing of tissue with ultrasound and diffuse optics for large breasts [82–84]. He monitored the cancer treatment for six large breast carcinoma using the localization information from the ultrasound technique and able to measure the changes in hemoglobin distrubutions. The histologic microvessel density counts from six tumor samples correlate to hemoglobin distributions with a correlation coefficient of 0.64. While ultrasound provides an accurate localization, the diffuse optical tomography reconstruction can be done in fine and coarse grid method depending on the location of the heterogeneity.

In all of the above cases, the diffuse optical tomography uses guidance of other imaging modalities to decrease the reconstruction error. In this proposal, we shall provide a combined scheme of tactile and diffuse optical imaging in order to obtain the absorption coefficients. In our approach, the tactile sensing provides the *a priori* location information for diffuse optical system. However, our goal is to obtain the mechanical properties from the absorption coefficient variation along the cross section of tissue. In order to achieve that we shall introduce the dynamic positioning of source-detector.

1.3 Research Goal

The research questions investigated in this dissertation are:

- Does dynamic positioning of the source and detector of the imaging system lead to more accurate tumor characterization?
- Can we get a more accurate tumor characterization by combining information from two imaging modalities?

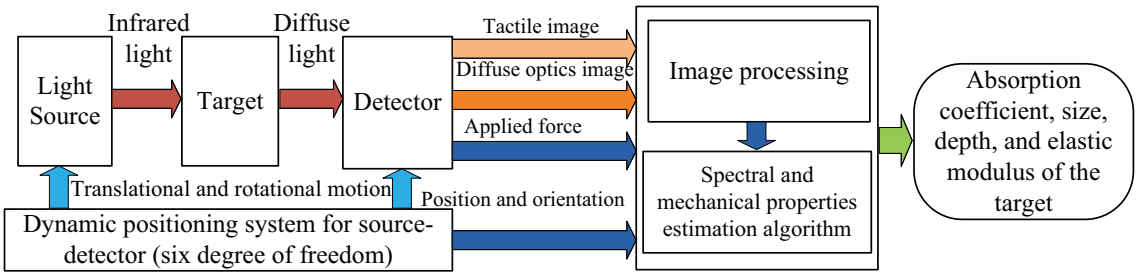

Figure 1.6: Conceptual diagram of bimodal dynamic imaging system

The overall research goal of this dissertation is to find out whether dynamic positioning and multimodality improve tumor characterization. To meet the research goal, three research objectives are established.

The primary research objective is to develop a dynamic positioning method with six degree of freedom motion in source-detector setup for improved tumor characterization. The dynamic positioning method will adopt a multimodal imaging approach with two imaging modalities to improve the tumor characterization performance. The second research objective is to develop a coordination control scheme for the source and the detector of the bimodal dynamic imaging system. The third research objective is to develop a bimodal dynamic imaging system prototype with six degree of freedom motion of the source and the detector. The prototype will use two imaging modalities for estimating mechanical and spectral properties of tumor. The mechanical and spectral properties of tumor are important since these properties vary in case of healthy tissue and tumor (benign and malignant). The tactile sensing imaging (also known as tactile imaging) and diffuse optical imaging are two candidates for mechanical and spectral properties estimation. The application of the bimodal imaging system is towards improving characterization of tumor in a non-invasive manner. In other words, screening (tumor versus no tumor) is not the targeted use of the bimodal imaging system. Fig. 1.6 shows a conceptual diagram of the proposed bimodal dynamic imaging system.

Fig. 1.7 shows a setup for the bimodal dynamic imaging system implemented with Baxter. The laser is mounted on one end-effector of the right arm. The tactile imaging sensor is mounted on another end-effector of the left arm. A computer is utilized for image

acquisition using the tactile imaging sensor. Another computer is utilized for maneuvering the Baxter arms.

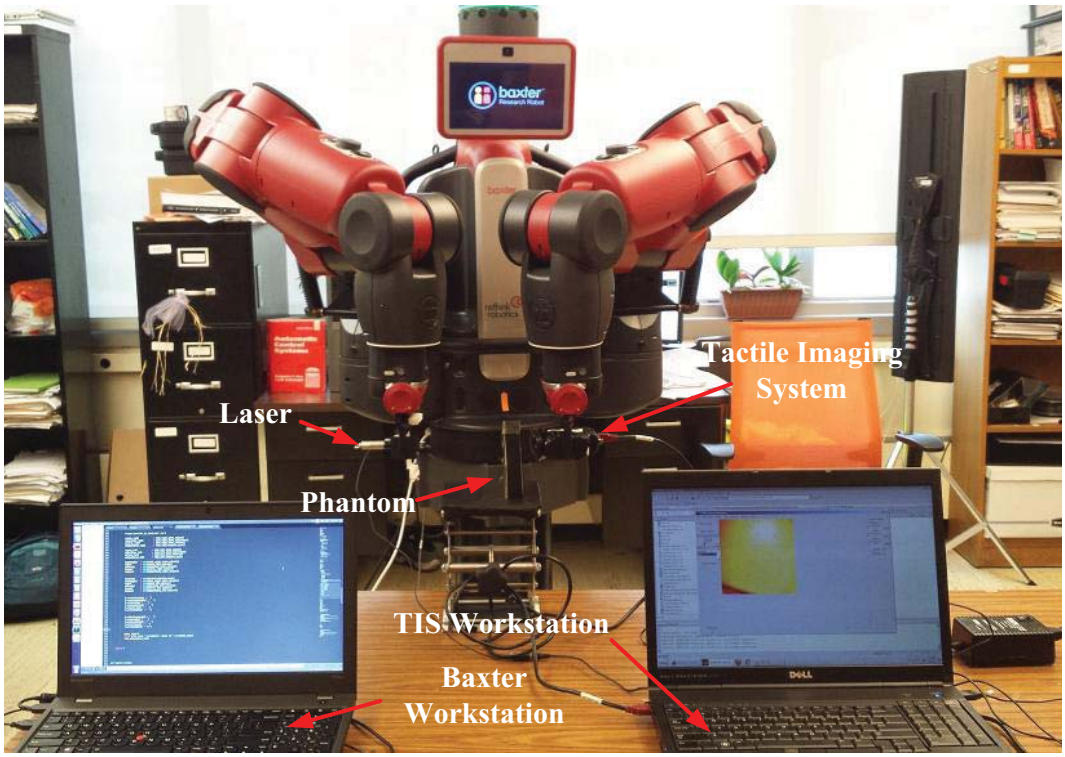

Figure 1.7: Bimodal dynamic imaging system implemented with the Baxter robot

1.4 Contributions

The major contributions of this dissertation are as follows.

- A new bimodal dynamic imaging approach is presented for an embedded tumor characterization. The bimodal dynamic imaging approach has two aspects: bimodal and dynamic imaging. The two modalities: tactile and spectral are used in this method for improving tumor characterization performance. The method employs dynamic positioning of the source and the detector while interrogating a target.
- A new open-loop Stackelberg minimal cost variance control scheme is derived for controlling the source and detector of the bimodal dynamic imaging setup with a numerical simulation. The Stackelberg game control considers the source and the detector maneuvering system as the leader and the follower. The proposed open-loop Stackelberg minimal cost variance control ensures the minimized variance of the leader cost function, while the mean of the follower cost function is being optimized.
- A new linear model is derived for a dual-arm robotic manipulator with seven degree of freedom for each arm. The model was derived in order to be simulated with the proposed control scheme.
- A new hybrid hierarchical statistical control scheme is presented to simulate the motion of robotic manipulators during bimodal dynamic imaging. This controller was applied on the linear model of the dual-arm robot Baxter in simulations. The simulation studies show accurate sequential task execution of the bimodal dynamic imaging system using the hybrid hierarchical statistical control scheme.

1.5 Publications

Here is a list of peer-reviewed publications by the author of this dissertation:

Peer-reviewed Journal Articles

1. **F. Saleheen** and C. -H. Won, “Bimodal Dynamic Imaging System for Embedded Inclusion Characterization", *Sensors Journal, IEEE*, Vol.16 (5), pp. - 6062-6071, 2016.
2. A. Sahu, **F. Saleheen**, V. Oleksyuk, C. McGoverin, N. Pleshko, A. Harati, J. Picone

and C. -H. Won, “Characterization of Mammary Tumors Using Noninvasive Tactile and Hyperspectral Imaging Sensors", *Sensors Journal, IEEE*, Vol.14 (10), pp. - 3337-3344, 2014.

3. **F. Saleheen** and C.-H. Won, “A Hybrid Hierarchical Statistical Control Architecture for Bimodal Dynamic Imaging System Using a Dual-Arm Robot”, *Automation Science and Engineering, IEEE Transactions on*, 2017 (Submitted).
4. **F. Saleheen**, Z. Wang, J. Picone, B. Butz, C.-H. Won, “Efficacy of a Virtual Teaching Assistant in an Open Laboratory Environment for Circuits”, *Advances in Engineering Education*, 2017 (Submitted).

Conference Papers

1. **F. Saleheen**, W.-C. Cheng, and A. Badano “Evaluating Color Performance of Whole-Slide Imaging Devices by Multispectral-Imaging of Biological Tissues", *SPIE Medical Imaging: Digital Pathology Conference*, Orlando, FL: USA, Feb 2017.
2. V. Oleksyuk, **F. Saleheen**, D. Caroline, and C.-H. Won, “Classification of Breast Masses using Tactile Imaging System and Machine Learning Algorithms", *Signal Processing in Medicine and Biology Symposium (SPMB), 2016 IEEE*, Philadelphia, PA: USA, Dec 2016.
3. **F. Saleheen**, Z. Wang, W. Moser, V. Oleksyuk, J. Picone, and C.-H. Won, “Effectiveness of Virtual Open Laboratory Teaching Assistant for Circuits Laboratories", *123rd ASEE Annual Conference and Exposition*, New Orleans, LA: USA, Jun 2016.
4. V. Oleksyuk, **F. Saleheen**, Y. Chen, and C.-H. Won, “Tactile Imaging System for Inclusion Size and Stiffness Characterization", *Signal Processing in Medicine and Biology Symposium (SPMB), 2015 IEEE*, Philadelphia, PA: USA, Dec 2015.
5. **F. Saleheen**, and C.-H. Won, “Dynamic positioning sensing system for estimating size and depth of embedded object", *Sensors, 2015 IEEE*, Busan: Korea, Nov 2015.
6. **F. Saleheen**, and C.-H. Won, “Dynamic Imaging System for Mechanical and Spectral Properties Estimation", *Biomedical Circuits and Systems (BioCAS) 2015*, Atlanta, GA: USA, Oct 2015.
7. **F. Saleheen**, S. Giorgi, Z. Smith, J. Picone, and C.-H. Won, “Design and Evaluation of a Web-based Virtual Open Laboratory Teaching Assistant (VOLTA) for Circuits

Laboratory", *122nd ASEE Annual Conference and Exposition*, Seattle, WA: USA, Jun 2015.

8. **F. Saleheen**, S. Giorgi, Z. Smith, J. Picone, and C.-H. Won, “Virtual Teaching Assistant for Electrical Engineering Science: Initial Study", *Spring 2015 Mid-Atlantic ASEE Conference*, Villanova, PA: USA, April 2015.
9. A. Sahu, **F. Saleheen**, V. Oleksyuk, Y. Chen, and C.-H. Won, “Tactile and hyperspectral imaging sensors for mammary tumor characterization", *Sensors, 2013 IEEE*, Baltimore, MD:USA, Nov 2013.
10. **F. Saleheen**, V. Oleksyuk, A. Sahu, and C.-H. Won, “Non-invasive mechanical properties estimation of embedded objects using tactile imaging sensor", *Proc. SPIE 8719*, Smart Biomedical and Physiological Sensor Technology X, 87190K; Baltimore, MD:USA, May 2013.
11. S. Giorge, **F. Saleheen**, F. Ferrese, and C.-H. Won, “Adaptive Neural replication and resilient control despite malicious attacks", *Resilient Control Systems (ISRCS), 2012 5th International Symposium on*. Salt Lake City, UT:USA, August 2012.
12. **F. Saleheen**, A. Sahu, V. Oleksyuk, and C.-H. Won “Normal force estimation using tactile imaging sensor", *Bioengineering Conference (NEBEC), 2012 38th Annual Northeast*, Philadelphia, PA:USA, March 2012.

1.6 Dissertation Outline

This dissertation proposal is composed of eight chapters. Chapter 2 presents a tactile imaging sensor. The wave-optics analysis and numerical simulation are carried out to verify the imaging principle used in building the sensor. Then, we present the mechanical properties estimation methods for measuring size, depth, and elastic modulus of an embedded inclusion. Chapter 2 ends with the phantom validation experiment results.

Chapter 3 describes the spectral properties estimation method based on the diffuse optics theory. The absorption coefficient determination method is formulated for estimating the coefficient from the diffuse optics image collected by the charged-coupled device camera. We present the results of the phantom validation experiment at the end of this chapter.

Chapter 4 presents the bimodal dynamic imaging method. By dynamic imaging, we

mean the sensors physically moves around the target for imaging. The spectral properties are estimated using the formula described in Chapter 3. Then, we describe the mechanical parameter estimation method using the bimodal dynamic imaging. We discuss the phantom validation experiment results. The bimodal dynamic imaging performance is then compared to that of the tactile imaging system.

Chapter 5 discusses the Stackelberg game control strategy in order to maneuver the source and the detector in the bimodal dynamic imaging system. Under two-player nonzero-sum game frame work, a solution is proposed for the problem of minimizing the leader cost variance, while the follower cost mean is optimized. The theory has been numerically simulated with a simple linear system model.

Chapter 6 derives a linearized model for a dual arm seven degree-of-freedom robot Baxter, which will be used as test-bed for the bimodal dynamic imaging method. The linearized model is validated with an experimental study.

Chapter 7 discusses a hybrid statistical control for the dual arm robot model. Numerical simulations of a hybrid statistical controlled dual-arm robot are presented.

Chapter 8 presents conclusions and future research.

CHAPTER 2

TACTILE IMAGING SENSOR

In this chapter, we describe the imaging principle of the tactile imaging sensor. The imaging principal is verified using wave optics analysis and simulation. Then, we present the overview the tactile imaging sensor. We develop the algorithm for estimating size, depth, and elastic modulus of an embedded inclusion. Finally, we present a preliminary result in order to validate the algorithm.

2.1 Tactile Imaging Principle

The tactile imaging sensor operates on the principle of total internal reflection. According to Snell's law [85], the air which surrounds the waveguide has lower refractive index than that of the waveguide. The incident light directed into the waveguide in such a way that it is trapped inside because of total internal reflection phenomenon. When there is no pressure applied on the waveguide, the camera records no light information since the light is totally internally reflected within the waveguide. The pressure applied on the waveguide makes the trapped light scattered towards the camera. The camera captures the light information, and the computer unit registers it in pixel information. Fig. 2.1 shows the conceptual diagram of the sensing principle of the tactile imaging sensor.

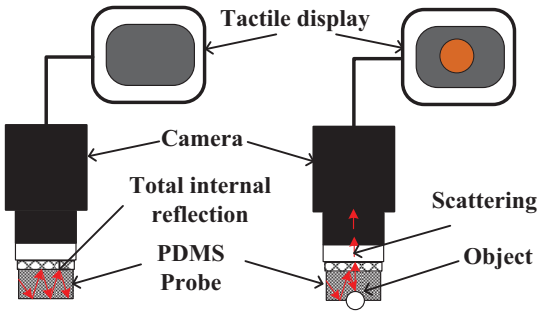

Figure 2.1: Total internal reflection occurs when the illuminated probe compresses the object.

2.1.1 Wave Optics Analysis

In this section, the imaging principle is analyzed using the wave optics analysis method. Fig. 2.2 shows an optical waveguide schematic consisting of a single layer PDMS with a glass plate layer on top. The layer 1 is PDMS with the refractive index η_1 and the height h_1, and the layer 2 is borosillicate glass plate with the refractive index η_2 and the height h_2. The refractive indices η_0 and η_3 are the refractive indices of the surrounding medium around the waveguide. In our case, the surrounding medium is air. Hence, $\eta_0 = \eta_3 = 1$. The waveguide layers are positioned in the order of increasing refractive index, $\eta_1 > \eta_2 > \eta_3 = \eta_0$. The light propagates in z-direction, and the layers are positioned in the x-direction. An infinite length in planar y-direction is assumed.

We begin with the Maxwell wave equation in time domain describing light propagation in an optical waveguide [86],

$$\nabla^2 \mathscr{E} - \frac{\eta^2}{c^2}\frac{\partial^2 \mathscr{E}}{\partial t^2} = 0, \tag{2.1}$$

where $\mathscr{E}$ is the electric field, η is the refractive index, and c is the speed of light in vacuum. The argument for $\mathscr{E}$ is (x,y,z,t), which is omitted for simplification. For monochromatic waves with frequency ω, the solution of (2.1) becomes,

$$\mathscr{E} = \mathscr{E}_{xyz} e^{j\omega t}, \tag{2.2}$$

Substituting (2.2) into (2.1), the spatial distribution of electric field $\mathscr{E}_{xyz}$ becomes

$$\frac{\partial^2 \mathscr{E}_{xyz}}{\partial x^2} + \frac{\partial^2 \mathscr{E}_{xyz}}{\partial y^2} + \frac{\partial^2 \mathscr{E}_{xyz}}{\partial z^2} + k_0^2 \eta^2 \mathscr{E}_{xyz} = 0, \tag{2.3}$$

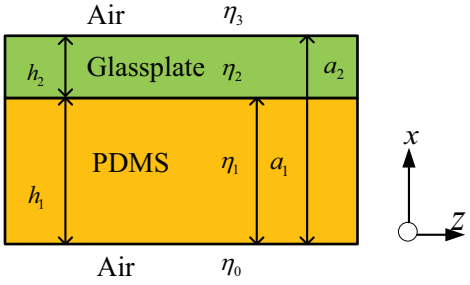

Figure 2.2: Structure of waveguide

where k_0 is the wave vector in vacuum: $k_0 = \omega/c$. The waveguide is uniform in z-direction. Therefore, the planar wave solution becomes,

$$\mathscr{E} = \mathscr{E}_{xy} e^{-j\beta z}, \tag{2.4}$$

where β is the propagation constant. The plane wave solutions are independent of y-direction, the field distribution varies only across x-direction. Then, the spatial distribution of electric field can be written as $\mathscr{E}_{xy} = \mathscr{E}_x$.

Further, we consider the solution for the transverse y-component of the electric field. We assume that $\mathscr{E}_x = \varepsilon_x \hat{j}$, where $\hat{j}$ is the unit vector along the y-direction. Substituting (2.4) into (2.3), we obtain

$$\frac{d^2\varepsilon_x}{dx^2} + \left(k_0^2\eta^2 - \beta^2\right)\varepsilon_x = 0. \tag{2.5}$$

The refractive indices η_0, η_1, η_2, and η_3 are for the respective regions.

$$\frac{d^2\varepsilon_x}{dx^2} + \left(k_0^2\eta_0^2 - \beta^2\right)\varepsilon_x = 0, \qquad x < 0 \tag{2.6}$$

$$\frac{d^2\varepsilon_x}{dx^2} + \left(k_0^2\eta_1^2 - \beta^2\right)\varepsilon_x = 0, \qquad 0 < x < a_1 \tag{2.7}$$

$$\frac{d^2\varepsilon_x}{dx^2} + \left(k_0^2\eta_2^2 - \beta^2\right)\varepsilon_x = 0, \qquad a_1 < x < a_2 \tag{2.8}$$

$$\frac{d^2\varepsilon_x}{dx^2} + \left(k_0^2\eta_3^2 - \beta^2\right)\varepsilon_x = 0. \qquad x > a_2 \tag{2.9}$$

Here, the regions $x < 0$ and $x > a_2$ are outside the waveguide, and the regions $0 < x < a_1$ and $a_1 < x < a_2$ are inside the waveguide. Since no light propagates outside the waveguide, the assumed solution in the region $x < 0$ and $x > a_2$ must decay exponentially with the distance from the surface. On the otherhand, the propagating lights in the region $0 < x < a_1$ and $a_1 < x < a_2$ are oscillating, and have sinusoidal form. Then the solution of (2.5) for all the regions are as follows:

$$\varepsilon_x = \varepsilon_0 e^{\alpha_0 x}, \qquad x < 0 \tag{2.10}$$

$$\varepsilon_x = \varepsilon_1 \cos\left(\alpha_1 x + \phi_1\right), \qquad 0 < x < a_1 \tag{2.11}$$

$$\varepsilon_x = \varepsilon_2 \cos\left(\alpha_2 x + \phi_2\right), \qquad a_1 < x < a_2 \tag{2.12}$$

$$\varepsilon_x = \varepsilon_3 e^{\alpha_3 x}, \qquad x > a_2. \tag{2.13}$$

These solutions are with the unknown parameters such as amplitudes ε_i, transverse wave vectors α_i, and phases ϕ_i, $i = 1,2$, which are determined from the boundary conditions by matching the fields in different regions. Substituting these solutions in (2.5) for their respective region, we have the following relations:

$$-\alpha_i^2 + \beta^2 = k_i^2 \varepsilon_i^2, \tag{2.14}$$

where $i = 0,1,2,3$ for the respective regions.

In order to apply the boundary conditions and match the field components, we determine the magnetic field from Maxwell equation [85]. For the magnetic field $\mathscr{H}$ the Maxwell equation is:

$$\nabla^2 \mathscr{H} - \frac{\eta^2}{c^2} \frac{\partial^2 \mathscr{H}}{\partial t^2} = 0. \tag{2.15}$$

The solution of this equation has a similar form to the electric field with a one nonzero component along the z-direction.

$$\mathscr{H}_{xyz} = h_x e^{(-j\beta z + j\omega t)} \hat{k}, \tag{2.16}$$

where $\hat{k}$ is the unit vector along z-direction. Substituting (2.4) and (2.16) into the Maxwell equation,

$$\nabla \times \mathscr{E} = -\frac{1}{c} \frac{\partial \mathscr{H}}{\partial t}, \tag{2.17}$$

we obtain the general solution for the magnetic field, expressed through the same parameters, as the electric field:

$$h_x = -\varpi \alpha_0 \varepsilon_0 e^{\alpha_0 x}, \qquad x < 0 \tag{2.18}$$

$$h_x = \varpi \alpha_1 \varepsilon_1 \sin(\alpha_1 x + \phi_1), \qquad 0 < x < a_1 \tag{2.19}$$

$$h_x = \varpi \alpha_2 \varepsilon_2 \sin(\alpha_2 x + \phi_2), \qquad a_1 < x < a_2 \tag{2.20}$$

$$h_x = \varpi \alpha_3 \varepsilon_3 e^{\alpha_3 x}. \qquad x > a_2 \tag{2.21}$$

where $\varpi = jc/\omega$. The ratio between the field amplitude of the electric and magnetic fields, $h(x)/e(x)$, is called impedance. The impedance should be continuous on all boundaries at

$x = 0$, $x = a_1$, $x = a_2$, i.e. $h_x = \varepsilon_x$. Thus we have the following results.

$$\alpha_0 = -\alpha_1 \tan\phi_1, \quad x = 0 \tag{2.22}$$

$$\alpha_1 \tan(\alpha_1 a_1) = \alpha_2 \tan(\alpha_2 a_1 + \phi_2), \quad x = a_1 \tag{2.23}$$

$$\alpha_2 \tan(\alpha_2 a_2 + \phi_2) = \alpha_3, \quad x = a_2 \tag{2.24}$$

where the following substitutions must be made.

$$\phi_1 = -\arctan(\alpha_0/\alpha_1), \tag{2.25}$$

$$\phi_2 = \arctan[(\alpha_1/\alpha_2)\tan(\alpha_1 a_1 + \phi_1)] - \alpha_2 a_1, \tag{2.26}$$

$$\alpha_0 = (\beta^2 - k_0^2\eta_0^2)^{\frac{1}{2}}, \tag{2.27}$$

$$\alpha_1 = (k_0^2\eta_1^2) - \beta^2)^{\frac{1}{2}}, \tag{2.28}$$

$$\alpha_2 = (k_0^2\eta_2^2 - \beta^2)^{\frac{1}{2}}, \tag{2.29}$$

$$\alpha_3 = (\beta^2 - k_0^2\eta_3^2)^{\frac{1}{2}}. \tag{2.30}$$

The field amplitudes ε are also determined from the boundary conditions.

$$\varepsilon_1 = \varepsilon_0 \cos\phi_1, \quad x = 0 \tag{2.31}$$

$$\varepsilon_2 = \varepsilon_1 \frac{\cos(\alpha_1 a_1 + \phi_1)}{\cos(\alpha_2 a_1 + \phi_2)}, \quad x = a_1 \tag{2.32}$$

$$\varepsilon_3 = \varepsilon_2 \cos(\alpha_2 a_2 + \phi_2), \quad x = a_2 \tag{2.33}$$

After substituting Eqs. (2.25)-(2.30) into (2.22) to (2.24), the only remaining variable we have is the propagation constant β. Light is an electromagnetic wave phenomenon, where the wave propagates in the form of two mutually coupled vector waves, an electric field wave $\mathscr{E}$ and a magnetic field wave $\mathscr{H}$. Thus the solutions of Eqs. (2.22)-(2.24) provide the complete spectrum of the light propagation in the waveguide.

2.1.2 Numerical Simulations

In this section, we simulated the imaging principle using (2.22)-(2.24). We obtained the electromagnetic wave pattern in the single layer optical waveguide and demonstrated the total internal reflection. We also showed that if an optical waveguide is deformed by an external force, the light is scattered and seen from the surface of an optical waveguide.

In order to simplify the simulation, we assume the waveguide is very thin. For a few millimeter thick waveguide, the wave can be approximated as a ray that uses the geometric optics approximation method.

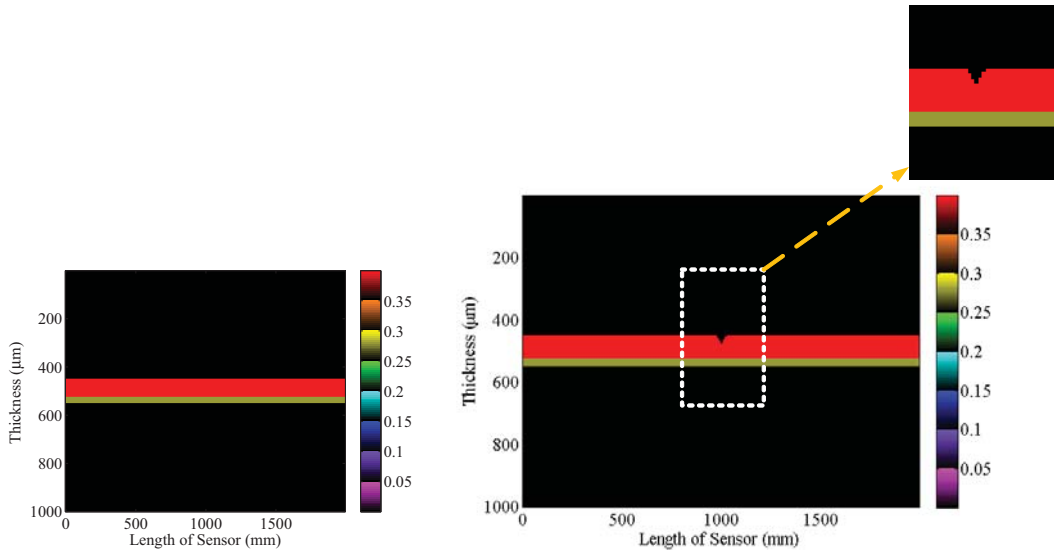

Figure 2.3: (a) The optical waveguide, as seen from its side without deformation, the red layer indicates PDMS. (b) The optical waveguide, as seen from its side with a deformation; the deformation is shown by a black cone shape in top PDMS layer.

Fig. 2.3a shows an optical waveguide prior to the light injection, as seen from its side. PDMS and glass plate layer are represented by the separate colors. The top layer here is PDMS which is the sensing probe, and the bottom layer is glass plate. The light is injected from the left side of the waveguide without and with deformation. The result is shown in Fig. 2.4a and 2.4b. Once the light is injected into the waveguide, a small portion of light diffracts away because of the discontinuity of the media, air and the waveguide. Because of Snell's law, the sinusoidal oscillation of the other light can be seen, and it continues to propagate in the waveguide.

Also, the formation of tactile image was simulated. We captured the scattered light from the top surface of the optical waveguide. Fig. 2.5a shows the result. We can verify that since the light is completely reflected in the optical waveguide, there is no light scattering. Next,

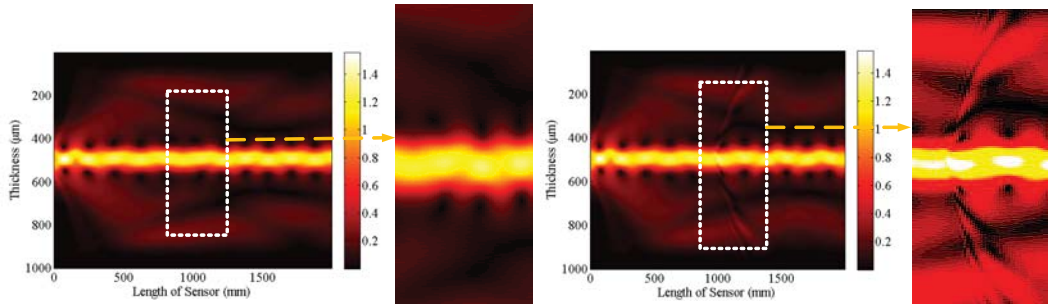

(a) (b)

Figure 2.4: (a) The light oscillation in the optical waveguide due to the Snell's law; the zoomed view shows the light is trapped inside waveguide, and no scattering occurs due to TIR (b) The light scattering in the waveguide due to deformation; the zoomed view shows the scattering.

we investigate the light scattering when the waveguide is deformed. In this simulation, the waveguide is compressed with 20 mm radius tip for about 10 mm deep.

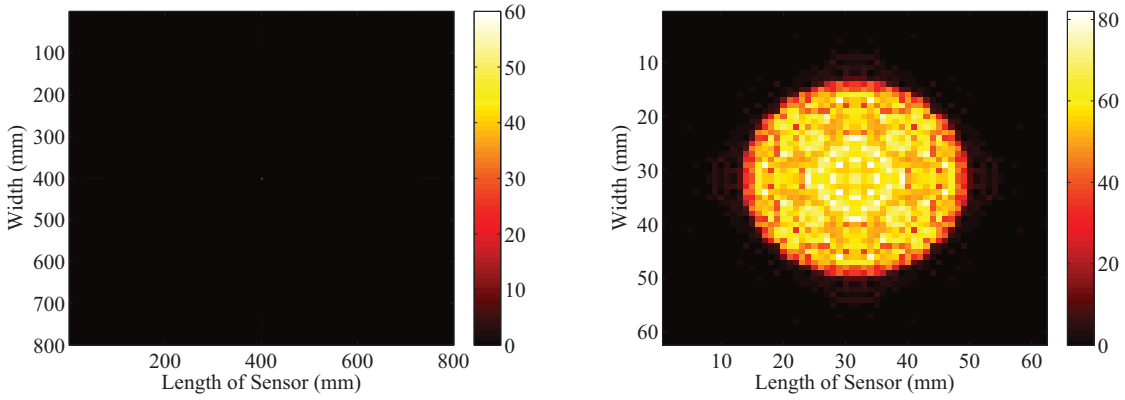

(a) (b)

Figure 2.5: (a) The captured image from the top surface of waveguide before deformation; TIR occurs (b) The captured image from the top surface of waveguide after deformation.

2.1.3 Geometric Optics Approximation

The wave optics analysis becomes too complex for the probe with few milimeter thickness or larger. Therefore, to analyze the critical angle and acceptance angle of the light we consider geometric optics approximation. The acceptance angle is the maximum angle within which light is accepted for the total internal reflection. Now, the light wave is considered as ray. This allows us to calculate the direction of the injected light into PDMS. Considering the geometry shown in Fig. 2.6, the propagation angle γ in each layer i, $i = 1, 2$

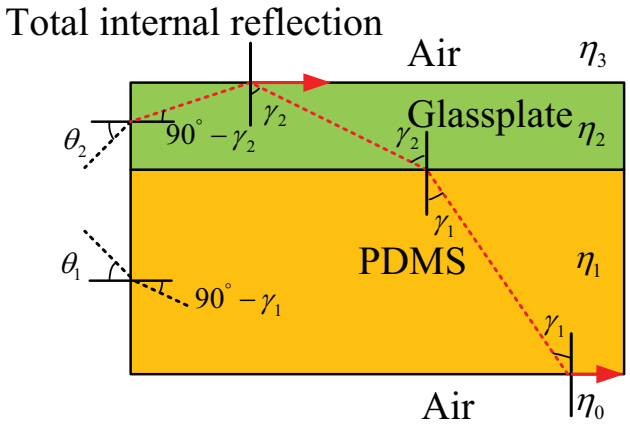

Figure 2.6: Light propagation as a ray inside waveguide.

are bound by the following relationships because of Snell's law,

$$\eta_1 sin\gamma_1 = \eta_0 sin\gamma_0, \tag{2.34}$$

$$\eta_2 sin\gamma_2 = \eta_1 sin\gamma_1, \tag{2.35}$$

$$\eta_3 sin\gamma_3 = \eta_2 sin\gamma_2. \tag{2.36}$$

The total internal reflection occurs when $\gamma_0 = \gamma_3 = 90^\circ$ at the boundaries of air and waveguide. If the light travels with angle $\geq \gamma_i$ in the corresponding layer, then it will be trapped inside the layer. So the minimum propagation angle can be found from the critical angle. The propagation angle γ_i and the acceptance angle θ_i are related by,

$$sin\theta_i = \eta_i sin(90^\circ - \gamma_i) = \eta_i cos\gamma_i = \sqrt{\eta_i^2 - \eta_i^2 sin^2\gamma_i}, \tag{2.37}$$

which gives

$$\theta_i = arcsin\left(\sqrt{\eta_i^2 - \eta_i^2 sin^2\gamma_i}\right). \tag{2.38}$$

Since $eta_i sin\gamma_i = \eta_0 = 1$ for air, Eq. (2.39) becomes

$$\theta_i = arcsin\left(\sqrt{\eta_i^2 - 1}\right). \tag{2.39}$$

We consider the PDMS refractive index as 1.41, and obtain $\theta_1 = 39.2^\circ$. In our design, we chose the light emitting diode with the spatial radiation angle less than 39.2°.

2.2 TIS Prototype Description

The tactile imaging sensor is used to capture tactile images, force information. The sensor consists of a sensing probe, a LED unit, and a lens-coupled CCD camera unit. The LED unit has four white LEDs (4×1500 mcd) with a dimmer circuit. The LED unit illuminates the sensing probe. A pressure on the probe causes the light inside the probe scattered towards the CCD camera, and a tactile image is formed. The sensing probe utilizes one layer of soft and transparent polydimethylsiloxane (PDMS) optical waveguide with dimensions of 20 mm $\times$ 23 mm $\times$ 14 mm and elastic modulus of 27.16 ± 0.57 kPa. The near infrared CCD camera (Guppy F-044, Allied Vision Technologies, Exton, PA) with resolution 752 pixels $\times$ 480 pixels is used for capturing scattered or diffused light. An external force gauge (Mark-10 Series 3, Mark-10, Long Island, NY) attached on the top of the camera body measures the applied force. The range of the measured force is from 0 to 50 N with the resolution of 10 mN. Fig. 2.7 shows the prototype design.

2.3 Mechanical Properties Estimation Algorithm

In this section, we describe the mechanical properties estimation algorithm. The properties of interest are size, depth, and elastic modulus of the embedded inclusion.

2.3.1 Size Estimation

The TIS size estimation algorithm is based on a 3D interpolation model built using tactile data. This model captures the dependency among applied normal force, F, number of

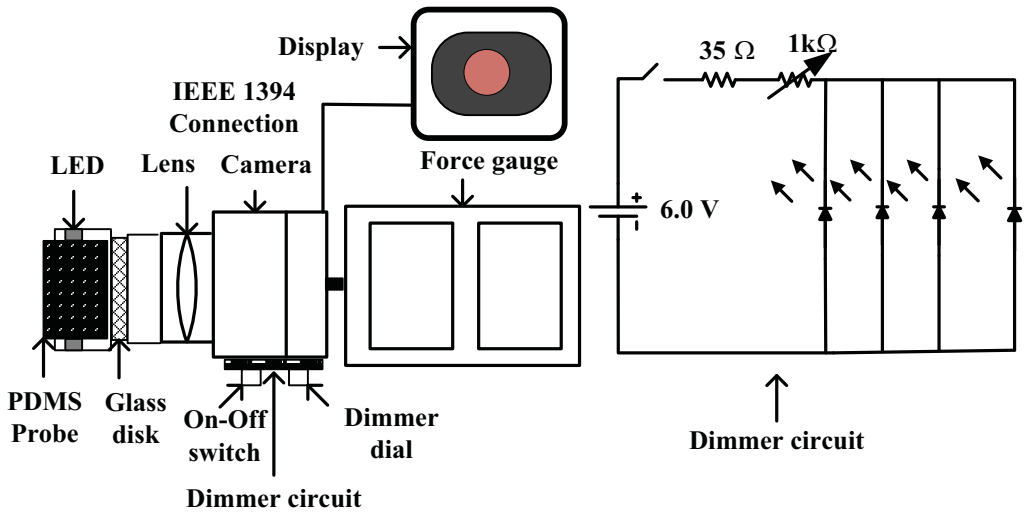

Figure 2.7: Tactile imaging sensor prototype schematics

pixels on the compression-induced image, N_p, and the diameter of the imaged inclusion, $l(F,N_p)$. The tactile images were pre-processed before size estimation. We applied an intensity based threshold which was found from the histogram distribution of the phantom experiment data. Using the number of pixels and applied force information, we calculated the size of the tumor region from the following model,

$$l = p_{00} + p_{10}F + p_{01}N_p + p_{20}F^2 + p_{11}FN_p + p_{30}F^3 + p_{21}F^2N_p. \tag{2.40}$$

2.3.2 Depth Estimation

For the depth estimation, we used a model based on depth and minimum force required to produce the first tactile image. This is given as follows:

$$b = \frac{F_{\min} - c_1}{c_2} \tag{2.41}$$

where b is depth from one surface of the phantom, $F_{\min}$ is the minimum force, c_1 and c_2 are constants determined from the experiment. Then the distance of inclusion from another surface of the phantom can be determined as follows:

$$h = L - l - b, \tag{2.42}$$

where L is the total phantom length and l is the estimated inclusion length.

2.3.3 Elastic Modulus Estimation

Elastic modulus is used to describe the stiffness of an object. It is defined as the slope of stress-strain curve in the elastic deformation region. The stress is defined as the force per unit area. The strain is defined as the fractional change of size because of stress. To calculate stress σ_i for each tactile image, the following formula is used:

$$\sigma_i = \frac{F_i}{A_{probe}}, \tag{2.43}$$

where F_i are the applied forces, i is the index of applied forces, and A_{probe} is the tactile sensor probe surface area.

To estimate the strain ε_i for each pair of tactile images, the following formula is used:

$$\varepsilon_i = \frac{|I_i - I_{\min}|}{I_{\min}} \tag{2.44}$$

where I_i is the sum of pixel values of tactile image captured with i-th force and $I_{\min}$ is the sum of pixel values of tactile image captured at minimum force level. Finally, the elastic modulus is determined from the stress-strain curve.

2.4 Phantom Experiment and Results

In order to validate the TIS method, a rectangular-shape opaque phantom ($90 \times 90 \times 17$ mm^3) with an embedded inclusion ($10 \times 10 \times 10$ mm^3) was fabricated from PDMS (Polydimethylsiloxane). The elastic moduli of the inclusion and the background were calculated as 45 kPa and 355 kPa, found by using the Instron material properties testing equipment. The diagonal length of the inclusion cube is 11.90 mm. The inclusion was embedded at 1 mm depth from one side and 6 mm depth from other side. Fig. 2.8 shows the phantom.

During the tactile image collection, TIS was pressed against the inclusion with 0-20 N forces. A graphical user built in Matlab was used to capture 752×480 pixel image for each force instance. A brightness threshold of 52 was applied on those tactile images. Then the mechanical properties of the embedded object were determined.

We found the coefficients $p_{00} = 4.758$, $p_{10} = 0.4975$, $p_{01} = 6.171 \times 10^{-5}$, $p_{20} = -0.04179$, $p_{11} = -1.326 \times 10^{-6}$, $p_{30} = 0.0007419$ for (2.40). These coefficients were

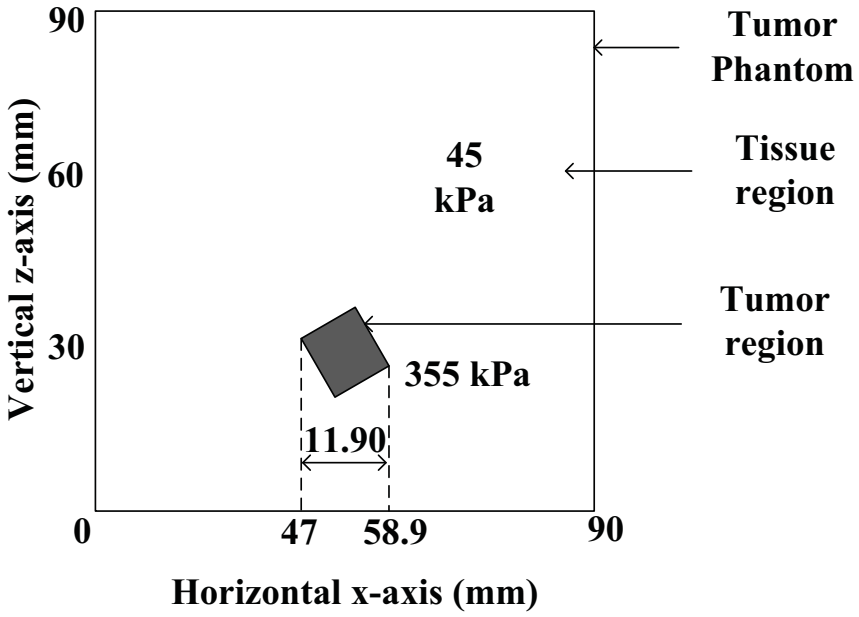

Figure 2.8: Tissue phantom used in TIS experiment

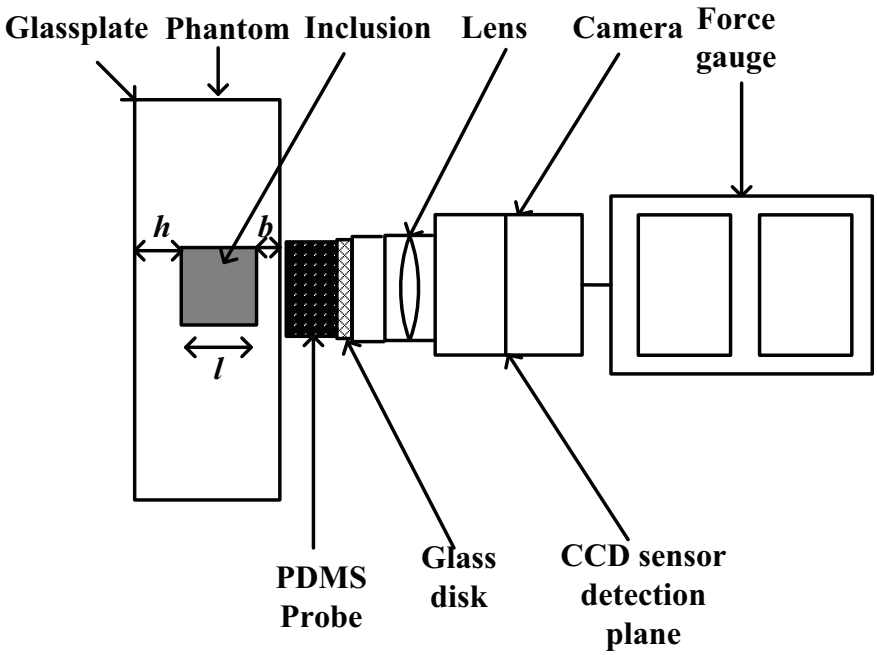

Figure 2.9: Experiment setup for TIS

chosen based on the estimated depth *b* of 2.47 mm. Using these values, we estimated the embedded object size as 11.04 mm. Then we estimated the depth of embedded object from the laser side surface *h* as 3.49 mm.

Table 2.1: TIS experimental results

Properties	True measurement	TIS estimation	Error (%)
l (mm)	11.90	11.04	7.23
h (mm)	6.00	3.49	41.83
E (kPa)	355.00	11.34	96.80

In order to determine elastic modulus, we calculated stress and strain using the TIS method. From stress-strain curve shown in Fig. 2.10, we obtained the linear regression curve for 40% strain. The TIS elastic modulus was found to be 11.34 kPa. The size, depth and elastic modulus estimation results are shown in Table 2.1.

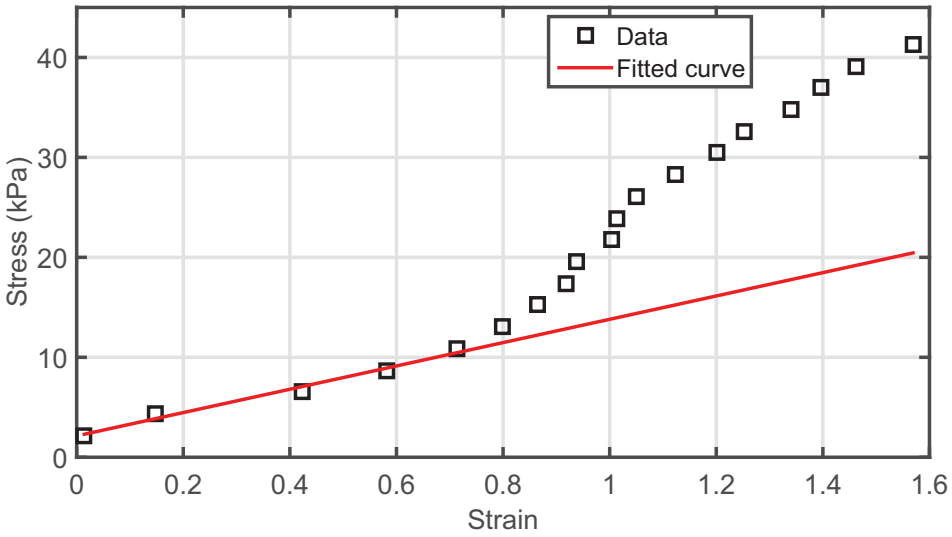

Figure 2.10: Stress-strain curve for TIS

2.5 Discussion

In this chapter, we present the TIS methods for determining size, depth, and elastic modulus, which are verified using a phantom experiment at the end. The experimental results

show that the TIS method work moderately well for the size estimation with 7.23% error. However, the depth and elastic modulus estimation showed large deviations from the true measurement 41.83% and 96.80%, respectively. In order to improve the mechanical properties estimation performance, we propose a dynamic positioning method, which utilizes the spectral properties and the dynamic positioning information of the inclusion. In the next chapter, we develop a method for determining the spectral properties such as absorption coefficient and reduced scattering coefficient of the inclusion.

CHAPTER 3

DIFFUSE OPTICAL IMAGING

In this chapter, we develop absorption and reduced scattering coefficient determination method using diffuse optics theory. In order to validate the method, we performed a phantom experiment.

3.1 Absorption and Reduced Scattering Coefficient Determination

We consider a setup for determining the spectral properties of a turbid medium as shown in Fig. 3.1. A continuous wave point source is located at $r_{s,laser}$. We define the origin O at the exit plane of the turbid medium. The light is incident on the surface of the phantom (turbid medium) at position r_s. Inside the medium, the propagation of light is affected by randomized scattering event and absorption. When photons reach the exit plane of the turbid medium at r_d, they are detected by a CCD camera at $r_{d,ccd}$. Next, we formulate the absorption coefficient determination method using diffuse optics theory.

In diffuse optics theory, light radiance is a key quantity, denoted by $L(r,\hat{\Omega},t)$. The light radiance is defined as the light power per unit area travelling in the $\hat{\Omega}$ direction at position r and time t. This quantity is governed by the radiation transport equation (RTE), which is a conservation equation for the radiance in each infinitesimal volume element within a sample. Assuming a nearly isotropic light source and using a numerical method called “P1 approximation", the light radiance can be expressed in terms of photon fluence rate $\Phi(r,t)$ and photon flux $J(r,t)$ as

$$L(r,\hat{\Omega},t) = \frac{1}{4\pi}\Phi(r,t) + \frac{3}{4\pi}J(r,t)\hat{\Omega}. \tag{3.1}$$

The photon fluence rate $\Phi(r,t)$, is defined as the total power per area moving radially outward from the infinitesimal volume element at position r and time t. The photon flux $J(r,t)$ is defined as the power per area traveling in the $\hat{\Omega}$ direction at position r and time t. Assuming isotropic sources and slow temporal variation in photon flux, the RTE can be

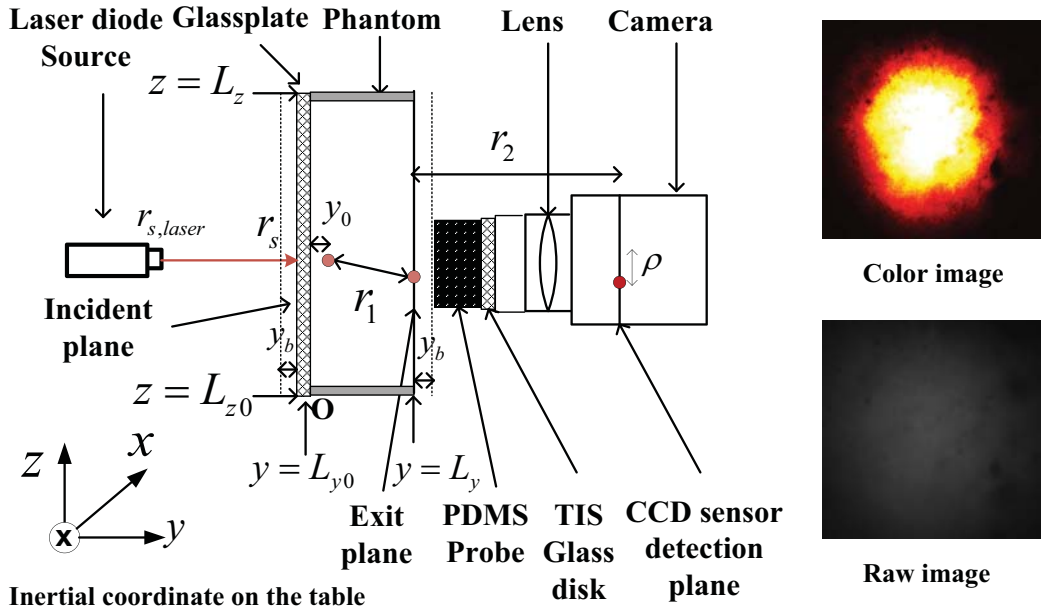

Figure 3.1: Schematic of diffuse optics imaging instrument for a phantom (left), color and raw images (right).

approximated as the photon diffusion equation (PDE) in time domain:

$$\nabla.(D(r)\nabla\Phi(r,t)) - \upsilon\mu_a\Phi(r,t) - \frac{\partial\Phi(r,t)}{\partial t} = -\upsilon S(r,t). \tag{3.2}$$

Here, $S(r,t)$ is the total power per volume emitted radially outward from position r and time t, the light velocity in the medium is υ, and μ_a is the absorption coefficient of the medium. The photon diffusion coefficient $D(r)$ is defined as

$$D(r) = \frac{\upsilon}{3\left[\mu_a(r) + \mu_s'(r)\right]}. \tag{3.3}$$

Here, $\mu_s'(r)$ is the reduced scattering coefficient. The photon diffusion model validity depends on the isotropy of the light source, which requires the condition

$$\mu_s'(r) >> \mu_a(r). \tag{3.4}$$

The rule of thumb is $\mu_s'(r) > 10\mu_a(r)$. In frequency domain, the source term $S(r,t)$ can be divided in dc and ac parts. For the homogeneous media, (3.2) can be written in frequency domain as follows:

$$\left(\nabla^2 - \mu_e^2\right)\Phi(r) = -\frac{\upsilon}{D}S(r). \tag{3.5}$$

Here, the diffusion coefficient is assumed to be constant $D(r) = D$, and μ_e is the effective optical attenuation coefficient, which is defined by

$$\mu_e^2 = \frac{\upsilon\mu_a - i\omega}{D}. \tag{3.6}$$

For a continuous wave source, the angular frequency $\omega = 0$, and (3.6) becomes

$$\mu_e^2 = \frac{\upsilon\mu_a}{D}. \tag{3.7}$$

Using the condition in (3.4) and the relation in (3.3), we write (3.7) as

$$\mu_e^2 \approx 3\mu_a\mu_s'. \tag{3.8}$$

In our case, the wave is generated by a continuous wave laser source with constant power S. We used the Dirac δ function because of the point source assumption. Then, (3.5) can be written as:

$$\left\{\nabla^2 - \mu_e^2\right\}\Phi(r) = -\frac{\upsilon S}{D}\delta(r). \tag{3.9}$$

From (3.8), we see that if μ_e and μ_s' are known, we can determine the absorption coefficient μ_a.

In order to determine μ_e analytically, we need to solve (3.9). For that, we need to find a respective Green's function. Then this Green's function can be used to construct the general solution. In diffuse optical spectroscopy, the most commonly used models for approximating tissue is a homogeneous semi-infinite medium [87]. In this geometry, a method of images is employed to find the diffusion equation Green's functions, subject to extrapolated boundary condition. Fig. 3.1 shows a few important parameters regarding the extrapolated boundary. The cylindrical coordinates are used to specify position, i.e., $r = (\rho, y)$, where ρ is the lateral separation between the source and the detector. We suppose a collimated beam is incident upon the turbid medium at $r_s = (\rho = 0, y = 0)$, and then consider a single normalized isotropic point source at position $r_s = (\rho = 0, y = y_0)$. For a detector at (ρ, y), the Green's function can be written as

$$G_0(\rho, y) = \frac{1}{4\pi}\left[\frac{\mathrm{e}^{-\mu_e r_1}}{r_1} - \frac{\mathrm{e}^{-\mu_e r_2}}{r_2}\right]. \tag{3.10}$$

Here, r_1 is the distance between two points located on the light incident and exit surface of the phantom or medium, and r_2 is the distance between two points located at exit surface and detector sensor. They are defined as,

$$r_1 = \left[(y-y_0)^2+\rho^2\right]^{\frac{1}{2}}, \tag{3.11}$$

$$r_2 = \left[(y+2y_b+y_0)^2+\rho^2\right]^{\frac{1}{2}}. \tag{3.12}$$

Here, y_b is the distance from the air-phantom boundary to extrapolated boundary and $y_0 = \frac{1}{\mu_s'}$. For details about the extrapolated boundary condition, see [87].

Assuming the phantom or turbid medium is well modeled by the homogeneous semi-infinite geometry, the fluence rate can be written as:

$$\Phi(\rho,y) = \frac{S\upsilon G_0}{D} = \frac{S\upsilon}{4\pi D}\left[\frac{e^{-\mu_e r_1}}{r_1} - \frac{e^{-\mu_e r_2}}{r_2}\right]. \tag{3.13}$$

In case of the large source detector separation, we have $\rho >> (2y_b+y_0)$. By setting $y=0$, from (3.11) we get,

$$r_1 = \left[y_0^2+\rho^2\right]^{\frac{1}{2}} = \rho\left[1+\frac{y_0^2}{\rho^2}\right]^{\frac{1}{2}} \approx \rho\left[1+\frac{1}{2}\frac{y_0^2}{\rho^2}\right]. \tag{3.14}$$

The higher order terms are neglected in the above expansion. Similarly, from (3.12), we write

$$\begin{aligned} r_2 = \left[(2y_b+y_0)^2+\rho^2\right]^{\frac{1}{2}} &= \rho\left[1+\frac{(2y_b+y_0)^2}{\rho^2}\right]^{\frac{1}{2}} \\ &\approx \rho\left[1+\frac{1}{2}\frac{(2y_b+y_0)^2}{\rho^2}\right]. \end{aligned} \tag{3.15}$$

Using the relations in (3.14) and (3.15), Eq. (3.13) can be written as

$$\begin{aligned}
\Phi(\rho,y) &= \frac{S\upsilon}{4\pi D}\left[\frac{e^{(-\mu_e r_1)}}{r_1} - \frac{e^{(-\mu_e r_2)}}{r_2}\right] \\
&= A_0\left[\frac{e^{\left\{-\mu_e\rho\left(1+\frac{1}{2}\frac{{y_0}^2}{\rho^2}\right)\right\}}}{\rho\left(1+\frac{1}{2}\frac{{y_0}^2}{\rho^2}\right)} - \frac{e^{\left\{-\mu_e\rho\left(1+\frac{1}{2}\frac{(2y_b+y_0)^2}{\rho^2}\right)\right\}}}{\rho\left(1+\frac{1}{2}\frac{(2y_b+y_0)^2}{\rho^2}\right)}\right] \\
&= A_0\frac{e^{-\mu_e\rho}}{\rho}\left[\frac{e^{\left\{-\mu_e\rho\left(\frac{1}{2}\frac{{y_0}^2}{\rho^2}\right)\right\}}}{\left(1+\frac{1}{2}\frac{{y_0}^2}{\rho^2}\right)} - \frac{e^{\left\{-\mu_e\rho\left(\frac{1}{2}\frac{(2y_b+y_0)^2}{\rho^2}\right)\right\}}}{\left(1+\frac{1}{2}\frac{(2y_b+y_0)^2}{\rho^2}\right)}\right] \\
&= A_0\frac{e^{-\mu_e\rho}}{\rho}\left[\left\{1-\frac{\mu_e {y_0}^2}{2\rho}+h.o.t.\right\}\left(1-\frac{1}{2}\frac{{y_0}^2}{\rho^2}+h.o.t.\right)\right] \\
&- A_0\frac{e^{-\mu_e\rho}}{\rho}\left\{1-\frac{\mu_e(2y_b+y_0)^2}{2\rho}+h.o.t.\right\}\left(1-\frac{1}{2}\frac{(2y_b+y_0)^2}{\rho^2}+h.o.t.\right) \\
&\approx A_0\frac{e^{-\mu_e\rho}}{\rho}\left[1-\frac{\mu_e {y_0}^2}{2\rho}-\frac{1}{2}\frac{{y_0}^2}{\rho^2}+\frac{\mu_e {y_0}^4}{4\rho^3}-1\right. \\
&\left.+\frac{\mu_e(2y_b+y_0)^2}{2\rho}+\frac{1}{2}\frac{(2y_b+y_0)^2}{\rho^2}-\frac{\mu_e(2y_b+y_0)^4}{4\rho^3}\right]. \qquad (3.16)
\end{aligned}$$

Here, the constant term is written as $A_0 = \frac{\upsilon S}{4\pi D}$. Also, we neglect the third, fourth, seventh, eighth terms of (3.16) because of the large source-detector separation assumptions, $\rho >> (2y_b + y_0)$ and $\rho >> y_0$. Eq. (3.16) becomes

$$\begin{aligned}
\Phi(\rho,y) &\approx A_0\frac{e^{-\mu_e\rho}}{\rho}\left[\frac{\mu_e(2y_b+y_0)^2}{2\rho} - \frac{\mu_e {y_0}^2}{2\rho}\right] \\
&= A_0\frac{e^{-\mu_e\rho}}{\rho^2}\left[2\mu_e(2y_0y_b+y_b^2)\right]. \qquad (3.17)
\end{aligned}$$

Now, multiplying both sides of (3.17) with ρ^2 and then taking logarithm, we get

$$\ln(\rho^2\Phi(\rho)) = \ln A_0 - \mu_e\rho + \ln\left[2\mu_e(2y_0y_b+y_b^2)\right]. \qquad (3.18)$$

The last term in (3.18) is neglected, and we write

$$\ln(\rho^2\Phi(\rho)) = -\mu_e\rho + \ln A_0 \qquad (3.19)$$

Eq. (3.19) shows the relationship between the fluence rate $\Phi(\rho)$ and the source-detector pair lateral separation ρ. The negative slope of this linear relationship provides the effective

optical attenuation coefficient which is a function of absorption and reduced scattering coefficient. In our case, a CCD sensor is used as detector. Now, we shall establish a relationship between the fluence rate and CCD image parameter.

Choe *et al.* showed for a lens-coupled CCD camera, the CCD readout is proportional to fluence rate [88]. The proportional term accounts for the internal amplifier gain, the camera exposure time, quantum efficiency of the detector, and the source power.

We suppose a CCD image is obtained for each source position r_s. The optical signal detected at CCD plane is read as a set of discrete points of finite size (pixel), and these pixels form the CCD image. The position $r_{d,CCD}$ denotes the position on CCD detection plane. The power, P, received by the CCD plane is related to the radiance $L(r_s, r, \hat{\Omega})$ by:

$$P(r_s, r_{d,CCD}) = \iint\limits_{\substack{exit \\ plane}} d^2 r \int\limits_{\substack{solid \\ angle}} d\hat{\Omega} L(r_s, r_{d,CCD}, \hat{\Omega}) T_F(\hat{\Omega}) R(r, r_{d,CCD}, \hat{\Omega}). \tag{3.20}$$

The angular integral is extended over the whole half-space solid angle, and the spatial integral is extended over the exit plane. Here, $T_F(\hat{\Omega})$ is a Fresnel transmission factor at the boundary, and $R(r, r_{d,CCD}, \hat{\Omega})$ is a response function which provides the probability that the light emitted from the position r in the $\hat{\Omega}$ direction reached the pixel centered at the position, $r_{d,CCD}$. It is assumed that the response function attains a maximum value at $r = r_d$ for a small area of A centered on r_d in the exit plane, and for $\hat{\Omega}$ within the numerical aperture of the CCD detector. Otherwise, the response function is zero.

Eq. (3.20) can be evaluated using Fick's diffusion law, which relates photon fluence rate to photon flux,

$$J(r) = -\frac{D}{\upsilon} \nabla \Phi(r). \tag{3.21}$$

We applied the partial boundary condition for the radiance at the exit plane [89],

$$\Phi(r) = 2 \frac{1 + R_{eff}}{1 - R_{eff}} \frac{D}{\upsilon} \frac{\partial \Phi}{\partial y}, \tag{3.22}$$

where R_{eff} is the effective reflectance at boundary, and evaluated Eq. (3.20) becomes

$$P(r_s, r_{d,CCD}) \approx \Phi(r_s, r_d) A \xi(r_d). \tag{3.23}$$

Here, $\xi(r_d)$ accounts for the Fresnel factor integral over the system numerical aperture and the Vignetting effect. Hence, the CCD readout voltage, $N(r_s, r_{d,CCD})$, can be expressed as

$$N(r_s, r_{d,CCD}) = P(r_s, r_{d,CCD})\nu\psi\Delta t. \tag{3.24}$$

Here, ν is the quantum efficiency of the CCD system, ψ is the internal amplifier gain of the CCD system, and Δt is the exposure time. Substituting (3.24) into (3.23), we write

$$N(r_s, r_{d,CCD}) = \Phi(r_s, r_d)A\xi(r_d)\nu\psi\Delta t. \tag{3.25}$$

For a specific CCD system, the CCD readout voltage is proportional to the fluence rate,

$$N(r_s, r_{d,CCD}) \propto \Phi(r_s, r_d). \tag{3.26}$$

The CCD pixel value is the digitized version of CCD analog read out voltage [90]. Therefore, the sum of pixel values, $I(r_s, r_{d,CCD})$, is also proportional to the fluence rate. So, we write

$$\Phi(\rho) = \gamma I(r_s, r_{d,CCD}) \tag{3.27}$$

Here γ is the proportional constant term. The argument (r_s, r_d) is replaced by ρ. Then, substituting Eq. (3.27) into (3.19) we obtain,

$$\ln(\rho^2 I(r_s, r_{d,CCD})) = -\mu_e\rho + c_0, \tag{3.28}$$

where the constant term is given by $c_0 = \ln(A_0/\gamma)$. From (3.28) we see that the logarithmic decay of the intensity with increasing source–detector separation can be approximated by a line with a slope of $-\mu_e$. The source-detector separation r can be computed using the geometry of the sample of the turbid medium. The pixel intensity $I(r_s, r_{d,CCD})$ can be found from the CCD camera image.

Arridge and Lionheart showed that in diffuse optical imaging experiment employing continuous wave source, it is impossible to separate μ'_s from μ_a uniquely [91]. In order to circumvent this problem, Minagawa et al. selected the absorption coefficient of the water from the literature for μ_a, then measure the scattering coefficient only by fitting the effective attenuation coefficient μ_e [92]. In our case, we are interested in determining the

absorption coefficient. We, therefore, determine the effective attenuation coefficient from the measured light intensity by fitting, and then for a known reduced scattering coefficient, we obtain the absorption coefficient from:

$$\mu_a \approx \frac{\mu_e^2}{3\mu'_s}. \tag{3.29}$$

Eq. (3.28) and (3.29) are two used for determining the absorption coefficient from diffuse optics information.

3.2 Phantom Experiment and Results

In order to test the method in the above section, we performed an experiment on two phantoms with different absorption coefficient. The phantoms were rectangular shape with a dimension of $90 \times 90 \times 17mm^3$. They were made from PDMS (Polydimethylsiloxane). Carbon black and TiO_2 were used as the absorbing and scattering agents with PDMS. The absorption coefficient of phantom 'a' is 0.3 cm^{-1} and the coefficient of phantom 'b' is $0.08cm^{-1}$. The reduced scattering coefficient is 6.0 cm^{-1}. A 635 nm laser diode was used to as near infrared light source.

We used a CCD camera as a detector because the tactile imaging sensor uses the CCD camera. The camera was focused on a phantom surface of $90 \times 90mm^2$. Then, we collected 283 diffuse optical images from phantom 'a' and 276 images from phantom 'b'. We plotted $ln(r^2 I(r))$ versus r graph, where r is the source-detector separation and $I(r)$ is the pixel intensity. From these plots, we found two fitted curves. Comparing the slope of the fitted curves to (3.28), we determine the effective attenuation coefficient μ_e. Then, we used (3.29) for determining the absorption coefficients. The results are listed in Table 3.1.

3.3 Discussion

The phantom experiment showed us that the CCD camera of the tactile imaging sensor can be used to measure the spectral properties of the inclusion by utilizing the diffuse optics theory. The μ_a estimation errors were found to be 68.56% for the phantom 'a' and 26.37% for the phantom 'b'. The variations of the estimation errors were fairly small. This

Table 3.1: Phantom experiment results for determining absorption coefficient

Phantom	True value (cm^{-1})	Estimated value (cm^{-1})	Standard deviation	Error (%)
a	0.30	0.5056	0.0522	68.56
b	0.08	0.0589	0.0049	26.37

showed that the method can be used for measuring the spectral properties of the inclusion consistently. In the next chapter, we introduce the bimodal dynamic imaging method which utilizes the spectral properties estimation method described in this chapter.

CHAPTER 4

BIMODAL DYNAMIC IMAGING

In this chapter, we develop a bimodal dynamic imaging method for determining mechanical and spectral properties of embedded inclusion. The spectral properties are first estimated using diffuse optical imaging method described in the previous chapter. Then the mechanical properties are estimated using dynamic positioning imaging method which utilize the tactile information, source-detector position information, and estimated absorption coefficients. We describe this bimodal dynamic imaging method in the next section. In order to validate this method, we performed an experiment on a multimodal phantom.

4.1 Overview of bimodal dynamic imaging System Prototype

Fig. 4.1 shows the schematic of the system. An infrared light source is used to illuminate a target. A 635 nm laser diode with $<$5 mW power is used as a light source. A tactile imaging sensor is used as a detector. The tactile imaging sensor is used to capture tactile images, force information, and diffuse optical images. The sensor consists of a transparent sensing probe, a LED unit, and a lens-coupled CCD camera unit. The LED unit has four white LEDs (4 $\times$ 1500 mcd) with a dimmer circuit. The LED unit illuminates the sensing probe. A pressure on the probe causes the light inside the probe scattered towards the CCD camera, and a tactile image is formed. The sensing probe utilizes one layer of soft and transparent polydimethylsiloxane (PDMS) optical waveguide with dimensions. The near infrared CCD camera (Guppy F-044, Allied Vision Technologies, Exton, PA) with resolution 752 pixels $\times$ 480 pixels is used for capturing scattered or diffused light. An external force gauge (Mark-10 Series 3, Mark-10, Long Island, NY) attached on the top of the camera body measures the applied force. The laser diode is mounted on a mechanical scanning platform, which includes a 2-D linear motion controller and a two-axis gimbal (Newmark Inc., USA). The linear motion controller is used for controlling the laser position along the parallel axis of the phantom. The two-axis gimbal is used to control the angular

position of the laser diode with respect to the phantom.

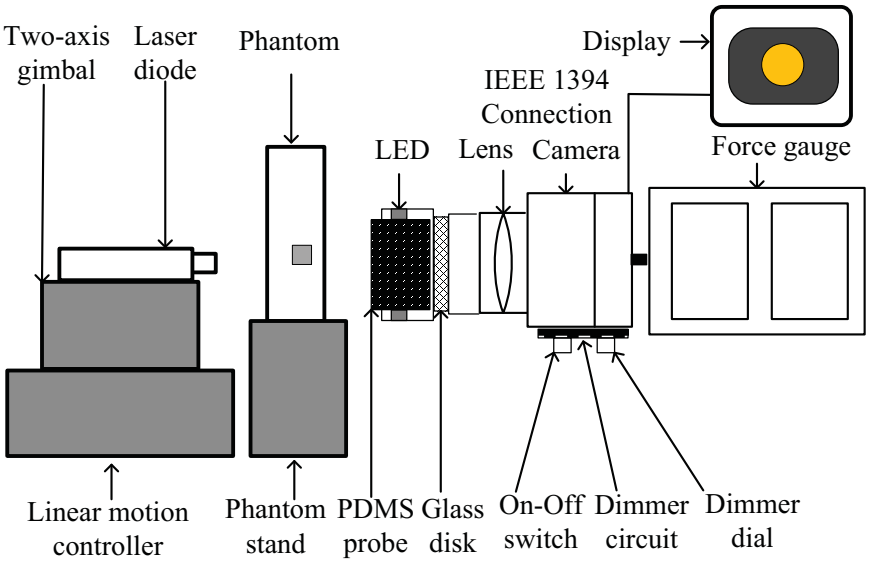

Figure 4.1: Bimodal dynamic imaging system schematic.

4.2 Mechanical Properties Estimation using BDI

In this section, we describe the mechanical properties estimation method using bimodal dynamic imaging. The mechanical properties are size, depth, and elastic modulus.

4.2.1 Size

For the size estimation, the laser diode and TIS are moved in parallel simultaneously along x-axis. The diffuse images are collected and processed. Then using eqs. (3.28) and (3.29), the absorption coefficient is determined for each position of laser diode. After this, the absorption coefficient versus position graph is plotted. We search the location and boundary of embedded object by looking at the variation of absorption coefficient with respect to position. The region with higher absorption coefficient value with small variation is considered the size of embedded object, l as shown in Fig. 4.2.

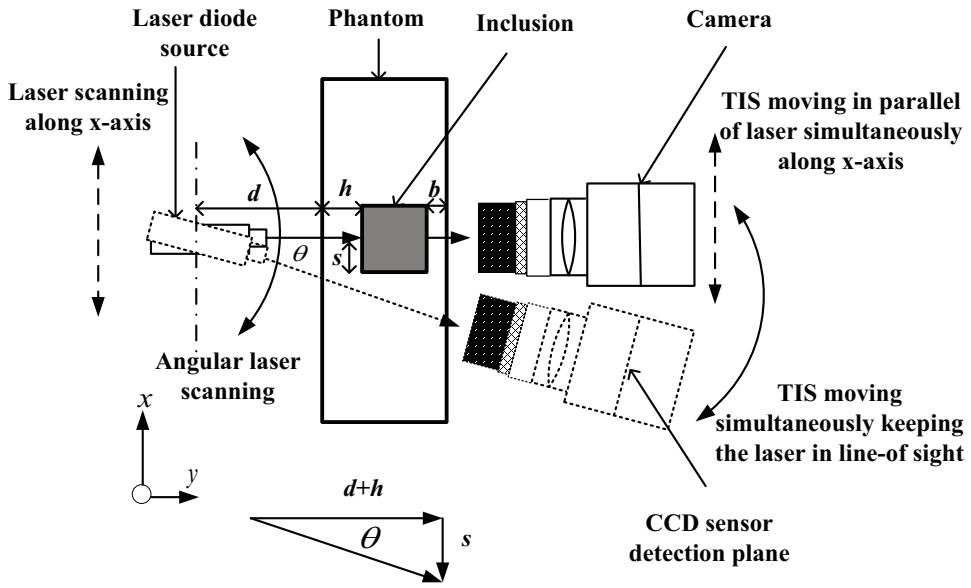

Figure 4.2: The BDIS linear and angular scanning.

4.2.2 Depth

After the size estimation, the laser is positioned at the half-length point of the object. The laser is then maneuvered angularly, with TIS in line of sight of the laser as shown in Fig. 4.2. The laser scanning angle, θ was measured from the current position of the laser and the initial position of laser when the laser beam was perpendicular to the phantom. The distance of the laser rotational axis from the phantom is denoted by d. The depth of embedded object from one surface of phantom (on the laser side) is h, and from the other surface is b. The initial position of laser, the current position of the laser, the half-length of embedded object forms a triangle. From this triangle, we estimate the depth of embedded object from laser side of the phantom as

$$h_{est} = \frac{s}{\tan\theta} - d \tag{4.1}$$

Here, s is the half-length of embedded object. For the depth estimation, the pixel intensity versus scanning angle is plotted. Then, we determine a point I_θ on the pixel intensity graph where the inclusion does not lie in the line-of-sight of the source and the detector. At this point, the pixel intensity will be a few times higher (depending on phantom geometry) than that of the initial position of the laser. The initial position corresponds to the angle 0° and

the angle corresponding to the point I_θ is considered as θ. Then (4.1) is used for the depth estimation.

4.2.3 Elastic Modulus

Elastic modulus is used to describe the stiffness of an object. It is defined as the slope of stress-strain curve in the elastic deformation region. The stress is defined as the force per unit area. The strain is defined as the fractional change of size because of stress. To calculate stress σ_i for each tactile image, the following formula is used:

$$\sigma_i = \frac{F_i}{A_{probe}}, \tag{4.2}$$

where F_i are the applied forces, i is the index of applied forces, and A_{probe} is the tactile sensor probe surface area. After that, the sizes of inclusion are estimated from μ_a versus x plot for multiple force values. Multiple force values produce multiple size estimates. The strain is then calculated as:

$$\varepsilon_i = \frac{|x_i - x_{i-1}|}{l}, \tag{4.3}$$

where x_i is the estimated size from i-th force and x_{i-1} is the previously estimated size. Finally, the elastic modulus is determined from the slope of stress-strain linear regression curve for a specific strain range.

4.3 Spectral Properties Estimation using BDI

We assume that the chromophores contributing to the absorption coefficient are principally oxyhemoglobin and deoxyhemoglobin. Then, the absorption coefficient of tissue can be expressed as a linear combination of chromophore concentrations:

$$\mu_a^\lambda = \varepsilon_{[HbO_2]}^\lambda [HbO_2] + \varepsilon_{[Hb]}^\lambda [Hb] \tag{4.4}$$

where $\varepsilon_{[chromophore]}^\lambda$ is the molar extinction coefficient of a given chromophore at wavelength λ, and $[HbO_2]$ and $[Hb]$ are concentrations of oxygenated and deoxygenated hemoglobin. The molar extinction coefficients $\varepsilon_{[HbO_2]}^\lambda, \varepsilon_{[Hb]}^\lambda$ are obtained from data collected by Scot Prahl [93].

In our case, the BDI size experiment differentiates the tissue and tumor region, the average absorption coefficients for 635 nm (μ_a^{635}) and for 808 nm (μ_a^{808}) are determined. Then the chromophore concentrations are found using the following expression derived from (4.4):

$$\begin{bmatrix} [HbO_2] \\ [Hb] \end{bmatrix} = \begin{bmatrix} \varepsilon_{[HbO_2]}^{635} & \varepsilon_{[Hb]}^{635} \\ \varepsilon_{[HbO_2]}^{808} & \varepsilon_{[Hb]}^{808} \end{bmatrix}^{-1} \begin{bmatrix} \mu_a^{635} \\ \mu_a^{808} \end{bmatrix} \tag{4.5}$$

We calculate two more physiological parameters, total hemoglobin concentration, $THC = [HbO_2] + [Hb]$ and blood oxygen saturation, $StO_2 = 100 \times {}^{[HbO_2]}/_{THC}$. These parameters are often substantially different in rapidly growing tumors; for example, high concentrations of hemoglobin with low oxygen saturation are suggestive of rapidly growing tumors [94, 95].

4.4 Phantom Experiment

In this section, we describe the bimodal phantom that was used in our experiment.

4.4.1 Bimodal Phantom

In order to validate the BDI method, we fabricated a bimodal phantom that emulates both mechanical and optical properties of human breast. The phantom was rectangular cube shape with an embedded cube shape inclusion. The elastic modulus (E) of the inclusion (tumor region) was kept higher than that of the background (tissue region) since the breast tumor tends to be stiffer than the surrounding tissue [54]. The tissue region was fabricated using the RTV 6136-D1 base agent ("A" component) and curing agent ("B" component) weight ratio of 1:1.3; the tumor region had A:B weight ratio of 1:10. The elastic moduli were determined by using the Instron material properties testing equipment. The tumor was embedded at 6 mm depth (h) from one surface of the phantom. The scanning length (l_d) of the cube shape tumor was calculated as 11.90 mm from its diagonal length because of its orientation as shown in Fig. 4.3. The absorption coefficient (μ_a) of the human breast tissue ranges from 0.02-0.12 cm^{-1}; for the reduced scattering coefficient (μ_s') the range is 6-15cm^{-1} [96]. In order to keep the optical coefficient values similar to the human breast tissue, we added carbon black and titanium dioxide (TiO_2) as absorbing and scattering

agents with PDMS, following a recipe given in [97]. The coefficients were then measured by a diffuse optical tomography instrument developed by the researchers in the University of Pennsylvania [97]. The tumor region had higher absorption coefficient value compared to the tissue region. The reduced scattering coefficient were kept similar for both regions and satisfied the assumption $\mu_s' >> \mu_a$. Table 4.1 lists the mechanical and optical properties of the bimodal phantom.

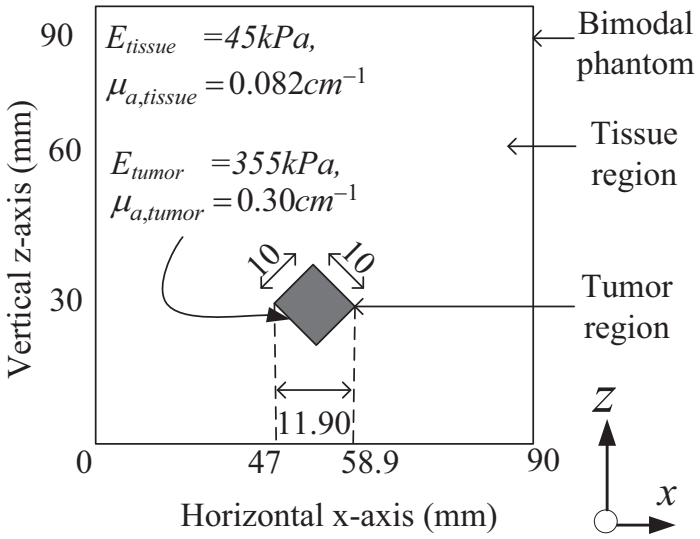

Figure 4.3: The bimodal phantom.

Table 4.1: Mechanical and optical properties of the phantom

Phantom region	Dimension (mm^3)	l_d (mm)	h (mm)	E (kPa)	μ_a (cm^{-1})	μ_s' (cm^{-1})
Tissue	90×90×17	-	-	45.00	0.082	6.80
Tumor	10×10×10	11.90	6.00	355.00	0.30	6.80

4.4.2 Experimental Procedure

During the dynamic positioning image collection, the laser was turned on, and the LED inside TIS was turned off. The laser diode was placed at a distance of 250 mm from light incident plane of the phantom. The phantom and the TIS were surrounded by a shielding box. TIS was kept close to the phantom. We moved the laser and TIS in parallel along x-axis in the same direction and by 4 mm distance. The first laser position (x,z) were on (28 mm, 34 mm) and the last laser position were (76 mm, 34 mm). The laser motion was controlled by the linear motion controller while the TIS was moved manually. For each source position, we obtained 480×480 pixel image. In the image pre-processing phase, we applied a brightness threshold value 52. For edge smoothing, we applied the Gaussian filter (with window of 9×9 and variance = 1) on the images. Using the filtered images, we plotted $\ln(r^2I(r))$ versus r. From this plot, we obtained the least square regression line. Comparing the slope of this regression line with the coefficient of r in (3.28), we calculated the effective attenuation coefficient μe. For calculating the absorption coefficient μ_a, we used the reduced scattering coefficient of the background region of the phantom in (3.29). For this experiment, the absorption coefficient variation between the tumor and tissue region with respect to the tissue region coefficient, $\left(\mu_{a,inc}-\mu_{a,bg}\right)/\mu_{a,bg}$ is 275%. This is much higher than the scattering coefficient variation $\left(\mu'_{s,inc}-\mu'_{s,bg}\right)/\mu'_{s,bg}$ = 11.76%. Therefore, we assume a constant value for the reduced scattering coefficient $\mu'_s=\mu'_{s,bg}=6.8$ cm^{-1}.

The size experiment was followed by the depth experiment. The laser was put at the position where the beam was incident on the center of the embedded object. This was the initial position corresponding to 0°. We moved the laser angularly, keeping TIS in the line-of-sight both clockwise and anticlockwise. The laser was moved using the yaw gimbal of a two-axis gimbal, and the TIS was moved manually. The laser was moved angularly from 0° to -12° and 0° to 12° with 1° increment. The distance between the laser rotation axis and inclusion d was measured as 81 mm. The images were collected and analyzed for the depth estimation using (4.1).

In BDI elastic modulus experiment, we collected images for horizontal position of 35 mm, 44-62 mm, and 68 mm. We used TIS and BDI size experiment results to choose these

horizontal position ranges. For the object location and its boundary with the background, we moved the laser source and camera at a step of 1 mm for 44-62 mm range. At each position, we applied 0-20 N force with 1 N interval and captured the images simultaneously.

4.5 Experimental Results

In this section, we present the experimental results for the bimodal dynamic imaging experiments. The first subsection shows the results from the single measurement of spectral properties, and the second subsection shows the results from the multiple measurements of spectral properties.

4.5.1 Mechanical and Spectral Properties Estimation from Single Measurement Experiment

Here, we present the estimated mechanical and spectral properties from the single measurement experiment. The desired mechanical properties are size, depth, and elastic modulus of the tumor phantom (inclusion). The desired spectral properties are the absorption coefficients of tumor (inclusion) and tissue (background) phantoms. The experimental results of size l, depth h, elastic modulus E, average phantom background absorption coefficient $\bar{\mu}_{a,bg}$, average inclusion absorption coefficient $\bar{\mu}_{a,inc}$ results are listed in Table 4.2.

4.5.1.1 Size Estimation

For the BDI size estimation, we obtained μ_a versus x as shown in Fig. 4.4. We found the object location between x = 48 mm to 60 mm where μ_a variation is less than 0.001. So, the size was found to be 12 mm.

4.5.1.2 Depth Estimation

For depth estimation, we plotted the sum of pixel intensity against the scanning angle as shown in Fig. 4.5. We observed that for this phantom, the pixel intensity increased at a higher rate after the pixel intensity became approximately two times higher than the initial position (0°). We found two such points on the intensity graph and their horizontal axis

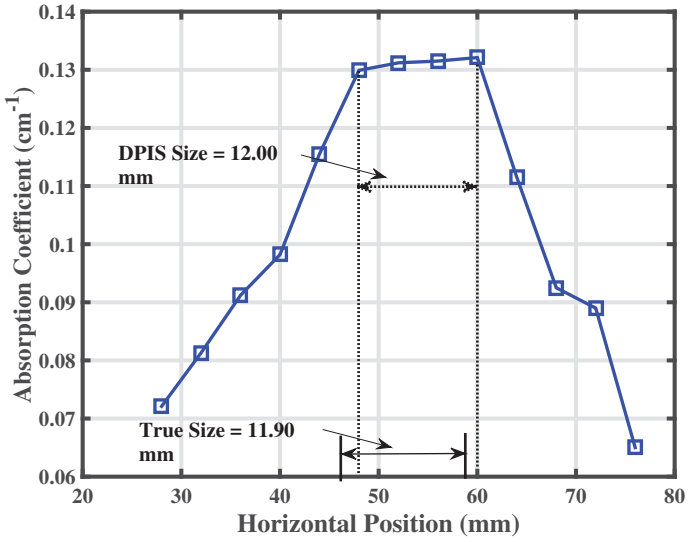

Figure 4.4: Absorption coefficient versus horizontal position graph from parallel scanning.

difference was $2\theta = 8°$. Therefore, we considered θ as 4°, and calculated the depth h as 4.80 mm using (4.1).

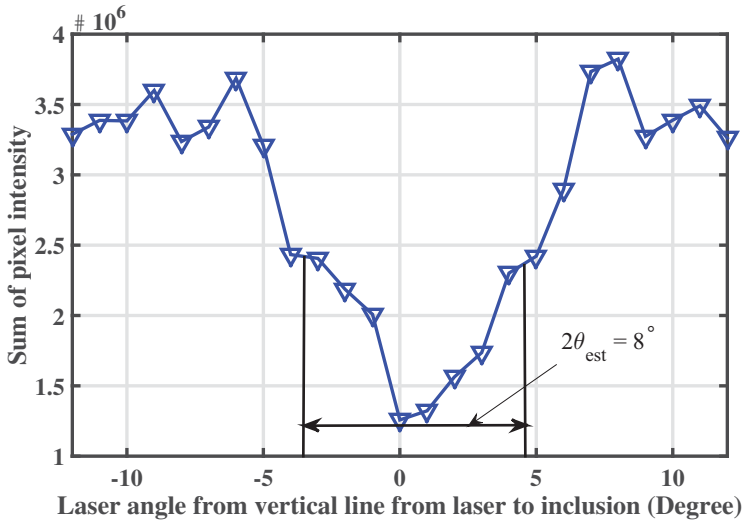

Figure 4.5: Integrated pixel values versus angle graph from angular scanning.

4.5.1.3 Elastic Modulus Estimation

In order to determine elastic modulus, we calculated stress and strain using the DPSS and TIS methods. From stress-strain curve, we obtained the linear regression curve for 40% strain. The TIS elastic modulus was found to be 11.34 kPa, while the BDI elastic modulus was found to be 89.48 kPa.

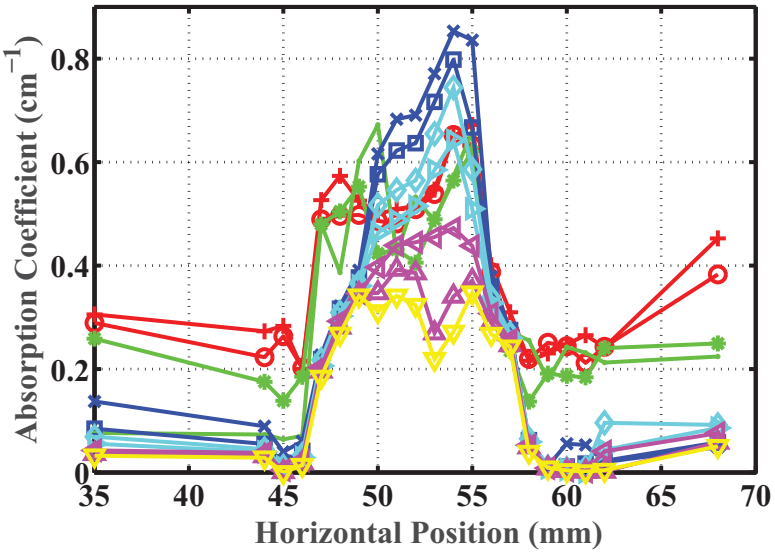

Figure 4.6: Absorption coefficient versus position for different forces.

4.5.1.4 Spectral Properties Estimation

We determined the average value of absorption of the phantom background and inclusion as 0.09 cm $^{-1}$ and 0.13 cm^{-1}. We attained absorption coefficient errors of 12.50% and 56.67% for the phantom background and inclusion.

4.5.2 Mechanical and Spectral Properties Estimation from Multiple Measurement Experiment

Here, we present the estimated mechanical and spectral properties from the multiple measurement experiment. The measurements were performed with 635 nm and 808 nm wavelengths of laser. Also, the absorption coefficients and average sum of pixel intensities were

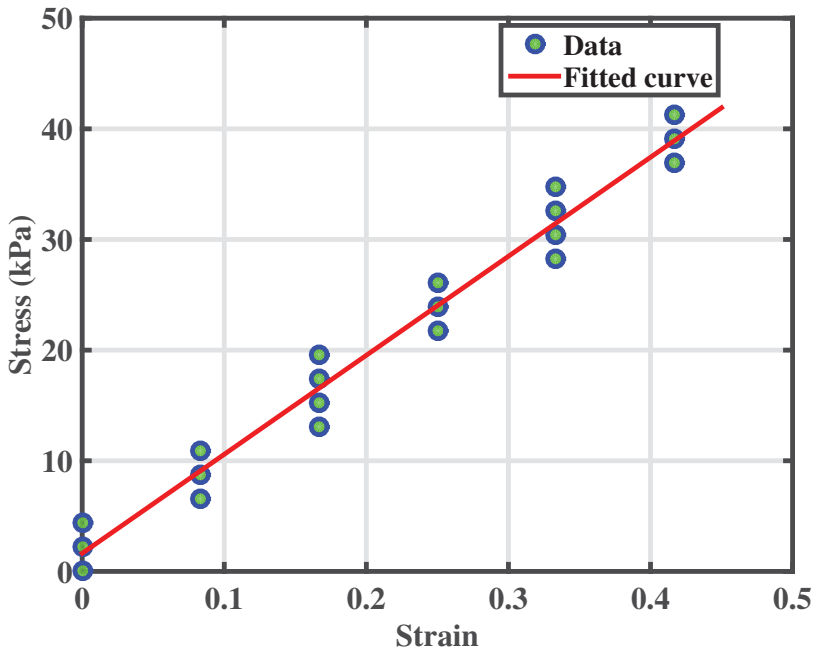

Figure 4.7: Stress-strain curve from elastic modulus experiment.

Table 4.2: Phantom experiment results for dynamic positioning and comparison with TIS results (Single measurement)

Properties	True measurement	TIS estimation	Error (%)	BDI estimation	Error (%)
l (mm)	11.90	11.04	7.23	12.00	0.80
h (mm)	6.00	3.49	41.83	4.76	20.00
E (kPa)	355.00	11.34	96.80	89.48	74.79
$\bar{\mu}_{a,bg}$ (cm^{-1})	0.08	-	-	0.09	12.50
$\bar{\mu}_{a,inc}$ (cm^{-1})	0.30	-	-	0.13	56.67

measured multiple times for each position and angle. The desired mechanical properties are size and depth of the tumor phantom (inclusion). These results can be found in Table

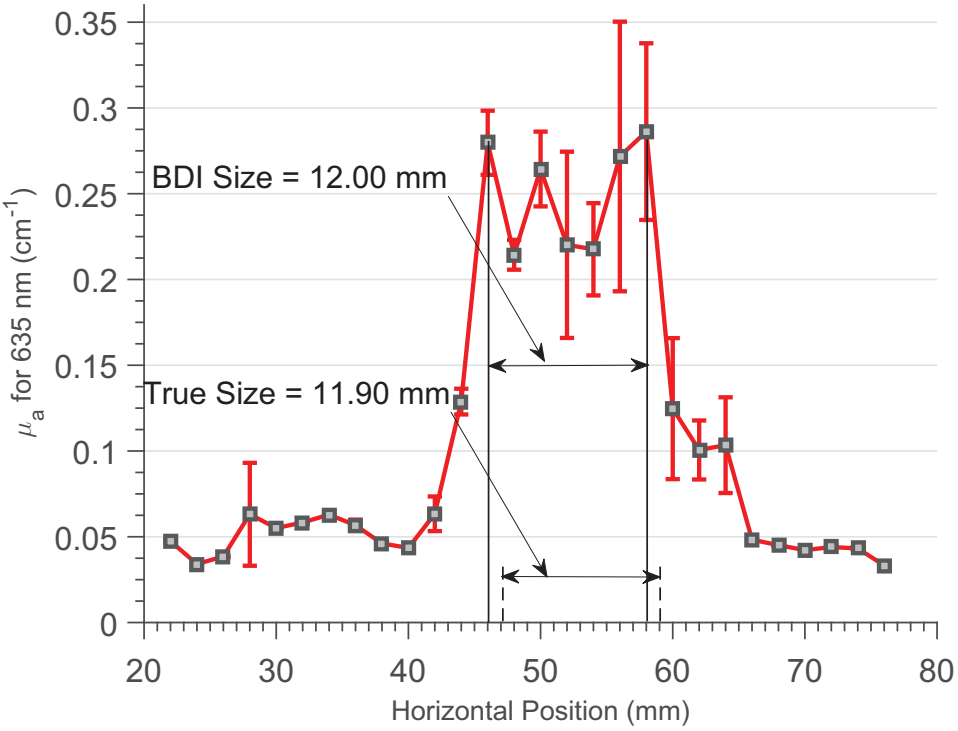

Figure 4.8: Absorption coefficient versus horizontal position graph for 635 nm from parallel scanning experiment.

4.3. The desired spectral properties are the absorption coefficients of tumor (inclusion) and tissue (background) phantoms. Also, we showed how chromophore concentrations can be determined from the absorption coefficient values. These results can be found in Table 4.4.

4.5.2.1 Size Estimation

For the BDI size estimation, we obtained μ_a versus x graph as shown in Fig. 4.8 for 635 nm and Fig. 5.2 for 808 nm. For each laser position, the mean value of μ_a with one standard deviation was shown as errorbar. The embedded inclusion location was estimated by observing the graph, where a sharp rise and a fall occurred. We estimated the inclusion (tumor) location between x= 46 mm to 58 mm. For both wavelengths, the size was found to be 12 mm.

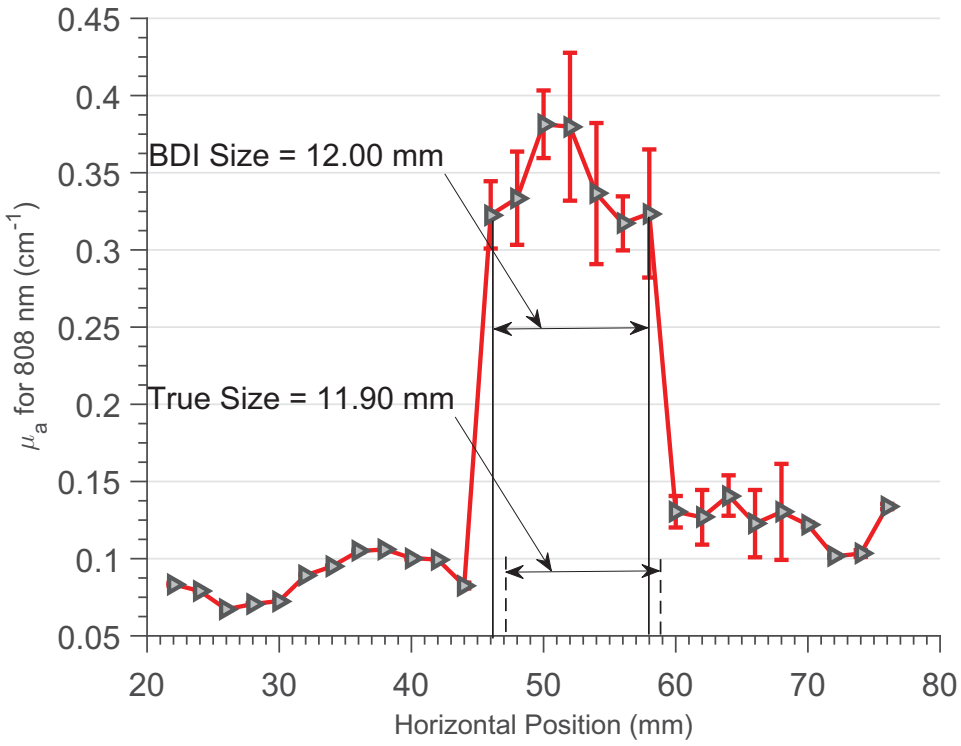

Figure 4.9: Absorption coefficient versus horizontal position graph for 808 nm from parallel scanning experiment.

4.5.2.2 Depth Estimation

The depth of the inclusion from TIS side surface b was determined as 2.47 mm from the tactile images. Then we estimated the depth of embedded object from the laser side surface h as 3.49 mm.

For the BDI depth estimation, we plotted the sum of pixel intensity against the scanning angle as shown in Fig. 4.10. We observed that for this phantom, the pixel intensity increased at a higher rate after the pixel intensity became approximately two times higher than the initial position (0°). We found two such points on the intensity graph and their horizontal axis difference was $2\theta = 8°$. Therefore, we considered θ as 4°, and calculated the depth h as 4.80 mm using (4.1).

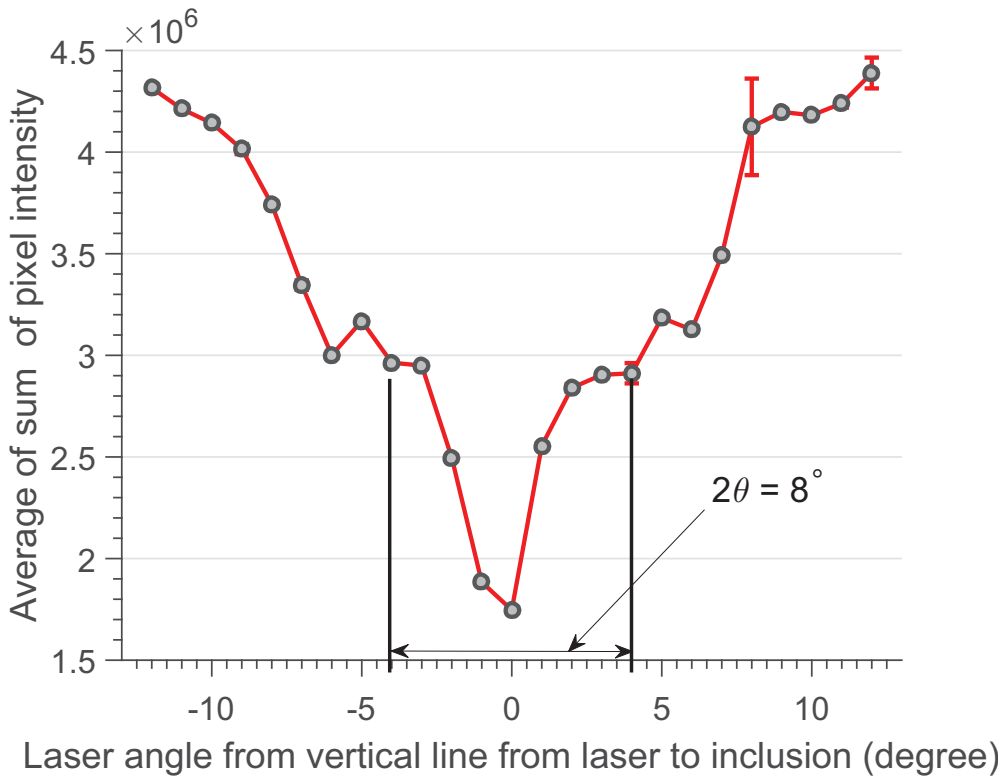

Figure 4.10: Average of sum of pixel values versus angle graph from ten angular scanning experiments.

Table 4.3: Mechanical properties estimation results from multiple measurement experiment

Mechanical Properties	True value	TIS est.	Error (%)	BDI est.	Error (%)
Size, l_d (mm)	11.90	11.04	7.23	12.00	0.80
Depth, h (mm)	6.00	3.49	41.83	4.76	20.00

4.5.2.3 Spectral Properties Estimation

After locating the tumor (embedded inclusion) region, we calculated the average absorption coefficients of tissue and tumor region for 635 nm and 808 nm. The tissue absorption coefficients were 0.0611 cm^{-1} and 0.1030 cm^{-1} for 635 nm and 808 nm. The tumor absorption

coefficients were 0.2506 cm^{-1} and 0.3421 cm^{-1} for 635 nm and 808 nm.

Then, we estimated the chromophore concentrations of oxygenated and deoxygenated hemoglobins using (4.5), and finally the total hemoglobin concentration and blood oxygen saturation. The spectral properties estimation results are listed in Table 4.4. Fig. 4.11 shows quantitative bar graphs of three physiological properties, oxygenated hemoglobin concentration [HbO_2], total hemoglobin concentration, THC, and blood oxygen saturation, StO_2. We observe an elevated level of [HbO_2] and StO_2 in case of tumor region compared to tissue region of the phantom. The total hemoglobin concentration for tumor was roughly three-fold greater than tissue. The blood oxygen saturation of tumor is slightly lower (3%) compared to tissue.

Table 4.4: Spectral properties estimation results from multiple measurement experiment

	Tissue			Tumor		
Spectral Properties	True value	Estimated value	Error (%)	True value	Estimated value	Error (%)
μ_a(cm^{-1})@635 nm	0.082	0.061 $\pm$0.028	25.50	0.30	0.251$\pm$0.032	16.47
μ_a(cm^{-1})@808 nm	0.082	0.103$\pm$0.002	25.55	0.30	0.342$\pm$0.027	14.03
[HbO_2] (μM)	-	120.031	-	-	389.181	-
[Hb] (μM)	-	0.351	-	-	12.386	-
THC (μM)	-	120.381	-	-	401.566	-
StO_2 (%)	-	99.709	-	-	96.916	-

4.6 Discussion

In this chapter, a bimodal dynamic imaging system was constructed. In order verify the performance of the system, we measured the size, depth, and elastic modulus of an embedded

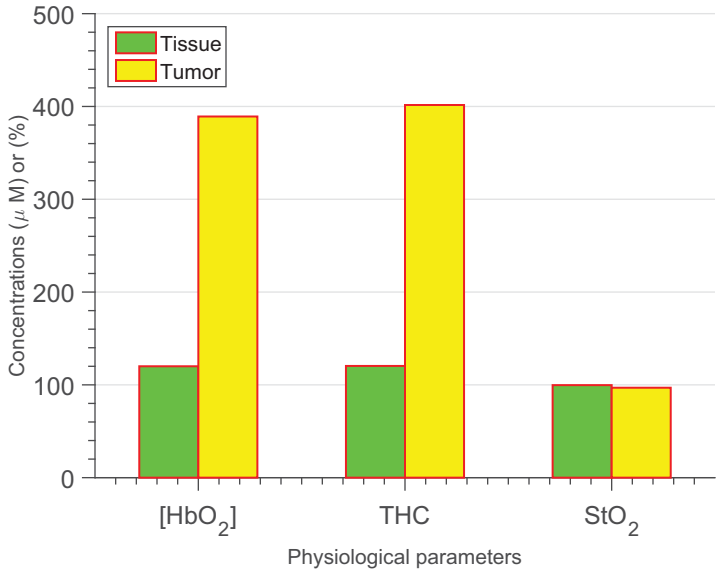

Figure 4.11: Physiological parameters for tissue and tumor.

inclusion inside a bimodal phantom. These measurements were compared to the TIS measurements. Also, we estimated absorption coefficients and chromophore concentrations of the tissue and tumor region of the bimodal phantom.

The experiments showed that BDI provides a better size estimation than TIS. The TIS size estimation error was 7.23% whereas the BDI method showed 0.80% error. The BDI size estimation was performed using 635 nm and 808 nm laser. In both cases, we found the estimation was same. The improved result of BDI was obtained at the cost of hardware and computation resources. For the depth estimation, the BDI method produced less error (20.00%) compared to the TIS only method (41.83%). In case of elastic modulus measurement, BDI showed 74.79% error, and TIS showed 96.80% error. The elastic modulus of soft tissue and cancerous tumor ranges from 10 kPa to 1 MPa [54]. Because of this large range, even with 100% elastic modulus measurement error, BDI can satisfy a resolution requirement of 1% of the entire variation range. Similar argument was given by Egorov and Sarvazyan in case of a large variation of elastic modulus measurement by their breast mechanical imager [61]. Strictly speaking, both TIS and BDI methods do not consider the effect of the soft indenter. TIS has a soft probe (indenter), so there is a mutual displacement of indenter and object during compression. We assume that this error is included in the total measurement error. The elastic modulus determined by the soft indenter of the

bimodal imaging system may correlate to the elastic modulus obtained by compression experiment using the instron instrument. Therefore, this data could still be useful. The further investigation can be conducted in future. Also, in our solid phantom the harder object (355 kPa) was embedded inside a softer background (45 kPa). Therefore, the probed area is not homogeneous and isotropic. The probed area consisting of two different elastic moduli lowered the effective elastic modulus of the region than that of the object. We only considered the inclusion elastic modulus for comparison. In the BDI method, the strain calculation is dependent on the positioning of the source and sensor. In our experimental setup, the minimum distance travelled by the laser and the camera is 1 mm. This pose a limitation for the strain calculation.

The accuracy of BDI method relies on the spectral property measurement of the inclusion and tissue background. We estimated the average absorption coefficients of tissue region with 25% error, and tumor region with 14-16% error. Using a similar spectral properties estimation method, Minagawa *et al.* reported the reduced scattering coefficient μ_s' with deviations of 23%-34% compared to a commercial time-resolved spectroscopy instrument measurement [92]. The embedded inclusion was surrounded by tissue background, therefore, the variations of absorption coefficient values in tumor region were observed in the BDI measurement.

The goal of determining chromophore concentrations is to verify whether BDI can differentiate between normal tissue and tumor. BDI measurement revealed an increase in THC for tumor compared to normal tissue. The increase in THC is associated with increased angiogenesis, a correlate of malignant development [68]. The similar trend was reported when the measurement was performed by photon migration spectroscopy [98], MR-guided diffuse optical spectroscopy [99], diffuse optical tomography [88], and ultrasound guided diffuse optical tomography [100]. The blood oxygen saturation StO_2 did not show a significant difference between normal tissue and tumor. Generally, StO_2 is expected to be lower because of high oxygen demand in cancerous tumor [101]. Choe also did not find StO_2 as a significant discriminator, though Tromberg reported a lower StO_2 in tumor compared to normal tissue [98].

In this chapter, we presented a bimodal dynamic imaging system prototype with meth-

ods to determine size, depth, and elastic modulus of an embedded inclusion. We found that the dynamic positioning method performs better than the TIS method. In order to improve the system performance further, an automatic control system is required for maneuvering the source and the detector. Under this circumstance, we require to find a control scheme which will ensure optimum performance for synchronous movement of the source and the detector. In the next chapter, we derived a game theoretic control strategy considering two players (the source and the detector) with asymmetric role (one player is leader, and the other is follower).

CHAPTER 5

OPEN-LOOP STACKELBERG STATISTICAL GAME CONTROL

In this chapter, we derive the Stackelberg solution of a two-player, nonzero-sum game, where the leader and the follower optimizes the system performance by shaping the n-th cumulant of their cost functions, while the follower minimizes the mean of a different cost function. We introduce the Stackelberg statistical game theory for the automatic control of the source and detector of the bimodal imaging system. The Stackelberg statistical game allows sequential and hierarchical moves for the players, while optimizing the n-th cumulant of each player's cost function.

5.1 Application of Game Theory for Biomodal Dynamic Imaging

In this section, we introduce the game theory, different types of games and their definitions, and discuss the application of Stackelberg equilibrium for bimodal dynamic imaging.

5.1.1 Introduction to Game Theory

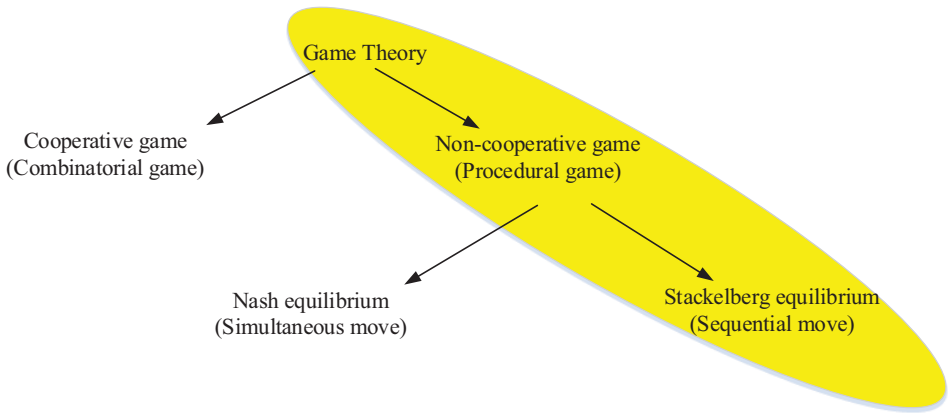

Figure 5.1: Game theory classification.

Fig. 5.1 shows a classification of game theory in context of our application. Game theory studies the mathematical model of conflict and cooperation among rational decision makers. It can be classified into two major branches: non-cooperative game theory and cooperative game theory. The non-cooperative game describes all the moves available to the decision makers. By contrast, the cooperative game theory describes the possible outcomes that results if the decision makers join together in different combinations. According to this notion, the non-cooperative game can be called as procedural game, while the cooperative game can be called as combinatorial game. The procedural game can have two types of equilibriums: Nash equilibrium and Stackelberg equilibrium. In Nash equilibrium, the decision makers act independently in a simultaneous manner, while in Stackelberg equilibrium, the decision makers interacts within a hierarchical structure in a sequential manner. Before justifying the use of Stackelberg equilibrium for our application, we will go through some preliminary materials of the game theory.

A game can be defined as a description of strategic interactions among multiple decision makers based on their interests and the constraints on their actions. The systematic description of different outcomes, which may emerge in a family of games, is called a *solution*. Game theory deals with the reasonable solutions of games and their properties [32].

In order to describe a game, we need to specify the following terms:

- *Players* (who are the decision makers?) may be interpreted as individuals or a group of individuals who make a decision [32].
- *Strategies* or decision rules (how do players move?) are the options that a player can choose. What actually will be done depends on the quantities not known yet, and not controlled by player or decision maker. When a player has fixed strategy, he cannot influence the course of events further. Any consequence of such a strategy, after the unknown quantities are realized, is called *actions* (also called controls) of that particular player.
- A *payoff function* (what motivates players?) is a numerical quantity which the players strive to minimize or maximize [32].

Equilibrium comprises the set of strategies such that every player will choose a payoff-maximization strategy. In equilibrium state, no player can benefit from changing his or her

strategy, while the other players keep their strategies unchanged.

A two-player game is called *zero-sum game* if the sum of the players' payoff functions is zero. If the sum is a nonzero constant, it is sometimes called *constant sum*. This type of game falls under zero-sum game category, because the sum can be made zero by appropriate scaling and translation. On the other hand, for a *nonzero-sum game*, the payoff functions cannot be made zero by any scaling and translation.

In a *finite game*, the players get to pick their actions out of a finite action set. The finite game is also known as a *matrix game*. If the action set is not finite, then the game is called *infinite game*. A *continuous-kernel game* is a type of infinite game, where the action sets and objective functions are continuous with respect to their action sets.

In a *deterministic game*, the players' actions determine uniquely the outcome, whereas in a *stochastic game*, at least one player's payoff function includes an additional variable with a known probability distribution.

In a *complete information game*, the description of the game (the players, the payoff functions, and the underlying probability distribution function (if stochastic)) is common information to all players; otherwise the game is called an *incomplete information game*.

A game is a *static game* if players have access to only the a priori information shared by all, and none of the players has access to information on the actions of any of the other players; otherwise we have *dynamic game*.

In this dissertation, we deal with *differential game*, a type of dynamic game, where the states of the players evolve with time variation, and the game is typically described by differential equations.

5.1.2 Non-cooperative and Cooperative Games

Dynamic games can be divided into two categories: non-cooperative games and cooperative games. These two categories of games differ in how they formalize the interdependence among the players.

In non-cooperative games, the players act independently; they do not communicate formally in an effort to coordinate their actions, even though they are aware of each other's existence.

On the other hand, in cooperative games (also known as coalitional games) the players form coalitions by making agreements about the distribution of payoffs or the choice of strategies, even if these agreements are not specified or implied by the rules of the game [102]. In other words, cooperative game theory considers two questions:

- Which player will cooperate with whom, that is, which coalition will tend to form?
- After formation of coalition, what will be the resulting distribution of wealth to each player?

A cooperative game is populated by a non-empty set $N = \{1, 2, \cdots, n\}$ of players. A coalition is a subset of the players N. The coalitions can be denoted by C^1. The grand coalition is the set of N of all players. In a coalition, the players are committed to some common actions. Each coalition is assigned a value of coalition, which can be divided among the members in any way that the members of coalition choose.

The primary difference between cooperative games and non-cooperative games is that cooperative games have a binding contract (agreement) among the players, to which every player must adhere. There is no options for binding agreement in non-cooperative game.

The terms 'non-cooperative' and 'cooperative' are not correlated with the degree of cooperation among the players. Non-cooperative game can model cooperation, while cooperative game can model competition. The non-cooperative game theory models all the moves available to the players. By contrast, the cooperative game theory abstracts away this level of details, and discusses the outcomes that result when the players come together in different combinations. From this point of view, a non-cooperative game can be termed as 'procedural game', and a cooperative game as 'combinatorial game' [103]. These terms indicate the distinction between non-cooperative and cooperative game theory.

5.1.3 Nash and Stackelberg Equilibrium

In game theory, the Nash equilibrium describes the solution concept of a non-cooperative game. Each player is assumed to know the equilibrium strategies of the other players, and no player can benefit from changing his strategy as long as the other players keep their strategies unchanged [35]. Such games are called Nash games. In Nash games, a single

player cannot dominate the decision making process.

On the other hand, the Stackelberg equilibrum has the following characteristics [37]

- The players interact with each other within a hierarchical structure. Because of the hierarchical structure, one player (designated as 'leader') has the ability to enforce his strategy on the other player (designated as 'follower'). There can be multiple levels of hierarchy with many leaders and followers. However, for the purpose of clarity, the discussion is limited to two players.
- The leader begins the game by announcing his strategy. The follower then executes his policy so as to optimize the follower's cost function. The leader assumes the follower's optimal response, and chooses a strategy which optimize his cost function. Unlike Nash games, the players make their moves sequentially.
- The decision of a player can impact the other player's cost function.

5.1.4 Justification of using Stackelberg Strategy for Our Application

For bimodal dynamic imaging, the robot manipulators for the source (laser) and detector (camera) requires to follow a specified trajectory. The camera and the laser will be in the line of sight with each other. The camera will track the diffused light from the laser on a stationary target and avoid any type of collision. Under these circumstances, the game theory can provide convenient mathematical tools for an efficient trajectory planning and target tracking for the bimodal dynamic imaging system.

In order to model all the movements of the robot manipulators, the procedural game model is selected. To maintain the sequential moves between the robot manipulators within a hierarchical structure, the Stackelberg equilibrium is chosen over the Nash equilibrium. In the Stackelberg equilibrium, the players make their moves in a sequential manner. The hierarchical structure of players' interaction lead one player to assume the role of a leader and the other as a follower. The leader gets to announce his policy first and makes the first move. The follower must act rationally and optimize his own cost function. Assuming that the follower wiil respond optimally, the leader optimizes his cost function, and attains the Stackelberg equilibrium solution. The hierarchical and sequential nature of players' interaction make the Stackelberg equilibrium a good candidate for the bimodal dynamic imaging

application. Additionally, the Stackelberg equilibrium ensures a reduced cost value for the leader compared to the Nash equilibrium.

For the bimodal imaging system, we intend to use a dual arm collaborative robot called Baxter. Human safety is the primary concern for this type of robot. A type of compliant actuator is used in Baxter as opposed to non-compliant or stiff actuator. A stiff actuator is a device, capable of moving to a specific position or tracking a pre-specified trajectory [104]. After reaching the specific position, it remains at that position despite the external forces exerted on the actuator (within the force limits of the device). A compliant device, on the other hand, permits deviation from its own equilibrium position, depending on the applied external force. The stiff actuator is popular in industrial robotics since it improves the precision, stability, and bandwidth of position-control. On the other hand, reducing the stiffness of interface provides less inadvertent damage to the environment, more accurate and stable force control, lower reflected inertia, greater shock tolerance, and the capacity for energy storage [105, 106]. Each link of Baxter is moved by a type of passive compliant actuator called “series elastic actuator" [107–109]. The series elastic actuator includes a spring between the motor/gearing elements and the output of the actuator [104]. The series elastic actuator offers inherent safety, because the springs in these actuators are deformable by human level input. This construction comes with the cost of the position accuracy of the robot manipulator.

With a more accurate positioning of the source and the detector while capturing diffused light information, the bimodal dynamic imaging system provides a better estimate of the absorption and reduced scattering coefficients of tumor. We can see from a previous experiment that the absorption coefficient values varied for each position (see Fig. 5.2). In order to reduce the variations, we require to point the source and the detector at the target with as little variation as possible. In our earlier work on controlling the two-axis gimbaled laser targeting system, we found that the statistical controller offered a better performance in minimizing the pointing variation [110]. Hence, we introduce the statistical control concept within the Stackelberg game theoretic control framework. Our Stackelberg statistical control scheme will allow the leader to minimize the variance of its cost function, which reduces the pointing variation.

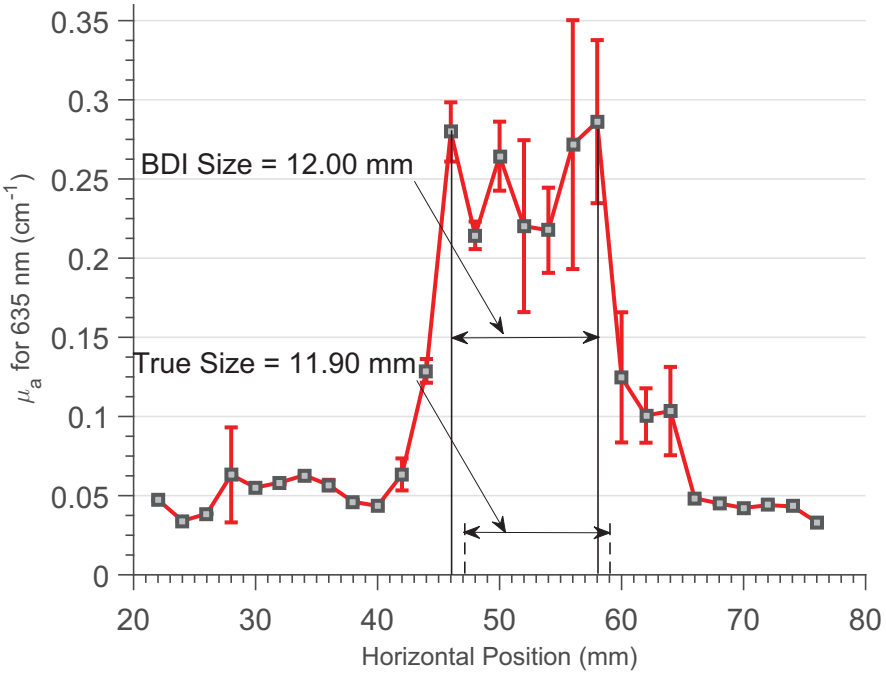

Figure 5.2: Absorption coefficient versus horizontal position graph for 635 nm from parallel scanning experiment (repeated from Chapter 4).

5.2 Mathematical Preliminaries for Differential Games and Stackelberg Equilibriums

5.2.1 Definitions of Differential Games

In this subsection, we describe the definitions related to differential games. Differential games discuss a class of decision problems, wherein the evolution of the state is described by a differential equation, and the players act throughout a time interval. The formulation of such games are given as follows [36]:

Definition 5.1. *A quantitative* **N***-person differential game of pre-specified fixed duration considers the following (See Def. 5 in Chapter 5 in [36]):*

1. *An index set* $\mathbf{N} = \{1, 2, \cdots, N\}$ *called the player's set,*
2. *A time interval* $[0, T]$ *which is specified a priori and which denotes the duration of the evolution of the game,*
3. *An infinite set* S_0 *with some topological structure, called the trajectory space of the game. The elements of* S_0 *are denoted as* $\{x(t), 0 \leq t \leq T\}$ *and constitute the*

permissible state trajectories of the game. Furthermore, for each fixed $t \in [0,T]$, $x(t) \in S_0$, *where* S_0 *is a subset of a finite-dimensional vector space.*

4. *An infinite set* U_k *with some topological structure defined for each* $i \in \mathbb{N}$. U_k *is called the control (action) space of player* **Pk**, *whose elements* $u_k(t), 0 \leq t \leq T$ *are the control functions or the controls of* **Pk**. *Furthermore, there exists a set* $S_k \subseteq \mathbf{R^{m_k}}$ *so that, for each fixed* $t \in [0,T]$, $u_k(t) \in S_k$.
5. *A differential equation is given as*

$$\dot{x}(t) = f(t,x(t),u_1(t),u_2(t),\cdots,u_N(t)), x(0) = x_0. \tag{5.1}$$

The solution of the above differential equation describes the state trajectory of the game corresponding to the N-tuple of control functions $u_k(t), 0 \leq t \leq T$ *and the given initial state* x_0.

6. *A set valued function* $\eta_k(\cdot)$ *defined for each* $k \in \mathbf{N}$ *as*

$$\eta_k(t) = \left\{x(s), 0 \leq s \leq \varepsilon_t^k\right\}, \quad 0 \leq \varepsilon_t^i \leq t, \tag{5.2}$$

where ε_t^k *is nondecreasing in* t. $\eta_k(t)$ *determines the state information gained and recalled by* **Pk** *at time* $t \in [0,T]$. *Specification of* $\eta_k(\cdot)$ *characterizes the information pattern (structure) of* **Pk**. *The collection of these information patterns over* $k \in \mathbf{N}$ *is the information patterns or information structures of the game.*

7. *A sigma-field* N_t^i *in* S_0, *generated for each* $k \in \mathbf{N}$ *by the cylinder sets* $x \in S_0, x(s) \in B$, *where* B *is a Borel set in* S_0 *and* $0 \leq s \leq \varepsilon_t$. $N_t^i, t \geq t_0$, *is called the information field of* **Pk**.
8. *A prespecified class* Γ_k *of mappings* $\gamma_i : [0T] \times S_0 \to S_k$, *with the property that* $u_k(t) = \gamma_k(t,x)$ *is* N_t^i*-measurable (i.e. it is adapted to the information field* N_t^i*).* Γ_k *is the strategy space of* **Pk**. *Each of its elements* γ_k *is a permissible strategy for* **Pk**.
9. *Two functionals* $q_k : S_0 \to \mathbf{R}; g_i : [0,T] \times S_0 \times S_1 \times \cdots \times S_N \to \mathbf{R}$ *defined for each* $i \in N$, *so that the composite functional*

$$L_k(u_1,u_2,\cdots,u_N) = \int_0^T g_i(t,x(t),u_1(t),u_2(t),\cdots,u_N(t))dt + q_k(x(T)), \tag{5.3}$$

is well defined for every $u_j(t) = \gamma_j(t,x), \gamma_j \in \Gamma_j (j \in \mathbf{N})$. *For each* $k \in \mathbf{N}$, L_k *is the cost functional of* **Pk** *in the differential game of fixed duration.*

For a well-defined differential game problem, we impose additional restrictions on f and Γ, so that the differential equation (5.1) admits a unique solution. We discuss these restriction in Section 5.4.

Now, there are several information structures within the context of deterministic differential games.

Definition 5.2. *In N-person continuous-time deterministic dynamic game of prespecified fixed duration* $[0,T]$, **Pk***'s information structure is called (See Def. 6 in Chapter 5 in [36])*

1. *open-loop (OL) pattern if* $\eta_k(t) = x_0$, $t \in [0,T]$,
2. *closed-loop perfect state (CLPS) pattern if* $\eta_k(t) = x(s), 0 \leq s \leq t$, $t \in [0,T]$,
3. ε*-delayed closed-loop perfect state (*ε*DCLPS) pattern*
   if $\eta_k(t) = \begin{cases} \eta_k(t) = \{x_0\}, 0 \leq t \leq \varepsilon, \\ \{x(s), 0 \leq s \leq t-\varepsilon\}, \varepsilon < t \end{cases}$ *, where* $\varepsilon > 0$ *is fixed.*
4. *memoryless perfect state (MPS) pattern if* $\eta_k(t) = \{x_0, x(t)\}$, $t \in [0,T]$,
5. *feedback (perfect state) (FB) pattern if* $\eta_k(t) = \{x(t)\}$, $t \in [0,T]$.

5.2.2 Definitions of Static Stackelberg Solution Concept

In this subsection, we describe the definitions related to Stackelberg solution concept within the context of a two-player finite game [36]. Let Γ_1 and Γ_2 be the pure strategy space of the players: the leader **P1** and the follower **P2**. Let $J_k(\gamma_1, \gamma_2)$ denote the cost incurred to **Pk** corresponding to a strategy pair $\{\gamma_1 \in \Gamma_1, \gamma_2 \in \Gamma_2\}$. Then we have the following definitions [36].

Definition 5.3. *In a two-player finite game, let* $D_2(\gamma_1) \subset \Gamma_2$ *be the rational reaction of* **P2** *to the strategy* $\gamma_1 \in \Gamma_1$. *The rational reaction set is then defined for each* $\gamma_1 \in \Gamma_1$ *by*

$$D_2(\gamma_1) = \{\xi \in \Gamma_2 : J_2(\gamma_1, \xi) \leq J_2(\gamma_1, \gamma_2), \quad \forall \gamma_2 \in \Gamma_2\}. \tag{5.4}$$

Definition 5.4. *In a two-player finite game where* **P1** *is the leader, a strategy* $\gamma_1 \in \Gamma_1$ *is called a Stackelberg equilibrium strategy for the leader, if*

$$\max_{\gamma_2 \in D_2(\gamma_1^*)} J_1(\gamma_1^*, \gamma_2) = \min_{\gamma_1 \in \Gamma_1} \max_{\gamma_2 \in D_2(\gamma_1)} J_1(\gamma_1, \gamma_2) \triangleq J_1^*, \tag{5.5}$$

where J_1^* *is the Stackelberg cost of the leader.*

Theorem 5.1. *Every two-player finite game admits a Stackelberg strategy for the leader.*

Proof: The proof is given in [36].

Remark 5.1. *The Stackelberg strategy for the leader does not necessarily have to be unique. Since the Stackelberg cost of the leader is unique, nonuniqueness of the equilibrium strategy does not create a problem in this scenario.*

Remark 5.2. *If* $D_2(\gamma_1)$ *is a singleton (a set with exactly one element) for each* $\gamma_1 \in \Gamma_1$*, there exists a mapping* $\mathfrak{T}_2 : \Gamma_1 \to \Gamma_2$ *such that* $\gamma_2 \in D_2(\gamma_1)$ *implies* $\gamma_2 = \mathfrak{T}_2\gamma_1$*. Thus the optimal response of the follower* $\mathfrak{T}_2$ *is unique for every strategy of the leader. It leads to the following simplified version of* (5.5) *in Definition 5.4:*

$$J_1(\gamma_1^*, \mathfrak{T}_2\gamma_1^*) = \min_{\gamma_1 \in \Gamma_1} J_1(\gamma_1, \mathfrak{T}_2\gamma_1) \triangleq J_1^*, \tag{5.6}$$

From the follower's point of view, the equilibrium strategy in a Stackelberg game is any optimal response to the announced Stackelberg strategy of the leader. This can be defined as:

Definition 5.5. *If* $\gamma_1^* \in \Gamma_1$ *is a Stackelberg strategy for the leader* **P1***, then any element* $\gamma_2^* \in R_2(\gamma_1^*)$ *is an optimal strategy for the follower* **P2***, that is in equilibrium with* γ_1^**. The strategy pair* $\{\gamma_1^*, \gamma_2^*\}$ *is a Stackelberg solution for the game with* **P1** *as the leader. The cost pair* $\{J_1(\gamma_1^*, \gamma_2^*), J_2(\gamma_1^*, \gamma_2^*)\}$ *is the corresponding Stackelberg equilibrium outcome.*

5.2.3 Stackelberg Stochastic Differential Game

In a two-player Stackelberg stochastic differential Game, the state evolves according to

$$\dot{x}(t) = [f(t, x(t), u_1(t), u_2(t))]dt + \sigma(t, x)dw(t), \quad x(t_0) = x_0,$$

where x is state vector, $u_1(.), u_2(.)$ are the control vectors for the leader and the follower, and x_0 is a deterministic initial condition. Here, $dw(t)$ is a Gaussian random process of dimension d with zero mean, covariance of $W(t)dt$. The random process is defined on a probability space $(\Omega_0, \mathscr{F}, \mathscr{P})$ where Ω_0 is a non-empty set, $\mathscr{F}$ is a σ-algebra of Ω_0, and $\mathscr{P}$ is a probability measure on $(\Omega_0, \mathscr{F})$. Let, $\{\mathscr{F}_t\}_{0\leq t\leq T}$ is the natural filtration generated by $w(t)$. The player 1 is the leader and the player 2 is the follower.

The cost functions are

$$L_k(u_1,u_2) = q_i(x(T)) + \int_0^T g_i(t,x(t),u_1(t),u_2(t))dt, \quad k = 1,2,$$

where $[0,T]$ is the duration of the game.

Earlier we describe the continuous-time deterministic differential game on fixed duration $[0,T]$ and its different information structure η according to the Defs. 5 and 6 in Chapter 5 in [36]. In stochastic case, the state equation is driven by a Brownian motion. Therefore, the players' decisions are affected by the filtration $\{\mathscr{F}_t\}_{0\leq t\leq T}$. Thus, the notions of the information structures are extended to stochastic settings:

- open-loop pattern if $\eta_k(t) = \{x_0, \mathscr{F}_t\}, t \in [0,T]$,
- closed-loop perfect state pattern if $\eta_k(t) = \{x(s), \mathscr{F}_t\}, 0 \leq s \leq t, t \in [0,T]$,
- memoryless perfect state pattern if $\eta_k(t) = \{x_0, x(t), \mathscr{F}_t\}, t \in [0,T]$,
- feedback pattern if $\eta_k(t) = \{x(t), \mathscr{F}_t\}, t \in [0,T]$.

5.3 Paper Summary: "Stackelberg Strategies in Linear-Quadratic Stochastic Differential Games" (Open Loop Case)

The theory developed in this chapter is an extension of the work described in [46]. The paper derives the Stackelberg solution to a two-player stochastic differential games described by a linear state dynamics and two quadratic objective functions. The information structure of the problem is such that the players make the measurement of the initial states, that is, the information structure is of open-loop. The players are allowed to construct their controls using the open-loop information structure.

Following are the steps considered for determining Stackelberg strategies in linear-quadratic stochastic differential games.

- Step 1: Describe a two-player linear stochastic differential game.
- Step 2: Describe the quadratic objective functions of two players.
- Step 3: Assign the leadership and the followership to the players and introduce the minimization problem. under Stackelberg framework.
- Step 4: Convert the game problem into an equivalent Stackelberg static game problem in Hilbert space using inner products and Volterra operators.
- Step 5: For a fixed leader strategy, solve the minimization problem for the follower.
- Step 6: Considering the follower solution, express the modified objective function for the leader. The leader faces a nonstandard stochastic optimization problem.
- Step 7: Solve the nonstandard stochastic optimization problem faced by the leader. This solution provides the Stackelberg strategy for the leader.

We put effort to use the similar symbols and notations used in the paper [46]. We use the player indices as subscript instead of superscript as in the paper [46].

5.3.0.1 Step 1: Linear State Dynamics

The two-player continuous-time nonzero-sum game is described by a Itô sense stochastic differential equation:

$$dx_t = [A(t)x_t + B_{1t}u_{1t} + B_{2t}u_{2t}]dt + F(t)dW_t, \quad t \geq t_0, x_{t_0} = x_0,$$

where x_0 is random vector with known statistics, such that $E\{|x_0|\} < \infty$ and $\{W_t, t \geq t_0\}$ is an n-dimensional standard Brownian motion. $A(\cdot)$, $B_1(\cdot)$, $B_2(\cdot)$, and $F(\cdot)$ are appropriate dimensional matrices with continuous entries on $[t_0, t_f]$. $\{u_{1t}, t \geq t_0\}$ and $\{u_{2t}, t \geq t_0\}$ are r_1-dimensional and r_2-dimensional stochastic processes denoting the controls of the player 1 and the player 2.

The players make independent noisy measurements of the initial state x_0, denoted by y_i, $i = 1, 2$. The conditional joint distribution of (y_1, y_2), given x_0 is *a priori* known. The information available to each player is static in nature.

Let H_i, $i = 1, 2$, denote the class of second-order stochastic processes defined on $[t_0, t_f]$, which are y_i-measurable. The strategy γ_i is a real Borel-measurable mapping. Let Γ be the space of all Borel-measurable functions. Therefore, each permissible γ_i requires to be in

Γ_i. So, $\gamma_i(\cdot, y_i)$ is in H_i.

5.3.0.2 Step 2: Quadratic Objective Functions

The quadratic objective functions are defined as follows:

$$J_1(\gamma_1,\gamma_2) = E\left\{x'_{t_f}Q_{1f}x_{t_f} + \int_{t_0}^{t_f}\left[x'_tQ_1(t)x_t + u'_{1t}u_{1t} + u'_{2t}R(t)u_{2t}\right]dt \mid u_{it} = \gamma_i(t,y_i), i = 1,2\right\},$$

$$J_2(\gamma_1,\gamma_2) = E\left\{x'_{t_f}Q_{2f}x_{t_f} + \int_{t_0}^{t_f}\left[x'_tQ_2(t)x_t + u'_{2t}u_{2t}+\right]dt \mid u_{it} = \gamma_i(t,y_i), i = 1,2\right\},$$

where

$$Q_{if} \geq 0, \quad Q_i(\cdot) \geq 0, \quad R(\cdot) \geq 0.$$

5.3.0.3 Step 3: Introduction of Stackelberg Solution Concept

This paper considers player 1 as the leader and player 2 is considered as the follower. For each $\bar{\gamma}_1 \in \Gamma_1$, there exists a unique $\bar{\gamma}_2 \in \Gamma_2$ that minimizes $J_2(\bar{\gamma}_1,\gamma_2)$ over Γ_2. This implies the existence of a unique map $T : \Gamma_1 \to \Gamma_2$ such that

$$J_2(\gamma_1, T\gamma_1) \leq J_2(\gamma_1,\gamma_2),$$

for all $\gamma_2 \in \Gamma_2$ and for every $\gamma_1 \in \Gamma_1$. Now, consider the minimization of the function $J_1(\gamma_1, T\gamma_1)$ over Γ_1. If $\gamma_{1o} \in \Gamma_1$ denote one minimizing solution; that is,

$$J_1(\gamma_{1o}, T\gamma_{1o}) \leq J_1(\gamma_1, T\gamma_1), \qquad \forall\gamma_1 \in \Gamma_1,$$

then, the pair $(\gamma_{1o}, \gamma_{2o} = T\gamma_{1o})$ provides a Stackelberg solution for the game problem under consideration.

5.3.0.4 Step 4: Conversion of Game Problem in Hilbert Space

This approach is identical as in [45]. The objective functions are re-expressed as follows:

$$\begin{aligned}
J_1(\gamma_1,\gamma_2) &= \langle \mathscr{Q}_1(\mathscr{L}_1\gamma_1(\cdot,y_1) + \mathscr{L}_2\gamma_2(\cdot,y_2) + r), (\mathscr{L}_1\gamma_1(\cdot,y_1) + \mathscr{L}_2\gamma_2(\cdot,y_2) + r)\rangle_f \\
&+ \langle\gamma_1(\cdot,y_1),\gamma_1(\cdot,y_1)\rangle_1 + \langle\gamma_2(\cdot,y_2), R\gamma_2(\cdot,y_2)\rangle_2, \\
J_2(\gamma_1,\gamma_2) &= \langle \mathscr{Q}_2(\mathscr{L}_1\gamma_1(\cdot,y_1) + \mathscr{L}_2\gamma_2(\cdot,y_2) + r), (\mathscr{L}_1\gamma_1(\cdot,y_1) + \mathscr{L}_2\gamma_2(\cdot,y_2) + r)\rangle_f \\
&+ \langle\gamma_2(\cdot,y_2),\gamma_2(\cdot,y_2)\rangle_2.
\end{aligned}$$

Following definitions are used to re-express the objective functions.

$$\langle u, v\rangle_i = E\left\{\int_{t_0}^{t_f} u_t'(\omega)v_t(\omega)dt\right\},$$

where $\{u \in H_1\}$, $\omega \in \Omega$, with $(\omega, \mathscr{B}, \mathscr{P})$ denoting underlying probability space. With these inner products, $H_i, \quad i = 1,2$ become Hilbert spaces.

$$\langle x, z\rangle_f = E\left\{x_{t_f}'(\omega)z_{t_f}(\omega) + \int_{t_0}^{t_f} x_t'(\omega)z_t(\omega)dt\right\},$$

$$(\mathscr{Q}_i x)_t = \begin{cases} Q_i(t)x_t(\omega), & t_0 \le t < t_f, \\ Q_{if}x_{t_f}(\omega), & t = t_f. \end{cases}$$

$$(\mathscr{L}_i u)_t(\omega) = \int_{t_0}^{t} \Phi(t,s)B_i(s)u_{is}(\omega)ds,$$

$$x(t) = \Phi(t,t_0)x_0 + \int_{t_0}^{t} \Phi(t,s)B_i(\tau)u_i(\omega)d\tau + \int_{t_0}^{t} \Phi(t,s)F(s)dW(\omega),$$

$$x(t) = r(t,\omega) + \int_{t_0}^{t} \Phi(t,s)B_i(\tau)u_i(\omega)d\tau.$$

5.3.0.5 Step 5: The Follower Solution For A Fixed Leader Strategy

For fixed $\gamma_1 \in \Gamma_1$, the minimization of $J_2(\gamma_1, \gamma_2)$ is equivalent to the control of minimizing the problem of minimizing

$$J_2(u_2) = \langle \mathscr{Q}_2(\mathscr{L}_1\gamma_1(\cdot,y_1) + \mathscr{L}_2u_2(\cdot,y_2) + r), (\mathscr{L}_1\gamma_1(\cdot,y_1) + \mathscr{L}_2u_2(\cdot,y_2) + r)\rangle_f + \langle u_2(\cdot,y_2), u_2(\cdot,y_2)\rangle_2.$$

for $u_2 \in H_2$. $J_2(u_2)$ has the unique minimum

$$u_2 = -(I + \mathscr{L}_2^*\mathscr{Q}_2\mathscr{L}_2)^{-1}\mathscr{L}_2^*\mathscr{Q}_2(\mathscr{L}_1\gamma_1(\cdot,y_1) + r).$$

Substituting the above control u_2 for $\gamma_2(\cdot,y_2)$ in the leader objective function gives an expression, by which the existence of a unique Stackelberg solution can be guaranteed.

5.3.0.6 Step 6: The Leader Objective Function Considering The Follower's Minimized Control

This step outlines a nonstandard optimization problem faced by the leader after the follower's minimized control. The details can be found in [111].

For each $\gamma_1 \in \Gamma_1$, the control $u_2 \in H_2$ that minimizes $J_2(u_2)$ is given by

$$u_{2t} = -B_2 \left[S_2(t) E \left\{ x_t | y_2 \right\} + k_{2t} \right],$$

where,

$$\begin{aligned}
&\dot{S}_2(t) = -A'(t)S_2(t) - S_2(t)A(t) - Q_2(t) + S_2(t)B_2(t)B_2'(t)S_2(t), \\
&S_2(t_f) = Q_{2f}, \\
&\dot{k}_{2t} = -\left[A'(t) - S_2(t)B_2(t)B_2'(t) \right] k_{2t} - S_2(t)B_1(t)E\left\{ \gamma_1(t,y_1) | y_2 \right\}, \\
&k_{2t_f} = 0.
\end{aligned}$$

Using the follower control expression and denoting $E\left\{\gamma_1(t,y_1)|y_2\right\}$ by $\hat{x}_{2t}$, we get the following expression from the state dynamics

$$\begin{aligned}
d\hat{x}_{2t} = \left[A(t) - B_2(t)B_2'(t)S_2(t) \right] \hat{x}_{2t} dt - B_2(t)B_2'(t)k_{2t}dt + B_1 E\left\{ \gamma_1(t,y_1)|y_2 \right\} dt, \\
\hat{x}_{2t_0} = E\left\{ x_{2t_0} | y_2 \right\} = E\left\{ x_0 | y_2 \right\}.
\end{aligned}$$

If $e_t = x_t - \hat{x}_{2t}$, then

$$de_t = A(t)e_t + B_1\gamma_1(t,y_1)dt - B_1(t)E\left\{\gamma_1(t,y_1)|y_2\right\}dt + F(t)dW_t,$$

with

$$e_{t_0} = x_0 - E\left\{x_0|y_2\right\}.$$

In terms of the new variables $\hat{x}_{2t}$, e_t, and k_{2t}, we can express the leader objective function as follows:

$$\begin{aligned}
&J_1(\gamma_1, T_2^1\gamma_1) = \hat{x}_{2t_f}'Q_{1f}\hat{x}_{2t_f} + e_{t_f}'Q_{1f}e_{t_f} \\
&+ \int_{t_0}^{t_f} \left[\hat{x}_{2t}'Q_1(t)\hat{x}_{2t} + e_t'Q_1(t)e_t \right] dt \\
&+ \int_{t_0}^{t_f} \left[\left\{ \hat{x}_2'(t)S_2(t)k_{2t}' \right\} B_2(t)R(t)B_2'(t)\left\{ S_2(t)\hat{x}_{2t} + k_{2t} \right\} + \gamma_1'(t,y_1)\gamma_1(t,y_1) \right] dt.
\end{aligned}$$

5.3.0.7 Step 7: Determination of Stackelberg Strategy

Theorem 5.2. *The two-person nonzero-sum stochastic differential game with static information admits a unique Stackelberg solution. The leader's Stackelberg strategy is given by*

$$\begin{aligned}
&\gamma_{1o}(t,\gamma_1) = -B_1(t)'\left[\left(\Psi'(t_f,t) - S_2(t)F'(t_f,t)\right)Q_{1f}\hat{\hat{x}}_{21t_f} + \Phi'(t_f,t)Q_{1f}\hat{e}_{1t_f}\right] \\
&- B_1(t)'\int_t^{t_f}\left[\left(\Psi'(\sigma,t) - S_2(t)F'(\sigma,t)\right)\left(Q_1(\sigma)\hat{\hat{x}}_{21\sigma} + S_2(\sigma)\hat{z}_\sigma\right) + \Phi'(\sigma,t)Q_1(\sigma)\hat{e}_{1\sigma}\right] \\
&+ B_1'S_2(t)\int_{t_0}^{t}\left[F(t,\sigma)\left(Q_1(\sigma)\hat{\hat{x}}_{21\sigma} + S_2(\sigma)\hat{z}_\sigma\right) - \Psi(t,\sigma)\hat{z}_\sigma\right]d\sigma,
\end{aligned}$$

where

$$\hat{z}_t = B_2(t)R(t)B_2'(t)\left[S_2(t)\hat{\hat{x}}_{21t} + \hat{k}_{21t}\right],$$

and $\hat{\hat{x}}_{21t}$, $\hat{e}_{1t}$, $\hat{k}_{21t}$ satisfy the differential equations

$$\begin{aligned}
&\dot{\hat{\hat{x}}}_{21t} = \left(A - B_2(t)B_2'(t)S_2(t)\right)\hat{\hat{x}}_{21t} + B_1(t)E\left\{E\left\{\gamma_{1o}(t,y_1)|y_2\right\}|y_1\right\} - B_2(t)B_2'(t)\hat{k}_{21t}, \\
&\dot{\hat{e}}_{1t} = A\hat{e}_{1t} + B_1(t)\gamma_{1o}(t,y_1) - B_1(t)E\left\{E\left\{\gamma_{1o}(t,y_1)|y_2\right\}|y_1\right\}, \\
&\dot{\hat{k}}_{21t} = -\left(A - S_2B_2(t)B_2'(t)\right)\hat{k}_{21t} - S_2(t)B_1(t)E\left\{E\left\{\gamma_{1o}(t,y_1)|y_2\right\}|y_1\right\}, \\
&\hat{\hat{x}}_{21t_0} = E\left\{E\left\{x_0|y_2\right\}|y_1\right\}, \\
&\hat{e}_{1t_0} = E\left\{x_0|y_1\right\} - E\left\{E\left\{x_0|y_2\right\}|y_1\right\}, \\
&\hat{k}_{21t_f} = 0.
\end{aligned}$$

The corresponding unique optimal response strategy of the follower is given by

$$\gamma_{2o}(t,\gamma_2) = -B_2\left[S_2(t)E\left\{\hat{x}_{2t}|y_2\right\} + k_{2t}\right].$$

The relevant terms are defined in step 5 and step 6. These are stated again below for convenience.

$$\hat{\hat{x}}_{21t} = E\left[\hat{x}_{21t} \mid y_1\right] = E\left[E\left[x_t \mid y_2\right] \mid y_1\right],$$
$$e_t = x_t - \hat{x}_{21t} = x_t - E\left[x_t \mid y_2\right],$$
$$\dot{k}_{21t} = -\left[A - S_2 B_2 B_2'\right] k_{2t} - S_2 B_1 E\left[\gamma_1 \mid y_2\right],$$
$$k_{2t_f} = 0,$$

where x_t is the state variable at time t, y_i is the noisy measurement of the states by the i-th player, and γ_i is the decision law (strategy) of the i-th player.

Proof:The proof is given in [46].

5.4 Open-Loop Statistical Stackelberg Problem Formulation

In this section, we formulate a two-player Stackelberg statistical game problem for a nonlinear system. We consider open-loop information structure for both players.

5.4.1 Preliminaries

We consider a two-player n-dimensional stochastic system described by a nonlinear Itô-sense stochastic differential equation.

$$dx(t) = [f(t,x(t),u_1(t),u_2(t))]dt + \sigma(t,x)dw(t), \tag{5.7}$$

where $t \in [t_0,t_f] = T$, $x(t) \in \mathbb{R}^n$ is the state vector, $x(t_0) = x_0$ is the initial state, and $x(t_f) = x_f$ is the final state. We denote the control of player 1 and player 2 by $u_1(t)$ and $u_2(t)$ which are a subset of the sets of admissible control $U_1 \subset \mathbb{R}^{r_1}$ and $U_2 \subset \mathbb{R}^{r_2}$. Player 1 is denoted by **P1** and player 2 is denoted by **P2**. Here, $dw(t)$ is a Gaussian random process of dimension d with zero mean, covariance of $W(t)dt$. The random process is defined on a probability space $(\Omega_0, \mathscr{F}, \mathscr{P})$, where Ω_0 is a non-empty set, $\mathscr{F}$ is a σ-algebra of Ω_0, and $\mathscr{P}$ is a probability measure on $(\Omega_0, \mathscr{F})$. Let, $\{\mathscr{F}_t\}_{0\leq t\leq T}$ is the natural filtration generated by $w(t)$.

The following conditions are sufficient for existence and uniqueness of the states $x(t)$ [112]. Let $Q_0 = \left[t_0,t_f\right) \times \mathbb{R}^n$ and let $\bar{Q}_0$ denote the closure of Q_0, where $\bar{Q}_0 = T \times \mathbb{R}^n$.

- We assume that $f : \bar{Q}_0 \times U_1 \times U_2 \to \mathbb{R}^n$ is $C^1(\bar{Q}_0 \times U_1 \times U_2)$ and $\sigma : \bar{Q}_0 \to \mathbb{R}^{n\times d}$ is $C^1(\bar{Q}_0)$. In other words, f and σ are defined and Borel measurable on the closure of $\bar{Q}_0$.
- In addition, f and σ satisfy linear growth conditions [112]. There exists a positive constant C such that,

$$\begin{aligned} \|f(t,x(t),u_1(t),u_2(t))\| &\leq C(1+\|x\|+u_1+u_2), \\ \sigma(t,x) &\leq C(1+\|x\|), \end{aligned} \tag{5.8}$$

  with $(t,x(t),u_1(t),u_2(t)) \in \bar{Q}_0 \times U_1 \times U_2 \to \mathbb{R}^n$, $(t,x(t)) \in \bar{Q}_0$, and $\|.\|$ is the Euclidean norm. The above condition (5.8) represents the linear growth, which prevents the state x from becoming unbounded in finite time.
- f and σ also satisfy local Lipschitz condition [112]. We assume that there exists a constant $\mathbb{K}$ such that

$$\begin{aligned} &\|[f(t,x(t),u_1(t),u_2(t)] - [f(t,\check{x}(t),\check{u}_1(t),\check{u}_2(t)]\| \leq \mathbb{K}(\|x-\check{x}\| + \sum_{k=1}^{2}\|u_k - \check{u_k}\|), \\ &\|\sigma(t,x) - \sigma(t,\check{x})\| \leq \mathbb{K}\|x-\check{x}\|, \end{aligned} \tag{5.9}$$

  with $t \in T$, $x,\check{x} \in \mathbb{R}^n$, and $u,\check{u} \in U_k$.

We consider a Stackelberg non-cooperative equilibrium solution concept, which is also known as the Stackelberg solution concept. In this concept, one of the players is the leader, the other one is the follower. Furthermore, it allows one of the players to have access to the strategy of the other player. Let **P1** be the leader and **P2** be the follower. The convention adopted in this chapter is that the leader **P1** announces his strategy first, and the follower **P2** reacts accordingly. For each of **P1**'s strategy, **P2** will choose an optimal strategy. If this is repeated for each of the **P1**'s strategies under a given information structure, then we obtain a rational reaction set or optimal response set for **P2**. Minimization of the cost function statistics over that reaction set yields the optimal strategy for **P1** under the Stackelberg solution concept [44, 45].

We assume that both the players make independent noisy measurements of the initial state x_0. We also assume that the information available to each player is static, that is, the

conditional joint distribution of (η_1, η_2), given x_0, is known *a priori*. This type of information structure is called open-loop (OL) pattern [36, p. 212]. The information structure of the leader is denoted by $\eta_1 = \{x_0, \mathscr{F}_t\}$. The information structure of the follower is denoted by $\eta_2 = \{x_0, u_1(.), \mathscr{F}_t\}$ because the follower makes his decision after the leader announces his strategy.

Let H_k, $k = 1,2$ denote the class of second-order stochastic processes defined on $[t_0, t_f]$ which are η_k-measurable. Let Γ_k be a class of real Borel-measurable mappings $\gamma_k : [t_0, t_f] \times R^{p_k} \to R^{r_k}$, where p_k is the dimension of η_k, and r_k is the dimension of u_k. Γ_k is the strategy space of **Pk**, where the Borel-measurable functions are $g : [t_0, t_f] \times R^{p_k} \to R^{r_k}$, with restriction of $E\left\{\int_{t_0}^{t_f} \|g(t, \eta_k)\|^2\right\} dt < \infty$. Each of Γ_k's elements γ_k is a permissible strategy for **Pk**. So, the controllers are defined as,

$$u_k(t) = \gamma_k(t, \eta_k), \tag{5.10}$$

where $\gamma_k(t, \eta_k) \in H_k$. For ease of notation, we suppress the dependence of t and η_k in the argument of γ_k. We assume that γ_k satisfies Lipschitz and linear growth conditions. Note that, for each pair of elements in $H_1 \times H_2$, the stochastic differential equation (5.7) admits a unique solution [113]. For an admissible pair of strategies $(\gamma_1 \in \Gamma_1, \gamma_2 \in \Gamma_2)$, the cost functions for the players are given by,

$$J_k(t, x(t), \gamma_k) = \psi_k(x(t_f)) + \int_t^{t_f} L_k(s, x(s), \gamma_k) ds \quad k = 1,2, \tag{5.11}$$

where $L_k : \bar{Q}_0 \times \Gamma_1 \times \Gamma_2 \to \mathbb{R}^+$ is $C(\bar{Q}_0 \times \Gamma_1 \times \Gamma_2)$ and $\psi_k : \bar{Q}_0 \to \mathbb{R}^+$ is $C(\bar{Q}_0)$ with both satisfying polynomial growth condition,

$$\|L_k(t, x(t), \gamma_k)\| \leq c_1(1 + \|x\| + \sum_{k=1}^{2} \|\gamma_k\|)^{c_2}, \tag{5.12}$$

$$\|\psi_k\| \leq c_1(1 + \|x\|)^{c_2}, \tag{5.13}$$

for constants c_1 and c_2. Here, L_k is the running cost and ψ_k is the terminal cost. These conditions allow the mean of the cost function to be finite [114].

Definition 5.6. *The i-th cost moment function M_k^i of the k-th player is defined by [40],*

$$M_k^i(t, x, \gamma_k) = E\left\{J_k^i(t, x, \gamma_k | x(t) = x\right\} = E_{tx}\left\{J_k^i(t, x, \gamma_k\right\}, \tag{5.14}$$

where $i = 1, 2, \ldots, m$, $k = 1, 2$, and $E_{tx} = E\{\cdot | x(t) = x\}$.

Definition 5.7. *A function $M : \bar{Q}_0 \to \mathbb{R}^+$ is an admissible mean cost function if there exists a strategy $\gamma_k(t,x)$ such that*

$$M_k^i(t,x) = M_k^i(t,x;\gamma_k), \quad k = 1,2, \quad i = 1,2 \quad for \quad t \in T, x \in \mathbb{R}^n \tag{5.15}$$

Definition 5.8. *Similarly, m-th cost cumulant function $V_k^m(t,x)$ of the k-th player in relation to the cost moment function is defined by [115],*

$$V_k^m(t,x,\gamma_k) = M_k^m(t,x) - \sum_{i=0}^{m-2} \frac{(m-1)!}{i!(m-1-i)!} M_k^{m-1-i}(t,x) V_k^{i+1}(t,x), \tag{5.16}$$

where $k = 1,2$, $t \in T = [t_0, t_f]$, $x(t_0) = x_0$, $x(t) \in \mathbb{R}^n$.

Also, V_k^m is the admissible m-th cost cumulant function for the k-th player related to the moment function through the moment-cumulant relation (5.16). Here, V_k^m is also called the m-th value function for the k-th player. **Note that the superscript of V_k^m indicates cumulant index and the subscript denotes the player index.**

5.4.2 Problem Definition

Now, we introduce Stackelberg solution concept for the differential game under statistical control framework. In stochastic Stackelberg game, the value function is the expected value (first cumulant) of the cost function. In statistical control, the concept of value function is extended, and generalized for second cumulant, third cumulant, and so on (up to m-th cumulant). Therefore, for statistical Stackelberg game, we shall introduce the value function used in statistical control, that is, the m-th cumulant of the cost function.

Let Γ_1^m and Γ_2^m be the strategy space of the players **P1** and **P2**. The cost incurred to the players are the value functions, that is, the m-th cost cumulants denoted by $V_1^m(t,x(t),\gamma_1^m,\gamma_2^m)$ and $V_2^m(t,x(t),\gamma_1^m,\gamma_2^m)$. Here, (γ_1^m,γ_2^m) is the strategy pair of the players **P1** and **P2** such that $\gamma_1^m \in \Gamma_1^m, \gamma_2^m \in \Gamma_2^m$. The player that selects his strategy first is called the leader, and the player that selects his strategy second is called the follower. Unless otherwise stated, the Stackelberg strategy will refer to the Stackelberg strategy with player **P1** as the leader, and **P2** as the follower.

Definition 5.9. *For any constant policy $\gamma_1^m \in \Gamma_1^m$, there exists a unique mapping $\mathfrak{T}_2^{mm} : \Gamma_1^m \to \Gamma_2^m$ such that*

$$V_2^m(\gamma_1^m, \mathfrak{T}_2^{mm}\gamma_1^m) \leq V_2^m(\gamma_1^m, \gamma_2^m), \quad \forall \gamma_2^m \in \Gamma_2^m, \tag{5.17}$$

and every $\gamma_1^m \in \Gamma_1^m$.

For ease of notation, we suppress t, $x(t)$ from the arguments of V_2^m. We shall also suppress the superscript of γ. The mapping functions for various combinations of strategy pair are listed in Table 5.1. Note that the first the superscript of $\mathfrak{T}$ indicates **P1**'s targeted cumulant index, and the second superscript indicates **P2**'s targeted cumulant index. The subscript denotes the player index as usual.

Table 5.1: Follower's mapping

	Follower's strategy		$\rightarrow$				
Leader's strategy		γ_2^1	γ_2^2	γ_2^3	γ_2^4	$\cdots$	γ_2^m
$\downarrow$	γ_1^1	$\mathfrak{T}_2^{11}$	$\mathfrak{T}_2^{12}$	$\mathfrak{T}_2^{13}$	$\mathfrak{T}_2^{14}$	$\cdots$	$\mathfrak{T}_2^{1m}$
	γ_1^2	$\mathfrak{T}_2^{21}$	$\mathfrak{T}_2^{22}$	$\mathfrak{T}_2^{23}$	$\mathfrak{T}_2^{24}$	$\cdots$	$\mathfrak{T}_2^{2m}$
	γ_1^3	$\mathfrak{T}_2^{31}$	$\mathfrak{T}_2^{32}$	$\mathfrak{T}_2^{33}$	$\mathfrak{T}_2^{34}$	$\cdots$	$\mathfrak{T}_2^{3m}$
	γ_1^4	$\mathfrak{T}_2^{41}$	$\mathfrak{T}_2^{42}$	$\mathfrak{T}_2^{43}$	$\mathfrak{T}_2^{44}$	$\cdots$	$\mathfrak{T}_2^{4m}$
	$\vdots$	$\vdots$	$\vdots$	$\vdots$	$\vdots$	$\vdots$	$\vdots$
	γ_1^m	$\mathfrak{T}_2^{m1}$	$\mathfrak{T}_2^{m2}$	$\mathfrak{T}_2^{m3}$	$\mathfrak{T}_2^{m4}$	$\cdots$	$\mathfrak{T}_2^{mm}$

The Stackelberg strategy is the optimal strategy for the leader if the follower reacts by playing rationally. Let the graph $D_2 = \left\{(\gamma_1, \gamma_2) \in \Gamma_1^m \times \Gamma_2^m : \gamma_2 = \mathfrak{T}_2^{mm}\gamma_1\right\}$ of the mapping $\mathfrak{T}_2^{mm}$ is a rational reaction set of the follower. This set represents the strategy pairs in $\Gamma_1^m \times \Gamma_2^m$, according to which the follower reacts to every strategy $\gamma_1 \in \Gamma_1^m$ chosen by the leader. By playing the according to the set D_2, the follower is considered to be a rational player.

We consider an open set $Q \subset Q_0$ and let the k-th player cost cumulant functions $V_k^j(t,x) \in C_p^{1,2}(Q) \cap C(\bar{Q})$ for $j = 1, 2, \ldots, m-1$ be admissible cumulant functions, where the set

$C_p^{1,2}(Q)\cap C(\bar{Q})$ means that the function V_k^j satisfy polynomial growth condition and is continuous in the first and second derivatives of Q, and continuous on the closure of Q. We assume that the existence of an optimal strategy for the leader $\gamma_1^* \in \Gamma_1^m$ and optimal value function $V_1^{m*}(t,x) \in C_p^{1,2}(Q)\cap C(\bar{Q})$ for the leader **P1**.

The leader **P1** first announces a constant policy. Then, the follower **P2** reacts optimally by adopting a unique strategy, which minimizes the follower m-th value function $V_2^m(\gamma_1,\gamma_2)$ over Γ_2^m. Now, we consider the minimization of the m-th cumulant function of the leader $V_1^m(\gamma_1,\mathfrak{T}_2^{mm}\gamma_1)$ over Γ_1^m. Let γ_1^* be a minimizing solution; that is

$$V_1^m(\gamma_1^*,\mathfrak{T}_2^{mm}\gamma_1^*) \le V_1^m(\gamma_1,\mathfrak{T}_2^{mm}\gamma_1) \qquad \forall \gamma_1 \in \Gamma_1^m, \tag{5.18}$$

where $\mathfrak{T}_2^{mm} : \Gamma_1^m \to \Gamma_2^m$ is a mapping for the m-th cumulant and V_1^m is m-th value function (m-th cost cumulant) of the leader **P1**. Then, we call the strategy pair $(\gamma_1^*,\gamma_2^*) \in \Gamma_1^m \times \Gamma_2^m$ the Stackelberg solution of the dynamic game problem considered above, with **P1** as the leader. Thus, the statistical game problem is to find the Stackelberg strategy pair (γ_1^*,γ_2^*) or $\gamma_1^*,\mathfrak{T}_2^{mm}\gamma_1^*$ which results in minimal m-th value function V_1^{m*} given as

$$V_1^m(\gamma_1^*,\mathfrak{T}_2^{mm}\gamma_1^*) = \min_{\gamma_1\in\Gamma_1^m} V_1^m(\gamma_1,\mathfrak{T}_2^{mm}\gamma_1) \triangleq V_1^{m*}. \tag{5.19}$$

Remark 5.3. *Note that the optimal value function for the leader $V_1^{m*}(t,x)$ will be found with the assumption that lower order cumulants, $V_k^j(t,x)$, are admissible for $j = 1,2,\ldots,m-1$. Same goes for the follower's m-th value function $V_2^{m*}(t,x)$ minimization. For instance, in the second cumulant minimization for the leader, all the strategies that give a pre-specified first cumulant are found and within this set, the optimal strategies that minimize the second cumulant value function are found.*

5.4.3 Special Case: Linear Quadratic System and Minimum Cost Variance for Leader

In this section, we formulate the above game problem for a linear system with quadratic cost functions.

We obtain the two-player n-dimensional linear stochastic system described by an Itô-sense stochastic differential equation by using the following relation,

$$f(t,x(t),u_k(t)) = A(t)x(t) + B_1(t)u_1(t) + B_2(t)u_2(t), \tag{5.20}$$

to substitute f, and $F(t)$ to substitute $\sigma(t,x)$ in (5.7). The linear system is given as,

$$dx(t) = [A(t)x(t) + B_1(t)u_1(t) + B_2(t)u_2(t)]dt + F(t)dw(t), \quad k = 1,2 \tag{5.21}$$

where $t \in [t_0, t_f] = T$, $x(t) \in \mathbb{R}^n$ is the state vector, $x(t_0) = x_0$ is the initial state, and $x(t_f) = x_f$ is the final state. We denote the control of the k-th player by $u_k(t)$ which is a subset of the sets of admissible control $\mathscr{U}_k \subset \mathbb{R}^{r_k}$, where $k = 1,2$. $A(\cdot)$, $B_1(\cdot)$, and $B_2(\cdot)$ are appropriate dimension matrices with continuous entries on T. Let γ_1 and γ_2 be permissible strategies belonging to permissible strategy space $\Gamma_k, k = 1,2$, such that the controls $u_1 = \gamma_1$ and $u_2 = \gamma_2$.

We consider the cost functions to be quadratic. In game theory, the quadratic cost functions are of particular interest for two reasons. First, they can be considered as the second-order approximation to other type of nonlinear cost functions. Second, the game problem with quadratic cost functions are analytically tractable and provides closed-form equilibrium solutions. We use the following relations,

$$\psi_k(x(t_f)) = x'(t_f)Q_{kf}x(t_f), \tag{5.22}$$

$$L_k(s,x(s),\gamma_1,\gamma_2) = x'(t)Q_kx(t) + \gamma_1'(t)R_{k1}(t)\gamma_1(t) + \gamma_2'(t)R_{k2}(t)\gamma_2(t), \quad k = 1,2 \tag{5.23}$$

to obtain the general quadratic cost function for **P1** and **P2**. The quadratic cost function can be written as,

$$J_k(t,x(t),\gamma_k) = x'(t_f)Q_{kf}x(t_f) + \int_{t_0}^{t_f} \left[x'(t)Q_kx(t) + \gamma_1'(t)R_{k1}(t)\gamma_1(t) + \gamma_2'(t)R_{k2}(t)\gamma_2(t)\right] dt, \tag{5.24}$$

for $k = 1,2$ with prime ($'$) denoting transpose of a matrix, where

$$Q_{kf} \geq 0, \quad Q_k(\cdot) \geq 0, \quad R_{k1}(\cdot) > 0, \quad R_{k2}(\cdot) > 0.$$

Because of the Stackelberg solution concept, the leader **P1** takes into account of the follower's choice of strategy into his own cost function. On the other hand, the follower **P2** only focuses on his own strategy. To accommodate this, we consider

$$R_{11} = I, \quad R_{12} = R, \quad R_{21} = O, \quad R_{22} = I,$$

where I is identity matrix and O is null matrix. This way, the leader cost function includes both leader and follower strategies, while the follower cost function only depends on the follower strategy. Now, we obtain the definition of the quadratic cost functional of **P1** and **P2** as follows

$$J_1(\gamma_1,\gamma_2) = x'(t_f)Q_{1f}x(t_f) + \int_{t_0}^{t_f} \left[x'(t)Q_1x(t) + \gamma_1'(t)\gamma_1(t) + \gamma_2'(t)R(t)\gamma_2(t)\right] dt, \quad (5.25)$$

$$J_2(\gamma_1,\gamma_2) = x'(t_f)Q_{2f}x(t_f) + \int_{t_0}^{t_f} \left[x'(t)Q_2x(t) + \gamma_2'(t)\gamma_2(t)\right] dt, \quad (5.26)$$

with prime denoting transpose of a matrix, where

$$Q_{1f} \geq 0, \quad Q_{2f} \geq 0, \quad Q_1(\cdot) \geq 0, \quad Q_2(\cdot) \geq 0, \quad R(\cdot) > 0.$$

We define the first and second cumulant of the cost function. The first cumulant of the cost function for the k-th player is defined by,

$$V_k^1(t,x,\gamma_k) = M_k^1(t,x) = E_{tx}\left\{J_k^1(t,x,\gamma_k)\right\}, \quad (5.27)$$

and the second cumulant of the cost function for the k-th player is defined by,

$$V_k^2(t,x,\gamma_k) = M_k^2(t,x) - \left[M_k^1(t,x)\right]^2 = E_{tx}\left\{J_k^2(t,x,\gamma_k)\right\} - \left[E_{tx}\left\{J_k^1(t,x,\gamma_k)\right\}\right]^2, \quad (5.28)$$

Note that the superscript of V indicates cumulant index and the subscript denotes the player index. In minimal cost variance problem, the second cumulant or variance of the cost function is minimized with a specified first cumulant or mean. We shall consider the minimization of cost variance of the leader in Stackelberg minimal cost variance problem.

Now, we introduce the Stackelberg solution concept for the above linear stochastic differential game. Let Γ_1^2 be the strategy space of the leader **P1** corresponding to second cost cumulant, and Γ_2^1 be the strategy space of the follower **P2** corresponding to the first cost cumulant. **P1** announces a constant policy first. For every $\gamma_1 \in \Gamma_1^2$, the follower **P2** reacts optimally by adopting a unique strategy $\gamma_2 \in \Gamma_2^1$, which minimizes the mean of the follower cost function $V_2^1(\gamma_1,\gamma_2)$ over Γ_2^1. This implies that there exists a unique mapping for the first cumulant $\mathfrak{T}_2^{21} : \Gamma_1^2 \to \Gamma_2^1$ such that

$$V_2^1(\gamma_1, \mathfrak{T}_1^{21}\gamma_1) \leq V_2^1(\gamma_1,\gamma_2), \quad \forall \gamma_2 \in \Gamma_2^1. \quad (5.29)$$

We assume that the existence of an optimal strategy for the leader $\gamma_1^* \in \Gamma_1^2$ and optimal value function $V_1^{2*}(t,x) \in C_p^{1,2}(Q) \cap C(\bar{Q})$ for the leader **P1**. Now, we consider the minimization of the second cumulant of the cost function of the leader $V_1^2(\gamma_1, \mathfrak{T}_2^{21}\gamma_1)$ over Γ_1^2. Let γ_1^* be a minimizing solution; that is

$$V_1^2(\gamma_1^*, \mathfrak{T}_2^{21}\gamma_1^*) \leq V_1^2(\gamma_1, \mathfrak{T}_2^{21}\gamma_1). \tag{5.30}$$

Thus, the statistical game problem is to find the Stackelberg strategy pair (γ_1^*, γ_2^*) or $\left(\gamma_1^*, \mathfrak{T}_2^{21}\gamma_1^*\right)$ which results in minimal second cost cumulant value function V_1^{2*} given as

$$V_1^2(\gamma_1^*, \mathfrak{T}_2^{21}\gamma_1^*) = \min_{\gamma_1 \in \Gamma_1^2} V_1^2(\gamma_1, \mathfrak{T}_2^{21}\gamma_1) \triangleq V_1^{2*}. \tag{5.31}$$

5.4.4 Stackelberg Minimal Cost Variance Problem Formulation

In this section, we first derive the optimal response of the follower to any announced policy of the leader. We then substitute the follower's response into the leader's problem to obtain Stackelberg minimal cost variance problem. We convert the game problem into an equivalent Stackelberg game problem in Hilbert space [46]. Hilbert space generalizes the notion of Euclidean space. Euclidean space refers to a finite dimensional linear space with an inner product. On the other hand, Hilbert space refers to an infinite dimensional linear inner product space, which is complete for the norm induced by the inner product [116]. Hilbert space allows the extension of vector algebra and calculus from the two dimensional Eucleadian plane and three dimensional space to spaces to any finite and infinite number of dimensions.

We introduce the definition of the inner product $\langle \cdot, \cdot \rangle$ on H_k through the relation,

$$\langle\, v_1, v_2 \rangle_k = E\left\{ \int_{t_0}^{t_f} v_1'(t,\omega) v_2(t,\omega) dt \right\} \tag{5.32}$$

for each pair $\{v_1 \in H_k, v_2 \in H_k\}$, $\omega \in \Omega_0$, with $(\Omega_0, \mathscr{F}, \mathscr{P})$ denoting the underlying probability space. Ω_0 is a non-empty set, $\mathscr{F}$ is a σ-algebra of Ω_0, and $\mathscr{P}$ is a probability measure on $(\Omega_0, \mathscr{F})$. With these inner products $H_k, k = 1,2$, become Hilbert spaces.

Let us denote the completion of the space of continuous functions from $\left[t_0, t_f\right] \times \Omega_0$ by

L_{2f} with the inner product

$$\langle x_1, x_2 \rangle_f = E\left\{ x_1'(t_f,\omega)x_2'(t_f,\omega) + \int_{t_0}^{t_f} x_1'(t,\omega)x_2(t,\omega)dt \right\}. \tag{5.33}$$

Let $\mathscr{Q}_k$, $k = 1,2$ be the bounded operators mapping $L_2[t_0,t_f] \times \Omega_0$ into itself, and $\mathscr{Q}_k$, $k = 1,2$ are defined by,

$$\mathscr{Q}_k x = \begin{cases} Q_k(t)x(t), & t_0 \le t < t_f, \\ Q_{kf}x(t_f), & t = t_f. \end{cases} \tag{5.34}$$

Then, we define Volterra operators $\mathscr{L}_k : H_k \to L_2[t_0,t_f] \times \Omega_0$, $k = 1,2$, by,

$$(\mathscr{L}_k u)(t,\omega) = \int_{t_0}^{t} \Phi(t,\tau)B_k(\tau)u(\tau,\omega)d\tau. \tag{5.35}$$

The state transition matrix $\Phi(t,\tau)$ comes from the solution of the stochastic differential equation (5.21):

$$x(t) = \Phi(t,t_0)x_0 + \int_{t_0}^{t} \Phi(t,\tau)B_k(\tau)u_k(\omega)d\tau + \int_{t_0}^{t} \Phi(t,\tau)F(\tau)dw(\tau,\omega)d\tau, \tag{5.36}$$

where $\Phi(t,\tau)$ is the state transition matrix function satisfying

$$\frac{d\Phi(t,\tau)}{dt} = A(t)\Phi(t,\tau), \quad \Phi(\tau,\tau) = I. \tag{5.37}$$

Further, let $r = L_{2f}\left([t_0,t_f] \times \Omega_0\right)$ be defined by

$$r(t,\omega) = \Phi(t,t_0)x_0(\omega) + \int_{t_0}^{t} \Phi(t,\tau)F(\tau)dw(\tau,\omega). \tag{5.38}$$

Using (5.38), we write (5.36) as,

$$x(t) = r(t,\omega) + \int_{t_0}^{t} \Phi(t,\tau)B_k(\tau)u_k(\omega)d\tau. \tag{5.39}$$

Then, using Volterra operators in (5.35), eq. (5.39) can be expressed as,

$$x(t) = r(t,\omega) + \mathscr{L}_1 u_1(t,\omega) + \mathscr{L}_2 u_2(t,\omega). \tag{5.40}$$

Then, using $u_k(t) = \gamma_k(t,\eta_k)$ from (5.10) in (5.40) we have,

$$x(t) = r(t,\omega) + \mathscr{L}_1\gamma_1(\cdot,\eta_1) + \mathscr{L}_2\gamma_2(\cdot,\eta_2). \tag{5.41}$$

For simplification, we suppress the argument (t,ω) and $(\cdot,\eta_1)$ and have

$$x(t) = r + \mathscr{L}_1\gamma_1 + \mathscr{L}_2\gamma_2. \tag{5.42}$$

Thus, the expected values of the cost functions of **P1** and **P2** in (5.25) and (5.26) can be written as,

$$E\{J_1(\gamma_1,\gamma_2)\} = \langle \mathscr{Q}_1 x, x\rangle + \langle \gamma_1,\gamma_1\rangle + \langle \gamma_2, R\gamma_2\rangle, \tag{5.43}$$

$$E\{J_2(\gamma_1,\gamma_2)\} = \langle \mathscr{Q}_2 x, x\rangle + \langle \gamma_2,\gamma_2\rangle. \tag{5.44}$$

Now, for fixed $\gamma_1 \in \Gamma_1$, the minimization of $V_2^1(\gamma_1,\gamma_2)$ i.e. the first cumulant of $J_2(\gamma_1,\gamma_2)$, is equivalent to the control problem of minimizing,

$$E\{J_2(\gamma_2)\} = \langle \mathscr{Q}_2 x, x\rangle + \langle \gamma_2,\gamma_2\rangle, \tag{5.45}$$

for $\gamma_2 \in H_2$ [117]. Substituting the value of x from (5.42) we write (5.45) as:

$$\begin{aligned} E\{J_2(\gamma_2)\} &= \langle \mathscr{Q}_2(r+\mathscr{L}_1\gamma_1+\mathscr{L}_2\gamma_2), (r+\mathscr{L}_1\gamma_1+\mathscr{L}_2\gamma_2)\rangle + \langle \gamma_2,\gamma_2\rangle \\ &= \langle \mathscr{Q}_2 r, r\rangle + \langle \mathscr{Q}_2 r, \mathscr{L}_1\gamma_1\rangle + \langle \mathscr{Q}_2 r, \mathscr{L}_2\gamma_2\rangle + \langle \mathscr{Q}_2\mathscr{L}_1\gamma_1, r\rangle + \langle \mathscr{Q}_2\mathscr{L}_1\gamma_1, \mathscr{L}_1\gamma_1\rangle + \langle \mathscr{Q}_2\mathscr{L}_1\gamma_1, \mathscr{L}_2\gamma_2\rangle \\ &+ \langle \mathscr{Q}_2\mathscr{L}_2\gamma_2, r\rangle + \langle \mathscr{Q}_2\mathscr{L}_2\gamma_2, \mathscr{L}_1\gamma_1\rangle + \langle \mathscr{Q}_2\mathscr{L}_2\gamma_2, \mathscr{L}_2\gamma_2\rangle + \langle \gamma_2,\gamma_2\rangle. \end{aligned} \tag{5.46}$$

Let $\mathscr{L}_2^*$ be the adjoint of the operator $\mathscr{L}_2$ in H_2. The concept of 'adjoint' applies for linear operators, which is similar to 'transpose' of matrices. One of the defining properties of adjoint is:

$$\langle x, \mathscr{L}_k\gamma_k\rangle = \langle \mathscr{L}_k^* x, \gamma_k\rangle. \tag{5.47}$$

Using (5.47), from (5.46) we write,

$$\begin{aligned} E\{J_2(\gamma_2)\} &= \langle \mathscr{Q}_2 r, r\rangle + \langle \mathscr{L}_1^*\mathscr{Q}_2 r, \gamma_1\rangle + \langle \mathscr{L}_2^*\mathscr{Q}_2 r, \gamma_2\rangle + \langle \mathscr{Q}_2\mathscr{L}_1\gamma_1, r\rangle + \langle \mathscr{L}_1^*\mathscr{Q}_2\mathscr{L}_1\gamma_1, \gamma_1\rangle \\ &+ \langle \mathscr{L}_2^*\mathscr{Q}_2\mathscr{L}_1\gamma_1, \gamma_2\rangle + \langle \mathscr{L}_2^*\mathscr{Q}_2 r, \gamma_2\rangle + \langle \mathscr{L}_2^*\mathscr{Q}_2\mathscr{L}_1\gamma_1, \gamma_2\rangle + \langle \mathscr{L}_2^*\mathscr{Q}_2\mathscr{L}_2\gamma_2, \gamma_2\rangle + \langle \gamma_2,\gamma_2\rangle. \end{aligned} \tag{5.48}$$

Taking the first of variation of $E\{J_2(\gamma_2)\}$ with respect to γ_2 and equate it to zero we have,

$$\delta E\{J_2(\gamma_2)\} = \langle (I + \mathscr{L}_2^*\mathscr{Q}_2\mathscr{L}_2)\gamma_2 + \mathscr{L}_2^*\mathscr{Q}_2(\mathscr{L}_1\gamma_1 + r), \delta\gamma_2\rangle = 0. \tag{5.49}$$

This gives us the necessary condition for the minimum as:

$$\gamma_2 = -(I + \mathscr{L}_2^* \mathscr{Q}_2 \mathscr{L}_2)^{-1} \mathscr{L}_2^* \mathscr{Q}_2 (\mathscr{L}_1 \gamma_1 + r). \tag{5.50}$$

Taking the second variation of $E\{J_2(\gamma_2)\}$ with respect to γ_2, we have

$$\delta^2 E\{J_2(\gamma_2)\} = \langle (I + \mathscr{L}_2^* \mathscr{Q}_2 \mathscr{L}_2), \delta^2 \gamma_2 \rangle. \tag{5.51}$$

Since, $\mathscr{L}_2$ is a Volterra operator, it is completely continuous and so is its adjoint $\mathscr{L}_2^*$. Besides, $\mathscr{Q}_2$ is a bounded operator. Therefore, the operator $(I + \mathscr{L}^* \mathscr{Q}_2 \mathscr{L})$ is strongly positive and has bounded inverse, for which (5.45) has a unique minimum

$$\gamma_2 = -(I + \mathscr{L}_2^* \mathscr{Q}_2 \mathscr{L}_2)^{-1} \mathscr{L}_2^* \mathscr{Q}_2 (\mathscr{L}_1 \gamma_1 + r). \tag{5.52}$$

Let us define $M_2 = (I + \mathscr{L}_2^* \mathscr{Q}_2 \mathscr{L}_2)^{-1}$, then (5.52) becomes,

$$\gamma_2 = -M_2 \mathscr{L}_2^* \mathscr{Q}_2 (\mathscr{L}_1 \gamma_1 + r). \tag{5.53}$$

Also,

$$\begin{aligned} M_2^* &= \left\{ (I + \mathscr{L}_2^* \mathscr{Q}_2 \mathscr{L}_2)^{-1} \right\}^* \\ &= \{ (I + \mathscr{L}_2^* \mathscr{Q}_2 \mathscr{L}_2)^* \}^{-1} \\ &= \{ I + (\mathscr{L}_2^* \mathscr{Q}_2 \mathscr{L}_2)^* \}^{-1} \\ &= (I + \mathscr{L}_2^* \mathscr{Q}_2 \mathscr{L}_2)^{-1} \\ &= M_2. \end{aligned} \tag{5.54}$$

Now,

$$E\{J_1\} = \langle \mathscr{Q}_1 x, x \rangle + \langle \gamma_1, \gamma_1 \rangle + \langle \gamma_2, R\gamma_2 \rangle, \tag{5.55}$$

Then, we substitute the value of x from (5.42) and the expression for γ_2 from (5.53) in

(5.55). The first term is as follows:

$$\langle \mathscr{Q}_1 x, x\rangle = \langle \mathscr{Q}_1(r+\mathscr{L}_1\gamma_1+\mathscr{L}_2\gamma_2),(r+\mathscr{L}_1\gamma_1+\mathscr{L}_2\gamma_2)\rangle$$
$$= \langle \mathscr{Q}_1 r, r\rangle + \langle \gamma_1, \mathscr{L}_1^*\mathscr{Q}_1\mathscr{L}_1\gamma_1\rangle + \langle \gamma_2, \mathscr{L}_2^*\mathscr{Q}_1\mathscr{L}_2\gamma_2\rangle + 2\langle \gamma_1, \mathscr{L}_1^*\mathscr{Q}_1 r\rangle + 2\langle \gamma_2, \mathscr{L}_2^*\mathscr{Q}_1 r\rangle$$
$$+ 2\langle \gamma_1, \mathscr{L}_1^*\mathscr{Q}_1\mathscr{L}_2\gamma_2\rangle$$
$$= \langle \mathscr{Q}_1 r, r\rangle + \langle \gamma_1, \mathscr{L}_1^*\mathscr{Q}_1\mathscr{L}_1\gamma_1\rangle + \langle \{-M_2\mathscr{L}_2^*\mathscr{Q}_2(\mathscr{L}_1\gamma_1+r)\}, \mathscr{L}_2^*\mathscr{Q}_1\mathscr{L}_2\{-M_2\mathscr{L}_2^*\mathscr{Q}_2(\mathscr{L}_1\gamma_1+r)\}\rangle$$
$$+ 2\langle \gamma_1, \mathscr{L}_1^*\mathscr{Q}_1 r\rangle + 2\langle \{-M_2\mathscr{L}_2^*\mathscr{Q}_2(\mathscr{L}_1\gamma_1+r)\}, \mathscr{L}_2^*\mathscr{Q}_1 r\rangle + 2\langle \gamma_1, \mathscr{L}_1^*\mathscr{Q}_1\mathscr{L}_2\{-M_2\mathscr{L}_2^*\mathscr{Q}_2(\mathscr{L}_1\gamma_1+r)\}\rangle$$
$$= \langle r, \mathscr{Q}_1 r\rangle + \langle \gamma_1, \mathscr{L}_1^*\mathscr{Q}_1\mathscr{L}_1\gamma_1\rangle + \langle \gamma_1, \mathscr{L}_1^*\mathscr{Q}_2\mathscr{L}_2 M_2\mathscr{L}_2^*\mathscr{Q}_1\mathscr{L}_2 M_2\mathscr{L}_2^*\mathscr{Q}_2\mathscr{L}_1\gamma_1\rangle$$
$$+ \langle r, \mathscr{Q}_2\mathscr{L}_2 M_2\mathscr{L}_2^*\mathscr{Q}_1\mathscr{L}_2 M_2\mathscr{L}_2^*\mathscr{Q}_2 r\rangle + 2\langle \gamma_1, \mathscr{L}_1^*\mathscr{Q}_2\mathscr{L}_2 M_2\mathscr{L}_2^*\mathscr{Q}_1\mathscr{L}_2 M_2\mathscr{L}_2^*\mathscr{Q}_2 r\rangle + 2\langle \gamma_1, \mathscr{L}_1^*\mathscr{Q}_1 r\rangle$$
$$- 2\langle \gamma_1, \mathscr{L}_1^*\mathscr{Q}_2\mathscr{L}_2 M_2\mathscr{L}_2^*\mathscr{Q}_1 r\rangle - 2\langle r, \mathscr{Q}_2\mathscr{L}_2 M_2\mathscr{L}_2^*\mathscr{Q}_1 r\rangle - 2\langle \gamma_1, \mathscr{L}_1^*\mathscr{Q}_1\mathscr{L}_2 M_2\mathscr{L}_2^*\mathscr{Q}_2\mathscr{L}_1\gamma_1\rangle$$
$$- 2\langle \gamma_1, \mathscr{L}_1^*\mathscr{Q}_1\mathscr{L}_2 M_2\mathscr{L}_2^*\mathscr{Q}_2 r\rangle. \tag{5.56}$$

The third term is as follows:

$$\langle \gamma_2, R\gamma_2\rangle = \langle \{-M_2\mathscr{L}_2^*\mathscr{Q}_2(\mathscr{L}_1\gamma_1+r)\}, R\{-M_2\mathscr{L}_2^*\mathscr{Q}_2(\mathscr{L}_1\gamma_1+r)\}\rangle$$
$$= \langle \gamma_1, \mathscr{L}_1^*\mathscr{Q}_2\mathscr{L}_2 M_2 R M_2\mathscr{L}_2^*\mathscr{Q}_2\mathscr{L}_1\gamma_1\rangle + \langle r, \mathscr{Q}_2\mathscr{L}_2 M_2 R M_2\mathscr{L}_2^*\mathscr{Q}_2 r\rangle$$
$$+ 2\langle \gamma_1, \mathscr{L}_1^*\mathscr{Q}_2\mathscr{L}_2 M_2 R M_2\mathscr{L}_2^*\mathscr{Q}_2 r\rangle. \tag{5.57}$$

Then,

$$E\{J_1\} = \langle r, \mathscr{Q}_1 r\rangle + \langle \gamma_1, \mathscr{L}_1^*\mathscr{Q}_1\mathscr{L}_1\gamma_1\rangle + \langle \gamma_1, \mathscr{L}_1^*\mathscr{Q}_2\mathscr{L}_2 M_2\mathscr{L}_2^*\mathscr{Q}_1\mathscr{L}_2 M_2\mathscr{L}_2^*\mathscr{Q}_2\mathscr{L}_1\gamma_1\rangle$$
$$+ \langle r, \mathscr{Q}_2\mathscr{L}_2 M_2\mathscr{L}_2^*\mathscr{Q}_1\mathscr{L}_2 M_2\mathscr{L}_2^*\mathscr{Q}_2 r\rangle + 2\langle \gamma_1, \mathscr{L}_1^*\mathscr{Q}_2\mathscr{L}_2 M_2\mathscr{L}_2^*\mathscr{Q}_1\mathscr{L}_2 M_2\mathscr{L}_2^*\mathscr{Q}_2 r\rangle + 2\langle \gamma_1, \mathscr{L}_1^*\mathscr{Q}_1 r\rangle$$
$$- 2\langle \gamma_1, \mathscr{L}_1^*\mathscr{Q}_2\mathscr{L}_2 M_2\mathscr{L}_2^*\mathscr{Q}_1 r\rangle - 2\langle r, \mathscr{Q}_2\mathscr{L}_2 M_2\mathscr{L}_2^*\mathscr{Q}_1 r\rangle - 2\langle \gamma_1, \mathscr{L}_1^*\mathscr{Q}_1\mathscr{L}_2 M_2\mathscr{L}_2^*\mathscr{Q}_2\mathscr{L}_1\gamma_1\rangle$$
$$- 2\langle \gamma_1, \mathscr{L}_1^*\mathscr{Q}_1\mathscr{L}_2 M_2\mathscr{L}_2^*\mathscr{Q}_2 r\rangle + \langle \gamma_1, \gamma_1\rangle + \langle \gamma_1, \mathscr{L}_1^*\mathscr{Q}_2\mathscr{L}_2 M_2 R M_2\mathscr{L}_2^*\mathscr{Q}_2\mathscr{L}_1\gamma_1\rangle +$$
$$\langle r, \mathscr{Q}_2\mathscr{L}_2 M_2 R M_2\mathscr{L}_2^*\mathscr{Q}_2 r\rangle + 2\langle \gamma_1, \mathscr{L}_1^*\mathscr{Q}_2\mathscr{L}_2 M_2 R M_2\mathscr{L}_2^*\mathscr{Q}_2 r\rangle. \tag{5.58}$$

After rearranging terms and substituting M_2, we get

$$E\{J_1\} = \langle \mathscr{Q}_1 x, x\rangle + \langle \gamma_1, \gamma_1\rangle + \langle \left[-(I+\mathscr{L}_2^*\mathscr{Q}_2\mathscr{L}_2)^{-1}\mathscr{L}_2^*\mathscr{Q}_2(\mathscr{L}_1\gamma_1+r)\right],$$
$$R\left[-(I+\mathscr{L}_2^*\mathscr{Q}_2\mathscr{L}_2)^{-1}\mathscr{L}_2^*\mathscr{Q}_2(\mathscr{L}_1\gamma_1+r)\right]\rangle,$$
$$= \langle \gamma_1, (I+\tilde{\mathscr{R}})\gamma_1\rangle + 2\langle \gamma_1, \tilde{\mathscr{L}}_1^*\mathscr{Q}_1\tilde{r}\rangle + \langle \mathscr{L}_1^*\mathscr{Q}_2\mathscr{L}_2(I+\mathscr{L}_2^*\mathscr{Q}_2\mathscr{L}_2)^{-1}R$$
$$(I+\mathscr{L}_2^*\mathscr{Q}_2\mathscr{L}_2)^{-1}\mathscr{L}_2^*\mathscr{Q}_2 r\rangle + J_{10}, \tag{5.59}$$

where

$$\tilde{\mathscr{R}} = \tilde{\mathscr{L}}_1^* \mathscr{Q}_1 \tilde{\mathscr{L}}_1 + \tilde{\mathscr{L}}_1^* \mathscr{Q}_2 \tilde{\mathscr{L}}_2 (I + \mathscr{L}_2^* \mathscr{Q}_2 \mathscr{L}_2)^{-1} R (I + \mathscr{L}_2^* \mathscr{Q}_2 \mathscr{L}_2)^{-1} \mathscr{L}_2^* \mathscr{Q}_2 \mathscr{L}_1, \quad (5.60)$$

$$\tilde{\mathscr{L}}_1 = \mathscr{L}_1 - \mathscr{L}_2 (I + \mathscr{L}_2^* \mathscr{Q}_2 \mathscr{L}_2)^{-1} \mathscr{L}_2^* \mathscr{Q}_2 \mathscr{L}_1, \quad (5.61)$$

$$\tilde{r} = (I - \mathscr{L}_2 (I + \mathscr{L}_2^* \mathscr{Q}_2 \mathscr{L}_2)^{-1} \mathscr{L}_2^* \mathscr{Q}_2) r. \quad (5.62)$$

J_{10} consists of the terms that are independent of γ_1 and $\tilde{\mathscr{L}}_1^*$ is the adjoint of $\tilde{\mathscr{L}}_1$. Since $(I + \mathscr{L}_2^* \mathscr{Q}_2 \mathscr{L}_2)^{-1}$ is strongly positive, and has a bounded inverse, taking variations with respect to γ_1, it can be shown that there exists a unique γ_1^* for which $E\{J_1\}$ has a minimum.

In order to express the control strategy of the follower in terms of the input matrices and the transition matrices, we need to determine the adjoint of $\mathscr{L}_1$ and $\mathscr{L}_2$. Let, the inner product $\mathscr{L}_k u_k$ be an arbitrary vector, that is

$$\mathscr{L}_k u_k(t,\omega) = \begin{bmatrix} \nu(t,\omega) & \nu(t_f,\omega) \end{bmatrix}'. \quad (5.63)$$

Then we write,

$$\begin{aligned} &\langle \nu_k, \mathscr{L}_k u_k \rangle \\ &= E\left\{ \int_{t_0}^{t_f} \nu_k'(t) \int_{t_0}^{t} \Phi(t,\tau) B_k(\tau) u_k(\tau,\omega) d\tau dt + \nu_k(t_f,\omega) \int_{t_0}^{t_f} \Phi(t_f,\tau) B_k(\tau) u_k(\tau,\omega) d\tau \right\} \\ &= E\left\{ \int_{t_0}^{t_f} u_k'(\tau,\omega) B_k'(\tau) \int_{t}^{t_f} \Phi'(t,\tau) \nu_k(t) dt d\tau + \nu_k(t_f,\omega) \int_{t_0}^{t_f} u_k'(\tau,\omega) B_k'(\tau) \Phi'(t_f,\tau) \right. \\ &\left. \times B_k(\tau) \nu_k(t_f,\omega) d\tau \right\}. \end{aligned} \quad (5.64)$$

Then, we find the adjoint of $\mathscr{L}_k$ is as follows:

$$\mathscr{L}_k^* \nu_k = B_k'(t) \int_t^{t_f} \Phi'(s,t) E\{\nu_k(s,\omega)|\sigma_k\} ds + B_k'(t) \Phi'(t_f,t) E\{\nu_k(t_f,\omega)|\sigma_k\}. \quad (5.65)$$

where σ_k indicates the sigma-algebra generated by the player information set of **Pk**.

Using (5.65) in (5.52) we obtain,

$$\gamma_2(t) = -B_2'(t) [S_2(t) E\{x(t)|\eta_2\} + \kappa_2(t)], \quad (5.66)$$

where,

$$\dot{S}_2(t) = -A'(t)S_2(t) - S_2(t)A(t) - Q_2(t) + S_2(t)B_2(t)B_2'(t)S_2(t), \tag{5.67}$$

$$S_2(t_f) = Q_{2f}, \tag{5.68}$$

$$\dot{\kappa}_2(t) = -\left[A'(t) - S_2(t)B_2(t)B_2'(t)\right]\kappa_2(t) - S_2(t)B_1(t)E\left\{\gamma_1(t,\eta_1)|\eta_2\right\}, \tag{5.69}$$

$$\kappa_2(t_f) = 0. \tag{5.70}$$

The detail derivation of (5.67)-(5.70) can be found in [111], [117].

Let us denote $E\{x|\eta_2\}$ by $\hat{x}_2(t)$. Then,

$$d\hat{x}_2(t) = \left[A(t) - B_2(t)B_2'(t)S_2(t)\right]\hat{x}_2(t)dt - B_2(t)B_2'(t)\kappa_2(t)dt + B_1E\left\{\gamma_1(t,\eta_1)|\eta_2\right\}dt, \tag{5.71}$$

$$\hat{x}_2(t_0) = E\left\{x(t_0)|\eta_2\right\} = E\left\{x_0|\eta_2\right\}. \tag{5.72}$$

Furthermore, if $\xi(t) = x(t) - \hat{x}_2(t)$, then

$$d\xi(t) = A(t)\xi(t) + B_1\gamma_1(t)dt - B_1(t)E\left\{\gamma_1(t)|\eta_2\right\}dt + F(t)dw(t), \quad \xi_{t_0} = x_0 - E\left\{x_0|\eta_2\right\}. \tag{5.73}$$

Note that at this point of derivation we are dealing with a different state dynamics (5.73) than in (5.21)

$$dx(t) = [A(t)x(t) + B_1(x)u_1(t) + B_2(x)u_2(t)]dt + F(t)dw(t), \qquad x(t_0) = x_0. \tag{5.74}$$

Now, in terms of the newly introduced variables $\hat{x}_2(t)$, $\xi(t)$, and $\kappa(t)$, we can express

$$\begin{aligned} J_1(\gamma_1, \mathfrak{T}_2^{21}\gamma_1) &= \hat{x}_2'(t_f)Q_{1f}\hat{x}_2(t_f) + \xi'(t_f)Q_{1f}\xi(t_f) \\ &+ \int_{t_0}^{t_f}\left[\hat{x}_2'(t)Q_1(t)\hat{x}_2(t) + \xi'(t)Q_1\xi(t)\right]dt \\ &+ \int_{t_0}^{t_f}\left[\left\{\hat{x}_2'(t)S_2(t)\kappa_2'(t)\right\}B_2(t)R(t)B_2'(t)\left\{S_2(t)\hat{x}_2(t) + \kappa_2(t)\right\} + \gamma_1'(t,\eta_1)\gamma_1(t,\eta_1)\right]dt. \end{aligned} \tag{5.75}$$

Thus, the statistical game problem is to determine the strategy $\gamma_1^*(t)$ of the leader to minimize

$$Var\left\{J_1(\gamma_1, \mathfrak{T}_2^{21}\gamma_1)\right\} = E\left\{J_1(\gamma_1, \mathfrak{T}_2^{21}\gamma_1) - E\left\{J_1(\gamma_1, \mathfrak{T}_2^{21}\gamma_1)\right\}\right\}^2, \tag{5.76}$$

with the constraints,

$$E\left\{J_1(\gamma_1, \mathfrak{T}_2^{21}\gamma_1)\right\} = M, \tag{5.77}$$

M is bounded below by the positive solution of the optimal $E\left\{J_1(\gamma_1, T_2^{21}\gamma_1)\right\}$. Here, we assume that the follower **P2** minimizes the mean of his cost function. In the earlier work, Bagchi and Başar [46] obtained the strategy for the leader to minimize $E\left\{J_1(\gamma_1, \mathfrak{T}_2^{11}\gamma_1)\right\}$.

5.4.5 Digression: Solution of A Special Open Loop MCV Control Problem

In this section, we derive a minimal cost variance control strategy for a special stochastic system. This is a special case, where the expected value of control input is considered in the stochastic system equation. The solution of this optimization problem will be used in the later section to derive the Stackelberg strategies.

Lemma 5.1. *We consider a problem of choosing a control strategy γ to minimize the variance of a quadratic cost function, $Var\{J(\gamma)\}$ such that the cost function is:*

$$J(\gamma) = x'(t_f)Q_f x(t_f) + \int_{t_0}^{t_f} [x'(t)Q(t)x(t) + \gamma'(t)R(t)\gamma(t)]dt, \tag{5.78}$$

with the constraint that the mean of the cost function $E\{J(\gamma)\} = M$, where M is bounded by the positive solution of the optimal $E\{J(\gamma)\}$. $Q(t)$, Q_f, and $R(t)$ are positive semi-definite matrices.

Also, we consider a stochastic system described by:

$$dx(t) = [A(t)x(t) + B(t)\gamma(t,\eta)]\,dt + C(t)E\{\gamma(t,\eta) \mid \phi\}\,dt + d\theta(t), \tag{5.79}$$

where the state $x(t)$ is a n-tuple vector, the observation η is a p-tuple vector, and ϕ is q-tuple random vector. The admissible control γ is such that $\gamma : [t_0, t_f] \times \mathbb{R}^p \to \mathbb{R}^m$, and γ is defined over Γ, where Γ is a linear vector space. The Brownian motion $\theta(t)$ is a n-tuple vector with zero mean and covariance $\Theta(t)$. We also assume that this noise process is independent of the initial state $x(t_0)$. This gives us:

$$E\{\theta(t)\} = 0,$$
$$E\left\{\theta(t)\theta'(t)\right\} = \Theta(t)\delta(t-\tau).$$

A, B, and C are appropriate dimension matrices.

A control strategy $\gamma \in \Gamma$ provides a minimizing solution to the stochastic optimal control problem if it satisfies the following equations:

$$\gamma^*(t) = -\frac{1}{2\mu} R^{-1}(t) B'(t) \rho(t), \tag{5.80}$$

if it satisfies the differential equations

$$dz(t) = A(t)z(t)dt - \frac{1}{2\mu} B(t)R^{-1}(t)B'(t)\rho(t)dt, \tag{5.81}$$

$$d\rho(t) = -A'(t)\rho(t)dt - 2\mu Q(t)z(t)dt - 8Q(t)\upsilon(t)dt, \tag{5.82}$$

$$d\upsilon(t) = A(t)\upsilon(t)dt + \left[C(t)E\left\{E\left\{\gamma(t,\eta)\right\}E\left\{\gamma'(t,\eta)\right\}\right\}C'(t) + \Theta\right]\varphi(t)dt, \tag{5.83}$$

$$d\varphi(t) = -A'(t)\varphi(t)dt - Q(t)z(t)dt. \tag{5.84}$$

with the boundary conditions

$$z(t_0) = x_0, \tag{5.85}$$

$$\rho(t_f) = 2\mu Q_f z(t_f) + 8Q_f \upsilon(t_f), \tag{5.86}$$

$$\upsilon(t_0) = 0, \tag{5.87}$$

$$\varphi(t_f) = Q_f z(t_f). \tag{5.88}$$

Proof. We consider a stochastic system described by the following stochastic differential equation,

$$dx(t) = [A(t)x(t) + B(t)\gamma(t,\eta)]\,dt + C(t)E\left\{\gamma(t,\eta) \mid \phi\right\}dt + d\theta(t), \tag{5.89}$$

with the quadratic cost function

$$J(\gamma) = x'(t_f)Q_f x(t_f) + \int_{t_0}^{t_f} [x'(t)Q(t)x(t) + \gamma'(t)R(t)\gamma(t)]dt. \tag{5.90}$$

Our problem is to determine $\gamma \in \Gamma$ for which the variance of the cost function $Var\{J(\gamma)\}$ attains a minimum with the constraint that the mean of the cost function $E\{J(\gamma)\} = M$, where M is a constant.

We decompose the state $x(t)$ into two parts $z(t)$ and $w(t)$, where $z(t)$ is deterministic and $w(t)$ is stochastic.

$$x(t) = z(t) + w(t), \tag{5.91}$$

These $z(t)$ and $w(t)$ are defined by,

$$dz(t) = [A(t)z(t) + B(t)\gamma(t)]dt, \quad z(t_0) = x_0, \tag{5.92}$$

$$dw(t) = A(t)dw(t) + C(t)E\{\gamma(t,\eta)|\psi\}dt + d\theta(t) \quad w(t_0) = 0, \tag{5.93}$$

where the mean and covariance of $w(t)$ is defined by,

$$E\{w(t)\} = 0, \tag{5.94}$$

$$E\left\{w(t)w'(t)\right\} = \mathscr{W}(t)\delta(t-\tau). \tag{5.95}$$

Therefore, $z(t)$ is the expected value of $x(t)$.

First, we determine the mean of the cost function in terms of $z(t)$ and $w(t)$. Let us calculate some necessary product terms which we need repeatedly. We start with

$$\begin{aligned} & x'(t)Q(t)x(t) \\ & = (z(t)+w(t))'Q(t)(z(t)+w(t)), \\ & = z'(t)Q(t)z(t) + z'(t)Q(t)w(t) + w'(t)Q(t)z(t) + w'(t)Q(t)w(t). \end{aligned} \tag{5.96}$$

Taking expectation on (5.96) we have,

$$\begin{aligned} & E\left\{x'(t)Q(t)x(t)\right\} \\ & = E\left\{z'(t)Q(t)z(t) + z'(t)Q(t)w(t) + w'(t)Q(t)z(t) + w'(t)Q(t)w(t)\right\}, \\ & = E\left\{z'(t)Q(t)z(t)\right\} + z'(t)Q(t)E\left\{w(t)\right\} + E\left\{w'(t)\right\}Q(t)z(t) + E\left\{w'(t)Q(t)w(t)\right\}, \\ & = E\left\{z'(t)Q(t)z(t)\right\} + E\left\{w'(t)Q(t)w(t)\right\}, \quad \text{(using (5.94))} \end{aligned} \tag{5.97}$$

Similarly,

$$\begin{aligned} & x'(t_f)Q_f x(t_f) \\ & = (z(t_f)+w(t_f))'Q_f(z(t_f)+w(t_f)), \\ & = z'(t_f)Q_f z(t_f) + z'(t_f)Q_f w(t_f) + w'(t_f)Q_f z(t_f) + w'(t_f)Q_f w(t_f), \end{aligned} \tag{5.98}$$

and

$$
\begin{aligned}
&E\left\{x'(t_f)Q_f x(t_f)\right\} \\
&= E\left\{z'(t_f)Q_f z(t_f) + z'(t_f)Q_f w(t_f) + w'(t_f)Q_f z(t_f) + w'(t_f)Q_f w(t_f)\right\}, \\
&= E\left\{z'(t_f)Q_f z(t_f)\right\} + z'(t_f)Q_f E\left\{w(t_f)\right\} + E\left\{w'(t_f)\right\}Q_f z(t_f) + E\left\{w'(t_f)Q_f w(t_f)\right\}, \\
&= E\left\{z'(t_f)Q_f z(t_f)\right\} + E\left\{w'(t_f)Q_f w(t_f)\right\}. \qquad (5.99)
\end{aligned}
$$

Now, taking expectation on (5.90), we have

$$
\begin{aligned}
E\{J\} &= E\left\{x'(t_f)Q_f x(t_f) + \int_{t_0}^{t_f}\left\{x'(t)Q(t)x(t) + \gamma'(t)R(t)\gamma(t)\right\}dt\right\}, \\
&= E\left\{x'(t_f)Q_f x(t_f)\right\} + E\left\{\int_{t_0}^{t_f} x'(t)Q(t)x(t)dt\right\} + E\left\{\int_{t_0}^{t_f}\gamma'(t)Q(t)\gamma(t)dt\right\}, \\
&= E\left\{z'(t_f)Q_f z(t_f)\right\} + E\left\{w'(t_f)Q_f w(t_f)\right\} + E\left\{\int_{t_0}^{t_f} z'(t)Q(t)z(t)dt\right\} \\
&+ E\left\{\int_{t_0}^{t_f} w'(t)Q(t)w(t)dt\right\} + \int_{t_0}^{t_f}\gamma'(t)R(t)\gamma(t)dt, \\
&= z'(t_f)Q_f z(t_f) + \int_{t_0}^{t_f}\left\{z'(t)Q(t)z(t) + \gamma'(t)R(t)\gamma(t)\right\}dt \\
&+ E\left\{w'(t_f)Q_f w(t_f)\right\} + E\left\{\int_{t_0}^{t_f} w'(t)Q(t)w(t)dt\right\}, \\
&= z'(t_f)Q_f z(t_f) + \int_{t_0}^{t_f}\left\{z'(t)Q(t)z(t) + \gamma'(t)R(t)\gamma(t)\right\}dt + E\{\alpha\}, \qquad (5.100)
\end{aligned}
$$

where

$$
\alpha = w'(t_f)Q_f w(t_f) + \int_{t_0}^{t_f} w'(t)Q(t)w(t)dt. \qquad (5.101)
$$

In order to determine the variance of the cost function, we use the following expression,

$$
Var\{J\} = E\left\{J^2\right\} - \{E\{J\}\}^2. \qquad (5.102)
$$

We determine $\{E\{J\}\}^2$ as follows:

$$
\begin{aligned}
&\{E\{J\}\}^2 \\
&= \left\{ z'(t_f)Q_f z(t_f) + \int_{t_0}^{t_f} \left\{ z'(t)Q(t)z(t) + \gamma'(t)R(t)\gamma(t) \right\} dt + E\left\{ w'(t_f)Q_f w(t_f) \right\} \right. \\
&\left. + E\left\{ \int_{t_0}^{t_f} w'(t)Q(t)w(t)dt \right\} \right\}^2 \\
&= \{z'(t_f)Q_f z(t_f)\{z'(t_f)Q_f z(t_f) + \int_{t_0}^{t_f}\int_{t_0}^{t_f} z'(t)Q(t)z(t)z'(s)Q(s)z(s)dsdt \\
&+ \int_{t_0}^{t_f}\int_{t_0}^{t_f} \gamma'(t)R(t)\gamma(t)\gamma'(s)R(s)\gamma(s)dt + E\left\{ w'(t_f)Q_f w(t_f) \right\} E\left\{ w'(t_f)Q_f w(t_f) \right\} \\
&+ E\left\{ \int_{t_0}^{t_f} w'(t)Q(t)w(t)dt \right\} E\left\{ \int_{t_0}^{t_f} w'(t)Q(t)w(t)dt \right\} + 2z'(t_f)Q_f z(t_f)\int_{t_0}^{t_f} z'(t)Q(t)z(t)dt \\
&+ 2\int_{t_0}^{t_f} z'(t)Q(t)z(t)dt \int_{t_0}^{t_f} \gamma'(s)R(s)\gamma(s)ds + 2\int_{t_0}^{t_f} \gamma'(t)R(t)\gamma(t)dt E\left\{ w'(t_f)Q_f w(t_f) \right\} \\
&+ 2E\left\{ w'(t_f)Q_f w(t_f) \right\} E\left\{ \int_{t_0}^{t_f} w'(t)Q(t)w(t)dt \right\} + 2z'(t_f)Q_f z(t_f)\int_{t_0}^{t_f} \gamma'(t)R(t)\gamma(t)dt \\
&+ 2z'(t_f)Q_f z(t_f)E\left\{ w'(t_f)Q_f w(t_f) \right\} + 2z'(t_f)Q_f z(t_f)E\left\{ \int_{t_0}^{t_f} w'(t)Q(t)w(t)dt \right\} \\
&+ 2\int_{t_0}^{t_f} z'(t)Q(t)z(t)dt E\left\{ w'(t_f)Q_f w(t_f) \right\} + 2\int_{t_0}^{t_f} z'(t)Q(t)z(t)dt E\left\{ \int_{t_0}^{t_f} w'(t)Q(t)w(t)dt \right\} \\
&+ 2\int_{t_0}^{t_f} \gamma'(t)R(t)\gamma(t)dt E\left\{ \int_{t_0}^{t_f} w'(t)Q(t)w(t)dt \right\}. \qquad (5.103)
\end{aligned}
$$

Next, we determine J^2 and the second moment of the cost function $E[J^2]$.

$$
\begin{aligned}
J^2 &= \left\{ x'(t_f)Q_f x(t_f) + \int_{t_0}^{t_f} [x'(t)Q(t)x(t) + \gamma'(t)R(t)\gamma(t)]dt \right\}^2 \\
&= x'(t_f)Q_f x(t_f)x'(t_f)Q_f x(t_f) \\
&+ \int_{t_0}^{t_f} [x'(t)Q(t)x(t) + \gamma'(t)R(t)\gamma(t)]dt \int_{t_0}^{t_f} [x'(s)Q(s)x(s) + \gamma'(s)R(s)\gamma(s)]ds \\
&+ 2x'(t_f)Q_f x(t_f)\int_{t_0}^{t_f} [x'(t)Q(t)x(t) + \gamma'(t)R(t)\gamma(t)]dt \\
&= Js_1 + Js_2 + Js_3 \qquad (5.104)
\end{aligned}
$$

By expanding the first term of (5.104), we have

$$
\begin{aligned}
Js_1 &= x'(t_f)Q_f x(t_f)x'(t_f)Q_f x(t_f) \\
&= \left\{z'(t_f)Q_f z(t_f) + z'(t_f)Q_f w(t_f) + w'(t_f)Q_f z(t_f) + w'(t_f)Q_f w(t_f)\right\} \\
&\left\{(z'(t_f)Q_f z(t_f) + z'(t_f)Q_f w(t_f) + w'(t_f)Q_f z(t_f) + w'(t_f)Q_f w(t_f)\right\} \\
&= z'(t_f)Q_f z(t_f)z'(t_f)Q_f z(t_f) + z'(t_f)Q_f z(t_f)z'(t_f)Q_f w(t_f) + z'(t_f)Q_f z(t_f)w'(t_f)Q_f z(t_f) \\
&+ z'(t_f)Q_f z(t_f)w'(t_f)Q_f(t_f)w(t_f) + z'(t_f)Q_f w(t_f)z'(t_f)Q_f z(t_f) \\
&+ z'(t_f)Q_f w(t_f)z'(t_f)Q_f w(t_f) + z'(t_f)Q_f w(t_f)w'(t_f)Q_f z(t_f) \\
&+ z'(t_f)Q_f w(t_f)w'(t_f)Q_f w(t_f) + w'(t_f)Q_f z(t_f)z'(t_f)Q_f z(t_f) \\
&+ w'(t_f)Q_f z(t_f)z'(t_f)Q_f w(t_f) + w'(t_f)Q_f z(t_f)w'(t_f)Q_f z(t_f) \\
&+ w'(t_f)Q_f z(t_f)w'(t_f)Q_f w(t_f) + w'(t_f)Q_f w(t_f)z'(t_f)Q_f z(t_f) \\
&+ w'(t_f)Q_f w(t_f)z'(t_f)Q_f w(t_f) + w'(t_f)Q_f w(t_f)w'(t_f)Q_f z(t_f) \\
&+ w'(t_f)Q_f w(t_f)w'(t_f)Q_f w(t_f). \qquad (5.105)
\end{aligned}
$$

Taking expectation on (5.105), we have,

$$
\begin{aligned}
E\{Js_1\} &= E\left\{z'(t_f)Q_f z(t_f)z'(t_f)Q_f z(t_f)\right\} + E\left\{z'(t_f)Q_f w(t_f)z'(t_f)Q_f w(t_f)\right\} \\
&+ E\left\{w'(t_f)Q_f z(t_f)w'(t_f)Q_f z(t_f)\right\} + E\left\{w'(t_f)Q_f w(t_f)w'(t_f)Q_f w(t_f)\right\} \qquad (5.106) \\
&+ 2E\left\{z'(t_f)Q_f z(t_f)w'(t_f)Q_f w(t_f)\right\} + 2E\left\{z'(t_f)Q_f w(t_f)w'(t_f)Q_f z(t_f)\right\}. \qquad (5.107)
\end{aligned}
$$

The second term of (5.104) gives,

$$
\begin{aligned}
Js_2 &= \int_{t_0}^{t_f}[x'(t)Q(t)x(t) + \gamma'(t)R(t)\gamma(t)]dt \int_{t_0}^{t_f}[x'(s)Q(s)x(s) + \gamma'(s)R(s)\gamma(s)]ds, \\
&= \int_{t_0}^{t_f}\int_{t_0}^{t_f} x'(t)Q(t)x(t)x'(s)Q(s)x(s)dsdt + \int_{t_0}^{t_f}\int_{t_0}^{t_f} \gamma'(t)R(t)\gamma(t)\gamma'(s)R(s)\gamma(s)dsdt \\
&+ 2\int_{t_0}^{t_f}\int_{t_0}^{t_f} x'(t)Q(t)x(t)\gamma'(s)R(s)\gamma(s)dsdt. \qquad (5.108)
\end{aligned}
$$

Taking expectation on (5.108), we have

$$
\begin{aligned}
&E\{Js_2\}\\
=&E\left\{\int_{t_0}^{t_f}\int_{t_0}^{t_f} x'(t)Q(t)x(t)x'(s)Q(s)x(s)dsdt+\int_{t_0}^{t_f}\int_{t_0}^{t_f}\gamma'(t)R(t)\gamma(t)\gamma'(s)R(s)\gamma(s)dsdt\right\}\\
&+2E\left\{\int_{t_0}^{t_f}\int_{t_0}^{t_f} x'(t)Q(t)x(t)\gamma'(s)R(s)\gamma(s)dsdt\right\}\\
&=E[\int_{t_0}^{t_f}\int_{t_0}^{t_f}[z'(t)Q(t)z(t)z'(t)Q(t)z(t)+z'(t)Q(t)z(t)z'(t)Q(t)w(t)+z'(t)Q(t)z(t)w'(t)Q(t)z(t)\\
&+z'(t)Q(t)z(t)w'(t)Q(t)w(t)+z'(t)Q(t)w(t)z'(t)Q(t)z(t)+z'(t)Q(t)w(t)z'(t)Q(t)w(t)\\
&+z'(t)Q(t)w(t)w'(t)Q(t)z(t)+z'(t)Q(t)w(t)w'(t)Q(t)w(t)+w'(t)Q(t)z(t)z'(t)Q(t)z(t)\\
&+w'(t)Q(t)z(t)z'(t)Q(t)w(t)+w'(t)Q(t)z(t)w'(t)Q(t)z(t)+w'(t)Q(t)z(t)w'(t)Q(t)w(t)\\
&+w'(t)Q(t)w(t)z'(t)Q(t)z(t)+w'(t)Q(t)w(t)z'(t)Q(t)w(t)+w'(t)Q(t)w(t)w'(t)Q(t)z(t)\\
&+w'(t)Q(t)w(t)w'(s)Q(s)w(s)]dsdt]+\int_{t_0}^{t_f}\int_{t_0}^{t_f}\gamma'(t)Q(t)\gamma(t)\gamma'(s)R(s)\gamma(s)dsdt\\
&+2\int_{t_0}^{t_f}\int_{t_0}^{t_f}\gamma'(s)R(s)\gamma(s)E[z'(t)Q(t)z(t)dsdt]+2\int_{t_0}^{t_f}\int_{t_0}^{t_f}\gamma'(s)R(s)\gamma(s)E[w'(s)Q(s)w(s)]dsdt,\\
&=E\left\{\int_{t_0}^{t_f}\int_{t_0}^{t_f} z'(t)Q(t)z(t)z'(s)Q(s)z(s)dsdt\right\}+E\left\{\int_{t_0}^{t_f}\int_{t_0}^{t_f} z'(t)Q(t)w(t)z'(s)Q(s)w(s)dsdt\right\}\\
&+E\left\{\int_{t_0}^{t_f}\int_{t_0}^{t_f} w'(t)Q(t)z(t)w'(s)Q(s)z(s)dsdt\right\}+E\left\{\int_{t_0}^{t_f}\int_{t_0}^{t_f} w'(t)Q(t)w(t)w'(s)Q(s)w(s)dsdt\right\}\\
&+2E\left\{\int_{t_0}^{t_f}\int_{t_0}^{t_f} z'(t)Q(t)w(t)w'(t)Q(t)z(t)dsdt\right\}+2E\left\{\int_{t_0}^{t_f}\int_{t_0}^{t_f} w'(t)Q(t)w(t)z'(s)Q(s)z(s)dsdt\right\}\\
&+\int_{t_0}^{t_f}\int_{t_0}^{t_f}\gamma'(t)Q(t)\gamma(t)\gamma'(s)R(s)\gamma(s)dsdt+2E\left\{\int_{t_0}^{t_f}\int_{t_0}^{t_f} z'(t)Q(t)z(t)\gamma'(s)R(s)\gamma(s)dsdt\right\}\\
&+2E\left\{\int_{t_0}^{t_f}\int_{t_0}^{t_f} w'(t)Q(t)w(t)\gamma'(s)R(s)\gamma(s)dsdt\right\}. \qquad (5.109)
\end{aligned}
$$

The third term of (5.104) gives,

$$
\begin{aligned}
Js_3&=2x'(t_f)Q_f x(t_f)\int_{t_0}^{t_f}[x'(t)Q(t)x(t)+\gamma'(t)R(t)\gamma(t)]dt,\\
&=2x'(t_f)Q_f x(t_f)\int_{t_0}^{t_f} x'(t)Q(t)x(t)dt+2x'(t_f)Q_f x(t_f)\int_{t_0}^{t_f}\gamma'(t)R(t)\gamma(t)dt,\\
&=2[z'(t_f)Q_f z(t_f)+z'(t_f)Q_f w(t_f)+w'(t_f)Q_f z(t_f)+w'(t_f)Q_f w(t_f)]\\
&\cdot\int_{t_0}^{t_f}[z'(t)Q(t)z(t)+z'(t)Q(t)w(t)+w'(t)Q(t)z(t)+w'(t)Q(t)w(t)]dt\\
&+2[z'(t_f)Q_f z(t_f)+z'(t_f)Q_f w(t_f)+w'(t_f)Q_f z(t_f)+w'(t_f)Q_f w(t_f)] \qquad (5.110)\\
&\times\int_{t_0}^{t_f}\gamma'(t)R(t)\gamma(t)dt. \qquad (5.111)
\end{aligned}
$$

Taking expectation on (5.111), we have

$$
\begin{aligned}
&E\{Js_3\} = E\left\{2[z'(t_f)Q_f z(t_f) + z'(t_f)Q_f w(t_f) + w'(t_f)Q_f z(t_f) + w'(t_f)Q_f w(t_f)\right\} \\
&\cdot \int_{t_0}^{t_f} [z'(t)Q(t)z(t) + z'(t)Q(t)w(t) + w'(t)Q(t)z(t) + w'(t)Q(t)w(t)] \\
&+ E\left\{2[z'(t_f)Q_f z(t_f) + z'(t_f)Q_f w(t_f) + w'(t_f)Q_f z(t_f) + w'(t_f)Q_f w(t_f)\right\} \\
&\cdot \int_{t_0}^{t_f} \gamma'(t)R(t)\gamma(t)dt], \\
&= 2E[z'(t_f)Q_f z(t_f) \int_{t_0}^{t} z'(t)Q_(t)z(t)dt + z'(t_f)Q_f z(t_f) \int_{t_0}^{t_f} z'(t)Q(t)w(t)dt \\
&+ z'(t_f)Q_f z(t_f) \int_{t_0}^{t_f} w'(t)Q(t)z(t)dt + z'(t_f)Q_f z(t_f) \int_{t_0}^{t_f} w'(t)Q(t)w(t)dt \\
&+ z'(t_f)Q_f w(t_f) \int_{t_0}^{t_f} z'(t)Q(t)z(t) + z'(t_f)Q_f w(t_f) \int_{t_0}^{t_f} z'(t)Q(t)w(t)dt \\
&+ z'(t_f)Q_f w(t_f) \int_{t_0}^{t_f} w'(t)Q(t)z(t)dt + z'(t_f)Q_f w(t_f) \int_{t_0}^{t_f} w'(t)Q(t)w(t)dt \\
&+ w'(t_f)Q_f z(t_f) \int_{t_0}^{t_f} z'(t)Q(t)z(t)dt + w'(t_f)Q_f z(t_f) \int_{t_0}^{t_f} z'(t)Q(t)w(t)dt \\
&+ w'(t_f)Q_f z(t_f) \int_{t_0}^{t_f} w'(t)Q(t)z(t)dt + w'(t_f)Q_f z(t_f) \int_{t_0}^{t_f} w'(t)Q(t)w(t)dt \\
&+ w'(t_f)Q_f w(t_f) \int_{t_0}^{t_f} z'(t)Q(t)z(t)dt + w'(t_f)Q_f w(t_f) \int_{t_0}^{t_f} z'(t)Q(t)w(t)dt \\
&+ w'(t_f)Q_f w(t_f) \int_{t_0}^{t_f} w'(t)Q(t)z(t)dt + w'(t_f)Q_f w(t_f) \int_{t_0}^{t_f} w'(t)Q(t)w(t)dt] \\
&+ 2E[z'(t_f)Q_f z(t_f) + w'(t_f)Q_f w(t_f)] \int_{t_0}^{t_f} \gamma'(t)R(t)\gamma(t)dt, \\
&= 2E\left\{z'(t_f)Q_f z(t_f) \int_{t_0}^{t_f} z'(t)Q(t)z(t)dt\right\} + 2E\left\{z'(t_f)Q_f z(t_f) \int_{t_0}^{t_f} w'(t)Q(t)w(t)dt\right\} \\
&+ 2E\left\{z'(t_f)Q_f w(t_f) \int_{t_0}^{t_f} z'(t)Q(t)w(t)dt\right\} + 2E\left\{z'(t_f)Q_f w(t_f) \int_{t_0}^{t_f} w'(t)Q(t)z(t)dt\right\} \\
&+ 2E\left\{w'(t_f)Q_f z(t_f) \int_{t_0}^{t_f} z'(t)Q(t)w(t)dt\right\} + 2E\left\{w'(t_f)Q_f z(t_f) \int_{t_0}^{t_f} w'(t)Q(t)z(t)dt\right\} \\
&+ 2E\left\{w'(t_f)Q_f w(t_f) \int_{t_0}^{t_f} z'(t)Q(t)z(t)dt\right\} + 2E\left\{w'(t_f)Q_f w(t_f) \int_{t_0}^{t_f} w'(t)Q(t)w(t)dt\right\} \\
&+ 2E\left\{z'(t_f)Q_f z(t_f) \int_{t_0}^{t_f} \gamma'(t)R(t)\gamma(t)dt\right\} + 2E\left\{w'(t_f)Q_f w(t_f) \int_{t_0}^{t_f} \gamma'(t)R(t)\gamma(t)dt\right\}.
\end{aligned}
\tag{5.112}
$$

Combining (5.107), (5.109), and (5.112) we have

$$
\begin{aligned}
&E\left\{J^2\right\} = E\left\{Js_1\right\} + E\left\{Js_2\right\} + E\left\{Js_3\right\},\\
&= E\left\{z'(t_f)Q_f z(t_f) z'(t_f)Q_f z(t_f)\right\} + E\left\{z'(t_f)Q_f w(t_f) z'(t_f)Q_f w(t_f)\right\}\\
&+ E\left\{w'(t_f)Q_f z(t_f) w'(t_f)Q_f z(t_f)\right\} + E\left\{w'(t_f)Q_f w(t_f) w'(t_f)Q_f w(t_f)\right\}\\
&+ 2E\left\{z'(t_f)Q_f z(t_f) w'(t_f)Q_f w(t_f)\right\} + 2E\left\{z'(t_f)Q_f w(t_f) w'(t_f)Q_f z(t_f)\right\}\\
&+ E\left\{\int_{t_0}^{t_f}\int_{t_0}^{t_f} z'(t)Q(t)z(t)z'(t)Q(t)z(t)dsdt\right\} + E\left\{\int_{t_0}^{t_f}\int_{t_0}^{t_f} z'(t)Q(t)w(t)z'(s)Q(s)w(s)dsdt\right\}\\
&+ E\left\{\int_{t_0}^{t_f}\int_{t_0}^{t_f} w'(t)Q(t)z(t)w'(s)Q(s)z(s)dsdt\right\} + E\left\{\int_{t_0}^{t_f}\int_{t_0}^{t_f} w'(t)Q(t)w(t)w'(s)Q(s)w(s)dsdt\right\}\\
&+ 2E\left\{\int_{t_0}^{t_f}\int_{t_0}^{t_f} z'(t)Q(t)w(t)w'(t)Q(t)z(t)dsdt\right\} + 2E\left\{\int_{t_0}^{t_f}\int_{t_0}^{t_f} w'(t)Q(t)w(t)z'(t)Q(t)z(t)dsdt\right\}\\
&+ \int_{t_0}^{t_f}\int_{t_0}^{t_f} \gamma'(t)Q(t)\gamma(t)\gamma'(s)R(s)\gamma(s)dsdt + 2E\left\{\int_{t_0}^{t_f}\int_{t_0}^{t_f} z'(t)Q(t)z(t)\gamma'(s)R(s)\gamma(s)dsdt\right\}\\
&+ 2E\left\{\int_{t_0}^{t_f}\int_{t_0}^{t_f} w'(t)Q(t)w(t)\gamma'(s)R(s)\gamma(s)dsdt\right\}\\
&+ 2E\left\{z'(t_f)Q_f z(t_f)\int_{t_0}^{t_f} z'(t)Q(t)z(t)dt\right\} + 2E\left\{z'(t_f)Q_f z(t_f)\int_{t_0}^{t_f} w'(t)Q(t)w(t)dt\right\}\\
&+ 2E\left\{z'(t_f)Q_f w(t_f)\int_{t_0}^{t_f} z'(t)Q(t)w(t)dt\right\} + 2E\left\{z'(t_f)Q_f w(t_f)\int_{t_0}^{t_f} w'(t)Q(t)z(t)dt\right\}\\
&+ 2E\left\{w'(t_f)Q_f z(t_f)\int_{t_0}^{t_f} z'(t)Q(t)w(t)dt\right\} + 2E\left\{w'(t_f)Q_f z(t_f)\int_{t_0}^{t_f} w'(t)Q(t)z(t)dt\right\}\\
&+ 2E\left\{w'(t_f)Q_f w(t_f)\int_{t_0}^{t_f} z'(t)Q(t)z(t)dt\right\} + 2E\left\{w'(t_f)Q_f w(t_f)\int_{t_0}^{t_f} w'(t)Q(t)w(t)dt\right\}\\
&+ 2E\left\{z'(t_f)Q_f z(t_f)\int_{t_0}^{t_f} \gamma'(t)R(t)\gamma(t)dt\right\} + 2E\left\{w'(t_f)Q_f w(t_f)\int_{t_0}^{t_f} \gamma'(t)R(t)\gamma(t)dt\right\}. \qquad (5.113)
\end{aligned}
$$

Substituting (5.113) and (5.103) in (5.102), we have

$$
\begin{aligned}
Var\{J\} &= E\left\{z'(t_f)Q_f z(t_f) z'(t_f)Q_f z(t_f)\right\} + E\left\{z'(t_f)Q_f w(t_f) z'(t_f)Q_f w(t_f)\right\} \\
&+ E\left\{w'(t_f)Q_f z(t_f) w'(t_f)Q_f z(t_f)\right\} + E\left\{w'(t_f)Q_f w(t_f) w'(t_f)Q_f w(t_f)\right\} \\
&+ 2E\left\{z'(t_f)Q_f z(t_f) w'(t_f)Q_f w(t_f)\right\} + 2E\left\{z'(t_f)Q_f w(t_f) w'(t_f)Q_f z(t_f)\right\} \\
&+ E\left\{\int_{t_0}^{t_f}\int_{t_0}^{t_f} z'(t)Q(t)z(t)z'(s)Q(s)z(s)dsdt\right\} + E\left\{\int_{t_0}^{t_f}\int_{t_0}^{t_f} z'(t)Q(t)w(t)z'(s)Q(s)w(s)dsdt\right\} \\
&+ E\left\{\int_{t_0}^{t_f}\int_{t_0}^{t_f} w'(t)Q(t)z(t)w'(s)Q(s)z(s)dsdt\right\} + E\left\{\int_{t_0}^{t_f}\int_{t_0}^{t_f} w'(t)Q(t)w(t)w'(s)Q(s)w(s)dsdt\right\} \\
&+ 2E\left\{\int_{t_0}^{t_f}\int_{t_0}^{t_f} z'(t)Q(t)w(t)w'(t)Q(t)z(t)dsdt\right\} + 2E\left\{\int_{t_0}^{t_f}\int_{t_0}^{t_f} w'(t)Q(t)w(t)z'(s)Q(s)z(s)dsdt\right\} \\
&+ \int_{t_0}^{t_f}\int_{t_0}^{t_f} \gamma'(t)Q(t)\gamma(t)\gamma'(s)R(s)\gamma(s)dsdt + 2E\left\{\int_{t_0}^{t_f}\int_{t_0}^{t_f} z'(t)Q(t)z(t)\gamma'(s)R(s)\gamma(s)dsdt\right\} \\
&+ 2E\left\{\int_{t_0}^{t_f}\int_{t_0}^{t_f} w'(t)Q(t)w(t)\gamma'(s)R(s)\gamma(s)dsdt\right\} \\
&+ 2E\left\{z'(t_f)Q_f z(t_f)\int_{t_0}^{t_f} z'(t)Q(t)z(t)dt\right\} + 2E\left\{z'(t_f)Q_f z(t_f)\int_{t_0}^{t_f} w'(t)Q(t)w(t)dt\right\} \\
&+ 2E\left\{z'(t_f)Q_f w(t_f)\int_{t_0}^{t_f} z'(t)Q(t)w(t)dt\right\} + 2E\left\{z'(t_f)Q_f w(t_f)\int_{t_0}^{t_f} w'(t)Q(t)z(t)dt\right\} \\
&+ 2E\left\{w'(t_f)Q_f z(t_f)\int_{t_0}^{t_f} z'(t)Q(t)w(t)dt\right\} + 2E\left\{w'(t_f)Q_f z(t_f)\int_{t_0}^{t_f} w'(t)Q(t)z(t)dt\right\} \\
&+ 2E\left\{w'(t_f)Q_f w(t_f)\int_{t_0}^{t_f} z'(t)Q(t)z(t)dt\right\} + 2E\left\{w'(t_f)Q_f w(t_f)\int_{t_0}^{t_f} w'(t)Q(t)w(t)dt\right\} \\
&+ 2E\left\{z'(t_f)Q_f z(t_f)\int_{t_0}^{t_f} \gamma'(t)R(t)\gamma(t)dt\right\} + 2E\left\{w'(t_f)Q_f w(t_f)\int_{t_0}^{t_f} \gamma'(t)R(t)\gamma(t)dt\right\} \\
&- z'(t_f)Q_f z(t_f) z'(t_f)Q_f z(t_f) - \int_{t_0}^{t_f}\int_{t_0}^{t_f} z'(t)Q(t)z(t)z'(s)Q(s)z(s)dsdt \\
&- \int_{t_0}^{t_f}\int_{t_0}^{t_f} \gamma'(t)R(t)\gamma(t)\gamma'(s)R(s)\gamma(s)dt - E\left\{w'(t_f)Q_f w(t_f)\right\} E\left\{w'(t_f)Q_f w(t_f)\right\} \\
&- E\left\{\int_{t_0}^{t_f} w'(t)Q(t)w(t)dt\right\} E\left\{\int_{t_0}^{t_f} w'(t)Q(t)w(t)dt\right\} - 2z'(t_f)Q_f z(t_f)\int_{t_0}^{t_f} z'(t)Q(t)z(t)dt \\
&- 2\int_{t_0}^{t_f} z'(t)Q(t)z(t)dt\int_{t_0}^{t_f} \gamma'(s)R(s)\gamma(s)ds - 2\int_{t_0}^{t_f} \gamma'(t)R(t)\gamma(t)dt E\left\{w'(t_f)Q_f w(t_f)\right\} \\
&- 2E\left\{w'(t_f)Q_f w(t_f)\right\} E\left\{\int_{t_0}^{t_f} w'(t)Q(t)w(t)dt\right\} - 2z'(t_f)Q_f z(t_f)\int_{t_0}^{t_f} \gamma'(t)R(t)\gamma(t)dt \\
&- 2z'(t_f)Q_f z(t_f) E\left\{w'(t_f)Q_f w(t_f)\right\} - 2z'(t_f)Q_f z(t_f) E\left\{\int_{t_0}^{t_f} w'(t)Q(t)w(t)dt\right\} \\
&- 2\int_{t_0}^{t_f} z'(t)Q(t)z(t)dt E\left\{w'(t_f)Q_f w(t_f)\right\} - 2\int_{t_0}^{t_f} z'(t)Q(t)z(t)dt E\left\{\int_{t_0}^{t_f} w'(t)Q(t)w(t)dt\right\} \\
&- 2\int_{t_0}^{t_f} \gamma'(t)R(t)\gamma(t)dt E\left\{\int_{t_0}^{t_f} w'(t)Q(t)w(t)dt\right\}
\end{aligned}
\tag{5.114}
$$

$$
\begin{aligned}
Var\{J\} &= E\left\{z'(t_f)Q_f w(t_f) z'(t_f)Q_f w(t_f)\right\} + E\left\{w'(t_f)Q_f z(t_f) w'(t_f)Q_f z(t_f)\right\} \\
&+ 2E\left\{z'(t_f)Q_f w(t_f) w'(t_f)Q_f z(t_f)\right\} + E\left\{\int_{t_0}^{t_f}\int_{t_0}^{t_f} z'(t)Q(t)w(t)z'(t)Q(t)w(t)dsdt\right\} \\
&+ E\left\{\int_{t_0}^{t_f}\int_{t_0}^{t_f} w'(t)Q(t)z(t)w'(t)Q(t)z(t)dsdt\right\} + 2E\left\{\int_{t_0}^{t_f}\int_{t_0}^{t_f} z'(t)Q(t)w(t)w'(t)Q(t)z(t)dsdt\right\} \\
&+ 2E\left\{z'(t_f)Q_f w(t_f)\int_{t_0}^{t_f} z'(t)Q(t)w(t)dt\right\} + 2E\left\{z'(t_f)Q_f w(t_f)\int_{t_0}^{t_f} w'(t)Q(t)z(t)dt\right\} \\
&+ 2E\left\{w'(t_f)Q_f z(t_f)\int_{t_0}^{t_f} z'(t)Q(t)w(t)dt\right\} + 2E\left\{w'(t_f)Q_f z(t_f)\int_{t_0}^{t_f} w'(t)Q(t)z(t)dt\right\} \\
&+ E\left\{w'(t_f)Q_f w(t_f) w'(t_f)Q_f w(t_f)\right\} + E\left\{\int_{t_0}^{t_f}\int_{t_0}^{t_f} w'(t)Q(t)w(t)w'(s)Q(s)w(s)dsdt\right\} \\
&+ 2E\left\{w'(t_f)Q_f w(t_f) w'(t_f)Q_f w(t_f)\int_{t_0}^{t_f} w'(t)Q(t)w(t)dt\right\} \\
&- E\left\{w'(t_f)Q_f w(t_f)\right\}E\left\{w'(t_f)Q_f w(t_f)\right\} - E\left\{\int_{t_0}^{t_f} w'(t)Q(t)w(t)dt\right\}E\left\{\int_{t_0}^{t_f} w'(t)Q(t)w(t)dt\right\} \\
&- 2E\left\{w'(t_f)Q_f w(t_f)\right\}E\left\{\int_{t_0}^{t_f} w'(t)Q(t)w(t)dt\right\}. \qquad (5.115)
\end{aligned}
$$

Now, we determine the variance of α. From (5.101), we write

$$
E\{\alpha\} = E\left\{w'(t_f)Q_f w(t_f)\right\} + E\left\{\int_{t_0}^{t_f} w'(t)Q(t)w(t)dt\right\}. \qquad (5.116)
$$

In order to determine the variance of α, we first evaluate $(E\{\alpha\})^2$ and $E\{\alpha^2\}$.

$$
\begin{aligned}
E\{\alpha\}^2 &= E\left\{w'(t_f)Q_f w(t_f)\right\} + E\left\{\int_{t_0}^{t_f} w'(t)Q(t)w(t)dt\right\} \\
&.E\left\{w'(t_f)Q_f w(t_f)\right\} + E\left\{\int_{t_0}^{t_f} w'(t)Q(t)w(t)dt\right\} \\
&= E\left\{w'(t_f)Q_f w(t_f)\right\}E\left\{w'(t_f)Q_f w(t_f)\right\} + E\left\{\int_{t_0}^{t_f} w'(t)Q(t)w(t)dt\right\}E\left\{\int_{t_0}^{t_f} w'(t)Q(t)w(t)dt\right\} \\
&+ 2E\left\{w'(t_f)Q_f w(t_f)\right\}E\left\{\int_{t_0}^{t_f} w'(t)Q(t)w(t)dt\right\}, \qquad (5.117)
\end{aligned}
$$

and

$$
\begin{aligned}
E\{\alpha^2\} &= E\left\{w'(t_f)Q_f w(t_f) w'(t_f)Q_f w(t_f)\right\} + E\left\{\int_{t_0}^{t_f}\int_{t_0}^{t_f} w'(t)Q(t)w(t)w'(s)Q(s)w(s)dsdt\right\} \\
&+ 2E\left\{w'(t_f)Q_f w(t_f) w'(t_f)Q_f w(t_f)\int_{t_0}^{t_f} w'(t)Q(t)w(t)dt\right\}. \qquad (5.118)
\end{aligned}
$$

$$
\begin{aligned}
&Var\{\alpha\} = E\left\{\alpha^2\right\} - \left(E\left\{\alpha\right\}\right)^2 \\
&= E\left\{w'(t_f)Q_f w(t_f) w'(t_f)Q_f w(t_f)\right\} + E\left\{\int_{t_0}^{t_f}\int_{t_0}^{t_f} w'(t)Q(t)w(t)w'(s)Q(s)w(s)dsdt\right\} \\
&+ 2E\left\{w'(t_f)Q_f w(t_f) w'(t_f)Q_f w(t_f)\int_{t_0}^{t_f} w'(t)Q(t)w(t)dt\right\} \\
&- E\left\{w'(t_f)Q_f w(t_f)\right\} E\left\{w'(t_f)Q_f w(t_f)\right\} - E\left\{\int_{t_0}^{t_f} w'(t)Q(t)w(t)dt\right\} \\
&.E\left\{\int_{t_0}^{t_f} w'(t)Q(t)w(t)dt\right\} - 2E\left\{w'(t_f)Q_f w(t_f)\right\} E\left\{\int_{t_0}^{t_f} w'(t)Q(t)w(t)dt\right\}. \qquad (5.119)
\end{aligned}
$$

Substituting the expression for the variance α from (5.119) into (5.115) we obtain

$$
\begin{aligned}
&Var\{J\} \\
&= E\left\{z'(t_f)Q_f w(t_f) z'(t_f)Q_f w(t_f)\right\} + E\left\{w'(t_f)Q_f z(t_f) w'(t_f)Q_f z(t_f)\right\} \\
&+ 2E\left\{z'(t_f)Q_f w(t_f) w'(t_f)Q_f z(t_f)\right\} + E\left\{\int_{t_0}^{t_f}\int_{t_0}^{t_f} z'(t)Q(t)w(t)z'(s)Q(s)w(s)dsdt\right\} \\
&+ E\left\{\int_{t_0}^{t_f}\int_{t_0}^{t_f} w'(t)Q(t)z(t)w'(s)Q(s)z(s)dsdt\right\} + 2E\left\{\int_{t_0}^{t_f}\int_{t_0}^{t_f} z'(t)Q(t)w(t)w'(s)Q(s)z(s)dsdt\right\} \\
&+ 2E\left\{z'(t_f)Q_f w(t_f)\int_{t_0}^{t_f} z'(t)Q(t)w(t)dt\right\} + 2E\left\{z'(t_f)Q_f w(t_f)\int_{t_0}^{t_f} w'(t)Q(t)z(t)dt\right\} \\
&+ 2E\left\{w'(t_f)Q_f z(t_f)\int_{t_0}^{t_f} z'(t)Q(t)w(t)dt\right\} + 2E\left\{w'(t_f)Q_f z(t_f)\int_{t_0}^{t_f} w'(t)Q(t)z(t)dt\right\} + Var\{\alpha\}.
\end{aligned}
\qquad (5.120)
$$

Eq. (5.120) has three types of terms apart from $Var\{\alpha\}$: product terms without any integrand (first three terms), product terms with a single integrand (fourth, fifth, and sixth terms), and product terms with a double integrand (seventh, eighth, ninth, and tenth terms). For the first three terms we write,

$$
\begin{aligned}
&Var\{J\}_1 = E\left\{z'(t_f)Q_f w(t_f) z'(t_f)Q_f w(t_f)\right\} + E\left\{w'(t_f)Q_f z(t_f) w'(t_f)Q_f z(t_f)\right\} \\
&+2E\left\{z'(t_f)Q_f w(t_f) w'(t_f)Q_f z(t_f)\right\} \\
&= E\left\{aa + a'a' + 2aa'\right\}, \qquad (\text{Let } a = z'(t_f)Q_f w(t_f), \text{ then } a' = w'(t_f)Q_f z(t_f)\ ) \\
&= 4E\left\{aa'\right\} \\
&= 4E\left\{z'(t_f)Q_f w(t_f) w'(t_f)Q_f z(t_f)\right\} \\
&= 4z'(t_f)Q_f w(t_f) E\left\{w(t_f)w'(t_f)\right\} Q_f z(t_f). \qquad (5.121)
\end{aligned}
$$

For the fourth, fifth, and sixth terms, we write

$$
\begin{aligned}
Var\{J\}_2 &= E\left\{\int_{t_0}^{t_f}\int_{t_0}^{t_f} z'(t)Q(t)w(t)z'(s)Q(s)w(s)dsdt\right\} \\
&+ E\left\{\int_{t_0}^{t_f}\int_{t_0}^{t_f} w'(t)Q(t)z(t)w'(s)Q(s)z(s)dsdt\right\} \\
&+ 2E\left\{\int_{t_0}^{t_f}\int_{t_0}^{t_f} z'(t)Q(t)w(t)w'(s)Q(s)z(s)dsdt\right\} \\
&= E\left\{\int_{t_0}^{t_f}\int_{t_0}^{t_f} (aa + a'a' + 2aa')dsdt\right\}; \qquad (a = z'(t)Q(t)w(t)) \\
&= 4E\left\{\int_{t_0}^{t_f}\int_{t_0}^{t_f} (aa'dsdt)\right\} \\
&= 4\int_{t_0}^{t_f}\int_{t_0}^{t_f} z'(t)Q(t)E\left\{w(t)w'(s)\right\}Q(s)z(s)dsdt. \qquad (5.122)
\end{aligned}
$$

For the seventh, eighth, ninth and tenth terms, we write

$$
\begin{aligned}
&Var\{J\}_3 \\
&= 2E\left\{z'(t_f)Q_f w(t_f)\int_{t_0}^{t_f} z'(t)Q(t)w(t)dt\right\} + 2E\left\{z'(t_f)Q_f w(t_f)\int_{t_0}^{t_f} w'(t)Q(t)z(t)dt\right\} \\
&+ 2E\left\{w'(t_f)Q_f z(t_f)\int_{t_0}^{t_f} z'(t)Q(t)w(t)dt\right\} + 2E\left\{w'(t_f)Q_f z(t_f)\int_{t_0}^{t_f} w'(t)Q(t)z(t)dt\right\} \\
&= 2E\left\{a'b' + a'b + ab' + ab\right\}; \quad (\text{Let } a = w'(t_f)Q_f z(t_f), b = \textstyle\int_{t_0}^{t_f} w'(t)Q(t)z(t)dt) \\
&= 8E\left\{a'b\right\} \\
&= 8E\left\{z'(t_f)Q_f w(t_f)\int_{t_0}^{t_f} w'(t)Q(t)z(t)dt\right\} \\
&= 8z'(t_f)Q_f E\left\{w(t_f)\int_{t_0}^{t_f} w'(t)Q(t)z(t)dt\right\}. \qquad (5.123)
\end{aligned}
$$

From (5.120), we have the following expression for the variance of cost using the expressions in (5.121), (5.122), and (5.123),

$$
\begin{aligned}
Var\{J\} &= 4z'(t_f)Q_f E\left\{w(t_f)w'(t_f)\right\}Q_f z(t_f) \\
&+ 4\int_{t_0}^{t_f}\int_{t_0}^{t_f} z'(t)Q(t)E\left\{w(t)w'(s)\right\}Q(s)z(s)dsdt \\
&+ 8z'(t_f)Q_f E\left\{w(t_f)\int_{t_0}^{t_f} w'(t)Q(t)z(t)dt\right\} + Var\{\alpha\}. \qquad (5.124)
\end{aligned}
$$

Now, we express $E\{w(t)w'(s)\}$, $E\{w(t_f)w'(t_f)\}$, $E\left\{w(t_f)\int_{t_0}^{t_f} w'(t)Q(t)z(t)dt\right\}$ in terms of the state transition matrix and covariance matrix. The state equation for $w(t)$ is stated as

(in (5.93)),

$$dw(t) = A(t)dw(t) + C(t)E\left\{\gamma(t,\eta)|\psi\right\}dt + d\theta(t) \quad w(t_0) = 0,$$

can be expressed as,

$$w(t) = \Phi(t,t_0)w(t_0) + \int_{t_0}^{t_f} \Phi(t,\tau)C(\tau)E\left\{\gamma(\tau)|\psi\right\}d\tau + \int_{t_0}^{t_f} \Phi(t,\tau)\theta(\tau)d\tau. \qquad (5.125)$$

where, $\Phi(t,\tau)$ is the transition matrix. Then

$$\begin{aligned} w(t)w'(s) = &\left[\Phi(t,t_0)w(t_0) + \int_{t_0}^{t_f} \Phi(t,\tau_1)C(\tau_1)E\left\{\gamma(\tau_1)|\psi\right\}d\tau_1 + \int_{t_0}^{t_f} \Phi(t,\tau_1)\theta(\tau_1)d\tau_1\right] \\ &.\left[\Phi(s,t_0)w(t_0) + \int_{t_0}^{t_f} \Phi(s,\tau_2)C(\tau_2)E\left\{\gamma(\tau_2)|\psi\right\}d\tau_2 + \int_{t_0}^{t_f} \Phi(s,\tau_2)\theta(\tau_2)d\tau_2\right]' \\ &= \int_{t_0}^{t_f}\int_{t_0}^{t_f} \Phi(t,\tau_1)C(\tau_1)E\left\{\gamma(\tau_1)|\psi\right\}E\left\{\gamma'(\tau_2)|\psi\right\}C'(\tau_2)\Phi'(s,\tau_2)d\tau_2 d\tau_1 \\ &+ \int_{t_0}^{t_f}\int_{t_0}^{t_f} \Phi(t,\tau_1)C(\tau_1)E\left\{\gamma(\tau_1)|\psi\right\}\theta'(\tau_2)\Phi'(s,\tau_2)d\tau_2 d\tau_1 \\ &+ \int_{t_0}^{t_f}\int_{t_0}^{t_f} \Phi(t,\tau_1)\theta(\tau_1)E\left\{\gamma'(\tau_2)|\psi\right\}C'(\tau_2)\Phi'(s,\tau_2)d\tau_2 d\tau_1 \\ &+ \int_{t_0}^{t_f}\int_{t_0}^{t_f} \Phi(t,\tau_1)\theta(\tau_1)\theta'(\tau_2)\Phi'(s,\tau_2)d\tau_2 d\tau_1. \quad w(t_0) = 0 \end{aligned} \qquad (5.126)$$

Taking expectation of (5.126), we obtain

$$
\begin{aligned}
&E\left\{w(t)w'(s)\right\}\\
&=E\left\{\int_{t_0}^{t_f}\int_{t_0}^{t_f}\Phi(t,\tau_1)C(\tau_1)E\left\{\gamma(\tau_1)|\psi\right\}E\left\{\gamma'(\tau_2)|\psi\right\}C'(\tau_2)\Phi'(s,\tau_2)d\tau_2 d\tau_1\right\}\\
&+E\left\{\int_{t_0}^{t_f}\int_{t_0}^{t_f}\Phi(t,\tau_1)C(\tau_1)E\left\{\gamma(\tau_1)|\psi\right\}\theta'(\tau_2)\Phi'(s,\tau_2)d\tau_2 d\tau_1\right\}\\
&+E\left\{\int_{t_0}^{t_f}\int_{t_0}^{t_f}\Phi(t,\tau_1)\theta(\tau_1)E\left\{\gamma'(\tau_2)|\psi\right\}C'(\tau_2)\Phi'(s,\tau_2)d\tau_2 d\tau_1\right\}\\
&+E\left\{\int_{t_0}^{t_f}\int_{t_0}^{t_f}\Phi(t,\tau_1)\theta(\tau_1)\theta'(\tau_2)\Phi'(s,\tau_2)d\tau_2 d\tau_1\right\}\\
&=\int_{t_0}^{t_f}\int_{t_0}^{t_f}\Phi(t,\tau_1)C(\tau_1)E\left\{E\left\{\gamma(\tau_1)|\psi\right\}E\left\{\gamma'(\tau_2)|\psi\right\}\right\}C'(\tau_2)\Phi'(s,\tau_2)d\tau_2 d\tau_1\\
&+\int_{t_0}^{t_f}\int_{t_0}^{t_f}\Phi(t,\tau_1)C(\tau_1)E\left\{E\left\{\gamma(\tau_1)|\psi\right\}\theta'(\tau_2)\right\}\Phi'(s,\tau_2)d\tau_2 d\tau_1\\
&+\int_{t_0}^{t_f}\int_{t_0}^{t_f}\Phi(t,\tau_1)E\left\{\theta(\tau_1)E\left\{\gamma'(\tau_2)|\psi\right\}\right\}C'(\tau_2)\Phi'(s,\tau_2)d\tau_2 d\tau_1\\
&+\int_{t_0}^{t_f}\int_{t_0}^{t_f}\Phi(t,\tau_1)E\left\{\theta(\tau_1)\theta'(\tau_2)\right\}\Phi'(s,\tau_2)d\tau_2 d\tau_1\\
&=\int_{t_0}^{t_f}\int_{t_0}^{t_f}\Phi(t,\tau_1)C(\tau_1)E\left\{E\left\{\gamma(\tau_1)|\psi\right\}E\left\{\gamma'(\tau_2)|\psi\right\}\right\}C'(\tau_2)\Phi'(s,\tau_2)d\tau_2 d\tau_1\\
&+\int_{t_0}^{t_f}\int_{t_0}^{t_f}\Phi(t,\tau_1)\Theta(t)\delta(t-\tau)\Phi'(s,\tau_2)d\tau_2 d\tau_1\\
&=\int_{t_0}^{t_f}\int_{t_0}^{t_f}\Phi(t,\tau_1)C(\tau_1)E\left\{E\left\{\gamma(\tau_1)|\psi\right\}E\left\{\gamma'(\tau_2)|\psi\right\}\right\}C'(\tau_2)\Phi'(s,\tau_2)d\tau_2 d\tau_1\\
&+\int_{t_0}^{\min(t,s)}\Phi(t,\tau_1)\Theta(t)\Phi'(s,\tau_2)d\tau_2\\
&=W(t,s).
\end{aligned}
\tag{5.127}
$$

Similarly,

$$
\begin{aligned}
&E\left\{w(t_f)w'(t_f)\right\}\\
&=\int_{t_0}^{t_f}\int_{t_0}^{t_f}\Phi(t_f,\tau_1)C(\tau_1)E\left\{E\left\{\gamma(\tau_1)|\psi\right\}E\left\{\gamma'(\tau_2)|\psi\right\}\right\}C'(\tau_2)\Phi'(t_f,\tau_2)d\tau_2 d\tau_1\\
&+\int_{t_0}^{\min(t,s)}\Phi(t_f,\tau_1)\Theta(t)\Phi'(t_f,\tau_2)d\tau_2\\
&=W(t_f,t_f).
\end{aligned}
\tag{5.128}
$$

$$
\begin{aligned}
&E\left\{w(t_f)\int_{t_0}^{t_f} w'(t)Q(t)z(t)dt\right\}\\
&=E\left\{\left[\int_{t_0}^{t_f}\Phi(t_f,\tau_1)C(\tau_1)E\left\{\gamma(\tau_1)|\psi\right\}d\tau_1+\int_{t_0}^{t_f}\Phi(t_f,\tau_1)\theta(\tau_1)d\tau_1\right]\right.\\
&\left.\cdot\int_{t_0}^{t_f}\left[\int_{t_0}^{t_f}\Phi(t,\tau_1)C(\tau_1)E\left\{\gamma(\tau_1)|\psi\right\}d\tau_1+\int_{t_0}^{t_f}\Phi(t,\tau_1)\theta(\tau_1)d\tau_1\right]' Q(t)z(t)dt\right\}\\
&=E\left\{\int_{t_0}^{t_f}\Phi(t_f,\tau_1)C(\tau_1)E\left\{\gamma(\tau_1)|\psi\right\}d\tau_1\right.\\
&\left.\cdot\int_{t_0}^{t_f}\left[\int_{t_0}^{t_f}\Phi(t,\tau_1)C(\tau_1)E\left\{\gamma(\tau_1)|\psi\right\}d\tau_1+\int_{t_0}^{t_f}\Phi(t,\tau_1)\theta(\tau_1)d\tau_1\right]' Q(t)z(t)dt\right\}\\
&+E\left\{\int_{t_0}^{t_f}\Phi(t_f,\tau_1)\theta(\tau_1)d\tau_1\right.\\
&\left.\cdot\int_{t_0}^{t_f}\left[\int_{t_0}^{t_f}\Phi(t,\tau_1)C(\tau_1)E\left\{\gamma(\tau_1)|\psi\right\}d\tau_1+\int_{t_0}^{t_f}\Phi(t,\tau_1)\theta(\tau_1)d\tau_1\right]' Q(t)z(t)dt\right\}\\
&=\int_{t_0}^{t_f}\Phi(t_f,\tau_1)C(\tau_1)E\left\{E\left\{\gamma(\tau_1)|\psi\right\}\int_{t_0}^{t_f}\int_{t_0}^{t_f}E\left\{\gamma'(\tau_2)|\psi\right\}C'(\tau_2)\Phi'(t,\tau_2)Q(t)z(t)d\tau_2 d\tau_1 dt\right\}\\
&+\int_{t_0}^{t_f}\Phi(t_f,\tau_1)E\left\{\theta(\tau_1)\int_{t_0}^{t_f}\int_{t_0}^{t_f}\theta'(\tau_2)\Phi'(t,\tau_2)Q(t)z(t)d\tau_2 d\tau_1 dt\right\}\\
&=\int_{t_0}^{t_f}\Phi(t_f,\tau_1)C(\tau_1)E\left\{E\left\{\gamma(\tau_1)|\psi\right\}\int_{t_0}^{t_f}\int_{t_0}^{t_f}E\left\{\gamma'(\tau_2)|\psi\right\}C'(\tau_2)\Phi'(t,\tau_2)Q(t)z(t)d\tau_2 d\tau_1 dt\right\}\\
&+\int_{t_0}^{t_f}\Phi(t_f,\tau_1)\int_{t_0}^{t_f}\Theta\Phi'(t,\tau_2)Q(t)z(t)d\tau_2 dt\\
&=\int_{t_0}^{t_f}W(t_f,t)Q(t)z(t)dt. \qquad (5.129)
\end{aligned}
$$

Using (5.127), (5.128), and (5.129) in (5.124) we have,

$$
\begin{aligned}
Var\{J\}&=4z'(t_f)Q_fW(t_f,t_f)Q_fz(t_f)+4\int_{t_0}^{t_f}\int_{t_0}^{t_f}z'(t)Q(t)W(t,s)Q(s)z(s)dsdt\\
&+8z'(t_f)Q_f\int_{t_0}^{t_f}W(t_f,t)Q(t)z(t)dt+Var\{\alpha\}. \qquad (5.130)
\end{aligned}
$$

Let us repeat our goal in this section. We intend to minimize the variance of the cost function, $Var\{\alpha\}$ stated in (5.130) keeping the mean of the cost function, $E\{\alpha\}$ equal to some M. The constraint stated in (5.92) is $dz(t)=[A(t)z(t)+B(t)\gamma(t)]dt, \quad z(t_0)=x_0$. To put this minimization problem in the framework of calculus of variations, we define an augmented cost function,

$$
\tilde{V}(\gamma)=Var\{J\}+\mu\left[E\{J\}-M\right]+\int_{t_0}^{t_f}\langle\{A(t)z(t)+B(t)\gamma(t)-\dot{z}(t)\},\rho(t)\rangle, \qquad (5.131)
$$

where μ is a Lagrange multiplier and $\rho(t)$ is a costate variable.

Now using Eqs. (5.100) and (5.130), Eq. (5.131) can be written as,

$$\begin{aligned}
&\tilde{V}(\gamma) = 4z'(t_f)Q_f W(t_f,t_f)Q_f z(t_f) + 4\int_{t_0}^{t_f}\int_{t_0}^{t_f} z'(t)Q(t)W(t,s)Q(s)z(s)dsdt \\
&+ 8z'(t_f)Q_f \int_{t_0}^{t_f} W(t_f,t)Q(t)z(t)dt + K_v + \mu\left[z'(t_f)Q_f z(t_f) + \int_{t_0}^{t_f}[z'(t)Q(t)z(t) + \gamma'(t)R(t)\gamma(t)]dt\right] \\
&+ \mu\left[K_m - M\right] + \int_{t_0}^{t_f}\left\langle\left\{A(t)z(t) + B(t)\gamma(t) - \dot{z}(t)\right\},\rho(t)\right\rangle \\
&= 8z'(t_f)Q_f \int_{t_0}^{t_f} W(t_f,t)Q(t)z(t)dt + 4\int_{t_0}^{t_f}\int_{t_0}^{t_f} z'(t)Q(t)W(t,s)Q(s)z(s)dsdt \\
&+ \mu\int_{t_0}^{t_f} z'(t)Q(t)z(t)dt + \mu\int_{t_0}^{t_f}\gamma'(t)R(t)\gamma(t)dt + K_v + \mu(K_m - M) + \\
&+ \int_{t_0}^{t_f}\left\langle\left\{A(t)z(t) + B(t)\gamma(t) - \dot{z}(t)\right\},\rho(t)\right\rangle + 4z'(t_f)Q_f W(t_f,t_f)Q_f z(t_f) + \mu z'(t_f)Q_f z(t_f). \quad (5.132)
\end{aligned}$$

where we denote the mean and variance of α by $K_m = E\{\alpha\}$ and $K_v = Var\{\alpha\}$.

Taking the first variation of $\tilde{V}(\gamma)$ we have,

$$\delta\tilde{V}(\gamma) = 8\int_{t_0}^{t_f}\langle Q'(t)W'(t_f,t)Q'_f z(t_f),\delta z(t)\rangle dt + 8\int_{t_0}^{t_f}\langle Q_f W(t_f,t)Q(t)z(t),\delta z(t_f)\rangle dt$$
$$+4\int_{t_0}^{t_f}\langle\left(\int_{t_0}^{t_f}Q(t)W(t,s)Q(s)z(s)ds\right),\delta z(t)\rangle dt + 4\int_{t_0}^{t_f}\langle\left(\int_{t_0}^{t_f}Q'(s)W'(s,t)Q'(t)z(t)dt\right),$$
$$\delta z(s)\rangle ds + 2\mu\int_{t_0}^{t_f}\langle Q(t)z(t),\delta z(t)\rangle dt + 2\mu\int_{t_0}^{t_f}\langle R(t)\gamma(t),\delta\gamma(t)\rangle dt$$
$$+\int_{t_0}^{t_f}\langle A(t)'(t)\rho(t),\delta z(t)\rangle dt + \int_{t_0}^{t_f}\langle B'(t)\rho(t),\delta\gamma(t)\rangle dt - \langle\rho(t_f),\delta z(t_f)\rangle$$
$$+\int_{t_0}^{t_f}\langle\dot{\rho}(t),\delta z(t)\rangle + 8\langle Q_f W(t_f,t_f)Q_f z(t_f),\delta z(t_f)\rangle + 2\mu\langle Q_f z(t_f),\delta z(t_f)\rangle$$
$$= 8\int_{t_0}^{t_f}\langle Q'(t)W'(t_f,t)Q'_f z(t_f),\delta z(t)\rangle dt + 8\int_{t_0}^{t_f}\langle Q_f W(t_f,t)Q(t)z(t),\delta z(t_f)\rangle dt +$$
$$+4\int_{t_0}^{t_f}\langle\left(\int_{t_0}^{t_f}Q(t)W(t,s)Q(s)z(s)ds\right),\delta z(t)\rangle dt + 4\int_{t_0}^{t_f}\langle\left(\int_{t_0}^{t_f}Q'(s)W'(s,t)Q'(t)z(t)dt\right),$$
$$\delta z(s)\rangle ds + 2\mu\int_{t_0}^{t_f}\langle Q(t)z(t),\delta z(t)\rangle dt + 2\mu\int_{t_0}^{t_f}\langle R(t)\gamma(t),\delta\gamma(t)\rangle dt$$
$$+\left[\langle z(t),\rho(t)\rangle\Big|_{t_0}^{t_f} - \int_{t_0}^{t_f}\langle z(t),\dot{\rho}(t)\rangle dt\right] + \int_{t_0}^{t_f}\langle A(t)'(t)\rho(t),\delta z(t)\rangle dt + \int_{t_0}^{t_f}\langle B'(t)\rho(t),\delta\gamma(t)\rangle dt$$
$$-\langle\rho(t_f),\delta z(t_f)\rangle + \int_{t_0}^{t_f}\langle\dot{\rho}(t),\delta z(t)\rangle + 8\langle Q_f W(t_f,t_f)Q_f z(t_f),\delta z(t_f)\rangle + 2\mu\langle Q_f z(t_f),\delta z(t_f)\rangle$$
$$= 8\int_{t_0}^{t_f}\langle Q'(t)W'(t_f,t)Q'_f z(t_f),\delta z(t)\rangle dt + 8\int_{t_0}^{t_f}\langle Q_f W(t_f,t)Q(t)z(t),\delta z(t_f)\rangle dt$$
$$+4\int_{t_0}^{t_f}\langle\left(\int_{t_0}^{t_f}Q(t)W(t,s)Q(s)z(s)ds\right),\delta z(t)\rangle dt + 4\int_{t_0}^{t_f}\langle\left(\int_{t_0}^{t_f}Q'(s)W'(s,t)Q'(t)z(t)dt\right),$$
$$\delta z(s)\rangle ds + 2\mu\int_{t_0}^{t_f}\langle Q(t)z(t),\delta z(t)\rangle dt + 2\mu\int_{t_0}^{t_f}\langle R(t)\gamma(t),\delta\gamma(t)\rangle dt$$
$$+\left[\langle z(t_f),\rho(t_f)\rangle - \langle z(t_0),\rho(t_0)\rangle - \int_{t_0}^{t_f}\langle z(t),\dot{\rho}(t)\rangle dt\right] + \int_{t_0}^{t_f}\langle A(t)'(t)\rho(t),\delta z(t)\rangle dt$$
$$+\int_{t_0}^{t_f}\langle B'(t)\rho(t),\delta\gamma(t)\rangle dt - \langle\rho(t_f),\delta z(t_f)\rangle + \int_{t_0}^{t_f}\langle\dot{\rho}(t),\delta z(t)\rangle$$
$$+8\langle Q_f W(t_f,t_f)Q_f z(t_f),\delta z(t_f)\rangle + 2\mu\langle Q_f z(t_f),\delta z(t_f)\rangle$$
$$= 8\int_{t_0}^{t_f}\langle Q'(t)W'(t_f,t)Q'_f z(t_f),\delta z(t)\rangle dt + 8\int_{t_0}^{t_f}\langle Q_f W(t_f,t)Q(t)z(t),\delta z(t_f)\rangle dt$$
$$+4\int_{t_0}^{t_f}\langle\left(\int_{t_0}^{t_f}Q(t)W(t,s)Q(s)z(s)ds\right),\delta z(t)\rangle dt + 4\int_{t_0}^{t_f}\langle\left(\int_{t_0}^{t_f}Q'(s)W'(s,t)Q'(t)z(t)dt\right),$$
$$\delta z(s)\rangle ds + 2\mu\int_{t_0}^{t_f}\langle Q(t)z(t),\delta z(t)\rangle dt + 2\mu\int_{t_0}^{t_f}\langle R(t)\gamma(t),\delta\gamma(t)\rangle dt$$
$$+\left[\langle z(t_f),\rho(t_f)\rangle - \int_{t_0}^{t_f}\langle z(t),\dot{\rho}(t)\rangle dt\right] + \int_{t_0}^{t_f}\langle A(t)'(t)\rho(t),\delta z(t)\rangle dt + \int_{t_0}^{t_f}\langle B'(t)\rho(t),\delta\gamma(t)\rangle dt$$
$$-\langle\rho(t_f),\delta z(t_f)\rangle + \int_{t_0}^{t_f}\langle\dot{\rho}(t),\delta z(t)\rangle + 8\langle Q_f W(t_f,t_f)Q_f z(t_f),\delta z(t_f)\rangle + 2\mu\langle Q_f z(t_f),\delta z(t_f)\rangle. \tag{5.133}$$

In order for γ to be minimum, it is necessary that $\delta\tilde{V}(\gamma)=0$. This gives us the necessary conditions with the following three equations:

$$\begin{aligned}
&2\mu\int_{t_0}^{t_f}\langle R(t)\gamma(t),\delta\gamma(t)\rangle dt+\int_{t_0}^{t_f}\langle B'(t)\rho(t),\delta\gamma(t)\rangle dt=0\\
&\gamma(t)=-\frac{1}{2\mu}R^{-1}(t)B'(t)\rho(t),
\end{aligned}\tag{5.134}$$

$$\begin{aligned}
&8\int_{t_0}^{t_f}\langle Q'(t)W'(t_f,t)Q_f'z(t_f),\delta z(t)\rangle dt+8\int_{t_0}^{t_f}\langle\left(\int_{t_0}^{t_f}Q(t)W(t,s)Q(s)z(s)ds\right),\delta z(t)\rangle dt\\
&+2\mu\int_{t_0}^{t_f}\langle Q(t)z(t),\delta z(t)\rangle dt+\int_{t_0}^{t_f}\langle A(t)'(t)\rho(t),\delta z(t)\rangle dt+\int_{t_0}^{t_f}\langle\dot{\rho}(t),\delta z(t)\rangle=0\\
&-\dot{\rho}(t)=8Q(t)W(t_f,t)Q_fz(t_f)+8\int_{t_0}^{t_f}Q(t)W(t,s)Q(s)z(s)ds+2\mu Q(t)z(t)+A(t)'(t)\rho(t),
\end{aligned}\tag{5.135}$$

$$\begin{aligned}
&8\int_{t_0}^{t_f}\langle Q_fW(t_f,t)Q(t)z(t),\delta z(t_f)\rangle dt+\langle\rho(t_f),\delta z(t_f)\rangle\\
&+8\langle Q_fW(t_f,t_f)Q_fz(t_f),\delta z(t_f)\rangle+2\mu\langle Q_fz(t_f),\delta z(t_f)\rangle=0\\
&\rho(t_f)=8\int_{t_0}^{t_f}Q_fW(t_f,t)Q(t)z(t)dt+8Q_fW(t_f,t_f)Q_fz(t_f)+2\mu Q_fz(t_f).
\end{aligned}\tag{5.136}$$

Now, taking the second variation of $\tilde{V}(\gamma)$, we have,

$$\begin{aligned}
&\delta^2\tilde{V}(\gamma)=4\int_{t_0}^{t_f}\langle Q'(t)W'(t_f,t)Q_f'z(t_f)\delta z(t_f),\delta z(t)\rangle dt+4\int_{t_0}^{t_f}\langle Q_fW(t_f,t)Q(t)\delta z(t),\delta z(t_f)\rangle dt\\
&+2\int_{t_0}^{t_f}\langle\left(\int_{t_0}^{t_f}Q(t)W(t,s)Q(s)\delta z(s)ds\right),\delta z(t)\rangle dt+2\int_{t_0}^{t_f}\langle\left(\int_{t_0}^{t_f}Q'(s)W'(s,t)Q'(t)\delta z(t)dt\right),\\
&\delta z(s)\rangle ds+\mu\int_{t_0}^{t_f}\langle Q(t)\delta z(t),\delta z(t)\rangle dt+\mu\int_{t_0}^{t_f}\langle R(t)\delta\gamma(t),\delta\gamma(t)\rangle dt\\
&+4\langle Q_fW(t_f,t_f)Q_f\delta z(t_f),\delta z(t_f)\rangle+\mu\langle Q_f\delta z(t_f),\delta z(t_f)\rangle.
\end{aligned}\tag{5.137}$$

Now, letting μ positive guarantees a minimum solution by ensuring $\delta^2\tilde{V}(\gamma)>0$. Eq. (5.137) gives the sufficient condition.

Here, the control strategy is a function of the costate variable which is dependent on the state variable. This makes the numerical evaluation of the control complex. In order to

circumvent the complexity, let us introduce two new variables υ and φ by an extension of the method of Baggeroer [118]:

$$\upsilon(t) = W(t,t_f)Q_f z(t_f) + \int_{t_0}^{t_f} W(t,s)Q(t)z(s)ds, \tag{5.138}$$

$$\varphi(t) = W(t_f,t)Q_f z(t_f) + \int_{t_0}^{t_f} \Phi(s,t)Q(t)z(s)ds. \tag{5.139}$$

In terms of these two new variables, (5.135) becomes,

$$d\rho(t) = -A'(t)\rho(t)dt - 2\mu Q(t)z(t)dt - 8Q(t)\upsilon(t)dt. \tag{5.140}$$

By taking derivatives of (5.138) and (5.139) gives,

$$d\upsilon(t) = A(t)\upsilon(t)dt + \left[C(t)E\left\{E\left\{\gamma(t,\eta)\right\}E\left\{\gamma'(t,\eta)\right\}\right\}C'(t) + \Theta\right]\varphi(t)dt, \tag{5.141}$$

$$\dot{\varphi}(t) = -A'(t)\varphi(t) - Q(t)z(t). \tag{5.142}$$

with an initial condition $\upsilon(t_0) = 0$ and a terminal condition $\varphi(t_f) = Q_f z(t_f)$. Also, (5.136) becomes,

$$\rho(t_f) = 2\mu Q_f z(t_f) + 8Q_f \upsilon(t_f). \tag{5.143}$$

Hence, (5.134) gives the control strategy for the stated problem in this section, if it satisfies the differential equations found from (5.92), (5.135), (5.140), and (5.140):

$$dz(t) = A(t)z(t)dt - \frac{1}{2\mu}B(t)R^{-1}(t)B'(t)\rho(t)dt, \tag{5.144}$$

$$d\rho(t) = -A'(t)\rho(t)dt - 2\mu Q(t)z(t)dt - 8Q(t)\upsilon(t)dt, \tag{5.145}$$

$$d\upsilon(t) = A(t)\upsilon(t)dt + \left[C(t)E\left\{E\left\{\gamma(t,\eta)\right\}E\left\{\gamma'(t,\eta)\right\}\right\}C'(t) + \Theta\right]\varphi(t)dt, \tag{5.146}$$

$$d\varphi(t) = -A'(t)\varphi(t)dt - Q(t)z(t)dt. \tag{5.147}$$

with the boundary conditions

$$z(t_0) = x_0, \tag{5.148}$$

$$\rho(t_f) = 2\mu Q_f z(t_f) + 8Q_f \upsilon(t_f), \tag{5.149}$$

$$\upsilon(t_0) = 0, \tag{5.150}$$

$$\varphi(t_f) = Q_f z(t_f). \tag{5.151}$$

□

5.5 Determination of Stackelberg Strategies

In this section, we determine the Stackelberg strategies for the minimal cost variance problem of a linear quadratic stochastic system derived in Section 5.4.4. We use Lemma 5.1 in Section 5.4.5 for solving our minimal cost variance problem. Note that after incorporating the follower's optimal control into the original linear stochastic system, the state variables are changed. Now the state variables are denoted by $\underline{x}(t) = \left[\hat{x}_2(t)\ \xi(t)\ \kappa_2(t).\right]'$ The state variables are described later in the proof. Accordingly, we used the 'bar' notation like $\underline{x}$ for the appropriate symbols.

Theorem 5.3. *The two-player nonzero-sum stochastic differential game with static information, as formulated in Section 5.4.4 admits a Stackelberg solution with **P1** as the leader **P1** with the cost function:*

$$J_1(\gamma_1, \mathfrak{T}_2^{21}\gamma_1) = \underline{x}_f' \underline{Q}_{1f} \underline{x}_f + \int_{t_0}^{t_f} \left[\underline{x}'(t)\underline{Q}(t)\underline{x}(t) + \gamma_1'(t)\gamma_1(t)\right] dt, \tag{5.152}$$

The Stackelberg statistical game problem is to minimize the variance of the cost function $Var\left\{J_1(\gamma_1, \mathfrak{T}_2^{21}\gamma_1)\right\}$ while keeping $E\left\{J_1(\gamma_1, \mathfrak{T}_2^{21}\gamma_1)\right\} = M$, where M is an arbitrary constant, and which is subject to the state dynamics

$$d\underline{x}(t) = [\underline{A}(t)\underline{x}(t) + \underline{B}(t)\gamma_1(t) + \underline{C}(t)E\left\{\gamma_1(t)|\eta_2\right\}] + \underline{F}(t)dw(t), \tag{5.153}$$

where the definitions of $\underline{x}, \underline{A}, \underline{B}, \underline{C}, \underline{F}, \underline{Q}(t), \underline{Q}_{1f}, \underline{Q}_{2f}$ are given inside the proof.

Then, the Stackelberg strategy $\gamma_1 \in \Gamma_1^2$ of the leader is given by

$$\gamma_1^*(t, \eta_1) = -\frac{1}{2\mu}\underline{B}'(t)\underline{\varrho}(t), \tag{5.154}$$

if it satisfies the differential equations

$$d\underline{z}(t) = \underline{A}(t)\underline{z}(t)dt - \frac{1}{\mu}\underline{B}(t)\underline{B}'(t)\underline{\varrho}(t)dt, \tag{5.155}$$

$$d\underline{\varrho}(t) = -\underline{A}'(t)\underline{\varrho}(t)dt - 2\mu\underline{Q}_1(t)\underline{z}(t)dt - 8\underline{Q}_1(t)\underline{\upsilon}(t)dt, \tag{5.156}$$

$$d\underline{\upsilon}(t) = \underline{A}(t)\underline{\upsilon}(t)dt + \left[\underline{C}(t)E\left\{E\left\{\gamma_1(t)|\eta_2)\right\}E\left\{\gamma_1'(t)|\eta_2)\right\}\right\}\underline{C}'(t) + \Theta\right]\underline{\varphi}(t)dt, \tag{5.157}$$

$$d\underline{\varphi}(t) = -\underline{A}'(t)\underline{\varphi}(t) - \underline{Q}_1(t)\underline{z}(t). \tag{5.158}$$

with the boundary conditions

$$\underline{z}(t_0) = \underline{x}_0, \tag{5.159}$$

$$\rho(t_f) = 2\mu Q_{1f}\underline{z}(t_f) + 8Q_{1f}\underline{\upsilon}(t_f), \tag{5.160}$$

$$\underline{\upsilon}(t_0) = 0, \tag{5.161}$$

$$\underline{\varphi}(t_f) = Q_{1f}\underline{z}(t_f). \tag{5.162}$$

Furthermore, the corresponding optimal response strategy of the follower ***P2*** *is given by,*

$$\gamma_2^*(t,\eta_2) = -B_2'(t)\left[S_2(t)E\left\{x(t)|\eta_2\right\} + \kappa_2(t)\right]. \tag{5.163}$$

where,

$$\dot{S}_2(t) = -A'(t)S_2(t) - S_2(t)A(t) - Q_2(t) + S_2(t)B_2(t)B_2'(t)S_2(t), \tag{5.164}$$

$$S_2(t_f) = Q_{2f}, \tag{5.165}$$

$$\dot{\kappa}_2(t) = -\left[A'(t) - S_2(t)B_2(t)B_2'(t)\right]\kappa_2(t) - S_2(t)B_1(t)E\left\{\gamma_1(t,\eta_1)|\eta_2\right\}, \tag{5.166}$$

$$\kappa_2(t_f) = 0. \tag{5.167}$$

Let us denote $E\{x|\eta_2\}$ *by* $\hat{x}_2(t)$*. Then,*

$$d\hat{x}_2(t) = \left[A(t) - B_2(t)B_2'(t)S_2(t)\right]\hat{x}_2(t)dt - B_2(t)B_2'(t)\kappa_2(t)dt + B_1E\left\{\gamma_1(t,\eta_1)|\eta_2\right\}dt, \tag{5.168}$$

$$\hat{x}_2(t_0) = E\left\{x(t_0)|\eta_2\right\} = E\left\{x_0|\eta_2\right\}. \tag{5.169}$$

Proof. We return to our original problem stated at the end of Section 5.4.4. We intend to minimize $Var\{J_1\}$ where,

$$\begin{aligned} J_1(\gamma_1, \mathfrak{T}_2^{21}\gamma_1) &= \hat{x}_2'(t_f)Q_{1f}\hat{x}_2(t_f) + \xi'(t_f)Q_{1f}\xi(t_f) \\ &+ \int_{t_0}^{t_f}\left[\hat{x}_2'(t)Q_1(t)\hat{x}_2(t) + \xi'(t)Q_1\xi(t)\right]dt \\ &+ \int_{t_0}^{t_f}\left[\left\{\hat{x}_2'(t)S_2(t)\kappa_2'(t)\right\}B_2(t)R(t)B_2'(t)\left\{S_2(t)\hat{x}_2(t) + \kappa_2(t)\right\} + \gamma_1'(t)\gamma_1(t)\right]dt \end{aligned} \tag{5.170}$$

with subject to the constraints,

$$E\{J_1\} = M, \tag{5.171}$$

$$d\hat{x}_2(t) = \left[A(t) - B_2(t)B_2'(t)S_2(t)\right]\hat{x}_2(t)dt - B_2(t)B_2'(t)\kappa_2(t)dt + B_1E\left\{\gamma_1(t,\eta_1)|\eta_2\right\}dt, \tag{5.172}$$

$$\hat{x}_2(t_0) = E\left\{x(t_0)|\eta_2\right\} = E\left\{x_0|\eta_2\right\}. \tag{5.173}$$

$$d\xi(t) = A(t)\xi(t) + B_1\gamma_1(t)dt - B_1(t)E\left\{\gamma_1(t)|\eta_2\right\}dt + \sigma(t)dw(t), \tag{5.174}$$

$$\xi_{t_0} = x_0 - E\left\{x_0|\eta_2\right\}. \tag{5.175}$$

$$\dot{\kappa}_2(t) = -\left[A'(t) - S_2(t)B_2(t)B_2'(t)\right]\kappa_2(t) - S_2(t)B_1(t)E\left\{\gamma_1(t,\eta_1)|\eta_2\right\}, \tag{5.176}$$

$$\kappa_2(t_f) = 0 \tag{5.177}$$

$$\dot{S}_2(t) = -A'(t)S_2(t) - S_2(t)A(t) - Q_2(t) + S_2(t)B_2(t)B_2'(t)S_2(t), \tag{5.178}$$

$$S_2(t_f) = Q_{2f}, \tag{5.179}$$

We define the new state vector,

$$\underline{x}(t) = \begin{bmatrix}\hat{x}_2(t) & \xi(t) & \kappa_2(t)\end{bmatrix}' \tag{5.180}$$

and the matrices,

$$\underline{A}(t) = \begin{bmatrix} A(t) - B_2(t)B_2'(t)S_2(t) & 0 & -B_2(t)B_2'(t) \\ 0 & A(t) & 0 \\ 0 & 0 & -\left[A'(t) - S_2(t)B_2(t)B_2'(t)\right] \end{bmatrix}, \tag{5.181}$$

$$\underline{B}(t) = \begin{bmatrix}0 & B_1(t) & 0\end{bmatrix}', \tag{5.182}$$

$$\underline{C}(t) = \begin{bmatrix}B_1(t) & -B_1(t) & -S_2(t)B_1(t)\end{bmatrix}', \tag{5.183}$$

$$\underline{F}(t) = \begin{bmatrix}0 & F(t) & 0\end{bmatrix}', \tag{5.184}$$

$$Q_{1f} = \begin{bmatrix} Q_{1f} & 0 & 0 \\ 0 & Q_{1f} & 0 \\ 0 & 0 & 0] \end{bmatrix}, \tag{5.185}$$

$$\underline{Q}_1 = \begin{bmatrix} Q_1(t) - S_2(t)B_2(t)R(t)B_2'(t)S_2(t) & 0 & -S_2(t)B_2(t)R(t)B_2'(t) \\ 0 & Q_1(t) & 0 \\ B_2(t)R(t)B_2'(t)S_2(t) & 0 & B_2(t)R(t)B_2'(t) \end{bmatrix} \tag{5.186}$$

Then, we have the following cost function for the leader **P1**:

$$J_1(\gamma_1, \mathfrak{T}_2^{21}\gamma_1) = \underline{x}_f' Q_{1f} \underline{x}_f + \int_{t_0}^{t_f} \left[\underline{x}'(t)Q(t)\underline{x}(t) + \gamma_1'(t)\gamma_1(t)\right] dt \tag{5.187}$$

We shall minimize $Var\left\{J_1(\gamma_1, \mathfrak{T}_2^{21}\gamma_1)\right\}$ while keeping $E\left\{J_1(\gamma_1, \mathfrak{T}_2^{21}\gamma_1)\right\} = M$, where M is an arbitrary constant, and which is subject to the state dynamics,

$$d\underline{x}(t) = [\underline{A}(t)\underline{x}(t) + \underline{B}(t)\gamma_1(t) + \underline{C}(t)E\left\{\gamma_1(t)|\eta_2\right\}]dt + \underline{F}(t)dw(t), \tag{5.188}$$

where $\hat{x}_2(t_0)$, $\xi(t_0)$ and $\kappa_2(t_f)$ are given. Then, from Lemma 5.1 we identify $\gamma(t)$ with $\gamma_1(t,\eta_1)$, η with η_1, ψ with η_2, and consider $R(t)$ as identity matrix. We rewrite the equations (5.138) and (5.139) as follows

$$\underline{\upsilon}(t) = \underline{W}(t,t_f)Q_{1f}\underline{z}(t_f) + \int_{t_0}^{t_f} \underline{W}(t,s)Q_1(t)\underline{z}(s)ds, \tag{5.189}$$

$$\underline{\varphi}(t) = \underline{W}(t_f,t)Q_{1f}\underline{z}(t_f) + \int_{t_0}^{t_f} \underline{\Phi}(s,t)Q_1(t)\underline{z}(s)ds, \tag{5.190}$$

with

$$\underline{z}(t) = E\left\{\underline{x}(t)\right\}, \qquad \underline{z}(t_0) = \underline{x}_0 = \begin{bmatrix} \hat{x}_2(t_0) & \xi(t_0) & \kappa_2(t_0) \end{bmatrix}'. \tag{5.191}$$

$$\underline{W}(t,s) = \int_{t_0}^{t_f}\int_{t_0}^{t_f} \underline{\Phi}(t,\tau_1)\underline{C}(\tau_1)E\left\{E\left\{\gamma_1(\tau_1,\eta_1)|\eta_2\right\}E\left\{\gamma_1'(\tau_2)|\eta_2\right\}\right\}\underline{C}'(\tau_2)\underline{\Phi}'(s,\tau_2)d\tau_2 d\tau_1$$
$$+ \int_{t_0}^{\min(t,s)} \underline{\Phi}(t,\tau_1)\Theta(t)\underline{\Phi}'(s,\tau_2)d\tau_2 \tag{5.192}$$

$$\underline{W}(t_f,t_f) = \int_{t_0}^{t_f}\int_{t_0}^{t_f} \underline{\Phi}(t_f,\tau_1)\underline{C}(\tau_1)E\left\{E\left\{\gamma_1(\tau_1,\eta_1)|\eta_2\right\}E\left\{\gamma_1'(\tau_2)|\psi\right\}\right\}\underline{C}'(\tau_2)\underline{\Phi}'(t_f,\tau_2)d\tau_2 d\tau_1$$
$$+ \int_{t_0}^{t_f} \underline{\Phi}(t_f,\tau_1)\Theta(t)\underline{\Phi}'(t_f,\tau_2)d\tau_2 \tag{5.193}$$

$$\int_{t_0}^{t_f} \underline{W}(t_f,t)Q_1(t)\underline{z}(t)dt$$
$$= \int_{t_0}^{t_f} \underline{\Phi}(t_f,\tau_1)\underline{C}(\tau_1)E\left\{E\left\{\gamma_1(\tau_1,\eta_1)|\eta_2\right\}\int_{t_0}^{t_f}\int_{t_0}^{t_f} E\left\{\gamma_1'(\tau_2)|\eta_2\right\}\underline{C}'(\tau_2)\underline{\Phi}'(t,\tau_2)Q_1(t)\underline{z}(t)d\tau_2 d\tau_1 dt\right\}$$
$$+ \int_{t_0}^{t_f} \underline{\Phi}(t_f,\tau_1)\int_{t_0}^{t_f} \Theta\underline{\Phi}'(t,\tau_2)Q_1(t)\underline{z}(t)d\tau_2 dt. \tag{5.194}$$

Now, according to Lemma 5.1, the control strategy of the leader is as follows:

$$\gamma_1^*(t,\eta_1) = -\frac{1}{2\mu}\underline{B}'(t)\underline{\rho}(t), \tag{5.195}$$

if it satisfies the differential equations

$$d\underline{z}(t) = \underline{A}(t)\underline{z}(t)dt - \frac{1}{2\mu}\underline{B}(t)\underline{B}'(t)\underline{\rho}(t)dt, \tag{5.196}$$

$$d\underline{\rho}(t) = -\underline{A}'(t)\underline{\rho}(t) - 2\mu Q_1(t)\underline{z}(t)dt - 8Q_1(t)\underline{\upsilon}(t)dt, \tag{5.197}$$

$$d\underline{\upsilon}(t) = \underline{A}(t)\underline{\upsilon}(t)dt + \left[\underline{C}(t)E\left\{E\left\{\gamma_1(t)|\eta_2\right)\right\}E\left\{\gamma_1'(t)|\eta_2\right)\right\}\underline{C}'(t) + \Theta\right]\underline{\varphi}(t)dt, \tag{5.198}$$

$$d\underline{\varphi}(t) = -\underline{A}'(t)\underline{\varphi}(t)dt - Q_1(t)\underline{z}(t)dt. \tag{5.199}$$

with the boundary conditions

$$\underline{z}(t_0) = \underline{x}_0, \tag{5.200}$$

$$\rho(t_f) = 2\mu Q_{1f}\underline{z}(t_f) + 8Q_{1f}\underline{\upsilon}(t_f), \tag{5.201}$$

$$\underline{\upsilon}(t_0) = 0, \tag{5.202}$$

$$\underline{\varphi}(t_f) = Q_{1f}\underline{z}(t_f). \tag{5.203}$$

Furthermore, the corresponding optimal response strategy of the follower is given by

$$\gamma_2^*(t,\eta_2) = -B_2'(t)\left[S_2(t)E\left\{x(t)|\eta_2\right\} + \kappa_2(t)\right]. \tag{5.204}$$

where,

$$\dot{S}_2(t) = -A'(t)S_2(t) - S_2(t)A(t) - Q_2(t) + S_2(t)B_2(t)B_2'(t)S_2(t), \tag{5.205}$$

$$S_2(t_f) = Q_{2f}, \tag{5.206}$$

$$\dot{\kappa}_2(t) = -\left[A'(t) - S_2(t)B_2(t)B_2'(t)\right]\kappa_2(t) - S_2(t)B_1(t)E\left\{\gamma_1(t,\eta_1)|\eta_2\right\}, \tag{5.207}$$

$$\kappa_2(t_f) = 0. \tag{5.208}$$

Hence, $(\gamma_1^*(t,\eta_1), \gamma_2^*(t,\eta_2))$ is the Stackelberg strategy pair for the above Stackelberg statistical game. □

5.6 Numerical Simulation of Stackelberg Statistical Controller

We consider a linear stochastic system described in [39], and modify it into a two-player linear stochastic system as follows

$$dx(t) = Ax(t) + B_1u_1(t) + B_2u_2(t) + Fdw(t), \quad x(t_0) = x_0, \tag{5.209}$$

where $A = \begin{bmatrix} -1 & 1 \\ 0 & -1 \end{bmatrix}$, $B_1 = \begin{bmatrix} 1 \\ 0 \end{bmatrix}$, $B_2 = \begin{bmatrix} 1 \\ 0 \end{bmatrix}$, $F = \begin{bmatrix} 1 \\ 1 \end{bmatrix}$. with the initial condition $x = [4\ 3]'$ and noise covariance $E\{dwdw'\} = 0.5$. Let γ_1 and γ_2 be permissible strategies belonging to permissible strategy space $\Gamma_k, k = 1,2$, such that the controls $u_1 = \gamma_1$ and $u_2 = \gamma_2$.

The cost functions for player 1 and player 2 are

$$J_1 = x'(t_f)Q_{1f}x(t_f) + \int_{t_0}^{t_f} \left[x'(t)Q_1x(t) + \gamma_1'(t)R_{11}(t)\gamma_1(t) + \gamma_2'(t)R_{12}(t)\gamma_2(t)\right] dt$$
$$J_2 = x'(t_f)Q_{2f}x(t_f) + \int_{t_0}^{t_f} \left[x'(t)Q_2x(t) + \gamma_1'(t)R_{21}(t)\gamma_1(t) + \gamma_2'(t)R_{22}(t)\gamma_2(t)\right] dt$$

The performance-measure weightings are
$Q_{1f} = \begin{bmatrix} 0 & 0 \\ 0 & 0 \end{bmatrix}$, $Q_1 = \begin{bmatrix} 1 & 0 \\ 0 & 1 \end{bmatrix}$, $Q_{2f} = \begin{bmatrix} 0 & 0 \\ 0 & 0 \end{bmatrix}$, $Q_2 = \begin{bmatrix} 1 & 0 \\ 0 & 1 \end{bmatrix}$, $R_{11} = I$, $R_{12} = I$, $R_{21} = O$, $R_{22} = I$.

Assuming the expected value of leader control $E\{\gamma_1 \mid \eta_2\} = 0.1$, we determine the Stackelberg control for the follower from Eqs. (5.204)-(5.208). The leader accounts the follower's response, which modifies the system considered by the leader to a new system of equations

$$d\underline{x}(t) = [\underline{A}(t)\underline{x}(t) + \underline{B}(t)\gamma_1(t) + \underline{C}(t)E\{\gamma_1(t)|\eta_2\}]dt + \underline{F}(t)dw(t), \tag{5.210}$$

where $\underline{A}$, $\underline{B}$, $\underline{C}$, and $\underline{F}$ can be determined from Eqs. (5.181), (5.182), (5.183), and (5.184). The cost function for the leader becomes

$$J_1 = \underline{x}_f'Q_{1f}\underline{x}_f + \int_{t_0}^{t_f} \left[\underline{x}'(t)Q_1(t)\underline{x}(t) + \gamma_1'(t)\gamma_1(t)\right] dt \tag{5.211}$$

where Q_1 and Q_{1f} can be determined from (5.186) and (5.185).

Assuming $E\{E\{\gamma_1(t)|\eta_2)\}E\{\gamma_1'(t)|\eta_2)\}\} = 0.1$ and $\Theta = 0.5$, we determine the Stackelberg control for the leader from Eqs. (5.195)-(5.203). In the simulation, the Lagrange multiplier μ was varied from 0.1 to 1.0. As the value of multiplier μ increases, the mean constraint gets emphasis as well as mean variance. Therefore, we observer some common characteristics to the state and control trajectories. For obtaining the state and control trajectories, we repeated the simulation 100 times with 100 different noise and recorded the average values. Running simulation multiple times with multiple noise reduce the deterministic characteristic from the system.

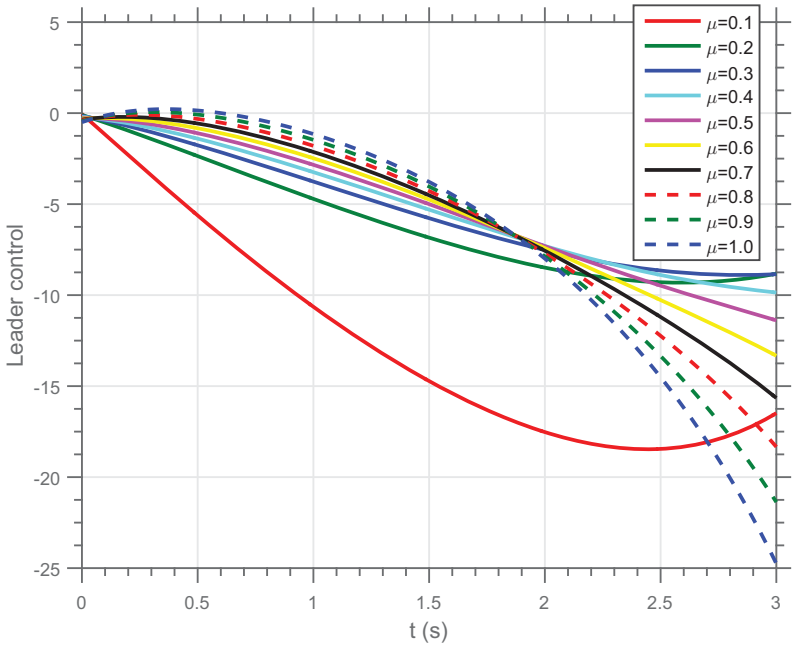

Figure 5.3: Player 1 (leader) control.

Fig. 5.3 shows the control action for the leader for varying μ. As the multiplier μ increases, the control action becomes smaller in value. Fig. 5.4 shows the control action for the follower, which look similar for all μ. The follower control action is independent of the value of μ. The variation occurs because of repetition of simulation with different random number seeds for noise generation. Figs. 5.5 and 5.6 show the mean and variance of the cost function for the leader. For the leader, we aim to minimize the variance of the leader cost function. Note that, as μ increase, the mean and the variance of the leader cost function decreases at first, and then increase. From the figures, we can determine an

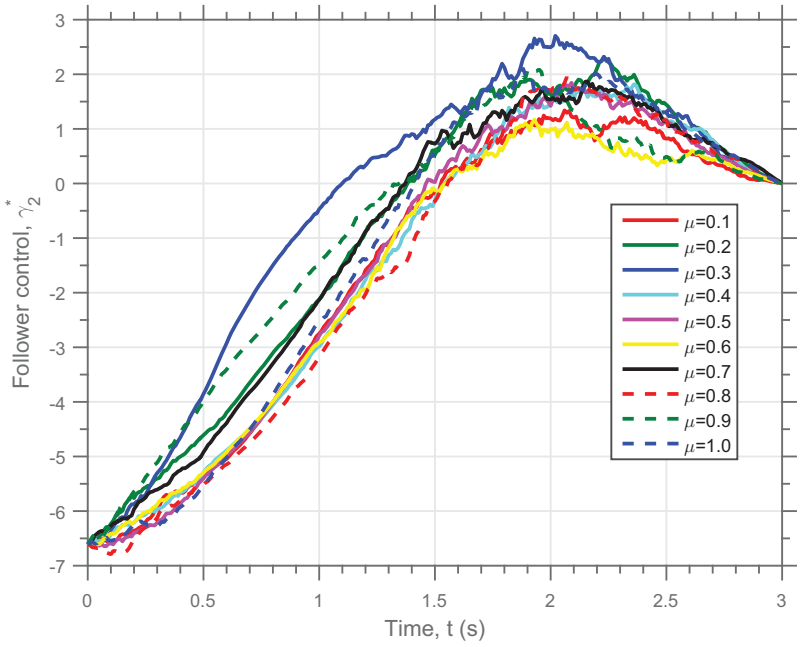

Figure 5.4: Player 2 (Follower) control.

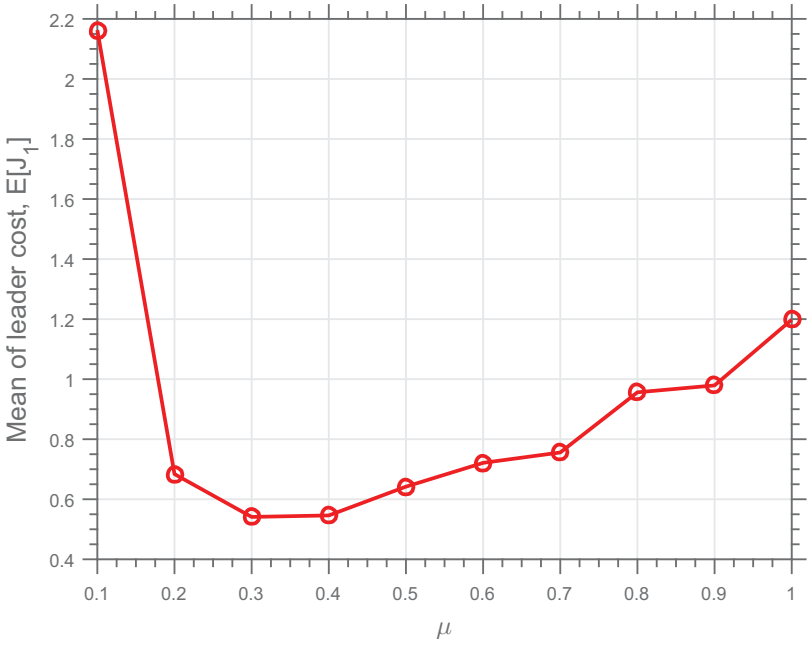

Figure 5.5: Mean of the leader cost function.

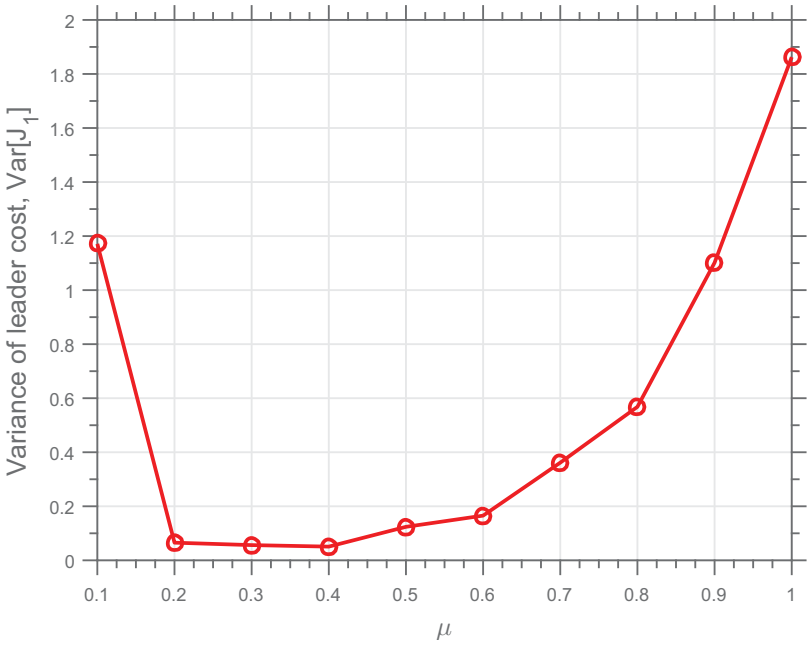

Figure 5.6: Variance of the leader cost function.

optimum value of μ.

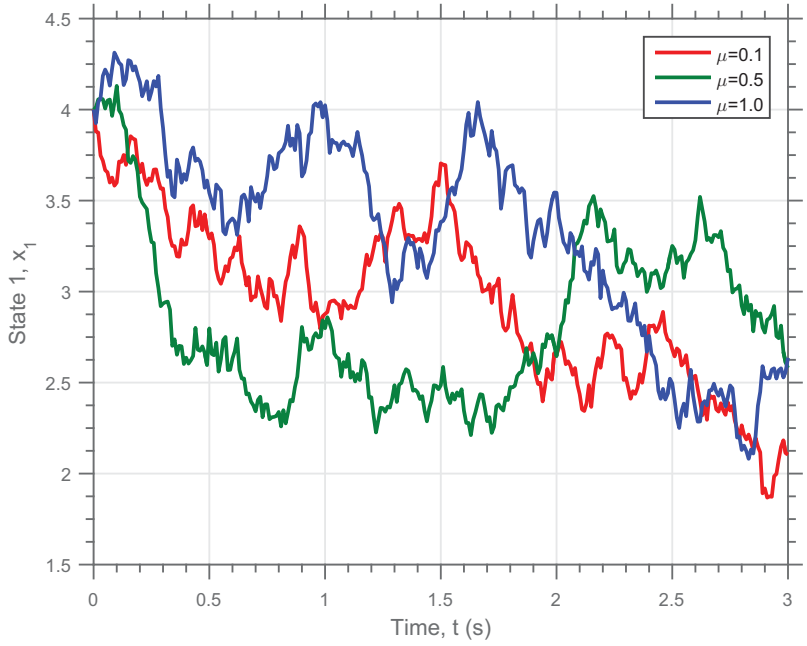

Figure 5.7: State 1 trajectories.

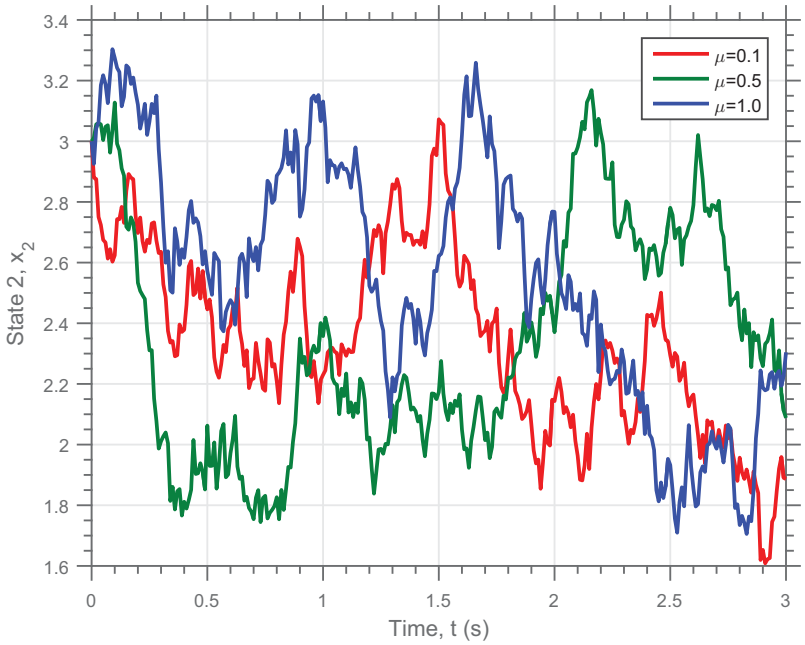

Figure 5.8: State 2 trajectories.

5.7 Review on Closed-loop Stackelberg Solutions of Differential Games

In two-player dynamic Stackelberg games, the decision depends on the type of information set the players have access to at any given time. When the leader has access to the closed-loop perfect state information, it leads to two types of equilibria – global Stackelberg solutions and feedback Stackelberg solutions.

The term 'global' indicates that the leader has a global advantage over the follower. In case feedback Stackelberg solutions, the continuous-time problem is viewed as the limit of discrete-time game, where the number of stages becomes unbounded in a finite interval. Then, the leader has stagewise or instantaneous advantage over the follower. In closed-loop paradigm, the follower may fail to attain the optimal response, because the leader's announced strategy comes with the memory of the state. Two approaches are considered to by-pass this problem: the team approach and the maximum principle approach.

In the team approach, the leader minimizes his cost function over the controls of the leader and the follower [119]. This gives a lower bound on the cost function and the team strategies for both players. Then, the leader attempts to find a closed-loop strategy so that

the follower's optimal response and the state trajectory coincide with the team strategy and team optimal trajectory.

In the maximum principle approach, the leader's strategy depends only on the initial and current states, and the leader solves a non-classical control problem [120]. Note that the follower's adjoint equation involves the derivative of the leader's strategy with respect to the state. Thus, after incorporating the follower's adjoint variable as augmented state, the leader faces a non-classical control problem, where both the control and its derivative appear in the controlled forward-backward ordinary differential equation [121].

In order to obtain the necessary conditions satisfied by the leader's optimal strategy, two approaches are considered by Papavassilopoulos and Cruz [122]. In the first approach, the variational techniques can be applied to the state system with mixed boundary conditions. In the second approach, an equivalent relationship is established between non-classical and classical problems. The second approach yields that the optimal strategy can be found in the space of affine functions.

Formally, in the second approach, the derivative of the control is considered as another new control variable, and a new classical control problem is formulated. Then, the equivalence between this new classical control problem and the original non-classical control problem is established. In the second approach, using Hamilton-Jacobi-Bellman equation yields a value function that depends on the whole function of the control. It becomes impossible for the leader to apply dynamic programming for his optimal strategy. Therefore, the maximum principle approach is considered more appropriate for closed-loop Stackelberg games [120].

The above discussion applies to the deterministic Stackelberg games. The stochastic formulation involves white noise terms. Therefore, the difficulty arises for Stackelberg game study under closed-loop information structure, because the the follower reaction may not be determined explicitly if the leader's strategy depends on the whole history of state. If the leader's strategy is restricted such that the leader's strategy depends only on the current state, then there is a way to solve the problem outlined by Papavassilopoulos and Cruz [122]. In the Stochastic Stackelberg game, the leader faces an optimal control problem in which there is a state equation consists of a stochastic differential equation and a

backward stochastic differential equation. Those equations feature leader's control u_1 and its derivative $\frac{\partial u_1}{\partial x}$. This gives rise to a difficult non-standard control problem. Using maximum principle approach, Bensoussan, Chen, and Shethi were able to prove the necessary condition and obtain the closed-loop Stackelberg solution [120]. They imposed a priori bounds on the derivative of the leader's control to keep the Hamiltonian finite. Since the derivative appears as part of the coefficient in the adjoint equation, its boundedness implies the well-posedness of the leader's problem when affine strategies are adopted. Bensoussan, Chen, and Shethi demonstrated the solution strategy with a one-dimensional linear quadratic game. However, the authors left the issue of the existence of the solution for future.

5.8 Discussion

In this chapter, the Stackelberg solution of two-player game was derived, where the leader is interested in optimizing the second cumulant of the cost function. The information patterns for both players are open-loop. Previously, Bagchi and Başar derived the Stackelberg solution of two player for open-loop linear quadratic Gaussian (LQG) control case [46]. Here, their work has been extended by deriving the open-loop minimal cost variance (MCV) Stackelberg solution. We presented a numerical simulation of a simple linear system using the developed open-loop MCV Stackelberg strategy. The next step of the Stackelberg theory development is solution of the Stackelberg game under closed-loop Stackelberg game, which would be more appropriate for the control of source and detector for the bimodal dynamic imaging.

CHAPTER 6

MODELING OF ROBOTIC MANIPULATOR

For automatic control of the bimodal imaging system, we intend to use a dual arm robot, “Baxter”. It is necessary to simulate the controller of a robot manipulator model before implementation. To simulate the controller, we require a mathematical model of the robot manipulator. We derive a non-linear mathematical model of n-link robot manipulator using Lagrange-Euler equations. Then we obtain a non-linear mathematical model of the Baxter robot. The perturbed linearized model is derived from the non-linear model using Taylor series approximation. We present the numerical simulations and experimental validation results for the linearized model of Baxter.

6.1 Robot Manipulator Model

6.1.1 Robot Manipulator Representation

For modeling, we consult these references [123], [124], [125], [126]. This section discusses the preliminary material required for a robot manipulator model.

6.1.1.1 Robot Manipulator Components and Geometries

Robot manipulators are composed of a set of bodies, called **links**, connected by **joints** into a kinematic chain. Robot manipulators are also known as “robot arms" in the literature. The motion in the robot manipulators occurs in the joints (analogous to human wrist and elbow); the links are of fixed construction (analogous to human forearms). The joints are typically rotary (revolute) and linear (prismatic). The revolute joints are hinges that allows relative rotation between two links. The prismatic joints allows relative linear motion between two links. The joints of most common robots are revolute. Fig. 6.1 shows revolute and prismatic joint types.

Each joint provides one degree-of-freedom (DOF) for the robot manipulator, either translational or rotational. In order to reach every point of its work environment with

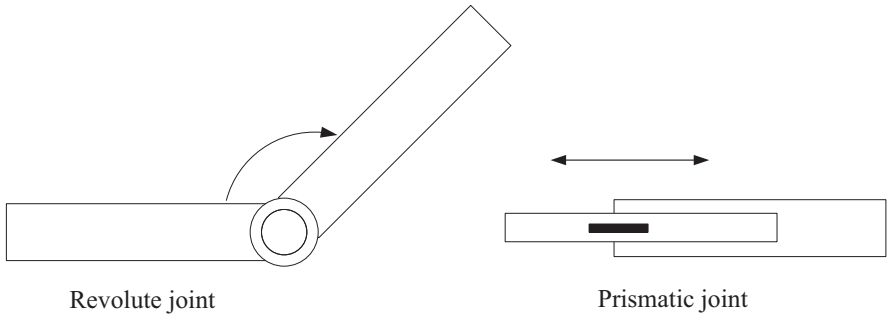

Figure 6.1: Type of joints.

arbitrary orientation, a robot manipulator requires to possess at least six joints. Six joints provide six independent DOF: three for position, and three for orientation.

6.1.1.2 Joint Variables, Homogeneous Transformation, and Arm T Matrices

Since each joint connects two links, a robot manipulator with n joints has $n+1$ links. For a manipulator, the joints are numbered from 1 to n, and the links are numbered from 0 to n [126]. Link 0 is the **base** of the manipulator, and link n holds the **end-effector or tool**. By this convention, joint i connects link $i-1$ and link i.

A link can be described by two parameters, its length, a_i, and its twist, α_i. A joint can be specified by two parameters: the joint angle, θ_i, and the link offset, d_i. The joint angle, θ_i, is the rotation of one link with respect to the next about the joint axis. The link offset, d_i denotes the distance from one link coordinate frame to the next along the joint axis. The i-th joint is associated with a joint variable, denoted by q_i. In the case of revolute joint, the joint angle is the joint variable. In the case of prismatic joint, the link offset is the joint variable. This means

$$q_i = \begin{cases} \theta_i, & \text{joint } i \text{ is revolute} \\ d_i, & \text{joint } i \text{ is prismatic.} \end{cases} \tag{6.1}$$

For an n-link robot, the generalized joint coordinates $\mathbf{q}$ is called the joint space. For the common case of an all-revolute robot, the joint coordinates are referred to as **joint angles** [126]. The joint coordinates are also referred to as the pose of the manipulator, which is not same as the pose of the end-effector. Fig. 6.2 shows a rigid object S to which a coor-

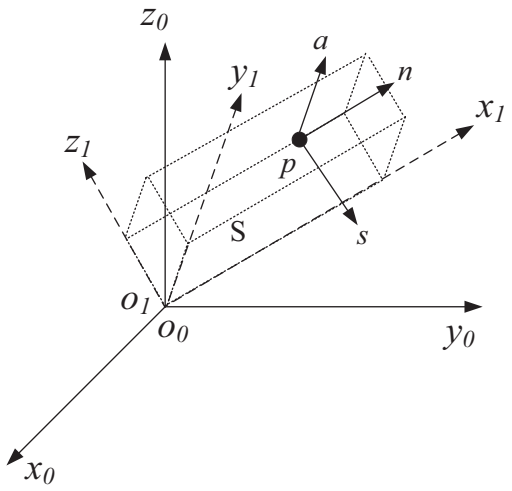

Figure 6.2: Coordinate frame attached to a rigid body.

dinate frame $o_1x_1y_1z_1$ is attached. The position and orientation of the point p on the rigid body can be expressed with respect to the frame $o_0x_0y_0z_0$ using a transformation matrix. In general, the position and orientation of i-th coordinate frame $o_ix_iy_iz_i$ can be expressed with respect to $(i-1)$-th coordinate frame $o_{i-1}x_{i-1}y_{i-1}z_{i-1}$ using a transformation matrix, A_i. The transformation matrix, A_i, a function of the joint variable q_i, varies as the robot configuration changes. Each homogeneous transformation matrix A_i is of the form,

$$A_i = A_i(q_i) = \begin{bmatrix} R_i^{i-1} & p_i \\ 0 & 1 \end{bmatrix} = \begin{bmatrix} n_x & s_x & a_x & p_x \\ n_y & s_y & a_y & p_y \\ n_z & s_z & a_z & p_z \\ 0 & 0 & 0 & 1 \end{bmatrix} = \begin{bmatrix} n & s & a & p \\ 0 & 0 & 0 & 1 \end{bmatrix}, \tag{6.2}$$

where R_i^{i-1} is an orthogonal rotation matrix and $p_i = [p_x\ p_y\ p_z]'$ is a translation vector. The vector $n = [n_x\ n_y\ n_z]'$ is represent the direction of x_1 in the $o_0x_0y_0z_0$ system, $s = [s_x\ s_y\ s_z]'$ represents the direction of y_1, and $a = [a_x\ a_y\ a_z]'$ represents the direction of z_1. The vector $d = [d_x\ d_y\ d_z]'$ represents the vector from the origin o_0 to the origin o_1 expressed in the frame $o_0x_0y_0z_0$.

6.1.1.3 Denavit-Hertenberg Notation

Denavit-Hertenverg (D-H) notation is a systematic way to describe the geometry of a robot manipulator made of serial chains of links and joints. The notation was proposed by Denavit and Hartenberg in 1955 [126].

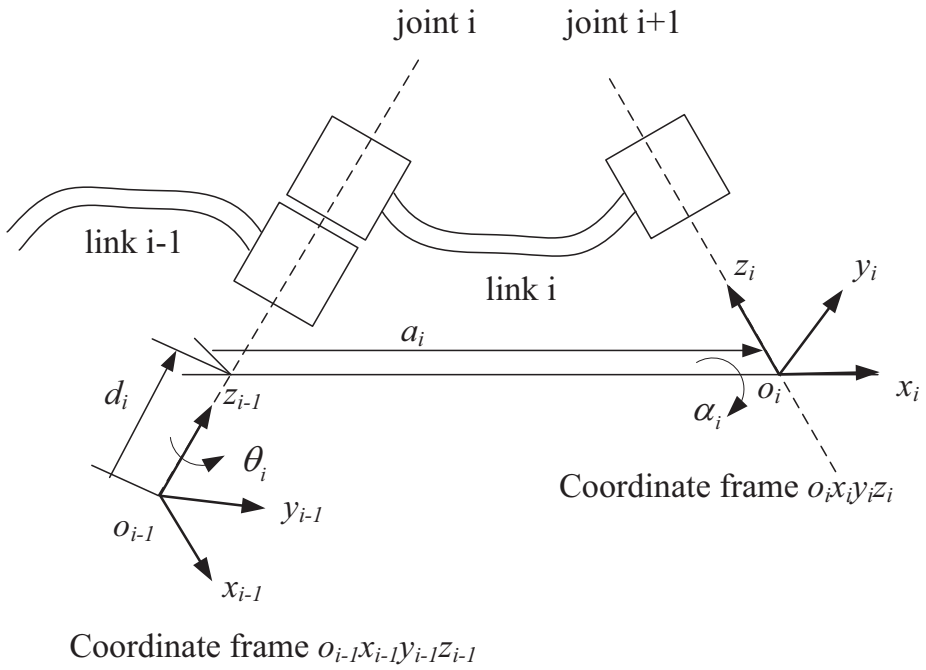

Figure 6.3: D-H parameters.

Fig. 6.3 illustrates D-H notation. The joint i connects link $(i-1)$ and link i. The frame $o_{i-1}x_{i-1}y_{i-1}z_{i-1}$ is attached to one end of link i. The axis of joint i is aligned with the z_{i-1}-axis. The frame $o_ix_iy_iz_i$ is attached to the other end of link i. The axis of joint $(i+1)$ is aligned with the z_i-axis. These link and joint parameters are expressed using four parameters defined in D-H convention. The four parameters are joint angle, θ_i, link offset, d_i, link length, a_i, and link twist, α_i. Their definitions are listed in Table 6.1. In D-H convention, each homogeneous transformation A_i is defined as a product of four basic

Table 6.1: D-H parameters

D-H parameter	Symbol	Definition
Joint angle	q_i	the angle between the x_{i-1} and x_i axes about the z_{i-1} axes. Revolute joint variable
Link offset	d_i	the distance from the origin o_{i-1} of frame $o_i x_i y_i z_i$ to the x_i axis along the z_{i-1} axis
Link length	a_i	the distance between the z_{i-1}- and z_i-axes along the x_i-axis
Link twist	α_i	the angle from the z_{i-1}-axis to the z_i-axis about the x_i-axis

transformations,

$$
\begin{aligned}
A_i =& Rot_{z,\theta_i} Trans_{z,d_i} Trans_{x,a_i} Rot_{x,\alpha_i}, \\
=& \begin{bmatrix} \cos\theta_i & -\sin\theta_i & 0 & 0 \\ \sin\theta_i & \cos\theta_i & 0 & 0 \\ 0 & 0 & 1 & 0 \\ 0 & 0 & 0 & 1 \end{bmatrix} \begin{bmatrix} 1 & 0 & 0 & 0 \\ 0 & 1 & 0 & 0 \\ 0 & 0 & 1 & d_i \\ 0 & 0 & 0 & 1 \end{bmatrix} \begin{bmatrix} 1 & 0 & 0 & a_i \\ 0 & 1 & 0 & 0 \\ 0 & 0 & 1 & 0 \\ 0 & 0 & 0 & 1 \end{bmatrix} \begin{bmatrix} 1 & 0 & 0 & 0 \\ 0 & \cos\alpha_i & -\sin\alpha_i & 0 \\ 0 & \sin\alpha_i & \cos\alpha_i & 0 \\ 0 & 0 & 0 & 1 \end{bmatrix} \\
=& \begin{bmatrix} \cos\theta_i & -\sin\theta_i\cos\alpha_i & \sin\theta_i\sin\alpha_i & a_i\cos\theta_i \\ \sin\theta_i & \cos\theta_i\cos\alpha_i & -\cos\theta_i\sin\alpha_i & a_i\sin\theta_i \\ 0 & \sin\alpha_i & \cos\alpha_i & d_i \\ 0 & 0 & 0 & 1 \end{bmatrix}.
\end{aligned} \tag{6.3}
$$

6.1.1.4 Forward and Inverse Kinematics and Dynamics

The pose of the end-effector consist of the position and the orientation of the end-effector. The pose of the end-effector has six DOF - three in translation and three in rotation. The forward kinematics problem for robot manipulators is: given the joint angles, find the pose of the end-effector expressed in the base frame. The inverse kinematics problem for robot manipulators is: given the pose of the end-effector expressed in the base frame, determine

the joint angles. The forward dynamics problem for robot manipulator is: given the joint torque, determine the motion of the robot manipulator. The inverse dynamics problem for robot manipulators is: given the pose, velocity, and acceleration, compute the required joint torques. In the following section, we use the Euler-Lagrange equation of motion to compute the inverse dynamics of n-link robot manipulators.

6.1.2 Mathematical Modeling of n-Link Robot Manipulators

In this section, we derive a differential equation for a n-link robot manipulator using Euler-Lagrange equation of motion.

6.1.3 Euler-Lagrange Equation of Motion

The Euler-Lagrange equation of motion for a system is given by [125]

$$\frac{d}{dt}\frac{\partial L}{\partial \dot{\mathbf{q}}} - \frac{\partial L}{\partial \mathbf{q}} = \tau, \tag{6.4}$$

where $\mathbf{q}$ is an n-vector of generalized coordinates q_i, $\dot{\mathbf{q}}$ is an n-vector of joint velocity $\dot{q}_i$, τ is an n-vector of generalized forces τ_i, and Lagrangian L is the difference between the kinetic and potential energies. In our case, $\mathbf{q}$ is the joint variable vector. Then, $\boldsymbol{\tau}$ is a n-vector of torques and forces.

6.1.4 Joint Velocities of n-Link Robot Manipulators

We consider a coordinate frame that is attached to each link of the robot. In particular, link i is attached to the frame $o_i x_i y_i z_i$. This implies that the coordinates of each point on link i are constant if expressed in the i-th coordinate frame $o_i x_i y_i z_i$. When joint i is actuated, link i with its attached frame $o_i x_i y_i z_i$ experience motion. The frame $o_0 x_0 y_0 z_0$, attached to the robot base, is referred to as the inertial frame.

In order to obtain the coordinates of a point in i-th frame in terms of j-th frame, a

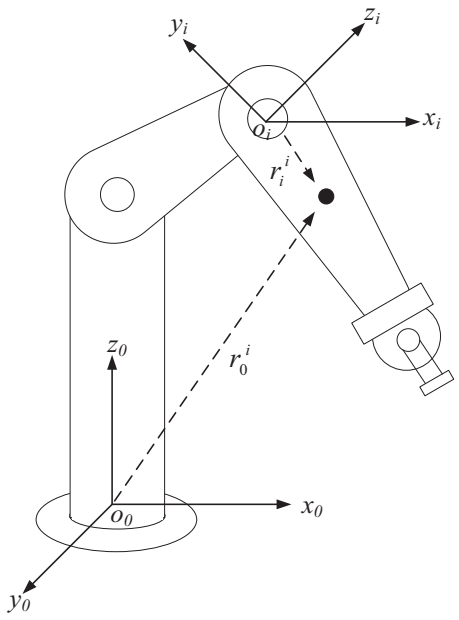

Figure 6.4: Coordinate frames for robot manipulator.

transformation matrix T_i^j is used, which is defined by

$$T_i^j = \begin{cases} A_{j+1}A_{j+2}\cdots A_{i-1}A_i, & i > j \\ I, & i = j \\ (T_i^j)^{-1}, & i < j \end{cases}, \tag{6.5}$$

where I is an identity matrix. Then, given the coordinates $r_i^i = [x_i\ y_i\ z_i\ 1]'$ of a point in the i-th frame, the coordinates of the same point in the base frame are given by,

$$r_i^0 = T_i^0\, r_i^i = (A_1A_2\cdots A_i)\, r_i^i = \left(T_1^0T_2^1\cdots T_i^{i-1}\right) r_i^i. \tag{6.6}$$

Let r_i^i be the coordinates of a point on link i with respect to frame i. This point can be expressed in the base frame as

$$r_0^i = \left(T_1^0T_2^1\cdots T_i^{i-1}\right) r_i^i, \tag{6.7}$$

where T_i^{i-1} is the 4×4 homogeneous transformation defined in (6.5). Here, T_i^{i-1} is a

function of joint variable q_i. Now, we write the velocity of the point in the base frame as

$$\begin{aligned} v_i = \frac{dr_i^0}{dt} &= \frac{d}{dt}\left(T_1^0 T_2^1 \cdots T_i^{i-1}\right) r_i^i \\ &= \dot{T}_1^0 T_2^1 \cdots T_i^{i-1} r_i^i + T_1^0 \dot{T}_2^1 \cdots T_i^{i-1} r_i^i + \cdots + T_1^0 T_2^1 \cdots \dot{T}_i^{i-1} r_i^i + T_i^0 \dot{r}_i^i \\ &= \left(\sum_{j=1}^{i} \frac{\partial T_i^0}{\partial q_j}\frac{\partial q_j}{\partial t}\right) r_i^i; \qquad \left(\text{velocity of } r_i^i \text{ expressed in } i\text{-th frame is zero, } \dot{r}_i^i = 0\right). \end{aligned} \tag{6.8}$$

Now, $\frac{\partial T_i^0}{\partial q_j}$ can be calculated using a matrix W_i, which will be stated below. Using (6.6) we get $T_i^{i-1} = A_i$, and then using (6.3) we write

$$T_i^{i-1} = A_i = \begin{bmatrix} \cos\theta_i & -\sin\theta_i\cos\alpha_i & \sin\theta_i\sin\alpha_i & a_i\cos\theta_i \\ \sin\theta_i & \cos\theta_i\cos\alpha_i & -\cos\theta_i\sin\alpha_i & a_i\sin\theta_i \\ 0 & \sin\alpha_i & \cos\alpha_i & d_i \\ 0 & 0 & 0 & 1 \end{bmatrix}. \tag{6.9}$$

Differentiating (6.9) with respect to $q_i = \theta_i$, we have

$$\begin{aligned} \frac{\partial T_i^{i-1}}{\partial q_i} &= \begin{bmatrix} -\sin\theta_i & -\cos\theta_i\cos\alpha_i & \cos\theta_i\sin\alpha_i & -a_i\sin\theta_i \\ \cos\theta_i & -\sin\theta_i\cos\alpha_i & -\sin\theta_i\sin\alpha_i & a_i\cos\theta_i \\ 0 & 0 & 0 & 0 \\ 0 & 0 & 0 & 0 \end{bmatrix} \\ &= \begin{bmatrix} 0 & -1 & 0 & 0 \\ 1 & 0 & 0 & 0 \\ 0 & 0 & 0 & 0 \\ 0 & 0 & 0 & 0 \end{bmatrix} \begin{bmatrix} \cos\theta_i & -\sin\theta_i\cos\alpha_i & \sin\theta_i\sin\alpha_i & a_i\cos\theta_i \\ \sin\theta_i & \cos\theta_i\cos\alpha_i & -\cos\theta_i\sin\alpha_i & a_i\sin\theta_i \\ 0 & \sin\alpha_i & \cos\alpha_i & d_i \\ 0 & 0 & 0 & 1 \end{bmatrix} \\ &= W_i T_i^0, \end{aligned} \tag{6.10}$$

where

$$W_i = \begin{bmatrix} 0 & -1 & 0 & 0 \\ 1 & 0 & 0 & 0 \\ 0 & 0 & 0 & 0 \\ 0 & 0 & 0 & 0 \end{bmatrix}; \qquad i = 1, 2, \cdots, n, \qquad \text{applicable for revolute joint.} \tag{6.11}$$

Now, we express the effect of the motion of joint j on all the points on link i using

$$\frac{\partial T_i^0}{\partial q_j} = \begin{cases} T_1^0 T_2^1 \cdots T_{j-1}^{j-2} W_j T_j^{j-1} \cdots T_i^{i-1}, & \text{for} \quad i \geq j \\ 0, & \text{for} \quad i < j \end{cases} \tag{6.12}$$

for $i = 1, 2, \cdots, n$, and

$$U_{ij} \equiv \frac{\partial T_i^0}{\partial q_j} = \begin{cases} T_{j-1}^0 W_j T_i^{j-1}, & \text{for} \quad i \geq j \\ 0, & \text{for} \quad i < j \end{cases} . \tag{6.13}$$

Using the relation in (6.13), we rewrite (6.8) as

$$v_i = \left(\sum_{j=1}^{i} \frac{\partial T_i^0}{\partial q_j} \frac{\partial q_j}{\partial t} \right) r_i^i = \left(\sum_{j=1}^{i} U_{ij} \dot{q}_j \right) r_i^i. \tag{6.14}$$

Note that the partial derivative of T_i^{i-1} with respect to q_i results into a matrix that does not preserve the structure of a homogeneous coordinate transformation matrix. For a revolute joint, the effect of pre-multiplying T_i^{i-1} by W_i is equivalent to interchanging the elements of the first two rows of T_i^{i-1}, then negating all the elements of the first row, and finally zeroing out all the elements of the third and fourth row.

Now, we need to find the interaction effects of the motion of joint j and joint k on all the points on link i as

$$\frac{\partial U_{ij}}{\partial q_k} \equiv U_{ijk} = \begin{cases} T_{j-1}^0 W_j T_{k-1}^{j-1} W_k T_i^{k-1}, & \text{for} \quad i \geq k \geq j \\ T_{k-1}^0 W_k T_{j-1}^{k-1} W_j T_i^{j-1}, & \text{for} \quad i \geq j \geq k \\ 0, & \text{for} \quad i < j \quad \text{or} \quad i < k \end{cases} . \tag{6.15}$$

6.1.5 Kinetic Energy of n-Link Robot Manipulators

Let dm be an infinitesimal mass at r_i^i with a velocity of $v = \begin{bmatrix} v_x^2 & v_y^2 & v_z^2 \end{bmatrix}'$. The differential kinetic energy of the mass is

$$\begin{aligned} dK_i &= \frac{1}{2}\left(v_x^2 + v_y^2 + v_z^2\right) dm, \\ &= \frac{1}{2}\operatorname{Tr}\left(v'v\right) dm, \\ &= \frac{1}{2}\operatorname{Tr}\left(vv'\right) dm, \\ &= \frac{1}{2}\operatorname{Tr}\left(\left[\left(\sum_{j=1}^{i} U_{ij}\dot{q}_j\right) r_i^i\right]\left[\left(\sum_{k=1}^{i} U_{ik}\dot{q}_k\right) r_i^i\right]'\right) dm, \\ &= \frac{1}{2}\operatorname{Tr}\left(\sum_{j=1}^{i}\sum_{k=1}^{i} U_{ij} r_i^i r_i^{i\prime} U_{ik}' \dot{q}_j \dot{q}_k\right) dm, \\ &= \frac{1}{2}\operatorname{Tr}\left(\sum_{j=1}^{i}\sum_{k=1}^{i} U_{ij}\left(r_i^i dm r_i^{i'}\right) U_{ik}' \dot{q}_j \dot{q}_k\right), \end{aligned} \tag{6.16}$$

where I_i is the 4×4 pseudo-inertia matrix defined as

$$\begin{aligned} I_i &= r_i^i dm r_i^{i'}, \\ &= \begin{bmatrix} \int x_i^2 dm & \int y_i x_i dm & \int z_i x_i dm & \int x_i dm \\ \int x_i y_i dm & \int y_i^2 dm & \int z_i y_i dm & \int y_i dm \\ \int x_i z_i dm & \int y_i z_i dm & \int z_i^2 dm & \int z_i dm \\ \int x_i dm & \int y_i dm & \int z_i dm & \int dm \end{bmatrix}, \end{aligned} \tag{6.17}$$

assuming $\bar{r}_i^i = \begin{bmatrix} \bar{x}_i & \bar{y}_i \bar{z}_i & 1 \end{bmatrix}'$ be the coordinates of the center of mass for dm in frame i. Here, I_i is the constant matrix depending on the geometry and mass distribution of link i. This inertia tensor can be expressed in an alternative form. In terms of the link i, moments of inertia are defined as

$$\begin{aligned} I_{xx} &= \int \left(y^2 + z^2\right) dm, \\ I_{yy} &= \int \left(x^2 + z^2\right) dm, \\ I_{zz} &= \int \left(x^2 + y^2\right) dm, \end{aligned}$$

cross-products of inertia

$$I_{xy} = \int xydm,$$
$$I_{xz} = \int xzdm,$$
$$I_{yz} = \int yzdm,$$

and first moments

$$m\bar{x} = \int xdm,$$
$$m\bar{y} = \int ydm,$$
$$m\bar{z} = \int zdm,$$

with m the total mass of link i, and $\bar{r}_i^i = [\bar{x}_i\ \bar{y}_i\bar{z}_i\ 1]'$ be the center of gravity of link i. Now we rewrite the inertia tensor as

$$I_i = \begin{bmatrix} \frac{-I_{xx}+I_{yy}+I_{zz}}{2} & I_{xy} & I_{xz} & m\bar{x}_i \\ I_{xy} & \frac{I_{xx}-I_{yy}+I_{zz}}{2} & I_{yz} & m\bar{y}_i \\ I_{xy} & I_{yz} & \frac{I_{xx}+I_{yy}-I_{zz}}{2} & m\bar{z}_i \\ m\bar{x}_i & m\bar{y}_i & m\bar{z}_i & m \end{bmatrix}. \tag{6.18}$$

These quantities can be computed from the manufacturer's specifications.

Now, the total kinetic energy of an n-link manipulator can be written as

$$\begin{aligned} K = \sum_{i=1}^{n} K_i &= \frac{1}{2}\sum_{i=1}^{n} \mathrm{Tr}\left[\sum_{j=1}^{i}\sum_{k=1}^{i} U_{ij} I_i U_{ik}' \dot{q}_j \dot{q}_k\right], \\ &= \frac{1}{2}\sum_{i=1}^{n}\sum_{j=1}^{i}\sum_{k=1}^{i} \left[\mathrm{Tr}\left(U_{ij} I_i U_{ik}'\right)\dot{q}_j \dot{q}_k\right]. \end{aligned} \tag{6.19}$$

Since $U_{ij} = 0$ for $j > i$, we can replace the upper summation limit by n in (6.19). Thus, we write the total kinetic energy

$$\begin{aligned} K = \sum_{i=1}^{n} K_i &= \frac{1}{2}\sum_{i=1}^{n} \frac{1}{2}\mathrm{Tr}\left[\sum_{j=1}^{i}\sum_{k=1}^{i} U_{ij} I_i U_{ik}' \dot{q}_j \dot{q}_k\right], \\ &= \frac{1}{2}\sum_{i=1}^{n}\sum_{j=1}^{n}\sum_{k=1}^{n} \left[\mathrm{Tr}\left(U_{ij} I_i U_{ik}'\right)\dot{q}_j \dot{q}_k\right]. \end{aligned} \tag{6.20}$$

6.1.6 Potential Energy of n-Link Robot Manipulators

Now, we obtain the total potential energy for an n-link manipulator. Let, m_i be a mass and ${}^i\bar{r}$ be a center of gravity of link i in frame i. Then, the potential energy of the link is

$$P_i = -m_i \mathbf{g} T_i^0 \bar{r}_i^i, \tag{6.21}$$

where the gravity vector $\mathbf{g} = [g_x \; g_y \; g_z \; 0] = [0 \; 0 \; -9.81 \; 0]$ with units of m/s^2, and with the assumption that the manipulator is level at sea level, and the base z axis is directed vertically upward.

The total potential energy, therefore, is

$$P = -\sum_{i=1}^{n} m_i \mathbf{g} T_i^0 \bar{r}_i^i. \tag{6.22}$$

6.1.7 Derivation of n-Link Robot Manipulator Dynamical Equation

The Lagrangian for the n-link robot manipulator can be written using (6.20) and (6.22)

$$L = K - P = \frac{1}{2} \sum_{i=1}^{n} \sum_{j=1}^{n} \sum_{k=1}^{n} \left[\mathrm{Tr}\left(U_{ij} I_i U_{ik}' \right) \dot{q}_j \dot{q}_k \right] + m_i g' T_i^0 \bar{r}_i^i. \tag{6.23}$$

The terms required in Euler-Lagrangian equation (6.4) are

$$\frac{\partial L}{\partial \dot{q}_k} = \frac{\partial K}{\partial \dot{q}_k} = \sum_{j=1}^{n} \sum_{i=1}^{n} \left[\mathrm{Tr}\left(U_{ik} I_i U_{ik}' \right) \dot{q}_j \right], \tag{6.24}$$

$$\begin{aligned}
\frac{d}{dt}\left(\frac{\partial L}{\partial \dot{q}_k} \right) &= \sum_{j=1}^{n} \sum_{i=1}^{n} \left[\mathrm{Tr}\left(U_{ij} I_i U_{ik}' \right) \ddot{q}_j \right] + \sum_{i=1}^{n} \sum_{j=1}^{n} \sum_{i=1}^{n} \left[\mathrm{Tr}\left\{ \frac{\partial}{\partial q_i} \left(U_{ij} I_i U_{ik}' \right) \right\} \right] \dot{q}_i \dot{q}_j, \\
&= \sum_{j=1}^{n} \sum_{i=1}^{n} \left[\mathrm{Tr}\left(U_{ij} I_i U_{ik}' \right) \ddot{q}_j \right] + \frac{1}{2} \sum_{i=1}^{n} \sum_{j=1}^{n} \sum_{i=1}^{n} \left[\mathrm{Tr}\left\{ \frac{\partial}{\partial q_i} \left(U_{ij} I_i U_{ik}' \right) \right\} \right] \dot{q}_i \dot{q}_j \\
&\quad + \frac{1}{2} \sum_{i=1}^{n} \sum_{j=1}^{n} \sum_{j=1}^{n} \left[\mathrm{Tr}\left\{ \frac{\partial}{\partial q_j} \left(U_{jk} I_j U_{ji}' \right) \right\} \right] \dot{q}_i \dot{q}_j,
\end{aligned} \tag{6.25}$$

where the second term on the first line is split by interchanging the order of summation and taking advantage of symmetry.

$$\frac{\partial L}{\partial q_k} = \frac{1}{2} \sum_{i=1}^{n} \sum_{j=1}^{n} \sum_{k=1}^{n} \left[\mathrm{Tr}\left\{ \frac{\partial}{\partial q_k} \left(U_{kj} I_k U_{ki}' \right) \right\} \right] \dot{q}_k \dot{q}_m - \sum_{j=i}^{n} m_j \mathbf{g} U_{ji} \bar{r}_j^j \tag{6.26}$$

Then, the dynamical equation for an n-link robot manipulators can be written using the Euler-Lagrangian equation (6.4) $\frac{d}{dt}\frac{\partial L}{\partial \dot{q}_k} - \frac{\partial L}{\partial q_k} = \tau_k$, and then using expression from (6.25) and (6.26)

$$\sum_{j=1}^{n}\sum_{i=1}^{n}\left[\mathrm{Tr}\left(U_{ij}I_iU_{ik}'\right)\ddot{q}_j\right] + \frac{1}{2}\sum_{i=1}^{n}\sum_{j=1}^{n}\sum_{i=1}^{n}\left[\mathrm{Tr}\left\{\frac{\partial}{\partial q_i}\left(U_{ij}I_iU_{ik}'\right)\right\}\right]\dot{q}_i\dot{q}_j \tag{6.27}$$

$$+\frac{1}{2}\sum_{i=1}^{n}\sum_{j=1}^{n}\sum_{j=1}^{n}\left[\mathrm{Tr}\left\{\frac{\partial}{\partial q_j}\left(U_{jk}I_jU_{ji}'\right)\right\}\right]\dot{q}_i\dot{q}_j - \frac{1}{2}\sum_{i=1}^{n}\sum_{j=1}^{n}\sum_{k=1}^{n}\left[\mathrm{Tr}\left\{\frac{\partial}{\partial q_k}\left(U_{kj}I_kU_{ki}'\right)\right\}\right]\dot{q}_k\dot{q}_m$$

$$+\sum_{j=i}^{n} m_j g' U_{ji}\bar{r}_j^j = \tau_k$$

$$= \sum_{j=1}^{n}\sum_{i=1}^{n}\left[\mathrm{Tr}\left(U_{ij}I_iU_{ik}'\right)\ddot{q}_j\right] + \frac{1}{2}\sum_{i=1}^{n}\sum_{j=1}^{n}\left[\frac{\partial}{\partial q_i}\left\{\sum_{i=1}^{n}\mathrm{Tr}\left(U_{ij}I_iU_{ik}'\right)\right\}\right.$$

$$\left.+\frac{\partial}{\partial q_j}\left\{\sum_{j=1}^{n}\mathrm{Tr}\left(U_{jk}I_jU_{ji}'\right)\right\} - \frac{\partial}{\partial q_k}\left\{\sum_{k=1}^{n}\mathrm{Tr}\left(U_{kj}I_kU_{ki}'\right)\right\}\right]\dot{q}_i\dot{q}_j$$

$$+\sum_{j=i}^{n} m_j \mathbf{g} U_{ji}\bar{r}_j^j = \tau_k. \tag{6.28}$$

We write the Euler-Lagrange equation in (6.28) as

$$\boxed{\sum_{j=1}^{n} M_{kj}\ddot{q}_j + \sum_{i=1}^{n}\sum_{j=1}^{n} V_{ijk}\dot{q}_i\dot{q}_j + G_i = \tau_k, \qquad k = 1,2,\cdots,n}. \tag{6.29}$$

In matrix form, (6.29) can be written as

$$\boxed{\mathbf{M}(\mathbf{q})\ddot{\mathbf{q}} + \mathbf{V}(\mathbf{q},\dot{\mathbf{q}}) + \mathbf{G}(\mathbf{q}) = \boldsymbol{\tau}}, \tag{6.30}$$

where

$\boldsymbol{\tau}$ is an $n \times 1$ generalized torque vector applied at joints $1,2,\cdots,n$, and can be expressed as,

$$\tau = \begin{bmatrix}\tau_1 & \tau_2 & \cdots \tau_n\end{bmatrix}'. \tag{6.31}$$

$\mathbf{q}$ is an $n \times 1$ vector of joint variables of the robot arm, and can be expressed as,

$$\mathbf{q} = \begin{bmatrix}q_1 & q_2 & \cdots q_n\end{bmatrix}'. \tag{6.32}$$

$\dot{\mathbf{q}}$ is an $n \times 1$ vector of joint velocity of the robot arm, and can be expressed as,

$$\dot{\mathbf{q}} = \begin{bmatrix}\dot{q}_1 & \dot{q}_2 & \cdots \dot{q}_n\end{bmatrix}'. \tag{6.33}$$

$\ddot{\mathbf{q}}$ is an $n \times 1$ vector of joint acceleration of the robot arm, and can be expressed as,

$$\ddot{\mathbf{q}} = \begin{bmatrix} \ddot{q}_1 & \ddot{q}_2 & \cdots \ddot{q}_n \end{bmatrix}'. \tag{6.34}$$

$\mathbf{M}$ is an $n \times n$ symmetric generalized inertia matrix, whose elements are

$$M_{kj} = \sum_{i=\max(k,j)}^{n} \mathrm{Tr}\left(U_{ij} I_i U_{ik}'\right), \qquad k, j = 1, 2, \cdots, n. \tag{6.35}$$

U_{ij} and U_{ik} are the product terms of transformation matrices defined in Eq. (6.13). $\mathbf{V}$ is an $n \times 1$ nonlinear Coriolis and centrifugal force vector, whose elements are

$$\mathbf{V} = \begin{bmatrix} V_1 & V_2 & \cdots V_n \end{bmatrix}'. \tag{6.36}$$

where

$$V_i = \sum_{i=1}^{n} \sum_{j=1}^{n} V_{ijk} \dot{q}_i \dot{q}_j \tag{6.37}$$

and

$$V_{ijk} = \frac{1}{2} \left[\frac{\partial}{\partial q_i} \left\{ \sum_{i=1}^{n} \mathrm{Tr}\left(U_{ij} I_i U_{ik}'\right) \right\} + \frac{\partial}{\partial q_j} \left\{ \sum_{j=1}^{n} \mathrm{Tr}\left(U_{jk} I_j U_{ji}'\right) \right\} - \frac{\partial}{\partial q_k} \left\{ \sum_{k=1}^{n} \mathrm{Tr}\left(U_{kj} I_k U_{ki}'\right) \right\} \right]. \tag{6.38}$$

Eq. (6.38) can be rewritten as,

$$V_{ijk} = \sum_{m=\max(i,j,k)}^{n} \mathrm{Tr}\left(U_{mjk} I_m U_{mi}'\right). \tag{6.39}$$

V_{ijk} is known as Christoffel symbols of the first kind.

$\mathbf{G}$ is an n gravity loading force vector, whose elements are

$$\mathbf{G} = \begin{bmatrix} G_1 & G_2 & \cdots G_n \end{bmatrix}' \tag{6.40}$$

where

$$G_i = \sum_{j=i}^{n} m_j \mathbf{g} U_{ji} \bar{r}_j^j. \tag{6.41}$$

Here the gravity vector is indicated by $\mathbf{g} = [g_x \; g_y \; g_z \; 0] = [0 \; 0 \; -9.81 \; 0]$ for mass m_j with the centers of gravity vector $\bar{r}_j^j = \begin{bmatrix} \bar{x}_j & \bar{y}_j & \bar{z}_j & 1 \end{bmatrix}'$.

Eq. (6.30) describes the robot manipulator rigid-body dynamics. The equation is also known as the inverse dynamics since given the pose, velocity, and accelerations it computes the required joint forces or torques.

6.2 Mathematical Modeling of Baxter Robot

The Baxter robot has seven links. Following the non-linear model of n-link robot in (6.30), we write the model for one manipulator or arm of Baxter robot

$$\mathbf{M}(\mathbf{q})\ddot{\mathbf{q}} + \mathbf{V}(\mathbf{q}, \dot{\mathbf{q}}) + \mathbf{G}(\mathbf{q}) = \boldsymbol{\tau}. \tag{6.42}$$

where the symmetric generalized inertia matrix is denoted by $\mathbf{M}$, Coriolis and centrifugal force vector by $\mathbf{V}$, gravity loading force vector by $\mathbf{G}$, joint variable vector by $\mathbf{q}$, and torque vector by $\boldsymbol{\tau}$. Next, we obtain the expressions for $\mathbf{M}$, $\mathbf{V}$, and $\mathbf{G}$ in terms of transformation matrices.

6.2.1 Generalized Inertia Matrix M

Here, we express $\mathbf{M}$ in terms of the transformation matrices.

$$\mathbf{M} = \begin{bmatrix} M_{11} & M_{12} & M_{13} & M_{14} & M_{15} & M_{16} & M_{17} \\ M_{12} & M_{22} & M_{23} & M_{24} & M_{25} & M_{26} & M_{27} \\ M_{13} & M_{23} & M_{33} & M_{34} & M_{35} & M_{36} & M_{37} \\ M_{14} & M_{24} & M_{34} & M_{44} & M_{45} & M_{46} & M_{47} \\ M_{15} & M_{25} & M_{35} & M_{45} & M_{55} & M_{56} & M_{57} \\ M_{16} & M_{26} & M_{36} & M_{46} & M_{56} & M_{66} & M_{67} \\ M_{17} & M_{27} & M_{37} & M_{47} & M_{57} & M_{67} & M_{77} \end{bmatrix}. \tag{6.43}$$

The elements of $\mathbf{M}$ can be written according to the expression in (6.35). Note that U_{ij} is the product terms of transformation matrices defined in Eq. (6.13), and I_i is the pseudo-inertia matrix. Now, we write the expression for each element in (6.43).

$$
\begin{aligned}
M_{11} &= \mathrm{Tr}(U_{11}I_1U'_{11}) + \mathrm{Tr}(U_{21}I_2U'_{21}) + \mathrm{Tr}(U_{31}I_3U'_{31}) + \mathrm{Tr}(U_{41}I_4U'_{41}) + \mathrm{Tr}(U_{51}I_5U'_{51}) \\
&\quad + \mathrm{Tr}(U_{61}I_6U'_{61}) + \mathrm{Tr}(U_{71}I_7U'_{71}), \\
M_{12} &= \mathrm{Tr}(U_{22}I_2U'_{21}) + \mathrm{Tr}(U_{32}I_3U'_{31}) + \mathrm{Tr}(U_{42}I_4U'_{41}) + \mathrm{Tr}(U_{52}I_5U'_{51}) + \mathrm{Tr}(U_{62}I_6U'_{61}) \\
&\quad + \mathrm{Tr}(U_{72}I_7U'_{71}), \\
M_{13} &= \mathrm{Tr}(U_{33}I_3U'_{31}) + \mathrm{Tr}(U_{43}I_4U'_{41}) + \mathrm{Tr}(U_{53}I_5U'_{51}) + \mathrm{Tr}(U_{63}I_6U'_{61}) + \mathrm{Tr}(U_{73}I_7U'_{71}), \\
M_{14} &= \mathrm{Tr}(U_{44}I_4U'_{41}) + \mathrm{Tr}(U_{54}I_5U'_{51}) + \mathrm{Tr}(U_{64}I_6U'_{61}) + \mathrm{Tr}(U_{74}I_7U'_{71}), \\
M_{15} &= \mathrm{Tr}(U_{55}I_5U'_{51}) + \mathrm{Tr}(U_{65}I_6U'_{61}) + \mathrm{Tr}(U_{75}I_7U'_{71}), \\
M_{16} &= \mathrm{Tr}(U_{66}I_6U'_{61}) + \mathrm{Tr}(U_{76}I_7U'_{71}), \\
M_{17} &= \mathrm{Tr}(U_{77}I_7U'_{71}),
\end{aligned}
$$

$$
\begin{aligned}
M_{22} &= \mathrm{Tr}(U_{22}I_2U'_{22}) + \mathrm{Tr}(U_{32}I_3U'_{32}) + \mathrm{Tr}(U_{42}I_4U'_{42}) + \mathrm{Tr}(U_{52}I_5U'_{52}) \\
&\quad + \mathrm{Tr}(U_{62}I_6U'_{62}) + \mathrm{Tr}(U_{72}I_7U'_{72}), \\
M_{23} &= \mathrm{Tr}(U_{33}I_3U'_{33}) + \mathrm{Tr}(U_{43}I_4U'_{43}) + \mathrm{Tr}(U_{53}I_5U'_{53}) + \mathrm{Tr}(U_{63}I_6U'_{63}) + \mathrm{Tr}(U_{73}I_7U'_{73}), \\
M_{24} &= \mathrm{Tr}(U_{44}I_4U'_{42}) + \mathrm{Tr}(U_{54}I_5U'_{52}) + \mathrm{Tr}(U_{64}I_6U'_{62}) + \mathrm{Tr}(U_{74}I_7U'_{72}), \\
M_{25} &= \mathrm{Tr}(U_{55}I_5U'_{52}) + \mathrm{Tr}(U_{65}I_6U'_{62}) + \mathrm{Tr}(U_{75}I_7U'_{72}), \\
M_{26} &= \mathrm{Tr}(U_{66}I_6U'_{62}) + \mathrm{Tr}(U_{76}I_7U'_{72}), \\
M_{27} &= \mathrm{Tr}(U_{77}I_7U'_{72}), \\
M_{33} &= \mathrm{Tr}(U_{33}I_3U'_{33}) + \mathrm{Tr}(U_{43}I_4U'_{43}) + \mathrm{Tr}(U_{53}I_5U'_{53}) + \mathrm{Tr}(U_{63}I_6U'_{63}) + \mathrm{Tr}(U_{73}I_7U'_{73}), \\
M_{34} &= \mathrm{Tr}(U_{44}I_4U'_{43}) + \mathrm{Tr}(U_{54}I_5U'_{53}) + \mathrm{Tr}(U_{64}I_6U'_{63}) + \mathrm{Tr}(U_{74}I_7U'_{73}), \\
M_{35} &= \mathrm{Tr}(U_{55}I_5U'_{53}) + \mathrm{Tr}(U_{65}I_6U'_{63}) + \mathrm{Tr}(U_{75}I_7U'_{73}), \\
M_{36} &= \mathrm{Tr}(U_{66}I_6U'_{63}) + \mathrm{Tr}(U_{76}I_7U'_{73}), \\
M_{37} &= \mathrm{Tr}(U_{77}I_7U'_{73}),
\end{aligned}
$$

$$M_{44} = \mathrm{Tr}(U_{44} I_4 U'_{44}) + \mathrm{Tr}(U_{54} I_5 U'_{54}) + \mathrm{Tr}(U_{64} I_6 U'_{64}) + \mathrm{Tr}(U_{74} I_7 U'_{74}),$$
$$M_{45} = \mathrm{Tr}(U_{55} I_5 U'_{54}) + \mathrm{Tr}(U_{65} I_6 U'_{64}) + \mathrm{Tr}(U_{75} I_7 U'_{74}),$$
$$M_{46} = \mathrm{Tr}(U_{66} I_6 U'_{64}) + \mathrm{Tr}(U_{76} I_7 U'_{74}),$$
$$M_{47} = \mathrm{Tr}(U_{77} I_7 U'_{74}),$$
$$M_{55} = \mathrm{Tr}(U_{55} I_5 U'_{55}) + \mathrm{Tr}(U_{65} I_6 U'_{65}) + \mathrm{Tr}(U_{75} I_7 U'_{75}),$$
$$M_{56} = \mathrm{Tr}(U_{66} I_6 U'_{65}) + \mathrm{Tr}(U_{76} I_7 U'_{75}),$$
$$M_{57} = \mathrm{Tr}(U_{77} I_7 U'_{75}),$$
$$M_{66} = \mathrm{Tr}(U_{66} I_6 U'_{66}) + \mathrm{Tr}(U_{76} I_7 U'_{76}),$$
$$M_{67} = \mathrm{Tr}(U_{77} I_7 U'_{76}),$$
$$M_{77} = \mathrm{Tr}(U_{77} I_7 U'_{77}).$$

Here U_{ij} is defined as in (6.13),

$$U_{ij} \equiv \frac{\partial T_i^0}{\partial q_i} = \begin{cases} T_{j-1}^0 W_j T_i^{j-1}, & \text{for} \quad i \geq j \\ 0, & \text{for} \quad i < j \end{cases} . \tag{6.44}$$

$$U_{11} = T_0^0 W_1 T_1^0,$$
$$U_{21} = T_0^0 W_1 T_2^0,$$
$$U_{22} = T_1^0 W_2 T_2^1,$$
$$U_{31} = T_0^0 W_1 T_2^0,$$
$$U_{32} = T_1^0 W_2 T_2^1,$$
$$U_{33} = T_2^0 W_3 T_3^2,$$
$$U_{41} = T_0^0 W_1 T_4^0,$$
$$U_{42} = T_1^0 W_2 T_4^1,$$
$$U_{43} = T_2^0 W_3 T_4^2,$$
$$U_{44} = T_3^0 W_4 T_4^3,$$

$$U_{51} = T_0^0 W_1 T_5^0,$$
$$U_{52} = T_1^0 W_2 T_5^1,$$
$$U_{53} = T_2^0 W_3 T_5^2,$$
$$U_{54} = T_3^0 W_4 T_5^3,$$
$$U_{55} = T_4^0 W_5 T_5^4,$$
$$U_{61} = T_0^0 W_1 T_6^0,$$
$$U_{62} = T_1^0 W_2 T_6^1,$$
$$U_{63} = T_2^0 W_3 T_6^2,$$
$$U_{64} = T_3^0 W_4 T_6^3,$$
$$U_{65} = T_4^0 W_5 T_6^4,$$
$$U_{66} = T_5^0 W_6 T_6^5,$$

$$U_{71} = T_0^0 W_1 T_7^0,$$
$$U_{72} = T_1^0 W_2 T_7^1,$$
$$U_{73} = T_2^0 W_3 T_7^2,$$
$$U_{74} = T_3^0 W_4 T_7^3,$$
$$U_{75} = T_4^0 W_5 T_7^4,$$
$$U_{76} = T_5^0 W_6 T_7^5,$$
$$U_{77} = T_6^0 W_6 T_7^6.$$

$$U_{12} = U_{13} = U_{14} = U_{15} = U_{16} = U_{17} = U_{23} = U_{24} = U_{25} = U_{26} = U_{27} = U_{34} = U_{35} = U_{36}$$
$$= U_{37} = U_{45} = U_{46} = U_{47} = U_{56} = U_{57} = U_{67} = 0.$$

The pseudo-inertia matrices are computed from (6.18)

$$I_i = \begin{bmatrix} \frac{-I_{xxi}+I_{yyi}+I_{zzi}}{2} & I_{xyi} & I_{xzi} & m\bar{x}_i \\ I_{xyi} & \frac{I_{xxi}-I_{yyi}+I_{zzi}}{2} & I_{yzi} & m\bar{y}_i \\ I_{xyi} & I_{yzi} & \frac{I_{xxi}+I_{yyi}-I_{zzi}}{2} & m\bar{z}_i \\ m\bar{x}_i & m\bar{y}_i & m\bar{z}_i & m \end{bmatrix}. \tag{6.45}$$

The homogeneous transformation matrices are computed from (6.5) and (6.9), which are stated as follows.

$$T_i^j = \begin{cases} A_{j+1}A_{j+2}\cdots A_{i-1}A_i, & i > j \\ I, & i = j \\ (T_i^j)^{-1}, & i < j \end{cases}. \tag{6.46}$$

$$T_i^{i-1} = A_i = \begin{bmatrix} \cos\theta_i & -\sin\theta_i\cos\alpha_i & \sin\theta_i\sin\alpha_i & a_i\cos\theta_i \\ \sin\theta_i & \cos\theta_i\cos\alpha_i & -\cos\theta_i\sin\alpha_i & a_i\sin\theta_i \\ 0 & \sin\alpha_i & \cos\alpha_i & d_i \\ 0 & 0 & 0 & 1 \end{bmatrix} \tag{6.47}$$

The following relationship are also necessary.

$$\begin{aligned} T_2^0 &= T_1^0 T_2^1, \\ T_3^0 &= T_1^0 T_2^1 T_3^2, \\ T_4^0 &= T_1^0 T_2^1 T_3^2 T_4^3, \\ T_5^0 &= T_1^0 T_2^1 T_3^2 T_4^3 T_5^4, \\ T_6^0 &= T_1^0 T_2^1 T_3^2 T_4^3 T_5^4 T_6^5, \\ T_7^0 &= T_1^0 T_2^1 T_3^2 T_4^3 T_5^4 T_6^5 T_7^6. \end{aligned}$$

6.2.2 Coriolis and Centrifugal Force Vector V

From (6.36) and (6.37), we write the Coriolis and Centrifugal vector

$$V_i = \dot{\mathbf{q}}' \mathbf{V}_{i,h} \dot{\mathbf{q}}, \tag{6.48}$$

$$\dot{\mathbf{q}}(t) = \begin{bmatrix} \dot{q}_1(t) & \dot{q}_2(t) & \dot{q}_3(t) & \dot{q}_4(t) & \dot{q}_5(t) & \dot{q}_6(t) & \dot{q}_7(t) \end{bmatrix}', \tag{6.49}$$

and

$$\mathbf{V}(\mathbf{q}, \dot{\mathbf{q}}) = \begin{bmatrix} V_1 \\ V_2 \\ V_3 \\ V_4 \\ V_5 \\ V_6 \\ V_7 \end{bmatrix} = \begin{bmatrix} \dot{\mathbf{q}}'\mathbf{V}_{1,h}\dot{\mathbf{q}} \\ \dot{\mathbf{q}}'\mathbf{V}_{2,h}\dot{\mathbf{q}} \\ \dot{\mathbf{q}}'\mathbf{V}_{3,h}\dot{\mathbf{q}} \\ \dot{\mathbf{q}}'\mathbf{V}_{4,h}\dot{\mathbf{q}} \\ \dot{\mathbf{q}}'\mathbf{V}_{5,h}\dot{\mathbf{q}} \\ \dot{\mathbf{q}}'\mathbf{V}_{6,h}\dot{\mathbf{q}} \\ \dot{\mathbf{q}}'\mathbf{V}_{7,h}\dot{\mathbf{q}} \end{bmatrix} \tag{6.50}$$

where $\mathbf{V}_{1,h}, \mathbf{V}_{2,h}, \cdots \mathbf{V}_{7,h}$ constitute a vector of matrices. Note that $\dot{\mathbf{q}}'$ is 1×7 vector, $\mathbf{V}_{i,h}$ is a 7×7 matrix, and $\dot{\mathbf{q}}$ is a 7×1 vector. The product of these three terms give V_i, which is 1×1. The elements of those matrices are defined by the expression given in (6.41). In general, we can express $\mathbf{V}_{i,h}$ as follows, where h represents 11, 12, 13, 14, 15, 16, 17, 22, 23, 24, 25, 26, 27, 33, 34, 35, 36, 37, 44, 45, 46, 47, 55, 56, 57, 66, 67, and 77.

$$V_{i,h} = \begin{bmatrix} V_{i11} & V_{i12} & V_{i13} & V_{i14} & V_{i15} & V_{i16} & V_{i17} \\ V_{i12} & V_{i22} & V_{i23} & V_{i24} & V_{i25} & V_{i26} & V_{i27} \\ V_{i13} & V_{i23} & V_{i33} & V_{i34} & V_{i35} & V_{i36} & V_{i37} \\ V_{i14} & V_{i24} & V_{i34} & V_{i44} & V_{i45} & V_{i46} & V_{i47} \\ V_{i15} & V_{i25} & V_{i35} & V_{i45} & V_{i55} & V_{i56} & V_{i57} \\ V_{i16} & V_{i26} & V_{i36} & V_{i46} & V_{i56} & V_{i66} & V_{i67} \\ V_{i17} & V_{i27} & V_{i37} & V_{i47} & V_{i57} & V_{i67} & V_{i77} \end{bmatrix}, \qquad i = 1, 2, \cdots, 7. \tag{6.51}$$

The elements of $V_{1,h}$ are

$$
\begin{aligned}
V_{111} &= \mathrm{Tr}(U_{111}I_1U'_{11}) + \mathrm{Tr}(U_{211}I_2U'_{21}) + \mathrm{Tr}(U_{311}I_3U'_{31}) + \mathrm{Tr}(U_{411}I_4U'_{41}) + \mathrm{Tr}(U_{511}I_5U'_{51}) \\
&\quad + \mathrm{Tr}(U_{611}I_6U'_{61}) + \mathrm{Tr}(U_{711}I_7U'_{71}) \\
V_{112} &= \mathrm{Tr}(U_{212}I_2U'_{21}) + \mathrm{Tr}(U_{312}I_3U'_{31}) + \mathrm{Tr}(U_{412}I_4U'_{41}) + \mathrm{Tr}(U_{512}I_5U'_{51}) + \mathrm{Tr}(U_{612}I_6U'_{61}) \\
&\quad + \mathrm{Tr}(U_{712}I_7U'_{71}) \\
V_{113} &= \mathrm{Tr}(U_{313}I_3U'_{31}) + \mathrm{Tr}(U_{413}I_4U'_{41}) + \mathrm{Tr}(U_{513}I_5U'_{51}) + \mathrm{Tr}(U_{613}I_6U'_{61}) + \mathrm{Tr}(U_{713}I_7U'_{71}) \\
V_{114} &= \mathrm{Tr}(U_{414}I_4U'_{41}) + \mathrm{Tr}(U_{514}I_5U'_{51}) + \mathrm{Tr}(U_{614}I_6U'_{61}) + \mathrm{Tr}(U_{714}I_7U'_{71}) \\
V_{115} &= \mathrm{Tr}(U_{515}I_5U'_{51}) + \mathrm{Tr}(U_{615}I_6U'_{61}) + \mathrm{Tr}(U_{715}I_7U'_{71}) \\
V_{116} &= \mathrm{Tr}(U_{616}I_6U'_{61}) + \mathrm{Tr}(U_{716}I_7U'_{71}) \\
V_{117} &= \mathrm{Tr}(U_{717}I_7U'_{71})
\end{aligned}
$$

$$
\begin{aligned}
V_{122} &= \mathrm{Tr}(U_{222}I_2U'_{21}) + \mathrm{Tr}(U_{322}I_3U'_{31}) + \mathrm{Tr}(U_{422}I_4U'_{41}) + \mathrm{Tr}(U_{522}I_5U'_{51}) + \mathrm{Tr}(U_{622}I_6U'_{61}) \\
&\quad + \mathrm{Tr}(U_{722}I_7U'_{71}), \\
V_{123} &= \mathrm{Tr}(U_{323}I_3U'_{31}) + \mathrm{Tr}(U_{423}I_4U'_{41}) + \mathrm{Tr}(U_{523}I_5U'_{51}) + \mathrm{Tr}(U_{623}I_6U'_{61}) + \mathrm{Tr}(U_{723}I_7U'_{71}), \\
V_{124} &= \mathrm{Tr}(U_{424}I_4U'_{41}) + \mathrm{Tr}(U_{524}I_5U'_{51}) + \mathrm{Tr}(U_{624}I_6U'_{61}) + \mathrm{Tr}(U_{724}I_7U'_{71}), \\
V_{125} &= \mathrm{Tr}(U_{525}I_5U'_{51}) + \mathrm{Tr}(U_{625}I_6U'_{61}) + \mathrm{Tr}(U_{725}I_7U'_{71}), \\
V_{126} &= \mathrm{Tr}(U_{626}I_6U'_{61}) + \mathrm{Tr}(U_{726}I_7U'_{71}), \\
V_{127} &= \mathrm{Tr}(U_{727}I_7U'_{71}),
\end{aligned}
$$

$$
\begin{aligned}
V_{133} &= \mathrm{Tr}(U_{333}I_3U'_{31}) + \mathrm{Tr}(U_{433}I_4U'_{41}) + \mathrm{Tr}(U_{533}I_5U'_{51}) + \mathrm{Tr}(U_{633}I_6U'_{61}) + \mathrm{Tr}(U_{733}I_7U'_{71}), \\
V_{134} &= \mathrm{Tr}(U_{434}I_4U'_{41}) + \mathrm{Tr}(U_{534}I_5U'_{51}) + \mathrm{Tr}(U_{634}I_6U'_{61}) + \mathrm{Tr}(U_{734}I_7U'_{71}), \\
V_{135} &= \mathrm{Tr}(U_{535}I_5U'_{51}) + \mathrm{Tr}(U_{635}I_6U'_{61}) + \mathrm{Tr}(U_{735}I_7U'_{71}), \\
V_{136} &= \mathrm{Tr}(U_{636}I_6U'_{61}) + \mathrm{Tr}(U_{736}I_7U'_{71}), \\
V_{137} &= \mathrm{Tr}(U_{736}I_7U'_{71}),
\end{aligned}
$$

$$V_{144} = \mathrm{Tr}(U_{444}I_4U'_{41}) + \mathrm{Tr}(U_{544}I_5U'_{51}) + \mathrm{Tr}(U_{644}I_6U'_{61}) + \mathrm{Tr}(U_{744}I_7U'_{71}),$$
$$V_{145} = \mathrm{Tr}(U_{545}I_5U'_{51}) + \mathrm{Tr}(U_{645}I_6U'_{61}) + \mathrm{Tr}(U_{745}I_7U'_{71}),$$
$$V_{146} = \mathrm{Tr}(U_{646}I_6U'_{61}) + \mathrm{Tr}(U_{746}I_7U'_{71}),$$
$$V_{147} = \mathrm{Tr}(U_{747}I_7U'_{71}),$$

$$V_{155} = \mathrm{Tr}(U_{555}I_5U'_{51}) + \mathrm{Tr}(U_{655}I_6U'_{61}) + \mathrm{Tr}(U_{755}I_7U'_{71}),$$
$$V_{156} = \mathrm{Tr}(U_{656}I_6U'_{61}) + \mathrm{Tr}(U_{756}I_7U'_{71}),$$
$$V_{157} = \mathrm{Tr}(U_{757}I_7U'_{71}),$$

$$V_{166} = \mathrm{Tr}(U_{666}I_6U'_{61}) + \mathrm{Tr}(U_{766}I_7U'_{71}),$$
$$V_{167} = \mathrm{Tr}(U_{767}I_7U'_{71}),$$

$$V_{177} = \mathrm{Tr}(U_{777}I_7U'_{71}).$$

$$\begin{aligned}V_{211} &= \mathrm{Tr}(U_{211}I_2U'_{22}) + \mathrm{Tr}(U_{311}I_3U'_{32}) + \mathrm{Tr}(U_{411}I_4U'_{42}) + \mathrm{Tr}(U_{511}I_5U'_{52}) + \mathrm{Tr}(U_{611}I_6U'_{62}) \\ &\quad + \mathrm{Tr}(U_{711}I_7U'_{72})\\ V_{212} &= \mathrm{Tr}(U_{212}I_2U'_{22}) + \mathrm{Tr}(U_{312}I_3U'_{32}) + \mathrm{Tr}(U_{412}I_4U'_{42}) + \mathrm{Tr}(U_{512}I_5U'_{52}) + \mathrm{Tr}(U_{612}I_6U'_{62}) \\ &\quad + \mathrm{Tr}(U_{712}I_7U'_{72})\\ V_{213} &= \mathrm{Tr}(U_{313}I_3U'_{32}) + \mathrm{Tr}(U_{413}I_4U'_{42}) + \mathrm{Tr}(U_{513}I_5U'_{52}) + \mathrm{Tr}(U_{613}I_6U'_{62}) + \mathrm{Tr}(U_{713}I_7U'_{72})\\ V_{214} &= \mathrm{Tr}(U_{414}I_4U'_{42}) + \mathrm{Tr}(U_{514}I_5U'_{52}) + \mathrm{Tr}(U_{614}I_6U'_{62}) + \mathrm{Tr}(U_{714}I_7U'_{72})\\ V_{215} &= \mathrm{Tr}(U_{515}I_5U'_{52}) + \mathrm{Tr}(U_{615}I_6U'_{62}) + \mathrm{Tr}(U_{715}I_7U'_{72})\\ V_{216} &= \mathrm{Tr}(U_{616}I_6U'_{62}) + \mathrm{Tr}(U_{716}I_7U'_{72})\\ V_{217} &= \mathrm{Tr}(U_{717}I_7U'_{72}),\end{aligned}$$

$$V_{222} = \mathrm{Tr}(U_{222}I_2U'_{22}) + \mathrm{Tr}(U_{322}I_3U'_{32}) + \mathrm{Tr}(U_{422}I_4U'_{42}) + \mathrm{Tr}(U_{522}I_5U'_{21}) + \mathrm{Tr}(U_{622}I_6U'_{62}) + \mathrm{Tr}(U_{722}I_7U'_{72}),$$

$$V_{223} = \mathrm{Tr}(U_{323}I_3U'_{32}) + \mathrm{Tr}(U_{423}I_4U'_{42}) + \mathrm{Tr}(U_{523}I_5U'_{21}) + \mathrm{Tr}(U_{623}I_6U'_{62}) + \mathrm{Tr}(U_{723}I_7U'_{72}),$$

$$V_{224} = \mathrm{Tr}(U_{424}I_4U'_{42}) + \mathrm{Tr}(U_{524}I_5U'_{21}) + \mathrm{Tr}(U_{624}I_6U'_{62}) + \mathrm{Tr}(U_{724}I_7U'_{72}),$$

$$V_{225} = \mathrm{Tr}(U_{525}I_5U'_{21}) + \mathrm{Tr}(U_{625}I_6U'_{62}) + \mathrm{Tr}(U_{725}I_7U'_{72}),$$

$$V_{226} = \mathrm{Tr}(U_{626}I_6U'_{62}) + \mathrm{Tr}(U_{726}I_7U'_{72}),$$

$$V_{227} = \mathrm{Tr}(U_{726}I_7U'_{72}),$$

$$V_{233} = \mathrm{Tr}(U_{333}I_3U'_{32}) + \mathrm{Tr}(U_{433}I_4U'_{42}) + \mathrm{Tr}(U_{533}I_5U'_{52}) + \mathrm{Tr}(U_{633}I_6U'_{62}) + \mathrm{Tr}(U_{733}I_7U'_{72}),$$

$$V_{234} = \mathrm{Tr}(U_{434}I_4U'_{42}) + \mathrm{Tr}(U_{534}I_5U'_{52}) + \mathrm{Tr}(U_{634}I_6U'_{62}) + \mathrm{Tr}(U_{734}I_7U'_{72}),$$

$$V_{235} = \mathrm{Tr}(U_{535}I_5U'_{52}) + \mathrm{Tr}(U_{635}I_6U'_{62}) + \mathrm{Tr}(U_{735}I_7U'_{72}),$$

$$V_{236} = \mathrm{Tr}(U_{636}I_6U'_{62}) + \mathrm{Tr}(U_{736}I_7U'_{72}),$$

$$V_{237} = \mathrm{Tr}(U_{737}I_7U'_{72}),$$

$$V_{244} = \mathrm{Tr}(U_{444}I_4U'_{44}) + \mathrm{Tr}(U_{544}I_5U'_{54}) + \mathrm{Tr}(U_{644}I_6U'_{64}) + \mathrm{Tr}(U_{744}I_7U'_{74}),$$

$$V_{245} = \mathrm{Tr}(U_{545}I_5U'_{54}) + \mathrm{Tr}(U_{645}I_6U'_{64}) + \mathrm{Tr}(U_{745}I_7U'_{74}),$$

$$V_{246} = \mathrm{Tr}(U_{646}I_6U'_{64}) + \mathrm{Tr}(U_{746}I_7U'_{74}),$$

$$V_{247} = \mathrm{Tr}(U_{747}I_7U'_{74}),$$

$$V_{255} = \mathrm{Tr}(U_{555}I_5U'_{52}) + \mathrm{Tr}(U_{655}I_6U'_{62}) + \mathrm{Tr}(U_{755}I_7U'_{72}),$$

$$V_{256} = \mathrm{Tr}(U_{656}I_6U'_{62}) + \mathrm{Tr}(U_{756}I_7U'_{72}),$$

$$V_{257} = \mathrm{Tr}(U_{757}I_7U'_{72}),$$

$$V_{266} = \mathrm{Tr}(U_{666}I_6U'_{62}) + \mathrm{Tr}(U_{766}I_7U'_{72}),$$

$$V_{267} = \mathrm{Tr}(U_{767}I_7U'_{72}),$$

$$V_{277} = \mathrm{Tr}(U_{777}I_7U'_{72}),$$

$$V_{311} = \mathrm{Tr}(U_{311}I_3U'_{33}) + \mathrm{Tr}(U_{411}I_4U'_{43}) + \mathrm{Tr}(U_{511}I_5U'_{53}) + \mathrm{Tr}(U_{611}I_6U'_{63}) + \mathrm{Tr}(U_{711}I_7U'_{73}),$$
$$V_{312} = \mathrm{Tr}(U_{312}I_3U'_{33}) + \mathrm{Tr}(U_{412}I_4U'_{43}) + \mathrm{Tr}(U_{512}I_5U'_{53}) + \mathrm{Tr}(U_{612}I_6U'_{63}) + \mathrm{Tr}(U_{712}I_7U'_{73}),$$
$$V_{313} = \mathrm{Tr}(U_{313}I_3U'_{33}) + \mathrm{Tr}(U_{413}I_4U'_{43}) + \mathrm{Tr}(U_{513}I_5U'_{53}) + \mathrm{Tr}(U_{613}I_6U'_{63}) + \mathrm{Tr}(U_{713}I_7U'_{73}),$$
$$V_{314} = \mathrm{Tr}(U_{414}I_4U'_{43}) + \mathrm{Tr}(U_{514}I_5U'_{53}) + \mathrm{Tr}(U_{614}I_6U'_{63}) + \mathrm{Tr}(U_{714}I_7U'_{73}),$$
$$V_{315} = \mathrm{Tr}(U_{515}I_5U'_{53}) + \mathrm{Tr}(U_{615}I_6U'_{63}) + \mathrm{Tr}(U_{715}I_7U'_{73}),$$
$$V_{316} = \mathrm{Tr}(U_{616}I_6U'_{63}) + \mathrm{Tr}(U_{716}I_7U'_{73}),$$
$$V_{317} = \mathrm{Tr}(U_{716}I_7U'_{73}),$$

$$V_{322} = \mathrm{Tr}(U_{322}I_3U'_{33}) + \mathrm{Tr}(U_{422}I_4U'_{43}) + \mathrm{Tr}(U_{522}I_5U'_{53}) + \mathrm{Tr}(U_{622}I_6U'_{63}) + \mathrm{Tr}(U_{722}I_7U'_{73}),$$
$$V_{323} = \mathrm{Tr}(U_{323}I_3U'_{33}) + \mathrm{Tr}(U_{423}I_4U'_{43}) + \mathrm{Tr}(U_{523}I_5U'_{53}) + \mathrm{Tr}(U_{623}I_6U'_{63}) + \mathrm{Tr}(U_{723}I_7U'_{73}),$$
$$V_{324} = \mathrm{Tr}(U_{424}I_4U'_{43}) + \mathrm{Tr}(U_{524}I_5U'_{53}) + \mathrm{Tr}(U_{624}I_6U'_{63}) + \mathrm{Tr}(U_{724}I_7U'_{73}),$$
$$V_{325} = \mathrm{Tr}(U_{525}I_5U'_{53}) + \mathrm{Tr}(U_{625}I_6U'_{63}) + \mathrm{Tr}(U_{725}I_7U'_{73}),$$
$$V_{326} = \mathrm{Tr}(U_{626}I_6U'_{63}) + \mathrm{Tr}(U_{726}I_7U'_{73}),$$
$$V_{327} = \mathrm{Tr}(U_{726}I_7U'_{73}),$$

$$V_{333} = \mathrm{Tr}(U_{333}I_3U'_{33}) + \mathrm{Tr}(U_{433}I_4U'_{43}) + \mathrm{Tr}(U_{533}I_5U'_{53}) + \mathrm{Tr}(U_{633}I_6U'_{63}) + \mathrm{Tr}(U_{733}I_7U'_{73}),$$
$$V_{334} = \mathrm{Tr}(U_{434}I_4U'_{43}) + \mathrm{Tr}(U_{534}I_5U'_{53}) + \mathrm{Tr}(U_{634}I_6U'_{63}) + \mathrm{Tr}(U_{734}I_7U'_{73}),$$
$$V_{335} = \mathrm{Tr}(U_{535}I_5U'_{53}) + \mathrm{Tr}(U_{635}I_6U'_{63}) + \mathrm{Tr}(U_{735}I_7U'_{73}),$$
$$V_{336} = \mathrm{Tr}(U_{636}I_6U'_{63}) + \mathrm{Tr}(U_{736}I_7U'_{73}),$$
$$V_{337} = \mathrm{Tr}(U_{737}I_7U'_{73}),$$

$$V_{344} = \mathrm{Tr}(U_{444}I_4U'_{43}) + \mathrm{Tr}(U_{544}I_5U'_{53}) + \mathrm{Tr}(U_{644}I_6U'_{63}) + \mathrm{Tr}(U_{744}I_7U'_{73}),$$
$$V_{345} = \mathrm{Tr}(U_{545}I_5U'_{53}) + \mathrm{Tr}(U_{645}I_6U'_{63}) + \mathrm{Tr}(U_{745}I_7U'_{73}),$$
$$V_{346} = \mathrm{Tr}(U_{646}I_6U'_{63}) + \mathrm{Tr}(U_{746}I_7U'_{73}),$$
$$V_{347} = \mathrm{Tr}(U_{747}I_7U'_{73}),$$

$$V_{355} = \mathrm{Tr}(U_{555}I_5U'_{53}) + \mathrm{Tr}(U_{655}I_6U'_{63}) + \mathrm{Tr}(U_{755}I_7U'_{73}),$$
$$V_{356} = \mathrm{Tr}(U_{656}I_6U'_{63}) + \mathrm{Tr}(U_{756}I_7U'_{73}),$$
$$V_{357} = \mathrm{Tr}(U_{757}I_7U'_{73}),$$

$$V_{366} = \mathrm{Tr}(U_{666} I_6 U'_{63}) + \mathrm{Tr}(U_{766} I_7 U'_{73}),$$
$$V_{367} = \mathrm{Tr}(U_{767} I_7 U'_{73}),$$

$$V_{377} = \mathrm{Tr}(U_{777} I_7 U'_{73}).$$

$$V_{411} = \mathrm{Tr}(U_{411} I_4 U'_{44}) + \mathrm{Tr}(U_{511} I_5 U'_{54}) + \mathrm{Tr}(U_{611} I_6 U'_{64}) + \mathrm{Tr}(U_{711} I_7 U'_{74}),$$
$$V_{412} = \mathrm{Tr}(U_{412} I_4 U'_{44}) + \mathrm{Tr}(U_{512} I_5 U'_{54}) + \mathrm{Tr}(U_{612} I_6 U'_{64}) + \mathrm{Tr}(U_{712} I_7 U'_{74}),$$
$$V_{413} = \mathrm{Tr}(U_{413} I_4 U'_{44}) + \mathrm{Tr}(U_{513} I_5 U'_{54}) + \mathrm{Tr}(U_{613} I_6 U'_{64}) + \mathrm{Tr}(U_{713} I_7 U'_{74}),$$
$$V_{414} = \mathrm{Tr}(U_{414} I_4 U'_{44}) + \mathrm{Tr}(U_{514} I_5 U'_{54}) + \mathrm{Tr}(U_{614} I_6 U'_{64}) + \mathrm{Tr}(U_{714} I_7 U'_{74}),$$
$$V_{415} = \mathrm{Tr}(U_{515} I_5 U'_{54}) + \mathrm{Tr}(U_{615} I_6 U'_{64}) + \mathrm{Tr}(U_{715} I_7 U'_{74}),$$
$$V_{416} = \mathrm{Tr}(U_{616} I_6 U'_{64}) + \mathrm{Tr}(U_{716} I_7 U'_{74}),$$
$$V_{417} = \mathrm{Tr}(U_{717} I_7 U'_{74}),$$

$$V_{422} = \mathrm{Tr}(U_{422} I_4 U'_{44}) + \mathrm{Tr}(U_{522} I_5 U'_{54}) + \mathrm{Tr}(U_{622} I_6 U'_{64}) + \mathrm{Tr}(U_{722} I_7 U'_{74}),$$
$$V_{423} = \mathrm{Tr}(U_{423} I_4 U'_{44}) + \mathrm{Tr}(U_{523} I_5 U'_{54}) + \mathrm{Tr}(U_{623} I_6 U'_{64}) + \mathrm{Tr}(U_{723} I_7 U'_{74}),$$
$$V_{424} = \mathrm{Tr}(U_{424} I_4 U'_{44}) + \mathrm{Tr}(U_{524} I_5 U'_{54}) + \mathrm{Tr}(U_{624} I_6 U'_{64}) + \mathrm{Tr}(U_{724} I_7 U'_{74}),$$
$$V_{425} = \mathrm{Tr}(U_{525} I_5 U'_{54}) + \mathrm{Tr}(U_{625} I_6 U'_{64}) + \mathrm{Tr}(U_{725} I_7 U'_{74}),$$
$$V_{426} = \mathrm{Tr}(U_{626} I_6 U'_{64}) + \mathrm{Tr}(U_{726} I_7 U'_{74}),$$
$$V_{427} = \mathrm{Tr}(U_{727} I_7 U'_{74}),$$

$$V_{433} = \mathrm{Tr}(U_{433} I_4 U'_{44}) + \mathrm{Tr}(U_{533} I_5 U'_{54}) + \mathrm{Tr}(U_{633} I_6 U'_{64}) + \mathrm{Tr}(U_{733} I_7 U'_{74}),$$
$$V_{434} = \mathrm{Tr}(U_{434} I_4 U'_{44}) + \mathrm{Tr}(U_{534} I_5 U'_{54}) + \mathrm{Tr}(U_{634} I_6 U'_{64}) + \mathrm{Tr}(U_{734} I_7 U'_{74}),$$
$$V_{435} = \mathrm{Tr}(U_{535} I_5 U'_{54}) + \mathrm{Tr}(U_{635} I_6 U'_{64}) + \mathrm{Tr}(U_{735} I_7 U'_{74}),$$
$$V_{436} = \mathrm{Tr}(U_{636} I_6 U'_{64}) + \mathrm{Tr}(U_{736} I_7 U'_{74}),$$
$$V_{437} = \mathrm{Tr}(U_{737} I_7 U'_{74}),$$

$$V_{444} = \mathrm{Tr}(U_{444}I_4U'_{44}) + \mathrm{Tr}(U_{544}I_5U'_{54}) + \mathrm{Tr}(U_{644}I_6U'_{64}) + \mathrm{Tr}(U_{744}I_7U'_{74}),$$
$$V_{445} = \mathrm{Tr}(U_{545}I_5U'_{54}) + \mathrm{Tr}(U_{645}I_6U'_{64}) + \mathrm{Tr}(U_{745}I_7U'_{74}),$$
$$V_{446} = \mathrm{Tr}(U_{646}I_6U'_{64}) + \mathrm{Tr}(U_{746}I_7U'_{74}),$$
$$V_{447} = \mathrm{Tr}(U_{747}I_7U'_{74}),$$

$$V_{455} = \mathrm{Tr}(U_{555}I_5U'_{54}) + \mathrm{Tr}(U_{655}I_6U'_{64}) + \mathrm{Tr}(U_{755}I_7U'_{74}),$$
$$V_{456} = \mathrm{Tr}(U_{656}I_6U'_{64}) + \mathrm{Tr}(U_{756}I_7U'_{74}),$$
$$V_{457} = \mathrm{Tr}(U_{757}I_7U'_{74}),$$

$$V_{466} = \mathrm{Tr}(U_{666}I_6U'_{64}) + \mathrm{Tr}(U_{766}I_7U'_{74}),$$
$$V_{467} = \mathrm{Tr}(U_{767}I_7U'_{74}),$$

$$V_{477} = \mathrm{Tr}(U_{777}I_7U'_{74}).$$

$$V_{511} = \mathrm{Tr}(U_{511}I_5U'_{55}) + \mathrm{Tr}(U_{611}I_6U'_{65}) + \mathrm{Tr}(U_{711}I_7U'_{75}),$$
$$V_{512} = \mathrm{Tr}(U_{512}I_5U'_{55}) + \mathrm{Tr}(U_{612}I_6U'_{65}) + \mathrm{Tr}(U_{712}I_7U'_{75}),$$
$$V_{513} = \mathrm{Tr}(U_{513}I_5U'_{55}) + \mathrm{Tr}(U_{613}I_6U'_{65}) + \mathrm{Tr}(U_{713}I_7U'_{75}),$$
$$V_{514} = \mathrm{Tr}(U_{514}I_5U'_{55}) + \mathrm{Tr}(U_{614}I_6U'_{65}) + \mathrm{Tr}(U_{714}I_7U'_{75}),$$
$$V_{515} = \mathrm{Tr}(U_{515}I_5U'_{55}) + \mathrm{Tr}(U_{615}I_6U'_{65}) + \mathrm{Tr}(U_{715}I_7U'_{75}),$$
$$V_{516} = \mathrm{Tr}(U_{616}I_6U'_{65}) + \mathrm{Tr}(U_{715}I_7U'_{75}),$$
$$V_{517} = \mathrm{Tr}(U_{717}I_7U'_{75}),$$

$$V_{522} = \mathrm{Tr}(U_{522}I_5U'_{55}) + \mathrm{Tr}(U_{622}I_6U'_{65}) + \mathrm{Tr}(U_{722}I_7U'_{75}),$$
$$V_{523} = \mathrm{Tr}(U_{523}I_5U'_{55}) + \mathrm{Tr}(U_{623}I_6U'_{65}) + \mathrm{Tr}(U_{723}I_7U'_{75}),$$
$$V_{524} = \mathrm{Tr}(U_{524}I_5U'_{55}) + \mathrm{Tr}(U_{624}I_6U'_{65}) + \mathrm{Tr}(U_{724}I_7U'_{75}),$$
$$V_{525} = \mathrm{Tr}(U_{525}I_5U'_{55}) + \mathrm{Tr}(U_{625}I_6U'_{65}) + \mathrm{Tr}(U_{725}I_7U'_{75}),$$
$$V_{526} = \mathrm{Tr}(U_{626}I_6U'_{65}) + \mathrm{Tr}(U_{725}I_7U'_{75}),$$
$$V_{527} = \mathrm{Tr}(U_{727}I_7U'_{75}),$$

$$V_{533} = \mathrm{Tr}(U_{533}I_5U'_{55}) + \mathrm{Tr}(U_{633}I_6U'_{65}) + \mathrm{Tr}(U_{733}I_7U'_{75}),$$
$$V_{534} = \mathrm{Tr}(U_{534}I_5U'_{55}) + \mathrm{Tr}(U_{634}I_6U'_{65}) + \mathrm{Tr}(U_{734}I_7U'_{75}),$$
$$V_{535} = \mathrm{Tr}(U_{535}I_5U'_{55}) + \mathrm{Tr}(U_{635}I_6U'_{65}) + \mathrm{Tr}(U_{735}I_7U'_{75}),$$
$$V_{536} = \mathrm{Tr}(U_{636}I_6U'_{65}) + \mathrm{Tr}(U_{735}I_7U'_{75}),$$
$$V_{537} = \mathrm{Tr}(U_{737}I_7U'_{75}),$$

$$V_{544} = \mathrm{Tr}(U_{544}I_5U'_{55}) + \mathrm{Tr}(U_{644}I_6U'_{65}) + \mathrm{Tr}(U_{744}I_7U'_{75}),$$
$$V_{545} = \mathrm{Tr}(U_{545}I_5U'_{55}) + \mathrm{Tr}(U_{645}I_6U'_{65}) + \mathrm{Tr}(U_{745}I_7U'_{75}),$$
$$V_{546} = \mathrm{Tr}(U_{646}I_6U'_{65}) + \mathrm{Tr}(U_{745}I_7U'_{75}),$$
$$V_{547} = \mathrm{Tr}(U_{747}I_7U'_{75}),$$

$$V_{555} = \mathrm{Tr}(U_{555}I_5U'_{55}) + \mathrm{Tr}(U_{655}I_6U'_{65}) + \mathrm{Tr}(U_{755}I_7U'_{75}),$$
$$V_{556} = \mathrm{Tr}(U_{656}I_6U'_{65}) + \mathrm{Tr}(U_{755}I_7U'_{75}),$$
$$V_{557} = \mathrm{Tr}(U_{757}I_7U'_{75}),$$

$$V_{566} = \mathrm{Tr}(U_{666}I_6U'_{65}) + \mathrm{Tr}(U_{765}I_7U'_{75}),$$
$$V_{567} = \mathrm{Tr}(U_{767}I_7U'_{75}),$$

$$V_{577} = \mathrm{Tr}(U_{777}I_7U'_{75}),$$

$$V_{611} = \mathrm{Tr}(U_{611}I_6U'_{66}) + \mathrm{Tr}(U_{711}I_7U'_{76}),$$
$$V_{612} = \mathrm{Tr}(U_{612}I_6U'_{66}) + \mathrm{Tr}(U_{712}I_7U'_{76}),$$
$$V_{613} = \mathrm{Tr}(U_{613}I_6U'_{66}) + \mathrm{Tr}(U_{713}I_7U'_{76}),$$
$$V_{614} = \mathrm{Tr}(U_{614}I_6U'_{66}) + \mathrm{Tr}(U_{714}I_7U'_{76}),$$
$$V_{615} = \mathrm{Tr}(U_{615}I_6U'_{66}) + \mathrm{Tr}(U_{715}I_7U'_{76}),$$
$$V_{616} = \mathrm{Tr}(U_{616}I_6U'_{66}) + \mathrm{Tr}(U_{716}I_7U'_{76}),$$
$$V_{617} = \mathrm{Tr}(U_{717}I_7U'_{76}),$$

$$V_{622} = \mathrm{Tr}(U_{622} I_6 U'_{66}) + \mathrm{Tr}(U_{722} I_7 U'_{76}),$$
$$V_{623} = \mathrm{Tr}(U_{623} I_6 U'_{66}) + \mathrm{Tr}(U_{723} I_7 U'_{76}),$$
$$V_{624} = \mathrm{Tr}(U_{624} I_6 U'_{66}) + \mathrm{Tr}(U_{724} I_7 U'_{76}),$$
$$V_{625} = \mathrm{Tr}(U_{625} I_6 U'_{66}) + \mathrm{Tr}(U_{725} I_7 U'_{76}),$$
$$V_{626} = \mathrm{Tr}(U_{626} I_6 U'_{66}) + \mathrm{Tr}(U_{726} I_7 U'_{76}),$$
$$V_{627} = \mathrm{Tr}(U_{727} I_7 U'_{76}),$$

$$V_{633} = \mathrm{Tr}(U_{633} I_6 U'_{66}) + \mathrm{Tr}(U_{733} I_7 U'_{76}),$$
$$V_{634} = \mathrm{Tr}(U_{634} I_6 U'_{66}) + \mathrm{Tr}(U_{734} I_7 U'_{76}),$$
$$V_{635} = \mathrm{Tr}(U_{635} I_6 U'_{66}) + \mathrm{Tr}(U_{735} I_7 U'_{76}),$$
$$V_{636} = \mathrm{Tr}(U_{636} I_6 U'_{66}) + \mathrm{Tr}(U_{736} I_7 U'_{76}),$$
$$V_{637} = \mathrm{Tr}(U_{737} I_7 U'_{76}),$$

$$V_{644} = \mathrm{Tr}(U_{644} I_6 U'_{66}) + \mathrm{Tr}(U_{744} I_7 U'_{76}),$$
$$V_{645} = \mathrm{Tr}(U_{645} I_6 U'_{66}) + \mathrm{Tr}(U_{745} I_7 U'_{76}),$$
$$V_{646} = \mathrm{Tr}(U_{646} I_6 U'_{66}) + \mathrm{Tr}(U_{746} I_7 U'_{76}),$$
$$V_{647} = \mathrm{Tr}(U_{747} I_7 U'_{76}),$$

$$V_{655} = \mathrm{Tr}(U_{655} I_6 U'_{66}) + \mathrm{Tr}(U_{755} I_7 U'_{76}),$$
$$V_{656} = \mathrm{Tr}(U_{656} I_6 U'_{66}) + \mathrm{Tr}(U_{756} I_7 U'_{76}),$$
$$V_{657} = \mathrm{Tr}(U_{757} I_7 U'_{76}),$$

$$V_{666} = \mathrm{Tr}(U_{666} I_6 U'_{66}) + \mathrm{Tr}(U_{766} I_7 U'_{76}),$$
$$V_{667} = \mathrm{Tr}(U_{767} I_7 U'_{76}),$$

$$V_{677} = \mathrm{Tr}(U_{777} I_7 U'_{76}),$$

$$V_{711} = \mathrm{Tr}(U_{711} I_7 U'_{77}),$$
$$V_{712} = \mathrm{Tr}(U_{712} I_7 U'_{77}),$$
$$V_{713} = \mathrm{Tr}(U_{713} I_7 U'_{77}),$$
$$V_{714} = \mathrm{Tr}(U_{714} I_7 U'_{77}),$$
$$V_{715} = \mathrm{Tr}(U_{715} I_7 U'_{77}),$$
$$V_{716} = \mathrm{Tr}(U_{716} I_7 U'_{77}),$$
$$V_{717} = \mathrm{Tr}(U_{717} I_7 U'_{77}),$$

$$V_{722} = \mathrm{Tr}(U_{722} I_7 U'_{77}),$$
$$V_{723} = \mathrm{Tr}(U_{723} I_7 U'_{77}),$$
$$V_{724} = \mathrm{Tr}(U_{724} I_7 U'_{77}),$$
$$V_{725} = \mathrm{Tr}(U_{725} I_7 U'_{77}),$$
$$V_{726} = \mathrm{Tr}(U_{726} I_7 U'_{77}),$$
$$V_{727} = \mathrm{Tr}(U_{727} I_7 U'_{77}),$$

$$V_{733} = \mathrm{Tr}(U_{733} I_7 U'_{77}),$$
$$V_{734} = \mathrm{Tr}(U_{734} I_7 U'_{77}),$$
$$V_{735} = \mathrm{Tr}(U_{735} I_7 U'_{77}),$$
$$V_{736} = \mathrm{Tr}(U_{736} I_7 U'_{77}),$$
$$V_{737} = \mathrm{Tr}(U_{737} I_7 U'_{77}),$$

$$V_{744} = \mathrm{Tr}(U_{744} I_7 U'_{77}),$$
$$V_{745} = \mathrm{Tr}(U_{745} I_7 U'_{77}),$$
$$V_{746} = \mathrm{Tr}(U_{746} I_7 U'_{77}),$$
$$V_{747} = \mathrm{Tr}(U_{747} I_7 U'_{77}),$$

$$V_{755} = \mathrm{Tr}(U_{755} I_7 U'_{77}),$$
$$V_{756} = \mathrm{Tr}(U_{756} I_7 U'_{77}),$$
$$V_{757} = \mathrm{Tr}(U_{757} I_7 U'_{77}),$$

$$V_{766} = \mathrm{Tr}(U_{766} I_7 U'_{77}),$$
$$V_{767} = \mathrm{Tr}(U_{767} I_7 U'_{77}),$$

$$V_{777} = \mathrm{Tr}(U_{777} I_7 U'_{77}).$$

Here U_{ijk} is defined as in (6.15)

$$\frac{\partial U_{ij}}{\partial q_k} \equiv U_{ijk} = \begin{cases} T^0_{j-1} W_j T^{j-1}_{k-1} W_k T^{k-1}_i, & \text{for} \quad i \geq k \geq j \\ T^0_{k-1} W_k T^{k-1}_{j-1} W_j T^{j-1}_i, & \text{for} \quad i \geq j \geq k \\ 0, & \text{for} \quad i < j \quad \text{or} \quad i < k \end{cases} . \tag{6.52}$$

$$U_{111} = T^0_0 W_1 T^0_0 W_1 T^0_1,$$
$$U_{222} = T^0_1 W_2 T^1_1 W_2 T^1_2,$$
$$U_{333} = T^0_2 W_3 T^2_2 W_3 T^2_3,$$
$$U_{444} = T^0_3 W_4 T^3_3 W_4 T^3_4,$$
$$U_{555} = T^0_4 W_5 T^4_4 W_5 T^4_5,$$
$$U_{666} = T^0_5 W_6 T^5_5 W_6 T^5_6,$$
$$U_{777} = T^0_6 W_7 T^6_6 W_7 T^6_7.$$

$$U_{211} = T^0_0 W_1 T^0_0 W_1 T^0_2,$$
$$U_{221} = T^0_0 W_1 T^0_1 W_2 T^1_2 = U_{212},$$
$$U_{222} = T^0_1 W_2 T^1_1 W_2 T^1_2.$$

$$
\begin{aligned}
U_{311} &= T_0^0 W_1 T_1^0 W_2 T_3^1, \\
U_{321} &= T_0^0 W_1 T_1^0 W_2 T_3^1 = U_{312}, \\
U_{322} &= T_1^0 W_2 T_1^0 W_2 T_3^1, \\
U_{331} &= T_0^0 W_1 T_2^0 W_3 T_3^2 = U_{313}, \\
U_{332} &= T_1^0 W_2 T_2^0 W_3 T_3^2 = U_{323}, \\
U_{333} &= T_2^0 W_3 T_2^2 W_3 T_3^2.
\end{aligned}
$$

$$
\begin{aligned}
U_{411} &= T_0^0 W_1 T_0^0 W_1 T_4^0, \\
U_{421} &= T_0^0 W_1 T_1^0 W_2 T_4^1 = U_{412}, \\
U_{422} &= T_1^0 W_2 T_1^1 W_2 T_4^1, \\
U_{431} &= T_0^0 W_1 T_2^0 W_3 T_4^2 = U_{413}, \\
U_{432} &= T_1^0 W_2 T_2^1 W_3 T_4^2 = U_{423}, \\
U_{433} &= T_2^0 W_3 T_2^2 W_3 T_4^2, \\
U_{441} &= T_0^0 W_1 T_3^0 W_4 T_4^3 = U_{414}, \\
U_{442} &= T_1^0 W_2 T_3^1 W_4 T_4^3 = U_{424}, \\
U_{443} &= T_2^0 W_3 T_3^2 W_4 T_4^3 = U_{434}, \\
U_{444} &= T_3^0 W_4 T_3^3 W_4 T_4^3,
\end{aligned}
$$

$$
\begin{aligned}
U_{511} &= T_0^0 W_1 T_0^0 W_1 T_5^0, \\
U_{521} &= T_0^0 W_1 T_1^0 W_2 T_5^1 = U_{512}, \\
U_{522} &= T_1^0 W_2 T_1^1 W_2 T_5^1, \\
U_{531} &= T_0^0 W_1 T_2^0 W_3 T_5^2 = U_{513}, \\
U_{532} &= T_1^0 W_2 T_2^1 W_3 T_5^2 = U_{523}, \\
U_{533} &= T_2^0 W_3 T_2^2 W_3 T_5^2, \\
U_{541} &= T_0^0 W_1 T_3^0 W_4 T_5^3 = U_{514}, \\
U_{542} &= T_1^0 W_2 T_3^1 W_4 T_5^3 = U_{524}, \\
U_{543} &= T_2^0 W_3 T_3^2 W_4 T_5^3 = U_{534}, \\
U_{544} &= T_3^0 W_4 T_3^3 W_4 T_5^3, \\
U_{551} &= T_0^0 W_1 T_4^0 W_5 T_5^4 = U_{515}, \\
U_{552} &= T_1^0 W_2 T_4^1 W_5 T_5^4 = U_{525}, \\
U_{553} &= T_2^0 W_3 T_4^2 W_5 T_5^4 = U_{535}, \\
U_{554} &= T_3^0 W_4 T_4^3 W_5 T_5^4 = U_{545}, \\
U_{555} &= T_4^0 W_5 T_4^4 W_5 T_5^4
\end{aligned}
$$

$$
\begin{aligned}
U_{611} &= T_0^0 W_1 T_0^0 W_1 T_6^0, \\
U_{621} &= T_0^0 W_1 T_1^0 W_2 T_6^1 = U_{612}, \\
U_{622} &= T_1^0 W_2 T_1^1 W_2 T_6^1, \\
U_{631} &= T_0^0 W_1 T_2^0 W_3 T_6^2 = U_{613}, \\
U_{632} &= T_1^0 W_2 T_2^1 W_3 T_6^2 = U_{623}, \\
U_{633} &= T_2^0 W_3 T_2^2 W_3 T_6^2, \\
U_{641} &= T_0^0 W_1 T_3^0 W_4 T_6^3 = U_{614}, \\
U_{642} &= T_1^0 W_2 T_3^1 W_4 T_6^3 = U_{624}, \\
U_{643} &= T_2^0 W_3 T_3^2 W_4 T_6^3 = U_{634}, \\
U_{644} &= T_3^0 W_4 T_3^3 W_4 T_6^3, \\
U_{651} &= T_0^0 W_1 T_4^0 W_5 T_6^4 = U_{615}, \\
U_{652} &= T_1^0 W_2 T_4^1 W_5 T_6^4 = U_{625}, \\
U_{653} &= T_2^0 W_3 T_4^2 W_5 T_6^4 = U_{635}, \\
U_{654} &= T_3^0 W_4 T_4^3 W_5 T_6^4 = U_{645}, \\
U_{655} &= T_4^0 W_5 T_4^4 W_5 T_6^4, \\
U_{661} &= T_0^0 W_1 T_5^0 W_6 T_6^5 = U_{616}, \\
U_{662} &= T_1^0 W_2 T_5^1 W_6 T_6^5 = U_{626}, \\
U_{663} &= T_2^0 W_3 T_5^2 W_6 T_6^5 = U_{636}, \\
U_{664} &= T_3^0 W_4 T_5^3 W_6 T_6^5 = U_{646}, \\
U_{665} &= T_4^0 W_5 T_5^4 W_6 T_6^5 = U_{656}, \\
U_{666} &= T_5^0 W_6 T_5^5 W_6 T_6^5,
\end{aligned}
$$

$$
\begin{aligned}
U_{711} &= T_0^0 W_1 T_0^0 W_1 T_7^0, \\
U_{721} &= T_0^0 W_1 T_1^0 W_2 T_7^1 = U_{712}, \\
U_{722} &= T_1^0 W_2 T_1^1 W_2 T_7^1, \\
U_{731} &= T_0^0 W_1 T_2^0 W_3 T_7^2 = U_{713}, \\
U_{732} &= T_1^0 W_2 T_2^1 W_3 T_7^2 = U_{723}, \\
U_{733} &= T_2^0 W_3 T_2^2 W_3 T_7^2, \\
U_{741} &= T_0^0 W_1 T_3^0 W_4 T_7^3 = U_{714}, \\
U_{742} &= T_1^0 W_2 T_3^1 W_4 T_7^3 = U_{724}, \\
U_{743} &= T_2^0 W_3 T_3^2 W_4 T_7^3 = U_{734}, \\
U_{744} &= T_3^0 W_4 T_3^3 W_4 T_7^3, \\
U_{751} &= T_0^0 W_1 T_4^0 W_5 T_7^4 = U_{715}, \\
U_{752} &= T_1^0 W_2 T_4^1 W_5 T_7^4 = U_{725}, \\
U_{753} &= T_2^0 W_3 T_4^2 W_5 T_7^4 = U_{735}, \\
U_{754} &= T_3^0 W_4 T_4^3 W_5 T_7^4 = U_{745}, \\
U_{755} &= T_4^0 W_5 T_4^4 W_5 T_7^4, \\
U_{761} &= T_0^0 W_1 T_5^0 W_6 T_7^5 = U_{716}, \\
U_{762} &= T_1^0 W_2 T_5^1 W_6 T_7^5 = U_{726}, \\
U_{763} &= T_2^0 W_3 T_5^2 W_6 T_7^5 = U_{736}, \\
U_{764} &= T_3^0 W_4 T_5^3 W_6 T_7^5 = U_{746}, \\
U_{765} &= T_4^0 W_5 T_5^4 W_6 T_7^5 = U_{756}, \\
U_{766} &= T_5^0 W_6 T_5^5 W_6 T_7^5,
\end{aligned}
$$

$$
\begin{aligned}
U_{771} &= T_0^0 W_1 T_6^0 W_7 T_7^6 = U_{717},\\
U_{772} &= T_1^0 W_2 T_6^1 W_7 T_7^6 = U_{727},\\
U_{773} &= T_2^0 W_3 T_6^2 W_7 T_7^6 = U_{737},\\
U_{774} &= T_3^0 W_4 T_6^3 W_7 T_7^6 = U_{747},\\
U_{775} &= T_4^0 W_5 T_6^4 W_7 T_7^6 = U_{757},\\
U_{776} &= T_5^0 W_6 T_6^5 W_7 T_7^6 = U_{767},\\
U_{777} &= T_6^0 W_7 T_6^6 W_7 T_7^6
\end{aligned}
$$

6.2.3 Gravity Loading Force Vector G

The gravity vector can be shown as

$$
\mathbf{G}(\theta) = \begin{bmatrix} G_1 & G_2 & G_3 & G_4 & G_5 & G_6 & G_7 \end{bmatrix}, \tag{6.53}
$$

where

$$
\begin{aligned}
G_1 &= -\left(m_1\mathbf{g}U_{11}\bar{r}_1^1 + m_2\mathbf{g}U_{21}\bar{r}_2^2 + m_3\mathbf{g}U_{31}\bar{r}_3^3 + m_4\mathbf{g}U_{41}\bar{r}_4^4 + m_5\mathbf{g}U_{51}\bar{r}_5^5 + m_6\mathbf{g}U_{61}\bar{r}_6^6 + m_7\mathbf{g}U_{71}\bar{r}_7^7\right),\\
G_2 &= -\left(m_2\mathbf{g}U_{22}\bar{r}_2^2 + m_3\mathbf{g}U_{32}\bar{r}_3^3 + m_4\mathbf{g}U_{42}\bar{r}_4^4 + m_5\mathbf{g}U_{52}\bar{r}_5^5 + m_6\mathbf{g}U_{62}\bar{r}_6^6 + m_7\mathbf{g}U_{72}\bar{r}_7^7\right),\\
G_3 &= -\left(m_3\mathbf{g}U_{32}\bar{r}_3^3 + m_4\mathbf{g}U_{42}\bar{r}_4^4 + m_5\mathbf{g}U_{52}\bar{r}_5^5 + m_6\mathbf{g}U_{62}\bar{r}_6^6 + m_7\mathbf{g}U_{72}\bar{r}_7^7\right),\\
G_4 &= -\left(m_4\mathbf{g}U_{44}\bar{r}_4^4 + m_5\mathbf{g}U_{54}\bar{r}_5^5 + m_6\mathbf{g}U_{64}\bar{r}_6^6 + m_7\mathbf{g}U_{74}\bar{r}_7^7\right),\\
G_5 &= -\left(m_5\mathbf{g}U_{55}\bar{r}_5^5 + m_6\mathbf{g}U_{65}\bar{r}_6^6 + m_7\mathbf{g}U_{75}\bar{r}_7^7\right),\\
G_6 &= -\left(m_6\mathbf{g}U_{66}\bar{r}_6^6 + m_7\mathbf{g}U_{76}\bar{r}_7^7\right),\\
G_7 &= -m_7\mathbf{g}U_{77}\bar{r}_7^7.
\end{aligned} \tag{6.54}
$$

6.3 Linearized Dynamics of Baxter Robot

In this section, we derive a linearized perturbed model for Baxter robot. We consider an n-link robot with the initial control torque vector $\hat{\boldsymbol{\tau}}$ is related to the initial joint position, velocity, and acceleration vectors $\hat{\mathbf{q}}$, $\hat{\dot{\mathbf{q}}}$, and $\hat{\ddot{\mathbf{q}}}$ by

$$
\mathbf{M}(\hat{\mathbf{q}})\hat{\ddot{\mathbf{q}}} + \mathbf{V}(\hat{\mathbf{q}}, \hat{\dot{\mathbf{q}}}) + \mathbf{G}(\mathbf{q}) = \hat{\boldsymbol{\tau}}. \tag{6.55}
$$

We suppose that the operating point corresponding to the initial condition of the robot is denoted by $\mathbf{Q_0} = \left(\hat{\mathbf{q}}, \hat{\dot{\mathbf{q}}}, \boldsymbol{\tau}\right)$. Also, we suppose that the control torque vector is perturbed with a small variation of $\Delta\boldsymbol{\tau}$, that is, $\boldsymbol{\tau} = \hat{\boldsymbol{\tau}} + \Delta\boldsymbol{\tau}$. The resulting perturbation in the joint variables are $\Delta\mathbf{q}$, $\Delta\dot{\mathbf{q}}$, and $\Delta\ddot{\mathbf{q}}$, that is, $\mathbf{q} = \hat{\mathbf{q}} + \Delta\mathbf{q}$, $\dot{\mathbf{q}} = \hat{\dot{\mathbf{q}}} + \Delta\dot{\mathbf{q}}$, and $\ddot{\mathbf{q}} = \hat{\ddot{\mathbf{q}}} + \Delta\ddot{\mathbf{q}}$. From the nonlinear robot model described in (6.42), we write

$$\mathbf{M}(\hat{\mathbf{q}} + \Delta\mathbf{q})(\hat{\ddot{\mathbf{q}}} + \Delta\ddot{\mathbf{q}}) + \mathbf{V}(\hat{\mathbf{q}} + \Delta\mathbf{q}, \hat{\dot{\mathbf{q}}} + \Delta\dot{\mathbf{q}}) + \mathbf{G}(\mathbf{q}) = \boldsymbol{\tau} + \hat{}\Delta\boldsymbol{\tau}. \tag{6.56}$$

Expanding the vectors $\mathbf{V}$ and $\mathbf{G}$ we obtain

$$\mathbf{V}(\hat{\mathbf{q}} + \Delta\mathbf{q}, \hat{\dot{\mathbf{q}}} + \Delta\dot{\mathbf{q}}) = \mathbf{V}(\hat{\mathbf{q}}, \hat{\dot{\mathbf{q}}}) + \left[\frac{\partial \mathbf{V}}{\partial \mathbf{q}}\right]_{\mathbf{Q_0}} \Delta\mathbf{q} + \left[\frac{\partial \mathbf{V}}{\partial \dot{\mathbf{q}}}\right]_{\mathbf{Q_0}} \Delta\dot{\mathbf{q}} + \cdots \tag{6.57}$$

$$\mathbf{G}(\hat{\mathbf{q}} + \Delta\mathbf{q}) = \mathbf{G}(\hat{\mathbf{q}}) + \left[\frac{\partial \mathbf{G}}{\partial \mathbf{q}}\right]_{\mathbf{Q_0}} \Delta\mathbf{q} + \cdots, \tag{6.58}$$

where $\left[\frac{\partial \mathbf{V}}{\partial \mathbf{q}}\right]$, $\left[\frac{\partial \mathbf{V}}{\partial \dot{\mathbf{q}}}\right]$, and $\left[\frac{\partial \mathbf{G}}{\partial \mathbf{q}}\right]$ are $n \times n$ matrices whose (i, j)-th elements are

$$\left[\frac{\partial \mathbf{V}}{\partial \mathbf{q}}\right]_{ij} = \left[\frac{\partial V_i}{\partial q_j}\right],$$
$$\left[\frac{\partial \mathbf{V}}{\partial \dot{\mathbf{q}}}\right]_{ij} = \left[\frac{\partial V_i}{\partial \dot{q}_j}\right],$$
$$\left[\frac{\partial \mathbf{G}}{\partial \mathbf{q}}\right]_{ij} = \left[\frac{\partial G_i}{\partial q_j}\right].$$

We approximated the infinite series in (6.58) using the first order term only. We also assume $\mathbf{M}(\hat{\mathbf{q}} + \Delta\mathbf{q}) \approx \mathbf{M}(\hat{\mathbf{q}})$. Then from (6.56) we can write

$$\mathbf{M}(\hat{\ddot{\mathbf{q}}}) + \mathbf{A_p}\Delta\ddot{\mathbf{q}} + \mathbf{V}(\hat{\mathbf{q}}, \hat{\dot{\mathbf{q}}}) + \mathbf{C_{p1}}\Delta\mathbf{q} + \mathbf{B_p}\Delta\dot{\mathbf{q}} + \mathbf{G}(\hat{\mathbf{q}}) + \mathbf{C_{p2}}\Delta\mathbf{q} = \hat{\boldsymbol{\tau}} + \Delta\boldsymbol{\tau}, \tag{6.59}$$

where $\mathbf{A_p}$, $\mathbf{B_p}$, $\mathbf{C_{p1}}$, and $\mathbf{C_{p2}}$ are defined as

$$\mathbf{A_p} = [\mathbf{M}]_{\mathbf{Q_o}}, \quad \mathbf{B_p} = \left[\frac{\partial \mathbf{V}}{\partial \dot{\mathbf{q}}}\right]_{\mathbf{Q_o}}, \quad \mathbf{C_{p1}} = \left[\frac{\partial \mathbf{V}}{\partial \mathbf{q}}\right]_{\mathbf{Q_o}}, \quad \mathbf{C_{p2}} = \left[\frac{\partial \mathbf{G}}{\partial \mathbf{q}}\right]_{\mathbf{Q_o}}. \tag{6.60}$$

Now, substituting (6.56) into (6.59), we obtain

$$\mathbf{A_p}\Delta\ddot{\mathbf{q}} + \mathbf{B_p}\Delta\dot{\mathbf{q}} + \mathbf{G}(\hat{\mathbf{q}}) + \left(\mathbf{C_{p1}} + \mathbf{C_{p2}}\right)\Delta\mathbf{q} = \Delta\boldsymbol{\tau}. \tag{6.61}$$

Equation (6.61) is incremental linearized model of the non-linear robot dynamics for small perturbations about the operating point $\mathbf{Q_o}$. This state-space representation of (6.61) can

be written as

$$\begin{bmatrix} \Delta\dot{\mathbf{q}} \\ \Delta\ddot{\mathbf{q}} \end{bmatrix} = \begin{bmatrix} 0_{n\times n} & \mathbf{I}_{n\times n} \\ -\mathbf{A_p^{-1}}(\mathbf{C_{p1}}+\mathbf{C_{p2}}) & -\mathbf{A_p^{-1}}\mathbf{B_p} \end{bmatrix} \begin{bmatrix} \Delta\mathbf{q} \\ \Delta\dot{\mathbf{q}} \end{bmatrix} + \begin{bmatrix} 0_{n\times n} \\ \mathbf{A_p^{-1}} \end{bmatrix} \Delta\boldsymbol{\tau}. \tag{6.62}$$

The above state-space model is of order $2n$ with the $2n\times 1$ incremental state vector $[\Delta\mathbf{q}\ \Delta\dot{\mathbf{q}}]'$, and the $n\times 1$ incremental control vector $\Delta\boldsymbol{\tau}$, and the $n\times 1$ incremental output vector $\Delta\mathbf{q}$.

Now, each manipulator of Baxter has seven DOF. Following the example in (6.62), we write a linearized dynamics of the left manipulator of Baxter as follows:

$$\underbrace{\begin{bmatrix} \Delta\dot{\mathbf{q}}_l \\ \Delta\ddot{\mathbf{q}}_l \end{bmatrix}}_{14\times 1} = \overbrace{\underbrace{\begin{bmatrix} 0_{7\times 7} & \mathbf{I}_{7\times 7} \\ -\mathbf{A_{pl}^{-1}}(\mathbf{C_{pl1}}+\mathbf{C_{pl2}}) & -\mathbf{A_{pl}^{-1}}\mathbf{B_{pl}} \end{bmatrix}}_{14\times 14}}^{\mathbf{A}_l} \underbrace{\begin{bmatrix} \Delta\mathbf{q}_l \\ \Delta\dot{\mathbf{q}}_l \end{bmatrix}}_{14\times 1} + \overbrace{\underbrace{\begin{bmatrix} 0_{7\times 7} \\ \mathbf{A_{pl}^{-1}} \end{bmatrix}}_{14\times 7}}^{\mathbf{B}_l} \underbrace{\Delta\boldsymbol{\tau}}_{7\times 1}. \tag{6.63}$$

we write a linearized dynamics of the right manipulator of Baxter as follows:

$$\underbrace{\begin{bmatrix} \Delta\dot{\mathbf{q}}_r \\ \Delta\ddot{\mathbf{q}}_r \end{bmatrix}}_{14\times 1} = \overbrace{\underbrace{\begin{bmatrix} 0_{7\times 7} & \mathbf{I}_{7\times 7} \\ -\mathbf{A_{pr}^{-1}}(\mathbf{C_{pr1}}+\mathbf{C_{pr2}}) & -\mathbf{A_{pr}^{-1}}\mathbf{B_{pr}} \end{bmatrix}}_{14\times 14}}^{\mathbf{A}_r} \underbrace{\begin{bmatrix} \Delta\mathbf{q}_r \\ \Delta\dot{\mathbf{q}}_r \end{bmatrix}}_{14\times 1} + \overbrace{\underbrace{\begin{bmatrix} 0_{7\times 7} \\ \mathbf{A_{pr}^{-1}} \end{bmatrix}}_{14\times 7}}^{\mathbf{B}_r} \underbrace{\Delta\boldsymbol{\tau}}_{7\times 1}. \tag{6.64}$$

Note that 'l' and 'r' denote the left and right manipulator, respectively.

For determining $\mathbf{A_p}$, we evaluate $\mathbf{M}$ in (6.43) at an operating condition $\mathbf{Q_o}$.

For determining $\mathbf{B_p}$, we first obtain $\frac{\partial \mathbf{V}}{\partial \dot{\mathbf{q}}}$, and then evaluate the obtained term at $\mathbf{Q_0}$. Here we show obtaining the partial derivative from (6.50).

$$\frac{\partial \mathbf{V}}{\partial \dot{\mathbf{q}}} = \begin{bmatrix} \frac{\partial V_1}{\partial \dot{q}_1} & \frac{\partial V_1}{\partial \dot{q}_2} & \frac{\partial V_1}{\partial \dot{q}_3} & \frac{\partial V_1}{\partial \dot{q}_4} & \frac{\partial V_1}{\partial \dot{q}_5} & \frac{\partial V_1}{\partial \dot{q}_6} & \frac{\partial V_1}{\partial \dot{q}_7} \\ \frac{\partial V_2}{\partial \dot{q}_1} & \frac{\partial V_2}{\partial \dot{q}_2} & \frac{\partial V_2}{\partial \dot{q}_3} & \frac{\partial V_2}{\partial \dot{q}_4} & \frac{\partial V_2}{\partial \dot{q}_5} & \frac{\partial V_2}{\partial \dot{q}_6} & \frac{\partial V_2}{\partial \dot{q}_7} \\ \frac{\partial V_3}{\partial \dot{q}_1} & \frac{\partial V_3}{\partial \dot{q}_2} & \frac{\partial V_3}{\partial \dot{q}_3} & \frac{\partial V_3}{\partial \dot{q}_4} & \frac{\partial V_3}{\partial \dot{q}_5} & \frac{\partial V_3}{\partial \dot{q}_6} & \frac{\partial V_3}{\partial \dot{q}_7} \\ \frac{\partial V_4}{\partial \dot{q}_1} & \frac{\partial V_4}{\partial \dot{q}_2} & \frac{\partial V_4}{\partial \dot{q}_3} & \frac{\partial V_4}{\partial \dot{q}_4} & \frac{\partial V_4}{\partial \dot{q}_5} & \frac{\partial V_4}{\partial \dot{q}_6} & \frac{\partial V_4}{\partial \dot{q}_7} \\ \frac{\partial V_5}{\partial \dot{q}_1} & \frac{\partial V_5}{\partial \dot{q}_2} & \frac{\partial V_5}{\partial \dot{q}_3} & \frac{\partial V_5}{\partial \dot{q}_4} & \frac{\partial V_5}{\partial \dot{q}_5} & \frac{\partial V_5}{\partial \dot{q}_6} & \frac{\partial V_5}{\partial \dot{q}_7} \\ \frac{\partial V_6}{\partial \dot{q}_1} & \frac{\partial V_6}{\partial \dot{q}_2} & \frac{\partial V_6}{\partial \dot{q}_3} & \frac{\partial V_6}{\partial \dot{q}_4} & \frac{\partial V_6}{\partial \dot{q}_5} & \frac{\partial V_6}{\partial \dot{q}_6} & \frac{\partial V_6}{\partial \dot{q}_7} \\ \frac{\partial V_7}{\partial \dot{q}_1} & \frac{\partial V_7}{\partial \dot{q}_2} & \frac{\partial V_7}{\partial \dot{q}_3} & \frac{\partial V_7}{\partial \dot{q}_4} & \frac{\partial V_7}{\partial \dot{q}_5} & \frac{\partial V_7}{\partial \dot{q}_6} & \frac{\partial V_7}{\partial \dot{q}_7} \end{bmatrix}. \tag{6.65}$$

For determining $\mathbf{C_{p1}}$, we first obtain $\frac{\partial \mathbf{V}}{\partial \mathbf{q}}$, and then evaluate the obtained term at $\mathbf{Q_0}$. Here we show obtaining the partial derivative.

$$\frac{\partial \mathbf{V}}{\partial \mathbf{q}} = \begin{bmatrix} \frac{\partial V_1}{\partial q_1} & \frac{\partial V_1}{\partial q_2} & \frac{\partial V_1}{\partial q_3} & \frac{\partial V_1}{\partial q_4} & \frac{\partial V_1}{\partial q_5} & \frac{\partial V_1}{\partial q_6} & \frac{\partial V_1}{\partial q_7} \\ \frac{\partial V_2}{\partial q_1} & \frac{\partial V_2}{\partial q_2} & \frac{\partial V_2}{\partial q_3} & \frac{\partial V_2}{\partial q_4} & \frac{\partial V_2}{\partial q_5} & \frac{\partial V_2}{\partial q_6} & \frac{\partial V_2}{\partial q_7} \\ \frac{\partial V_3}{\partial q_1} & \frac{\partial V_3}{\partial q_2} & \frac{\partial V_3}{\partial q_3} & \frac{\partial V_3}{\partial q_4} & \frac{\partial V_3}{\partial q_5} & \frac{\partial V_3}{\partial q_6} & \frac{\partial V_3}{\partial q_7} \\ \frac{\partial V_4}{\partial q_1} & \frac{\partial V_4}{\partial q_2} & \frac{\partial V_4}{\partial q_3} & \frac{\partial V_4}{\partial q_4} & \frac{\partial V_4}{\partial q_5} & \frac{\partial V_4}{\partial q_6} & \frac{\partial V_4}{\partial q_7} \\ \frac{\partial V_5}{\partial q_1} & \frac{\partial V_5}{\partial q_2} & \frac{\partial V_5}{\partial q_3} & \frac{\partial V_5}{\partial q_4} & \frac{\partial V_5}{\partial q_5} & \frac{\partial V_5}{\partial q_6} & \frac{\partial V_5}{\partial q_7} \\ \frac{\partial V_6}{\partial q_1} & \frac{\partial V_6}{\partial q_2} & \frac{\partial V_6}{\partial q_3} & \frac{\partial V_6}{\partial q_4} & \frac{\partial V_6}{\partial q_5} & \frac{\partial V_6}{\partial q_6} & \frac{\partial V_6}{\partial q_7} \\ \frac{\partial V_7}{\partial q_1} & \frac{\partial V_7}{\partial q_2} & \frac{\partial V_7}{\partial q_3} & \frac{\partial V_7}{\partial q_4} & \frac{\partial V_7}{\partial q_5} & \frac{\partial V_7}{\partial q_6} & \frac{\partial V_7}{\partial q_7} \end{bmatrix}. \tag{6.66}$$

Note that

$$\mathbf{V}(\mathbf{q}, \dot{\mathbf{q}}) = \begin{bmatrix} V_1 \\ V_2 \\ V_3 \\ V_4 \\ V_5 \\ V_6 \\ V_7 \end{bmatrix} = \begin{bmatrix} \dot{\mathbf{q}}' \mathbf{V}_{1,h} \dot{\mathbf{q}} \\ \dot{\mathbf{q}}' \mathbf{V}_{2,h} \dot{\mathbf{q}} \\ \dot{\mathbf{q}}' \mathbf{V}_{3,h} \dot{\mathbf{q}} \\ \dot{\mathbf{q}}' \mathbf{V}_{4,h} \dot{\mathbf{q}} \\ \dot{\mathbf{q}}' \mathbf{V}_{5,h} \dot{\mathbf{q}} \\ \dot{\mathbf{q}}' \mathbf{V}_{6,h} \dot{\mathbf{q}} \\ \dot{\mathbf{q}}' \mathbf{V}_{7,h} \dot{\mathbf{q}} \end{bmatrix} \tag{6.67}$$

Note that $\dot{\mathbf{q}}'$ is 1×7 vector, $\mathbf{V}_{i,h}$ is a 7×7 matrix, and $\dot{\mathbf{q}}$ is a 7×1 vector. The product of these three terms give V_i, which is 1×1. The elements of those matrices are defined by the expression given in (6.41). In general, we can express $\mathbf{V}_{i,h}$ as follows, where h represents 11, 12, 13, 14, 15, 16, 17, 22, 23, 24, 25, 26, 27, 33, 34, 35, 36, 37, 44, 45, 46, 47, 55, 56, 57, 66, 67, and 77.

$$V_{i,h} = \begin{bmatrix} V_{i11} & V_{i12} & V_{i13} & V_{i14} & V_{i15} & V_{i16} & V_{i17} \\ V_{i12} & V_{i22} & V_{i23} & V_{i24} & V_{i25} & V_{i26} & V_{i27} \\ V_{i13} & V_{i23} & V_{i33} & V_{i34} & V_{i35} & V_{i36} & V_{i37} \\ V_{i14} & V_{i24} & V_{i34} & V_{i44} & V_{i45} & V_{i46} & V_{i47} \\ V_{i15} & V_{i25} & V_{i35} & V_{i45} & V_{i55} & V_{i56} & V_{i57} \\ V_{i16} & V_{i26} & V_{i36} & V_{i46} & V_{i56} & V_{i66} & V_{i67} \\ V_{i17} & V_{i27} & V_{i37} & V_{i47} & V_{i57} & V_{i67} & V_{i77} \end{bmatrix}, \qquad i = 1,2,\cdots,7. \tag{6.68}$$

Therefore, we need to determine $\frac{\partial V_i}{\partial q_l} = \dot{\mathbf{q}}' \frac{\partial V_{i,h}}{\partial q_l} \dot{\mathbf{q}}$.

The following relationship will be required to determine $\frac{\partial V_i}{\partial q_l}$.

$$\frac{\partial U_{ijk}}{\partial q_l} \equiv U_{ijkl} = \begin{cases} T_{l-1}^0 W_l T_{k-1}^{l-1} W_k T_{k-1}^{j-1} W_j T_i^{j-1}, & \text{for} \quad i \geq j \geq k \geq l \\ T_{l-1}^0 W_l T_{l-1}^{j-1} W_j T_{k-1}^{j-1} W_k T_i^{k-1}, & \text{for} \quad i \geq k \geq j \geq l \\ T_{k-1}^0 W_k T_{l-1}^{k-1} W_j T_{j-1}^{l-1} W_j T_i^{j-1}, & \text{for} \quad i \geq j \geq l \geq k \\ T_{j-1}^0 W_j T_{l-1}^{j-1} W_l T_{k-1}^{l-1} W_k T_i^{k-1}, & \text{for} \quad i \geq k \geq l \geq j \\ 0, & \text{for} \quad i < j \quad \text{or} \quad i < k \quad i < l \end{cases} . \tag{6.69}$$

For determining $\mathbf{C_{p2}}$, we first obtain $\frac{\partial \mathbf{G}}{\partial \mathbf{q}}$, and then evaluate the obtained term at $\mathbf{Q_0}$. Here we show obtaining the partial derivative.

$$\frac{\partial \mathbf{G}}{\partial \mathbf{q}} = \begin{bmatrix} \frac{\partial G_1}{\partial q_1} & \frac{\partial G_1}{\partial q_2} & \frac{\partial G_1}{\partial q_3} & \frac{\partial G_1}{\partial q_4} & \frac{\partial G_1}{\partial q_5} & \frac{\partial G_1}{\partial q_6} & \frac{\partial G_1}{\partial q_7} \\ \frac{\partial G_2}{\partial q_1} & \frac{\partial G_2}{\partial q_2} & \frac{\partial G_2}{\partial q_3} & \frac{\partial G_2}{\partial q_4} & \frac{\partial G_2}{\partial q_5} & \frac{\partial G_2}{\partial q_6} & \frac{\partial G_2}{\partial q_7} \\ \frac{\partial G_3}{\partial q_1} & \frac{\partial G_3}{\partial q_2} & \frac{\partial G_3}{\partial q_3} & \frac{\partial G_3}{\partial q_4} & \frac{\partial G_3}{\partial q_5} & \frac{\partial G_3}{\partial q_6} & \frac{\partial G_3}{\partial q_7} \\ \frac{\partial G_4}{\partial q_1} & \frac{\partial G_4}{\partial q_2} & \frac{\partial G_4}{\partial q_3} & \frac{\partial G_4}{\partial q_4} & \frac{\partial G_4}{\partial q_5} & \frac{\partial G_4}{\partial q_6} & \frac{\partial G_4}{\partial q_7} \\ \frac{\partial G_5}{\partial q_1} & \frac{\partial G_5}{\partial q_2} & \frac{\partial G_5}{\partial q_3} & \frac{\partial G_5}{\partial q_4} & \frac{\partial G_5}{\partial q_5} & \frac{\partial G_5}{\partial q_6} & \frac{\partial G_5}{\partial q_7} \\ \frac{\partial G_6}{\partial q_1} & \frac{\partial G_6}{\partial q_2} & \frac{\partial G_6}{\partial q_3} & \frac{\partial G_6}{\partial q_4} & \frac{\partial G_6}{\partial q_5} & \frac{\partial G_6}{\partial q_6} & \frac{\partial G_6}{\partial q_7} \\ \frac{\partial G_7}{\partial q_1} & \frac{\partial G_7}{\partial q_2} & \frac{\partial G_7}{\partial q_3} & \frac{\partial G_7}{\partial q_4} & \frac{\partial G_7}{\partial q_5} & \frac{\partial G_7}{\partial q_6} & \frac{\partial G_7}{\partial q_7} \end{bmatrix} \tag{6.70}$$

$$G_1 = -\left(m_1 \mathbf{g} U_{11} \bar{r}_1^1 + m_2 \mathbf{g} U_{21} \bar{r}_2^2 + m_3 \mathbf{g} U_{31} \bar{r}_3^3 + m_4 \mathbf{g} U_{41} \bar{r}_4^4 + m_5 \mathbf{g} U_{51} \bar{r}_5^5 + m_6 \mathbf{g} U_{61} \bar{r}_6^6 + m_7 \mathbf{g} U_{71} \bar{r}_7^7 \right),$$

$$\frac{\partial G_1}{\partial q_1} = -\Big(m_1\mathbf{g}U_{111}\bar{r}_1^1 + m_2\mathbf{g}U_{211}\bar{r}_2^2 + m_3\mathbf{g}U_{311}\bar{r}_3^3 + m_4\mathbf{g}U_{411}\bar{r}_4^4 + m_5\mathbf{g}U_{511}\bar{r}_5^5 + m_6\mathbf{g}U_{611}\bar{r}_6^6 + m_7\mathbf{g}U_{711}\bar{r}_7^7\Big),$$

$$\frac{\partial G_1}{\partial q_2} = -\left(m_2\mathbf{g}U_{212}\bar{r}_2^2 + m_3\mathbf{g}U_{312}\bar{r}_3^3 + m_4\mathbf{g}U_{412}\bar{r}_4^4 + m_5\mathbf{g}U_{512}\bar{r}_5^5 + m_6\mathbf{g}U_{612}\bar{r}_6^6 + m_7\mathbf{g}U_{712}\bar{r}_7^7\right),$$

$$\frac{\partial G_1}{\partial q_3} = -\left(m_3\mathbf{g}U_{313}\bar{r}_3^3 + m_4\mathbf{g}U_{413}\bar{r}_4^4 + m_5\mathbf{g}U_{513}\bar{r}_5^5 + m_6\mathbf{g}U_{613}\bar{r}_6^6 + m_7\mathbf{g}U_{713}\bar{r}_7^7\right),$$

$$\frac{\partial G_1}{\partial q_4} = -\left(m_4\mathbf{g}U_{414}\bar{r}_4^4 + m_5\mathbf{g}U_{514}\bar{r}_5^5 + m_6\mathbf{g}U_{614}\bar{r}_6^6 + m_7\mathbf{g}U_{714}\bar{r}_7^7\right),$$

$$\frac{\partial G_1}{\partial q_5} = -\left(m_5\mathbf{g}U_{515}\bar{r}_5^5 + m_6\mathbf{g}U_{615}\bar{r}_6^6 + m_7\mathbf{g}U_{715}\bar{r}_7^7\right),$$

$$\frac{\partial G_1}{\partial q_6} = -\left(m_6\mathbf{g}U_{616}\bar{r}_6^6 + m_7\mathbf{g}U_{716}\bar{r}_7^7\right),$$

$$\frac{\partial G_1}{\partial q_7} = -m_7\mathbf{g}U_{717}\bar{r}_7^7,$$

$$G_2 = -\left(m_2\mathbf{g}U_{22}\bar{r}_2^2 + m_3\mathbf{g}U_{32}\bar{r}_3^3 + m_4\mathbf{g}U_{42}\bar{r}_4^4 + m_5\mathbf{g}U_{52}\bar{r}_5^5 + m_6\mathbf{g}U_{62}\bar{r}_6^6 + m_7\mathbf{g}U_{72}\bar{r}_7^7\right),$$

$$\frac{\partial G_2}{\partial q_1} = -\left(m_2\mathbf{g}U_{221}\bar{r}_2^2 + m_3\mathbf{g}U_{321}\bar{r}_3^3 + m_4\mathbf{g}U_{421}\bar{r}_4^4 + m_5\mathbf{g}U_{521}\bar{r}_5^5 + m_6\mathbf{g}U_{621}\bar{r}_6^6 + m_7\mathbf{g}U_{721}\bar{r}_7^7\right),$$

$$\frac{\partial G_2}{\partial q_2} = -\left(m_2\mathbf{g}U_{222}\bar{r}_2^2 + m_3\mathbf{g}U_{322}\bar{r}_3^3 + m_4\mathbf{g}U_{422}\bar{r}_4^4 + m_5\mathbf{g}U_{522}\bar{r}_5^5 + m_6\mathbf{g}U_{622}\bar{r}_6^6 + m_7\mathbf{g}U_{722}\bar{r}_7^7\right),$$

$$\frac{\partial G_2}{\partial q_3} = -\left(m_3\mathbf{g}U_{323}\bar{r}_3^3 + m_4\mathbf{g}U_{423}\bar{r}_4^4 + m_5\mathbf{g}U_{523}\bar{r}_5^5 + m_6\mathbf{g}U_{623}\bar{r}_6^6 + m_7\mathbf{g}U_{723}\bar{r}_7^7\right),$$

$$\frac{\partial G_2}{\partial q_4} = -\left(m_4\mathbf{g}U_{424}\bar{r}_4^4 + m_5\mathbf{g}U_{524}\bar{r}_5^5 + m_6\mathbf{g}U_{624}\bar{r}_6^6 + m_7\mathbf{g}U_{724}\bar{r}_7^7\right),$$

$$\frac{\partial G_2}{\partial q_5} = -\left(m_5\mathbf{g}U_{525}\bar{r}_5^5 + m_6\mathbf{g}U_{626}\bar{r}_6^6 + m_7\mathbf{g}U_{726}\bar{r}_7^7\right),$$

$$\frac{\partial G_2}{\partial q_6} = -\left(m_6\mathbf{g}U_{626}\bar{r}_6^6 + m_7\mathbf{g}U_{726}\bar{r}_7^7\right),$$

$$\frac{\partial G_2}{\partial q_7} = -\left(m_7\mathbf{g}U_{721}\bar{r}_7^7\right),$$

$$G_3 = -\left(m_3\mathbf{g}U_{32}\bar{r}_3^3 + m_4\mathbf{g}U_{42}\bar{r}_4^4 + m_5\mathbf{g}U_{52}\bar{r}_5^5 + m_6\mathbf{g}U_{62}\bar{r}_6^6 + m_7\mathbf{g}U_{72}\bar{r}_7^7\right),$$

$$\begin{aligned}
\frac{\partial G_3}{\partial q_1} &= -\left(m_3\mathbf{g}U_{321}\bar{r}_3^3 + m_4\mathbf{g}U_{421}\bar{r}_4^4 + m_5\mathbf{g}U_{521}\bar{r}_5^5 + m_6\mathbf{g}U_{621}\bar{r}_6^6 + m_7\mathbf{g}U_{721}\bar{r}_7^7\right),\\
\frac{\partial G_3}{\partial q_2} &= -\left(m_3\mathbf{g}U_{322}\bar{r}_3^3 + m_4\mathbf{g}U_{422}\bar{r}_4^4 + m_5\mathbf{g}U_{522}\bar{r}_5^5 + m_6\mathbf{g}U_{622}\bar{r}_6^6 + m_7\mathbf{g}U_{722}\bar{r}_7^7\right),\\
\frac{\partial G_3}{\partial q_3} &= -\left(m_3\mathbf{g}U_{323}\bar{r}_3^3 + m_4\mathbf{g}U_{423}\bar{r}_4^4 + m_5\mathbf{g}U_{523}\bar{r}_5^5 + m_6\mathbf{g}U_{623}\bar{r}_6^6 + m_7\mathbf{g}U_{723}\bar{r}_7^7\right),\\
\frac{\partial G_3}{\partial q_4} &= -\left(m_4\mathbf{g}U_{424}\bar{r}_4^4 + m_5\mathbf{g}U_{524}\bar{r}_5^5 + m_6\mathbf{g}U_{624}\bar{r}_6^6 + m_7\mathbf{g}U_{724}\bar{r}_7^7\right),\\
\frac{\partial G_3}{\partial q_5} &= -\left(m_5\mathbf{g}U_{525}\bar{r}_5^5 + m_6\mathbf{g}U_{625}\bar{r}_6^6 + m_7\mathbf{g}U_{725}\bar{r}_7^7\right),\\
\frac{\partial G_3}{\partial q_6} &= -\left(m_6\mathbf{g}U_{626}\bar{r}_6^6 + m_7\mathbf{g}U_{726}\bar{r}_7^7\right),\\
\frac{\partial G_3}{\partial q_7} &= -m_7\mathbf{g}U_{727}\bar{r}_7^7,
\end{aligned}$$

$$G_4 = -\left(m_4\mathbf{g}U_{44}\bar{r}_4^4 + m_5\mathbf{g}U_{54}\bar{r}_5^5 + m_6\mathbf{g}U_{64}\bar{r}_6^6 + m_7\mathbf{g}U_{74}\bar{r}_7^7\right),$$

$$\begin{aligned}
\frac{\partial G_4}{\partial q_1} &= -\left(m_4\mathbf{g}U_{441}\bar{r}_4^4 + m_5\mathbf{g}U_{541}\bar{r}_5^5 + m_6\mathbf{g}U_{641}\bar{r}_6^6 + m_7\mathbf{g}U_{741}\bar{r}_7^7\right),\\
\frac{\partial G_4}{\partial q_2} &= -\left(m_4\mathbf{g}U_{442}\bar{r}_4^4 + m_5\mathbf{g}U_{542}\bar{r}_5^5 + m_6\mathbf{g}U_{642}\bar{r}_6^6 + m_7\mathbf{g}U_{742}\bar{r}_7^7\right),\\
\frac{\partial G_4}{\partial q_3} &= -\left(m_4\mathbf{g}U_{443}\bar{r}_4^4 + m_5\mathbf{g}U_{543}\bar{r}_5^5 + m_6\mathbf{g}U_{643}\bar{r}_6^6 + m_7\mathbf{g}U_{743}\bar{r}_7^7\right),\\
\frac{\partial G_4}{\partial q_4} &= -\left(m_4\mathbf{g}U_{444}\bar{r}_4^4 + m_5\mathbf{g}U_{544}\bar{r}_5^5 + m_6\mathbf{g}U_{644}\bar{r}_6^6 + m_7\mathbf{g}U_{744}\bar{r}_7^7\right),\\
\frac{\partial G_4}{\partial q_5} &= -\left(m_5\mathbf{g}U_{545}\bar{r}_5^5 + m_6\mathbf{g}U_{645}\bar{r}_6^6 + m_7\mathbf{g}U_{745}\bar{r}_7^7\right),\\
\frac{\partial G_4}{\partial q_6} &= -\left(m_6\mathbf{g}U_{646}\bar{r}_6^6 + m_7\mathbf{g}U_{746}\bar{r}_7^7\right),\\
\frac{\partial G_4}{\partial q_7} &= -m_7\mathbf{g}U_{747}\bar{r}_7^7,
\end{aligned}$$

$$G_5 = -\left(m_5\mathbf{g}U_{55}\bar{r}_5^5 + m_6\mathbf{g}U_{65}\bar{r}_6^6 + m_7\mathbf{g}U_{75}\bar{r}_7^7\right),$$

$$\begin{aligned}
\frac{\partial G_5}{\partial q_1} &= -\left(m_5\mathbf{g}U_{551}\bar{r}_5^5 + m_6\mathbf{g}U_{651}\bar{r}_6^6 + m_7\mathbf{g}U_{751}\bar{r}_7^7\right),\\
\frac{\partial G_5}{\partial q_2} &= -\left(m_5\mathbf{g}U_{552}\bar{r}_5^5 + m_6\mathbf{g}U_{652}\bar{r}_6^6 + m_7\mathbf{g}U_{752}\bar{r}_7^7\right),\\
\frac{\partial G_5}{\partial q_3} &= -\left(m_5\mathbf{g}U_{553}\bar{r}_5^5 + m_6\mathbf{g}U_{653}\bar{r}_6^6 + m_7\mathbf{g}U_{753}\bar{r}_7^7\right),\\
\frac{\partial G_5}{\partial q_4} &= -\left(m_5\mathbf{g}U_{554}\bar{r}_5^5 + m_6\mathbf{g}U_{654}\bar{r}_6^6 + m_7\mathbf{g}U_{754}\bar{r}_7^7\right),\\
\frac{\partial G_5}{\partial q_5} &= -\left(m_5\mathbf{g}U_{555}\bar{r}_5^5 + m_6\mathbf{g}U_{655}\bar{r}_6^6 + m_7\mathbf{g}U_{755}\bar{r}_7^7\right),\\
\frac{\partial G_5}{\partial q_6} &= -\left(m_6\mathbf{g}U_{656}\bar{r}_6^6 + m_7\mathbf{g}U_{756}\bar{r}_7^7\right),\\
\frac{\partial G_5}{\partial q_7} &= -m_7\mathbf{g}U_{757}\bar{r}_7^7,
\end{aligned}$$

$$G_6 = -\left(m_6\mathbf{g}U_{66}\bar{r}_6^6 + m_7\mathbf{g}U_{76}\bar{r}_7^7\right),$$

$$\begin{aligned}
\frac{\partial G_6}{\partial q_1} &= -\left(m_6\mathbf{g}U_{661}\bar{r}_6^6 + m_7\mathbf{g}U_{761}\bar{r}_7^7\right),\\
\frac{\partial G_6}{\partial q_2} &= -\left(m_6\mathbf{g}U_{662}\bar{r}_6^6 + m_7\mathbf{g}U_{762}\bar{r}_7^7\right),\\
\frac{\partial G_6}{\partial q_3} &= -\left(m_6\mathbf{g}U_{663}\bar{r}_6^6 + m_7\mathbf{g}U_{763}\bar{r}_7^7\right),\\
\frac{\partial G_6}{\partial q_4} &= -\left(m_6\mathbf{g}U_{664}\bar{r}_6^6 + m_7\mathbf{g}U_{764}\bar{r}_7^7\right),\\
\frac{\partial G_6}{\partial q_5} &= -\left(m_6\mathbf{g}U_{665}\bar{r}_6^6 + m_7\mathbf{g}U_{765}\bar{r}_7^7\right),\\
\frac{\partial G_6}{\partial q_6} &= -\left(m_6\mathbf{g}U_{666}\bar{r}_6^6 + m_7\mathbf{g}U_{766}\bar{r}_7^7\right),\\
\frac{\partial G_6}{\partial q_7} &= -m_7\mathbf{g}U_{767}\bar{r}_7^7,
\end{aligned}$$

$$G_7 = -m_7 \mathbf{g} U_{77} \bar{r}_7^7.$$

$$\begin{aligned}
\frac{\partial G_7}{\partial q_1} &= -m_7 \mathbf{g} U_{771} \bar{r}_7^7, \\
\frac{\partial G_7}{\partial q_2} &= -m_7 \mathbf{g} U_{772} \bar{r}_7^7, \\
\frac{\partial G_7}{\partial q_3} &= -m_7 \mathbf{g} U_{773} \bar{r}_7^7, \\
\frac{\partial G_7}{\partial q_4} &= -m_7 \mathbf{g} U_{774} \bar{r}_7^7, \\
\frac{\partial G_7}{\partial q_5} &= -m_7 \mathbf{g} U_{775} \bar{r}_7^7, \\
\frac{\partial G_7}{\partial q_6} &= -m_7 \mathbf{g} U_{776} \bar{r}_7^7, \\
\frac{\partial G_7}{\partial q_7} &= -m_7 \mathbf{g} U_{777} \bar{r}_7^7,
\end{aligned}$$

6.4 Numerical Simulations and Validations of Baxter Linearized Model

In this section, we study the dynamic response of the Baxter linearized model derived in the earlier section, and present an experimental validation study.

6.4.1 Baxter Physical Parameters

The physical parameters of Baxter can be retrieved from a URDF (Unified Robot Description Format) file. The file consists of a series of frames and transformation description between frames with the kinematic information of the robot. The detail of the file is given in Appendix A.

Baxter robot has been developed by Rethink Robotics Inc. Baxter has two seven degree-of-freedom arms. The arm joints are named as: S0 (shoulder roll), S1 (shoulder pitch), E0 (elbow roll), E1 (elbow pitch), W0 (wrist roll), W1 (wrist pitch), W2 (wrist roll). Fig. 6.5

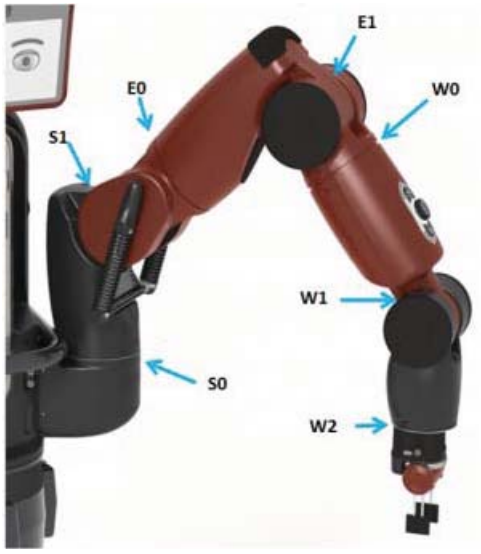

Figure 6.5: Baxter joint names (left arm).

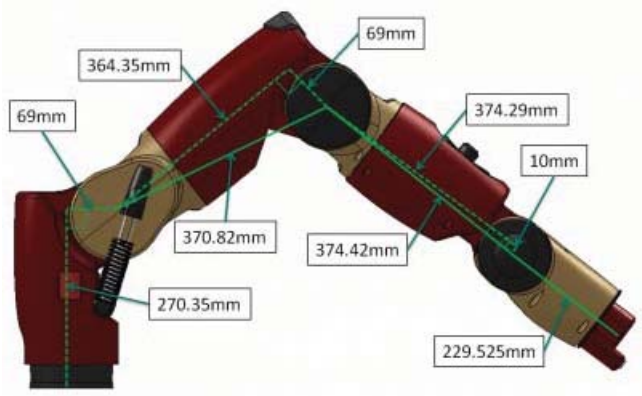

Figure 6.6: Baxter link lengths (left arm).

Table 6.2: D-H parameters of Baxter robot links from URDF file [3]

Link i	Joint angle q	Link offset d (m)	Link length a (m)	Link Twist α (rad)
1	q_1	0.2703	0.069	$-\frac{\pi}{2}$
2	q_2	0	0	$+\frac{\pi}{2}$
3	q_3	0.3644	0.069	$-\frac{\pi}{2}$
4	q_4	0	0	$+\frac{\pi}{2}$
5	q_5	0.3743	0.01	$-\frac{\pi}{2}$
6	q_6	0	0	$+\frac{\pi}{2}$
7	q_7	0.2295	0	0

shows the joint names and Fig. 6.6 shows the link length of left arm. The right arm joints are named with a similar convention.

Table 6.2 shows the D-H parameters for Baxter. Table 6.3 shows the centers of gravity and masses for the Baxter links. Table 6.4 shows moments of inertia for the Baxter links. Table 6.5 shows cross-products of inertia for the Baxter links.

Table 6.3: The centers of gravity and masses of Baxter robot links [3]

Link	$\bar{x}$ (m)	$\bar{y}$ (m)	$\bar{z}$ (m)	m (kg)
1	-0.051170	0.079080	0.000859	5.700440
2	0.002690	-0.005290	0.068449	3.226980
3	-0.071760	0.081490	0.001319	4.312720
4	0.001590	-0.011170	0.026179	2.072060
5	-0.011679	0.13111	0.004599	2.246650
6	0.006970	0.005999	0.060480	1.609790
7	0.005137	0.000957	-0.066823	0.542180

Table 6.4: Moment of inertia elements of Baxter robot links (unit: kgm^2) [3]

Link	I_{xx}	I_{yy}	I_{zz}
1	0.047091	0.035959	0.037669
2	0.027885	0.020787	0.011752
3	0.026617	0.012480	0.028443
4	0.013182	0.009268	0.007116
5	0.016677	0.003746	0.016754
6	0.007005	0.005527	0.003876
7	0.000816	0.000873	0.003876

Table 6.5: Cross-product of inertia elements of Baxter robot links(unit: kgm^2) [3]

Link	I_{xy}	I_{yz}	I_{xz}
1	-0.006149	-0.000781	0.000128
2	-0.000188	0.002077	-0.000300
3	-0.003921	-0.001084	0.000293
4	-0.000197	0.000745	0.000360
5	-0.000186	0.000647	0.000184
6	0.000153	-0.000211	-0.000444
7	0.000128	0.000106	0.000189

6.4.2 Dynamic Response and Stability of Linearized Model

Let the operating point of the robot be

$$\begin{aligned}\mathbf{Q_o} &= \begin{bmatrix} q_{1o} & q_{2o} & q_{3o} & q_{4o} & q_{5o} & q_{6o} & q_{7o} & \dot{q}_{1o} & \dot{q}_{2o} & \dot{q}_{3o} & \dot{q}_{4o} & \dot{q}_{5o} & \dot{q}_{6o} & \dot{q}_{7o} \end{bmatrix}', \\ &= \begin{bmatrix} -0.3137 & -0.5492 & -1.1950 & 1.5842 & 1.0051 & 1.2513 & 0.6604 & 0 & 0 & 0 & 0 & 0 & 0 & 0 \end{bmatrix}',\end{aligned}$$

corresponding to one “dexterous" configuration of Baxter’s left arm shown in Fig. 6.7. The joint angles of the operating point cause an initial pose of the end-effector that is suitable for the parallel or angular scanning experiment of the bimodal dynamic imaging system. The joint velocities of the operating are considered zero to capture the dynamics where the joints start to move from a stand-still position.

The submatrices in the linearized state-space model (6.63) evaluated at the operating point are

$$\mathbf{A_p^{-1}} = \begin{bmatrix} -0.2525 & 1.2359 & -1.3411 & 0.2171 & -0.6623 & -1.8760 & -0.7642 \\ 1.2359 & -0.0965 & -1.5473 & 0.1687 & -0.3324 & 0.1499 & -0.1311 \\ -1.3411 & -1.5473 & 15.137 & 0.1357 & 8.8677 & 16.7180 & 7.3466 \\ 0.2171 & 0.1687 & 0.1357 & 4.3447 & 8.6417 & 5.4724 & 4.0161 \\ -0.6623 & -0.3324 & 8.8677 & 8.6417 & 94.2320 & 18.7970 & 13.8300 \\ -1.8760 & 0.1499 & 16.7180 & 5.4724 & 18.7970 & 79.1160 & 46.2780 \\ -0.76416 & -0.1311 & 7.3466 & 4.0161 & 13.8300 & 46.2780 & 1847.9 \end{bmatrix},$$

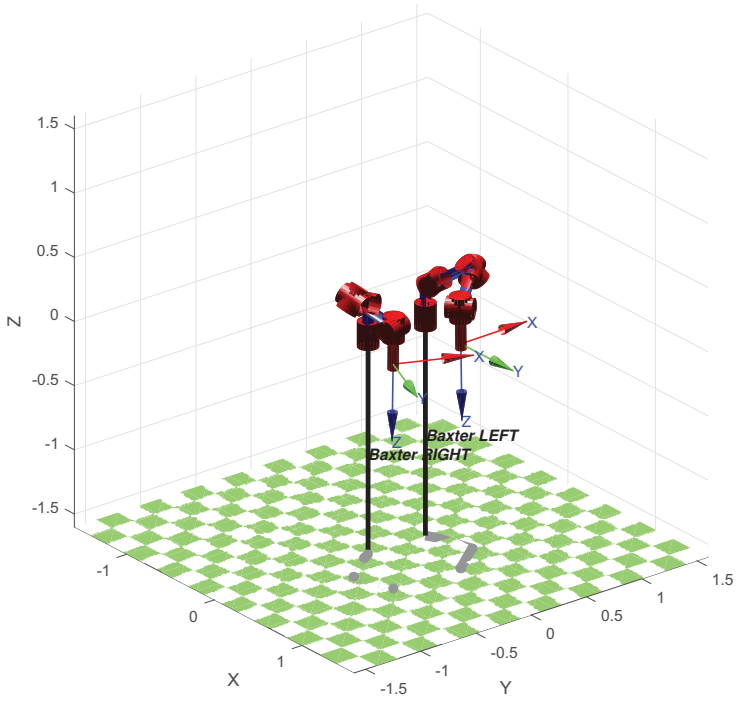

Figure 6.7: Dexterous pose of Baxter's left arm for a parallel scanning experiment

$$\mathbf{B_p} = 0_{7\times 7},$$

$$\mathbf{C_{p1}} = 0_{7\times 7},$$

$$\mathbf{C_{p2}} = \begin{bmatrix} 0 & -7.6493 & 0 & 0 & 0.0102 & 0 & 0 \\ -7.6493 & -21.607 & 5.3508 & 5.1614 & -1.2548 & -1.1767 & 0 \\ -7.6493 & -19.439 & 5.3508 & 5.1614 & -0.5213 & -1.1767 & -0.0035 \\ 0 & 5.1614 & 0.1947 & 6.5152 & -0.9189 & -0.44536 & -0.0194 \\ 0.01019 & -0.5213 & -0.0408 & -0.9189 & 0.1543 & -0.48784 & 0.0078 \\ 0 & -1.1767 & 0.0399 & -0.4454 & -0.4878 & -1.322 & 0.0059 \\ 0 & -0.00351 & -0.0013 & -0.0194 & 0.0078 & 0.0059444 & -0.0204 \end{bmatrix}.$$

Then, the linearized state-space model of one arm of the Baxter robot for perturbations about the operating point is found by plugging in the submatrices computed above into (6.63).

The eigenvalues of the system in (6.63) evaluated at the operating points are ± 11.6877, $\pm 8.5541i$, ± 6.1040, $\pm 5.0821i$, $\pm 4.0967i$, ± 2.1849, ± 0.3842. Since there are eigenvalues with positive real parts, the system is not stable. The number of uncontrollable states is 2. The number of unobservable state is zero. The time responses of seven joint positions to a small perturbation (1 μN) are shown in Fig. 6.8, exhibiting unstable behavior of the system. The initial investigation of the Baxter linearized model indicates that the robot is an unstable system at the operating point $\mathbf{Q_o}$.

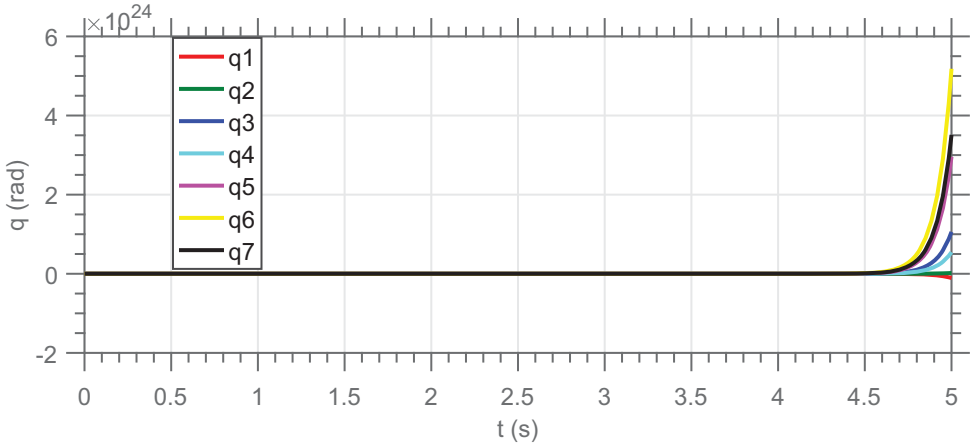

Figure 6.8: Time responses of the joint positions from the Baxter linearized model for 1 μN torque

6.4.3 Robot Stabilization and Regulation

In order to stabilize and regulate the robot model, we used seven Proportional-Integral-Derivative (PID) controller with a low-pass filter for seven joints. The PID controller with a low-pass filter has the form of

$$k_p + k_i \frac{1}{s} + k_d \frac{N}{1 + N\frac{1}{s}}$$

where k_p is the proportional gain, k_i is the integral gain, k_d is the derivative gain, and N is the filter coefficient. Note that the derivative gain is multiplied with the low-pass filter.

The parameters of the PID controller were tuned using Matlab's *pidtuner* function. Table 6.6 shows the tuned parameter values.

Table 6.6: PID controller parameters

Joint	k_p	k_i (m)	k_d	N
1	156.8636	529.3146	90.8136	355.4528
2	100.2464	459.1323	31.6649	291.3696
3	86.5436	436.9163	24.6351	454.3801
4	4.4047	28.1636	2.8559	238.7716
5	26.9042	621.3653	23.4639	298.6593
6	8.7855	652.8582	93.9565	295.7826
7	-1.2844	628.0802	5.4983	322.7994

The eigenvalues of the closed-loop PID-controlled system are $-161.55 \pm 51042i$, $-149.15 \pm 16956i$, $-157.49 \pm 12431i$, $-166.39 \pm 4845.3i$, $-237.7 \pm 1918.2i$, $-248.14 \pm 19.926i$, $-3.6076 \pm 11.039i$, $-0.04849 \pm 10.692i$, $-0.58862 \pm 5.4092i$, $-0.78861 \pm 5.0006i$, -0.86326, $-1.5166 \pm 3.349i$, $-0.074851 \pm 2.6545i$, $-0.64799 \pm 2.0434i$, -0.95214. The real part of the eigenvalues of the system is negative. Therefore, the PID controller is adequate to stabilize the robot linearized dynamics.

In order to test the Baxter linearized model's regulatory capability, i.e. the ability track or follow a reference command, we applied a step command of 0.1754 radian (10 degree) for each joint to the PID-controlled linearized model. All the joints reached the joint angle of 0.1754 radian (10 degree) and oscillate around 0.1754 radian (10 degree). Fig. 6.9 the simulation diagram. Figs. 6.15-6.16 show the time responses of the joint angles. For the first five joints, the robot achieved a satisfactory level of steady-state regulation for the step commands. For joints 6 and 7, we observed sustained oscillations around the step commands.

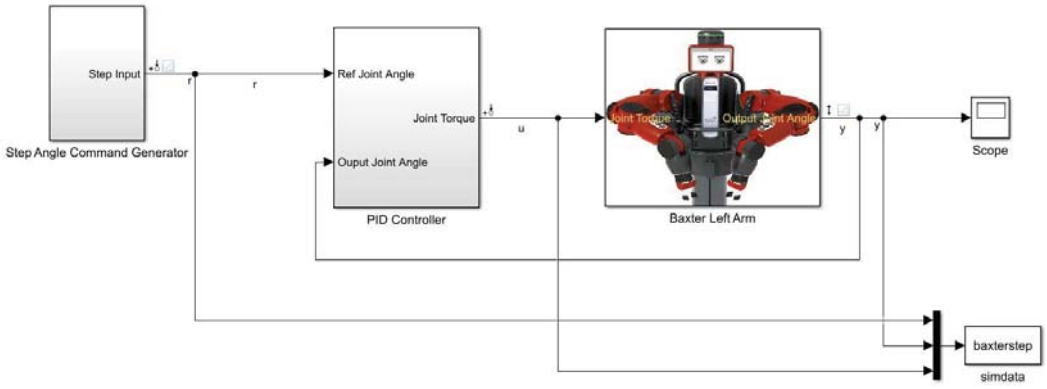

Figure 6.9: Step command tracking simulation diagram

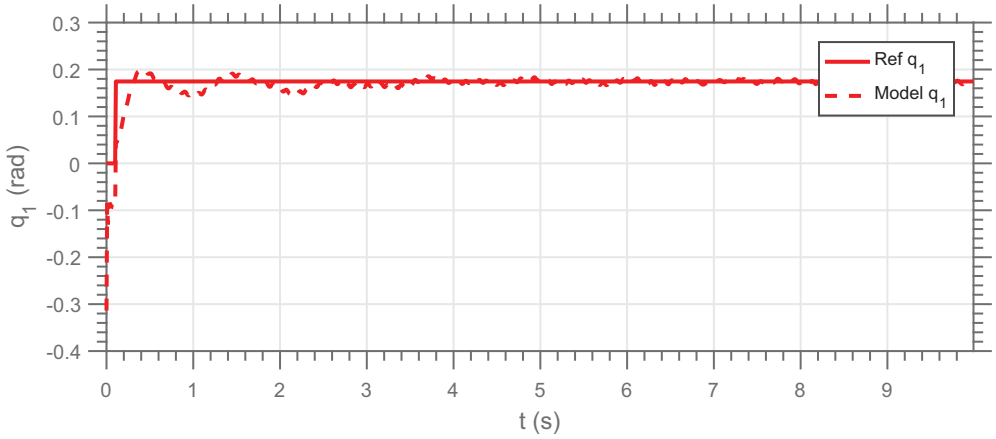

Figure 6.10: Step command tracking for Joint 1

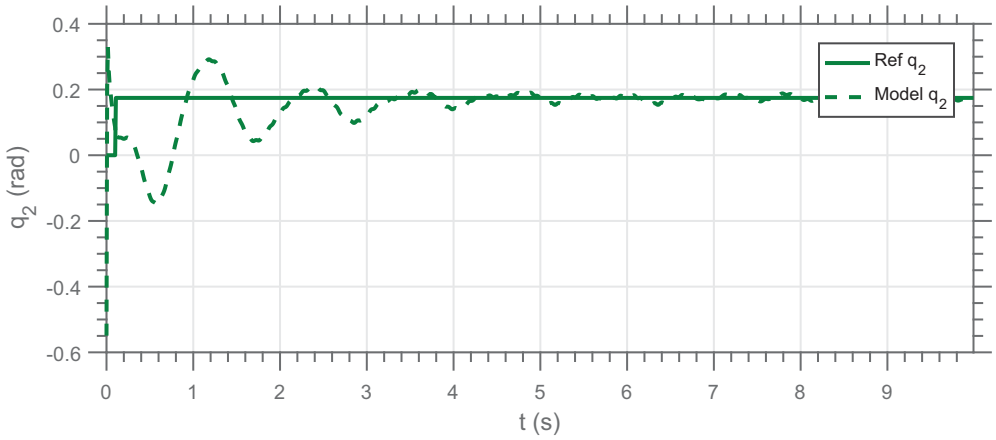

Figure 6.11: Step command tracking for Joint 2

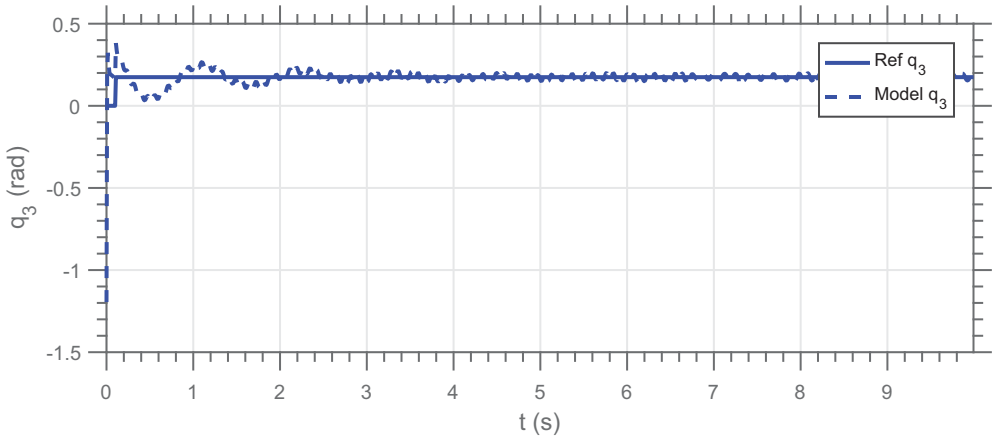

Figure 6.12: Step command tracking for Joint 3

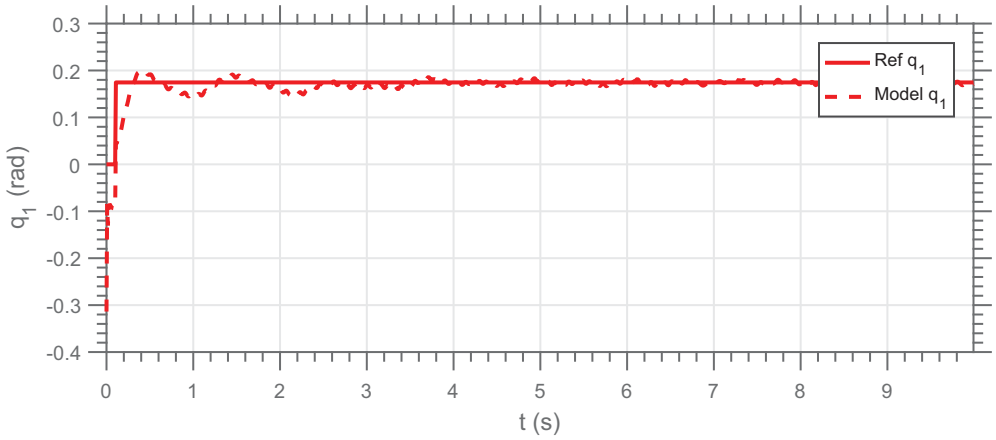

Figure 6.13: Step command tracking for Joint 4

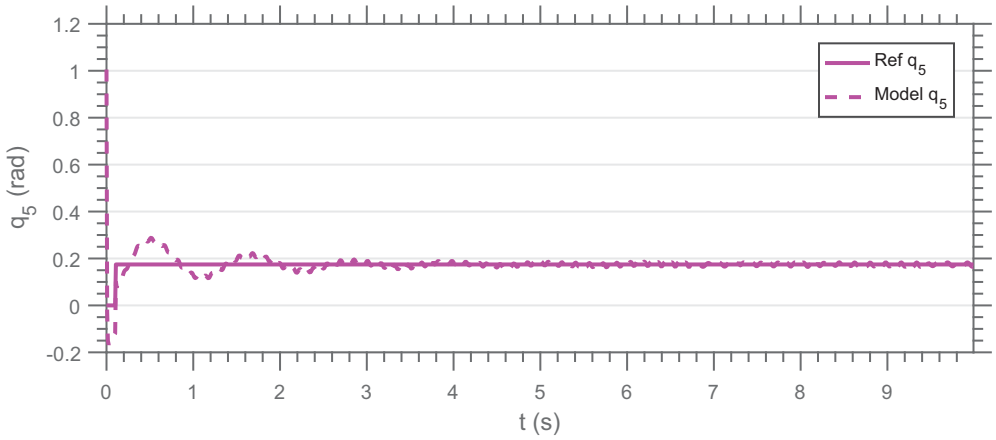

Figure 6.14: Step command tracking for Joint 5

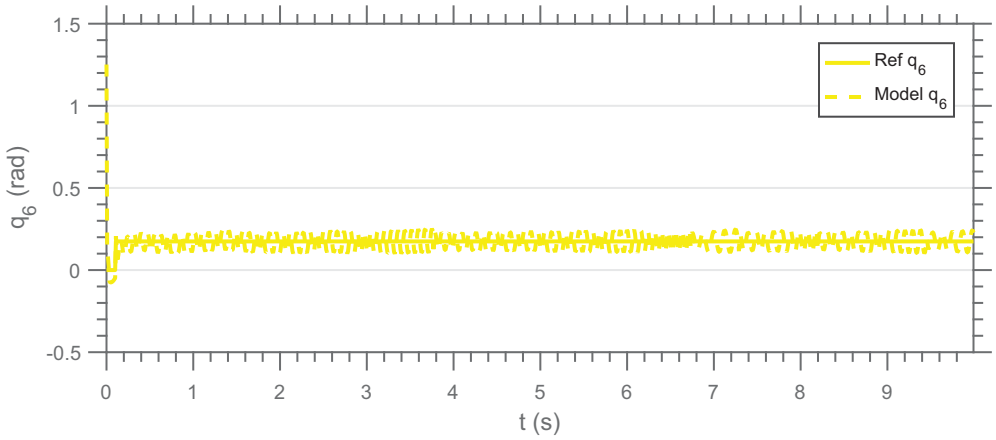

Figure 6.15: Step command tracking for Joint 6

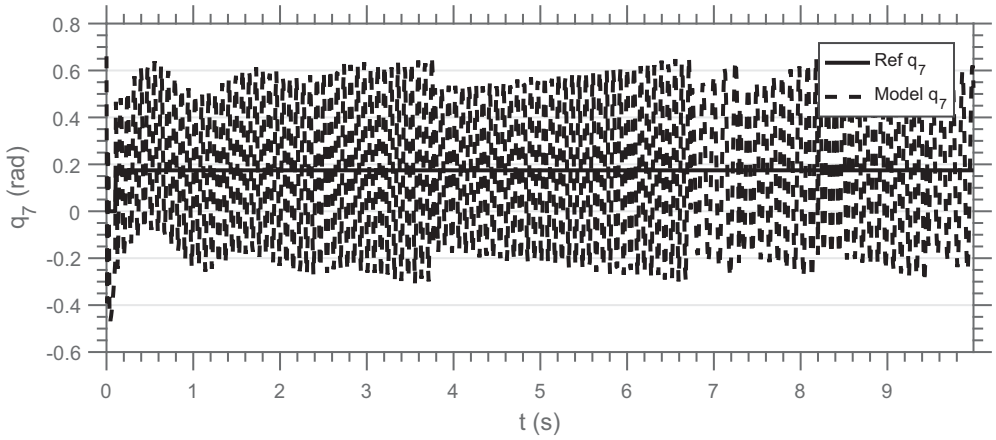

Figure 6.16: Step command tracking for Joint 7

6.4.4 Experimental Validation Study

We performed a validation study for the PID-controlled linearized model. The validation study workflow is shown in Fig. 6.17. In the study, the left manipulator of Baxter was driven along a straight line trajectory from one point (x = 0.657 m, y = 0.103 m, z = 0.038 m) to another point (x = 0.76 m, y = 0.103 m, z = 0.038 m) in Cartesian space. We employed an inverse kinematic solver to generate the reference joint angles which were fed to a PID position controller. From the Baxter robot, we collected reference joint angles and output joint angles.

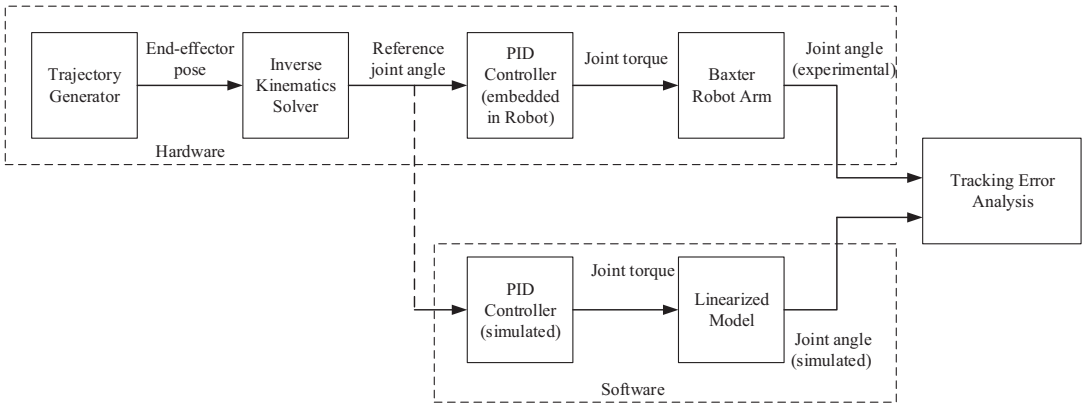

Figure 6.17: Validation study workflow

The collected reference joint angles were fed into the simulated PID-controlled Baxter model. The simulation diagram is shown in Fig. 6.18.

The tracking performance of the Baxter robot and the linearized model was evaluated by root mean squared error (RMSE) between the reference joint angles and the output joint angles. Table 6.7 shows the tracking error for seven joints. Based on the error, the Baxter robot performed better than the model. Figs. 6.19-6.25 shows joint trajectory tracking the Baxter robot and model. From the plots, we notice that until 3 to 4 seconds, the model shows overshoot characteristic, which contributed to the large tracking error. After 5 seconds, the model tracking performance was as good as the Baxter robot.

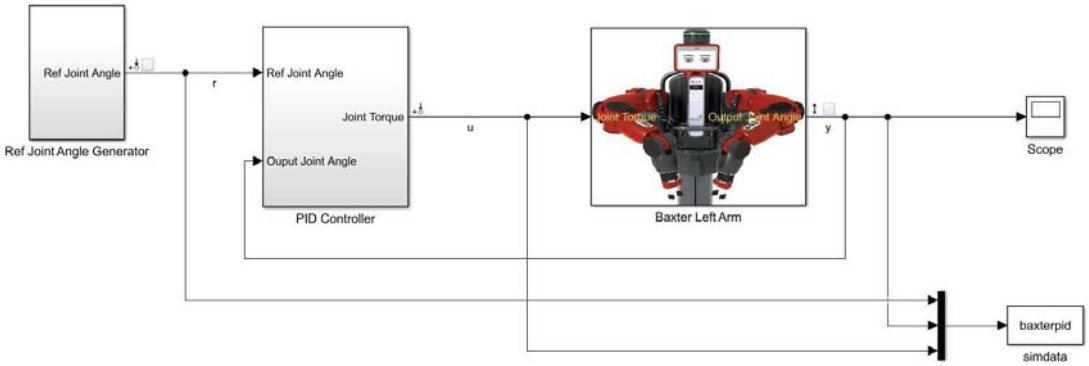

Figure 6.18: Trajectory tracking simulation diagram

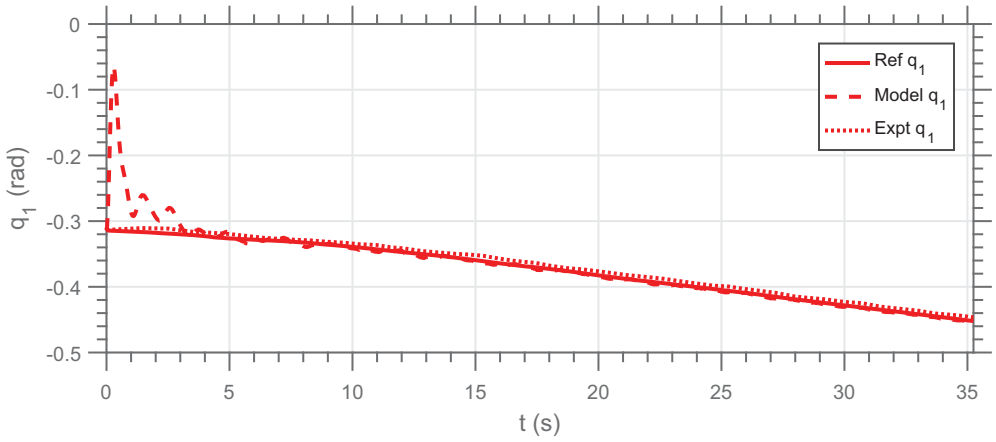

Figure 6.19: Trajectory tracking for Joint 1

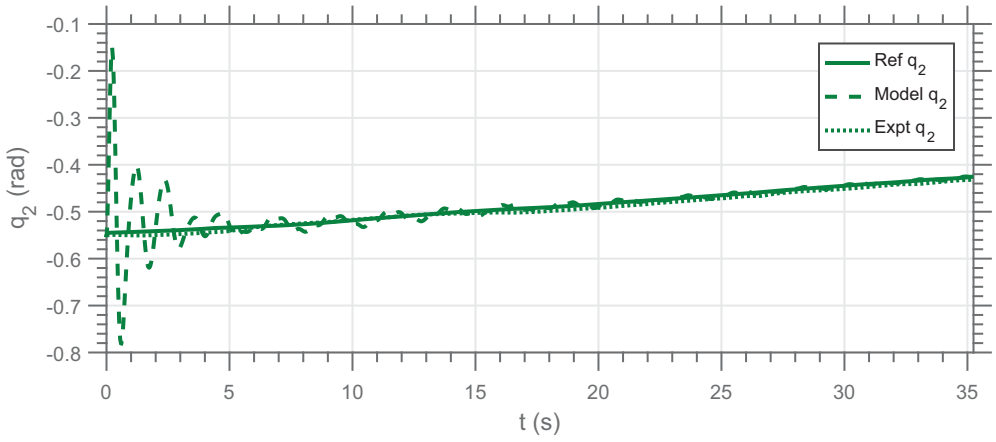

Figure 6.20: Trajectory tracking for Joint 2

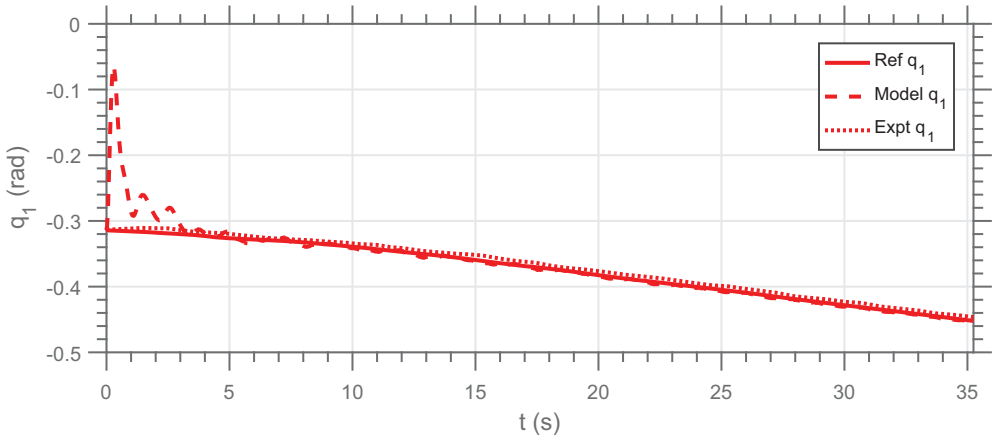

Figure 6.21: Trajectory tracking for Joint 3

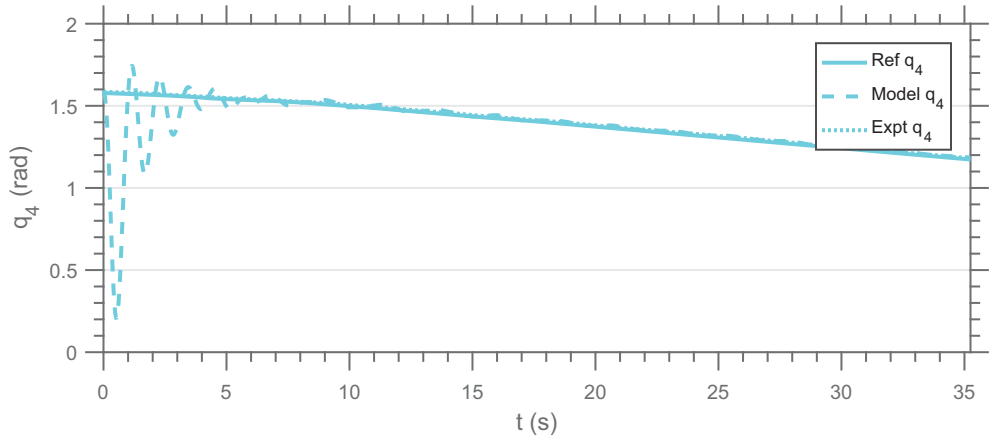

Figure 6.22: Trajectory tracking for Joint 4

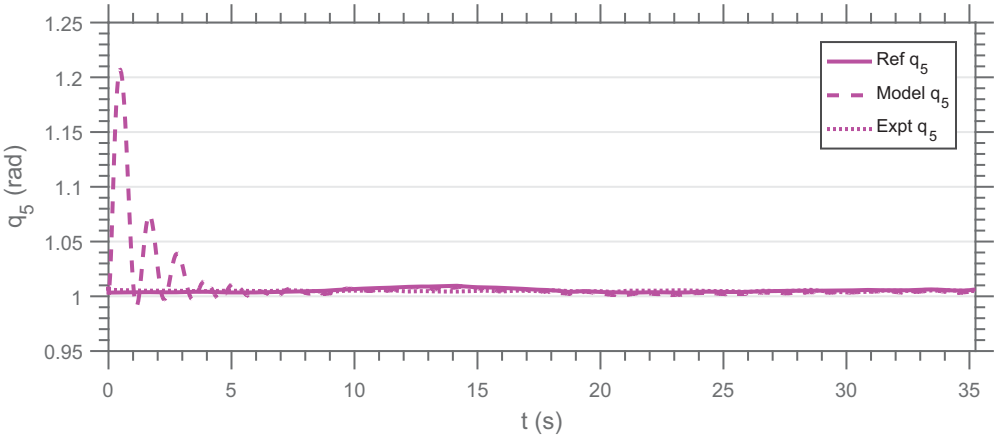

Figure 6.23: Trajectory tracking for Joint 5

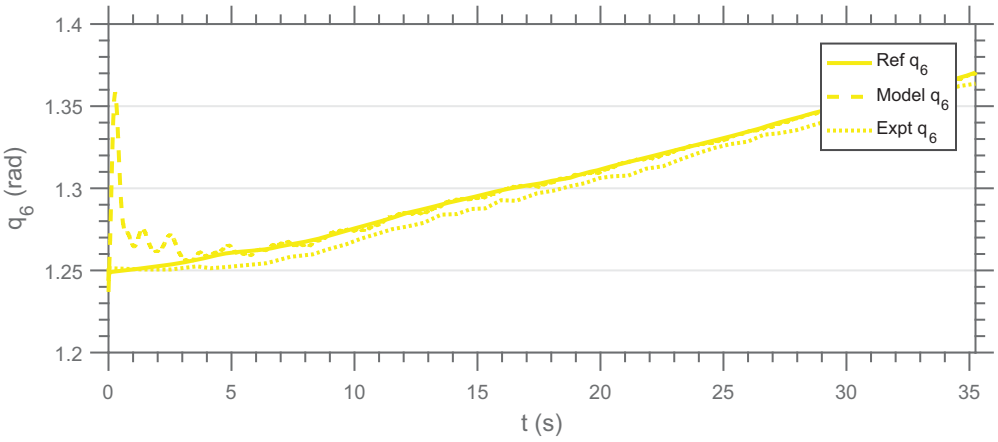

Figure 6.24: Trajectory tracking for Joint 6

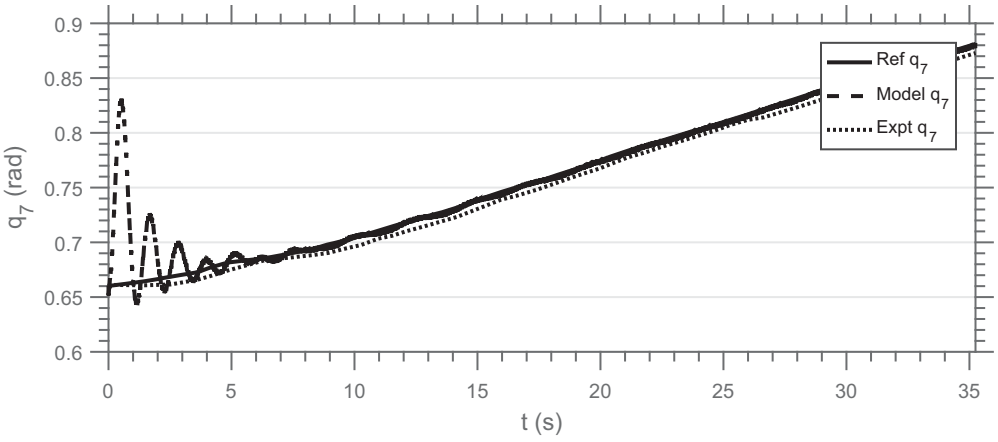

Figure 6.25: Trajectory tracking for Joint 7

Table 6.7: RMS Tracking Error of Joint Angles

Joint	Baxter (rad)	Linear Model (rad)
1	0.0056	0.0257
2	0.0060	0.0394
3	0.0040	0.0355
4	0.0077	0.1548
5	0.0020	0.0246
6	0.0066	0.0103
7	0.0072	0.0193

6.5 Discussion

In this chapter, we derived a linearized model for the dual arm Baxter robot from the Lagrange-Euler equation of motion. Then we presented numerical simulation of the model, and validated with the data found from the real Baxter robot. The validation study shows that the developed model can represent the real Baxter robot. Next, we discuss a hybrid statistical control approach to control this robot manipulator model.

CHAPTER 7

FEEDBACK CONTROL OF ROBOTIC MANIPULATORS: HYBRID HIERARCHICAL STATISTICAL CONTROL

In this chapter, we present a hybrid hierarchical statistical control approach for robotic manipulators. For the bimodal dynamic imaging system, these robotic manipulators are utilized to move the source and the detector. The bimodal dynamic imaging system contains both the continuous and discrete dynamics. Therefore, only statistical control is not sufficient to model the system dynamics. We consider the bimodal dynamic imaging system as a hybrid system. In this chapter, first we utilized a full-state feedback statistical controller to minimize the joint angle variations of the previously developed single robot manipulator model of Baxter. Then, we considered two such statistical-controlled manipulators as agents and developed a supervisory controller for coordination between the manipulators. The feasibility of the hybrid hierarchical statistical controller is demonstrated with numerical simulations.

7.1 Statistical Control

In this section, we simulated a single robot manipulator using the statistical controller. In statistical control paradigm, the cumulants of the cost function of the stochastic system is minimized. In our case, we intend to minimize the joint angle variation so that the end-effector pose is less affected. The less variation will ensure that the laser and the camera will be in line-of-sight during image acquisition for the bimodal imaging experiment. In this section, we selected the optimum design parameter for the statistical controller through numerical simulations.

7.2 Full-state Feedback Statistical Controller

In statistical control paradigm, because of the presence of the Gaussian white noise, the cost function becomes random. Therefore, the cumulants of the cost function of the stochastic

system is minimized. In our case, we intend to minimize the joint angle variation so that the end-effector pose is less affected. The less variation will ensure that the laser and the camera will be in line-of-sight during image acquisition for the bimodal imaging experiment. We utilize the full-state feedback statistical control, because Baxter has sensors to measure the joint angles, joint velocity, torque, and end-effector pose.

7.2.1 Statistical Control Preliminaries

We consider a stochastic linear time invariant dynamic system modelled on $[t_0, t_f]$. The dynamic process model is given by,

$$\begin{aligned} dx(t) &= Ax(t)dt + Bu(t)dt + Fdw(t), \\ x(t_0) &= x_0, \quad t \in [t_0, t_F] \end{aligned} \tag{7.1}$$

where $x(t) \in \mathbb{R}^n$ is an n-dimensional state vector at time t, $u(t) \in \mathbb{R}^m$ is an m-dimensional control vector at time t, x_0 is the initial condition. $A \in \mathbb{R}^{n\times n}$, $B \in \mathbb{R}^{n\times m}$, and $F \in \mathbb{R}^{n\times p}$ are matrices of appropriate order. Here, $dw(t)$ is a Gaussian random process of dimension p with zero mean, covariance of $W(t)dt$. The random process is defined on a probability space $(\Omega_0, \mathscr{F}, \mathscr{P})$ where Ω_0 is a non-empty set, $\mathscr{F}$ is a σ-algebra of Ω_0, and $\mathscr{P}$ is a probability measure on (Ω_0, F). Also, we consider the output equation:

$$y(t) = Cx(t) + Du(t), \tag{7.2}$$

where, C and D are matrices of appropriate order.

The quadratic random cost for the linear stochastic system is

$$J = x'(t_F)Q_F x(t_F) + \int_t^{t_F} \left[x'(\tau)Qx(\tau) + u'(\tau)Ru(\tau)d\tau\right], \tag{7.3}$$

where the state weighting symmetric matrix $Q \in \mathbb{R}^{n\times n}$ is positive semi-definite, the control effort weighting symmetric matrix $R \in \mathbb{R}^{m\times m}$ is positive definite, and the terminal penalty weighting symmetric matrix $Q_F \in \mathbb{R}^{n\times n}$ is positive semi-definite.

The statistical control problem is to determine a control law such that the n-th cost cumulant of the cost function in (7.3) is minimized, while keeping the rest of the $(n-1)$-th cumulants at pre-specified levels.

7.2.2 Statistical Control Law

In this paper, we utilize the statistical control that minimizes the second cumulant of the cost function for a fixed first cumulant. The second cumulant is the variance of the cost function, while the first cumulant is the mean of the cost function. In case of the second cost cumulant minimization, the full-state-feedback linear statistical control law has the form [40],

$$u(t) = -R^{-1}B'(\mathscr{M} + \gamma\mathscr{V})x(t) = -K_{stat}x(t), \tag{7.4}$$

where the positive semi-definite $\mathscr{M}$ and $\mathscr{V}$ are solutions of the coupled algebraic Riccati equations:

$$\begin{aligned} &A'\mathscr{M} + \mathscr{M}A + Q - \mathscr{M}BR^{-1}B'\mathscr{M} \\ &+ \gamma^2\mathscr{V}BR^{-1}B'\mathscr{V} = 0, \end{aligned} \tag{7.5}$$

$$\begin{aligned} &4\mathscr{M}FWF^T\mathscr{M} + A'\mathscr{V} + \mathscr{V}A - \mathscr{M}BR^{-1}B'\mathscr{V} \\ &- \mathscr{V}BR^{-1}B'\mathscr{M} - 2\gamma\mathscr{V}BR^{-1}B'\mathscr{V} = 0, \end{aligned} \tag{7.6}$$

with the boundary conditions $\mathscr{M}(t_F) = Q_F$ and $\mathscr{V}(t_F) = 0$ for a suitable Lagrange multiplier γ. We assume that $R > 0$, (A,B) is stabilizable, and $(\sqrt{Q},A)$ is detectable. In case of $\gamma = 0$, the above-mentioned statistical control law becomes

$$u(t) = -R^{-1}B'\mathscr{M}x(t), \tag{7.7}$$

where $\mathscr{M}$ is the solution of the following Riccati equation:

$$A'\mathscr{M} + \mathscr{M}A + Q - \mathscr{M}BR^{-1}B'\mathscr{M} = 0, \tag{7.8}$$

with the boundary condition $\mathscr{M}(t_F) = Q_F$.

Note that the statistical control with nonzero γ is known as 'Minimum Cost Variance' control, and the statistical control with $\gamma = 0$ is known as 'Linear Quadratic Gaussian' control.

For implementing the statistical control for non-zero reference tracking, we use the internal model principle to find a feedforward gain for a reference input [127]. The control law is rewritten as:

$$u = -K_{stat}x + \bar{N}r, \tag{7.9}$$

where

$$\bar{N} = N_u + K_{stat}N_x \tag{7.10}$$

is the feedforward controller gain. Note that we first design a state feedback gain K_{stat} using statistical control method such that $A - BK_{stat}$ is stable. Then, to obtain the values of N_x and N_u, we solve

$$\begin{bmatrix} A & B \\ C & D \end{bmatrix} \begin{bmatrix} N_x \\ N_u \end{bmatrix} = \begin{bmatrix} 0 \\ I \end{bmatrix}.$$

This feedforward control method is applicable for a slowly varying reference input.

7.2.3 Statistical Control Simulation of a Single Robot Manipulator

7.2.3.1 Simulation Parameters

The linearized state-space model of one arm of the Baxter robot for perturbations about the operating point is found from Eq. (6.63) using the operating point for joint angles $[0, 0.7854, 1.5708, 0, 0.7854, 0]$ and joint velocities $[0,0,0,0,0,0,0,0]'$. The system is found controllable and observable. The eigenvalues of the system are $\pm 11.58i$, ± 9.40, ± 7.52, ± 6.59, ± 5.22, $-0.62 \pm 0.66i$, and $0.62 \pm 0.66i$. In order to make the linear state-space model stochastic, we incorporate a zero-mean Gaussian white noise term dw with a covariance W in the model. Therefore, from the linear model of Eq. (6.63), we write the stochastic linear model for the left robot manipulator in this form:

$$dx_l(t) = A_l x_l(t)dt + B_l u_l(t)dt + F_l dw_l(t), \quad x_l(t_0) = x_{l0}, \quad t \in [t_0, t_F].$$

For set-point tracking we used the following diagram (Fig. 7.1) for simulation,

The initial joint angles are $[-0.3927, -1.1781, -1.9635, 1.1781, 1.1781, 0.3927, 0.3927]'$ and the reference joint angles are $[0, 0.7854, 1.5708, 0, 0.7854, 0, 0]'$.

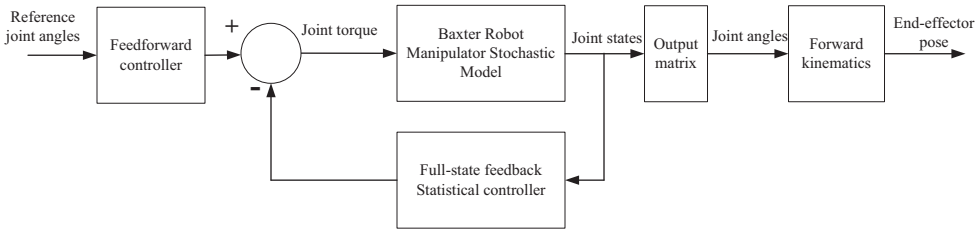

Figure 7.1: Set-point tracking with statistical control simulation diagram

Figs. 7.2, 7.3, 7.4, 7.5, 7.6 and 7.7 show the time response of the joint angle and end-effector position and error, and end-effector orientation and error with the statistical controller of $\gamma = 0$.

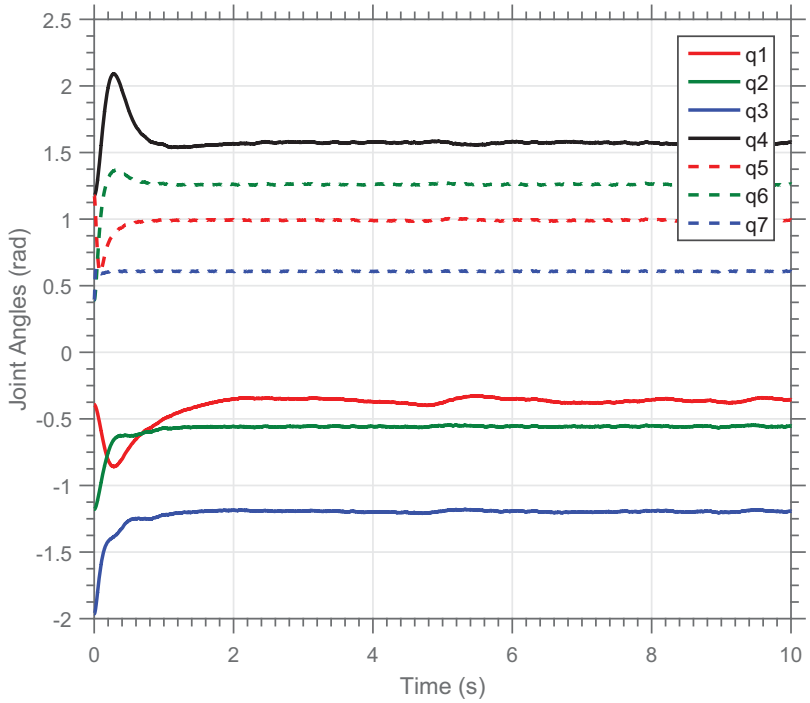

Figure 7.2: Joint angle tracking with statistical control $\gamma = 0$

7.2.3.2 Statistical Design Parameter Selection

In order to obtain the suitable statistical design parameter γ, we investigated the joint angle tracking, and end-effector position and orientation tracking error. We used the following two performance metrics to choose γ

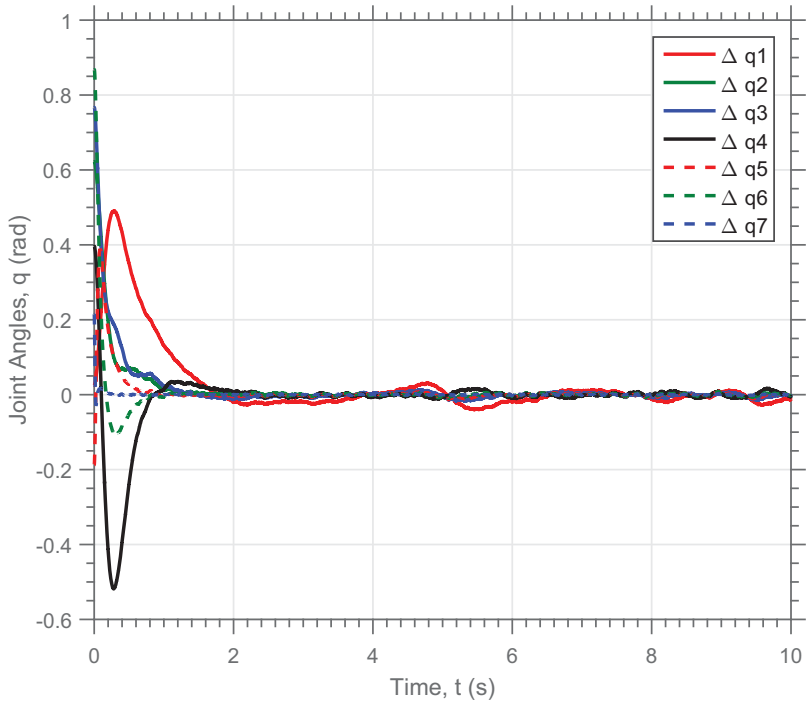

Figure 7.3: Joint angle tracking error with statistical control $\gamma = 0$

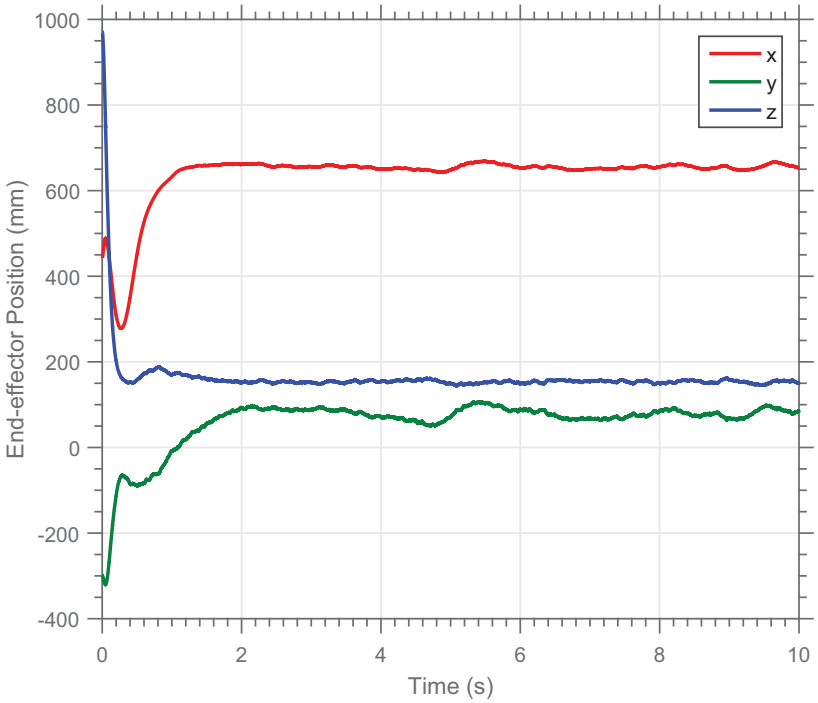

Figure 7.4: End-effector position tracking with statistical control $\gamma = 0$

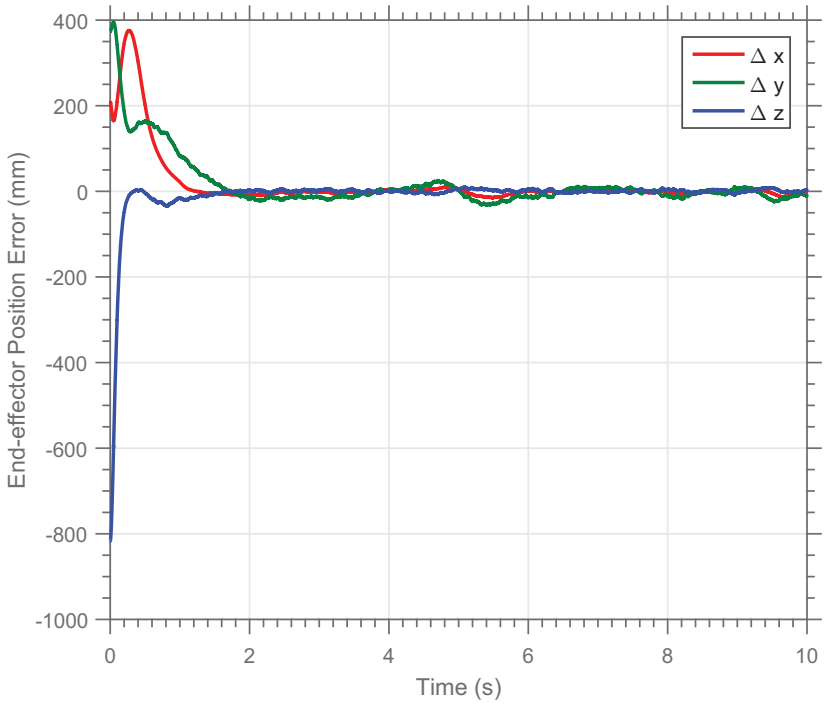

Figure 7.5: End-effector position tracking error with statistical control $\gamma = 0$

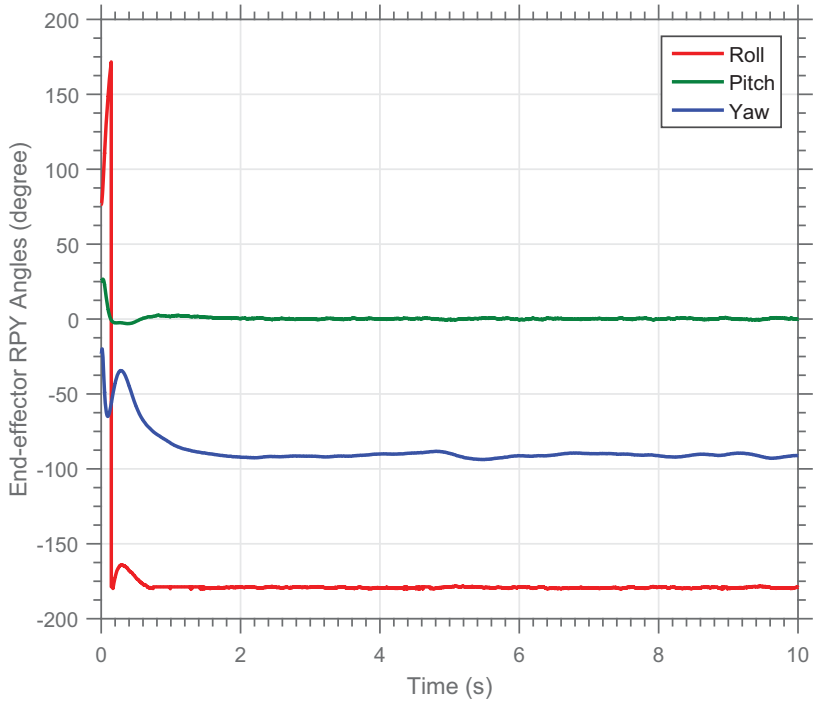

Figure 7.6: End-effector orientation tracking with statistical control $\gamma = 0$

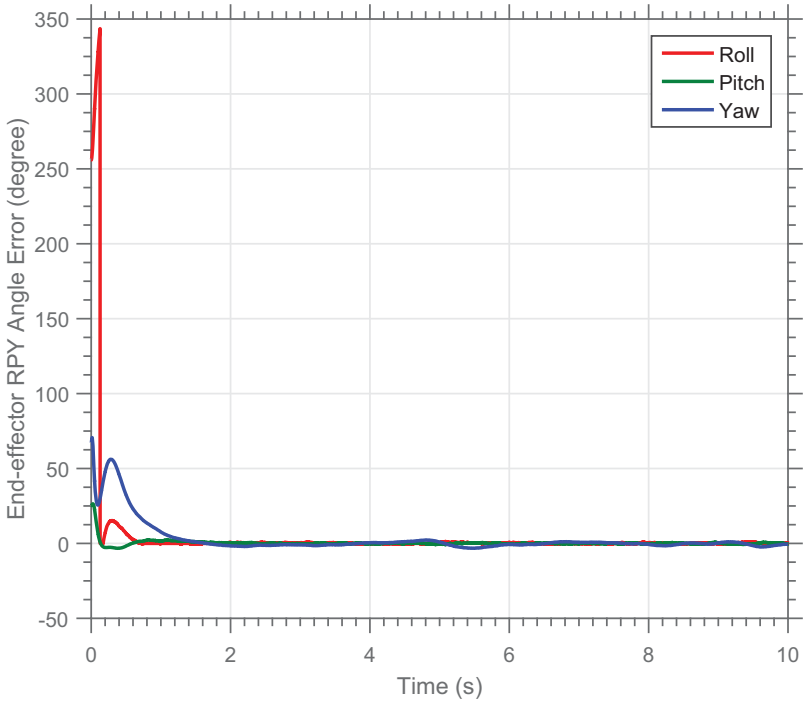

Figure 7.7: End-effector orientation tracking error with statistical control $\gamma = 0$

- Tracking error and root-mean-squared tracking error: The tracking error is the difference between the set-points and the outputs. The root mean squared tracking error is defined in (7.11):

$$\mu_\varepsilon = \sqrt{\frac{\sum_{t=0}^{t=t_f} \varepsilon^2(t)}{N_\varepsilon}},$$

where μ_ε is the root mean squared tracking error, ε is the error between the set-point and the current output value, N_ε is the number of samples.

- Standard deviation of tracking error : The standard deviation of the tracking error indicates the variation of the error from the mean error value. This is defined as:

$$\sigma_\varepsilon = \sqrt{\frac{\sum_{t=0}^{t=t_f} (\varepsilon(t) - \mu)^2}{N_\varepsilon - 1}}. \tag{7.11}$$

This formula is also referred as the corrected sample standard deviation. We are interested about the steady-state pointing performance of the system. Therefore, we calculated these metrics on the steady-state part of the joint angle and end-effector pose response.

In our simulation, we varied γ from 0 to 1 with 0.1 interval. For each γ we ran the simulation 100 times. Each time a randomized seed was used to generate Gaussian white noise. The simulation duration was 10 seconds. Finally, we averaged the response. In this manner, we ensured the stochastic nature of the simulation. We calculated the root-mean-squared tracking error and standard deviation based on the response from $t = 3s$.

Figs. 7.8 and 7.9 show the joint angle tracking error and error variation with the varying γ. Figs. 7.10 and 7.11 show the end-effector position tracking error and error variation with the varying γ. Figs. 7.12 and 7.13 show the end-effector orientation tracking error and error variation with the varying γ.

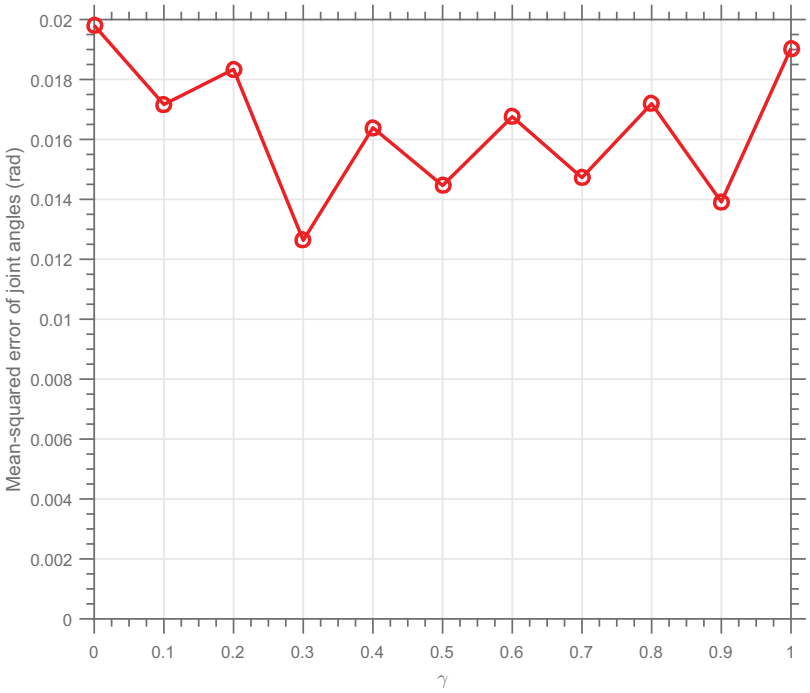

Figure 7.8: Joint angle tracking error versus γ

Table 7.1 shows tracking performance for $\gamma = 0$, 0.3, and 0.9. We observe that the $\gamma = 0.3$ and $\gamma = 0.9$ show better performance compared to $\gamma = 0$ case. $\gamma = 0.3$ produced the minimum tracking error in all cases (joint angles and end-effector pose). $\gamma = 0.9$ produced the minimum tracking error variation. Our control goal is to minimize the variation in the joint angle error, consequently, end-effector pose error. Therefore, we choose $\gamma = 0.9$ as

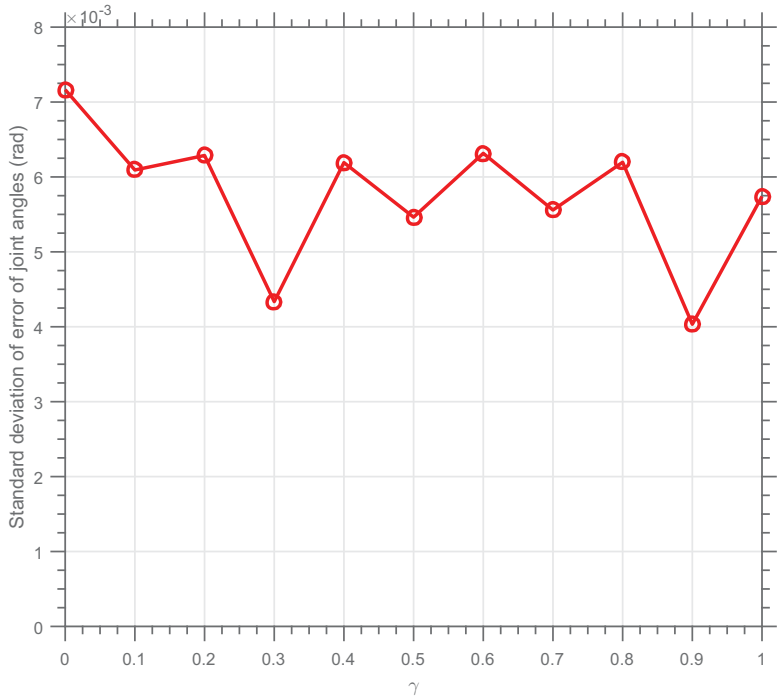

Figure 7.9: Joint angle tracking error variation versus γ

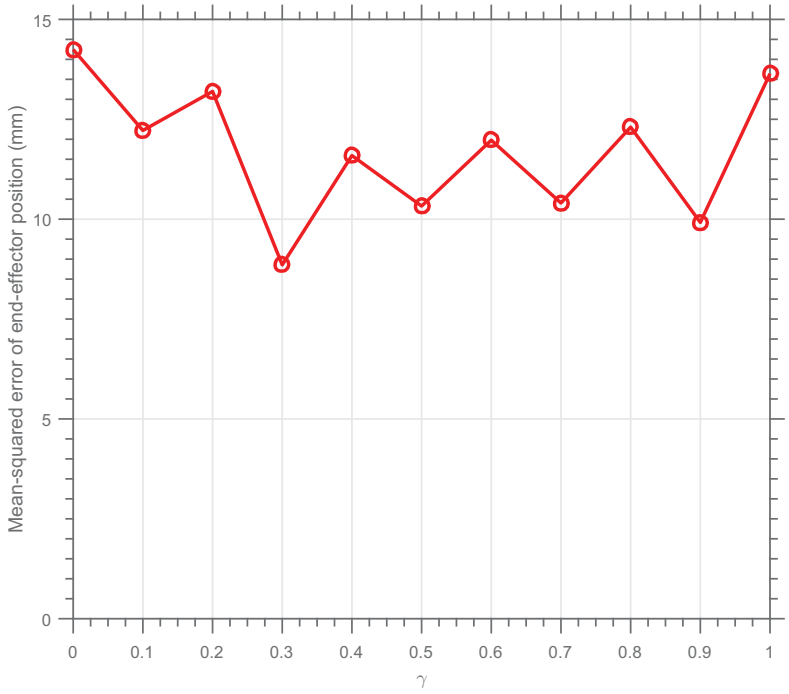

Figure 7.10: End-effector position tracking error versus γ

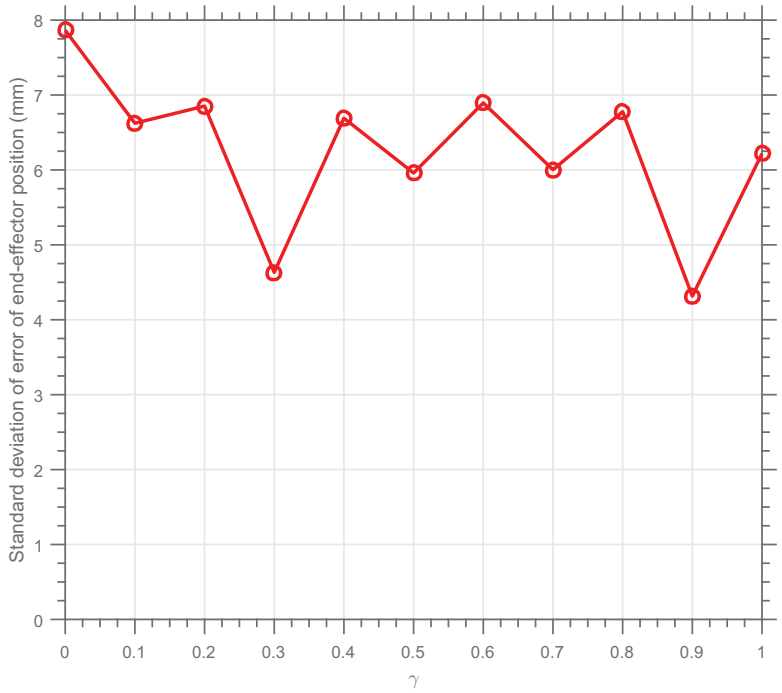

Figure 7.11: End-effector position tracking error variation versus γ

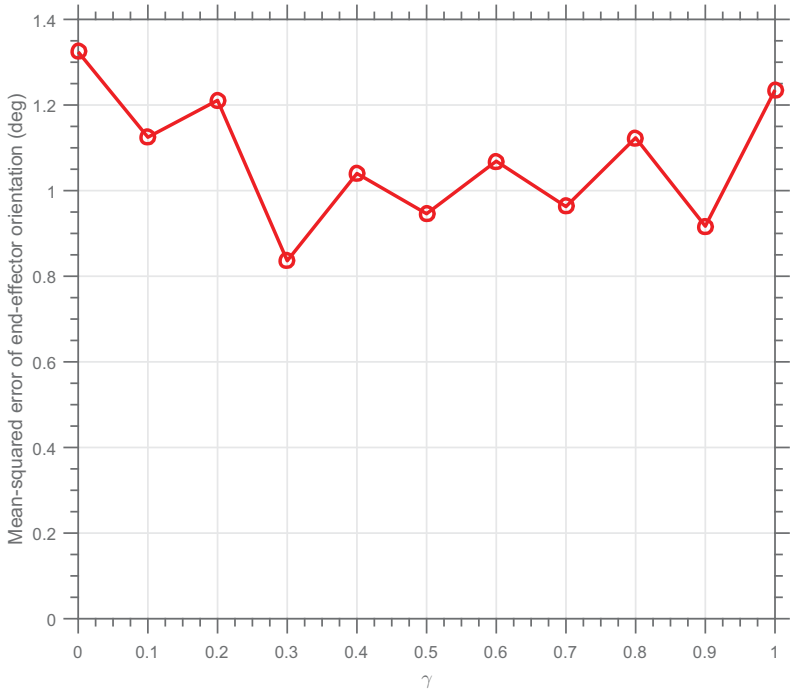

Figure 7.12: End-effector orientation tracking error versus γ

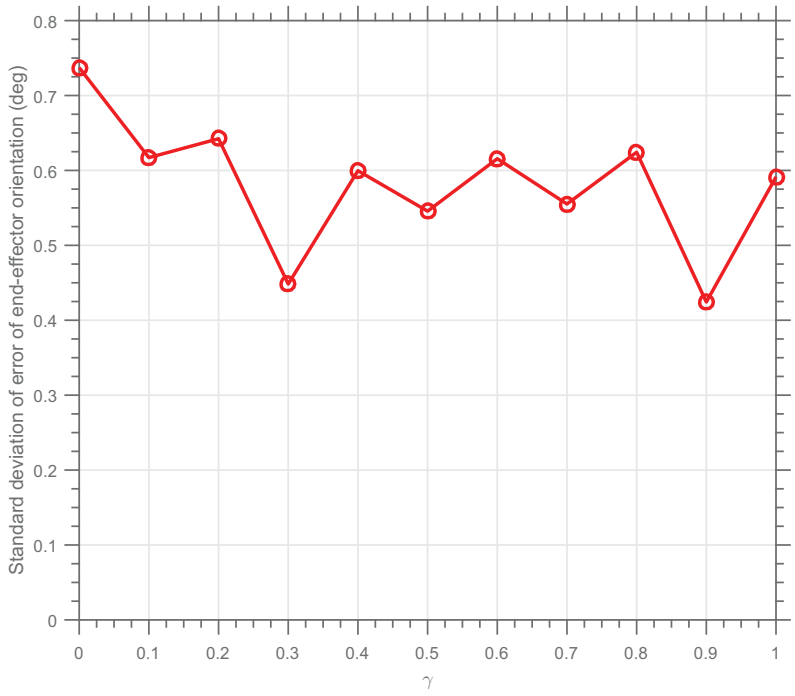

Figure 7.13: End-effector orientation tracking error variation versus γ

Table 7.1: Root-mean-squared tracking error (μ) and error variation (σ) results

	$\gamma = 0$		$\gamma = 0.3$		$\gamma = 0.9$	
Parameters	μ	σ	μ	σ	μ	σ
Joint angle (rad)	0.02	0.0071	0.0126	0.0043	0.0139	0.004
End-effector position (mm)	14.25	7.865	8.86	4.63	4.31	4.2506
End-effector orientation (deg)	1.32	0.7372	0.84	0.45	0.92	0.42

the best design parameter value for the statistical control of the left arm of Baxter robot.

7.2.3.3 Statistical Controller Simulation

Figs. 7.14, 7.15, 7.16, 7.17, 7.18 and 7.19 show the time response of the joint angle and end-effector position and error, and end-effector orientation and error with the statistical controller of $\gamma = 0.9$. The parameter $\gamma = 0.9$ yielded better tracking error variation for the end-effector position. Therefore, we selected $\gamma = 0.9$ as the design parameter value for our statistical controllers.

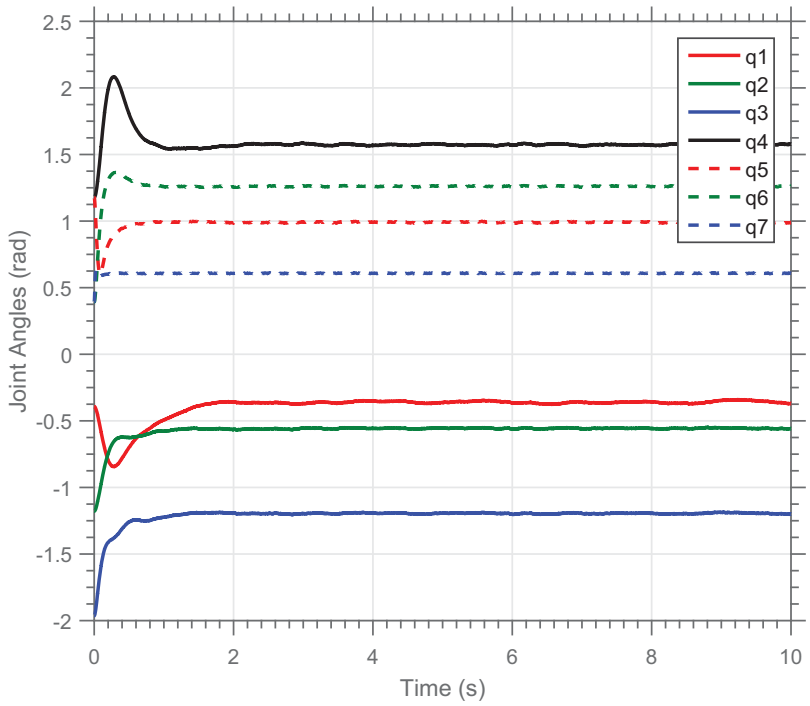

Figure 7.14: Joint angle tracking with statistical control $\gamma = 0.9$

7.3 Hybrid Hierarchical Statistical Control Architecture

We propose a system architecture for controlling the source and detector motion of Baxter robot arms for scanning the target. Fig. 7.20 shows the hierarchical hybrid agent control system architecture. The system consists of two tiers. The top tier is the supervisory controller, and the bottom tier component is called the agent. The supervisory controller

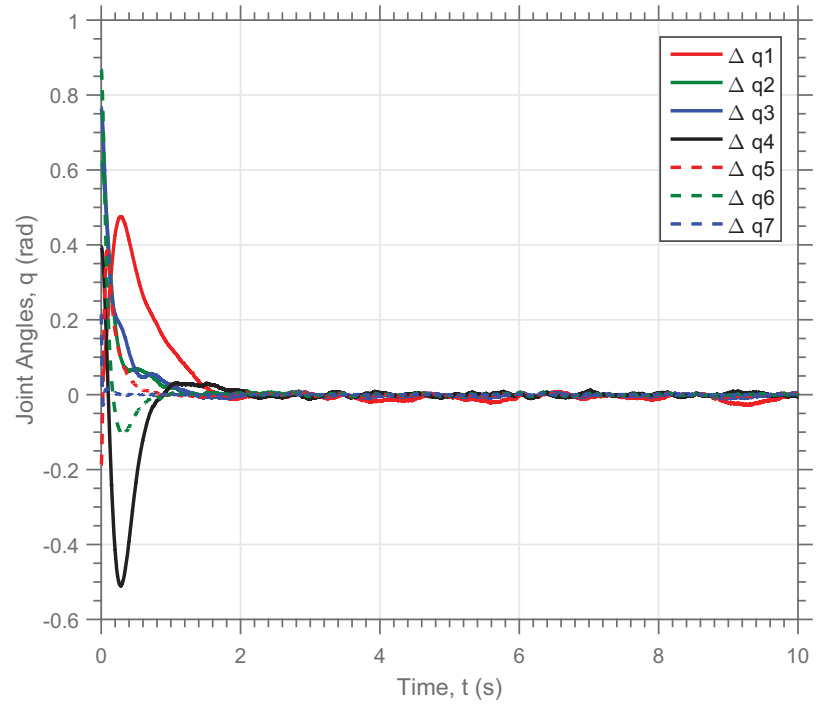

Figure 7.15: Joint angle tracking error with statistical control $\gamma = 0.9$

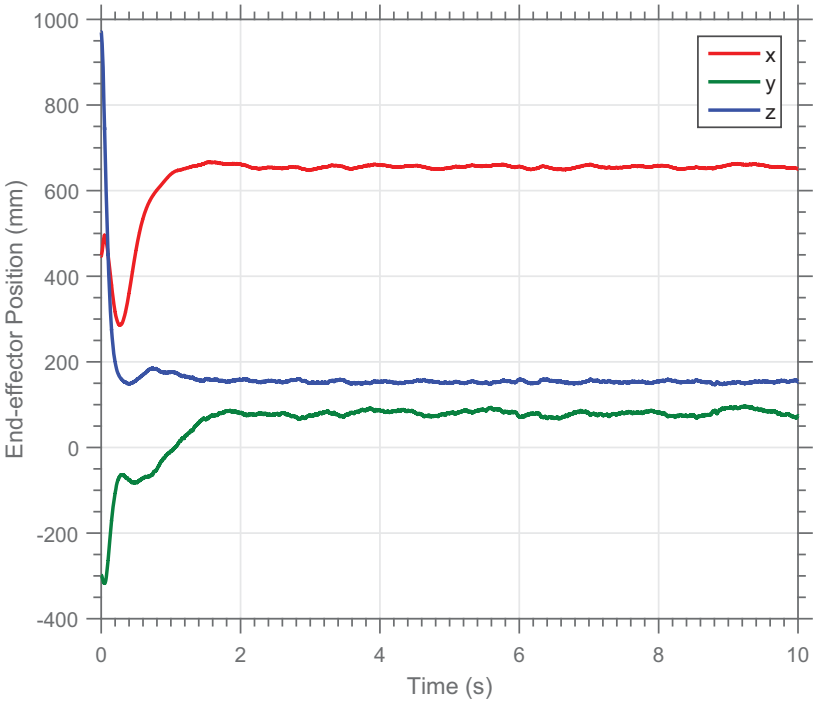

Figure 7.16: End-effector position tracking with statistical control $\gamma = 0.9$

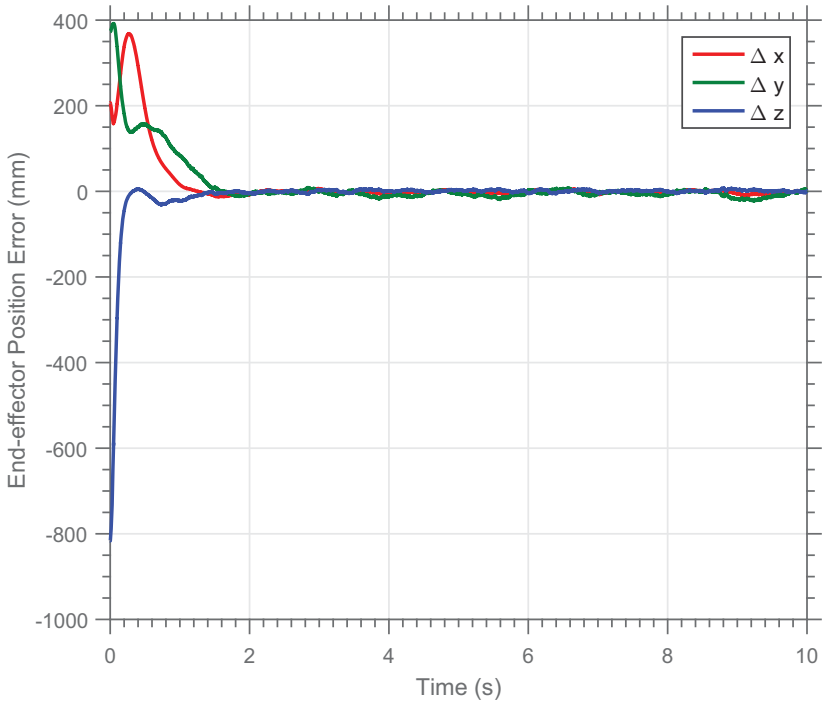

Figure 7.17: End-effector position tracking error with statistical control $\gamma = 0.9$

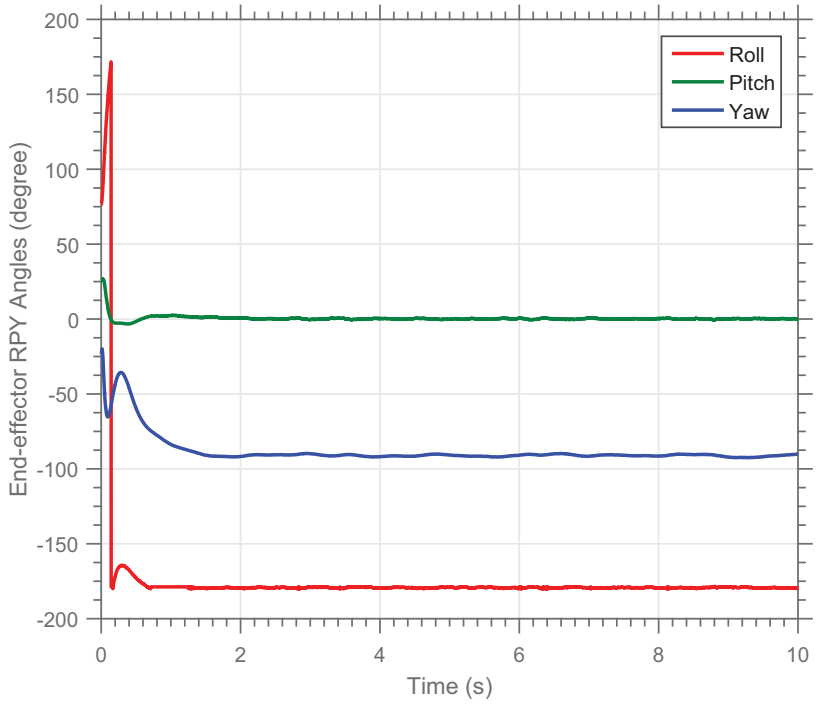

Figure 7.18: End-effector orientation tracking with statistical control $\gamma = 0.9$

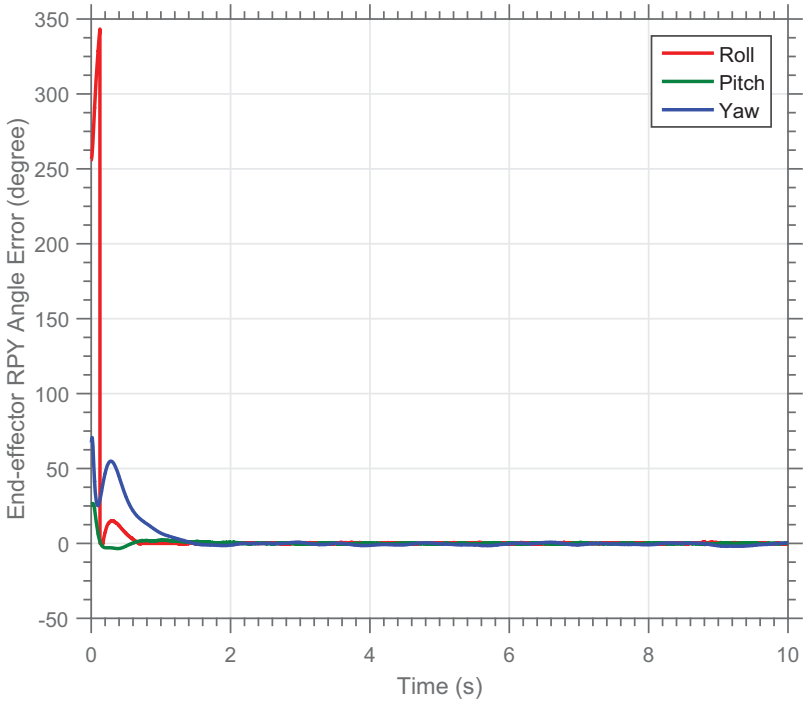

Figure 7.19: End-effector orientation tracking error with statistical control $\gamma = 0.9$

generates commands for scanning, monitors the status of agents, and coordinates between them. The two arms of Baxter can be considered as agents. They are equipped with actuators and sensors to complete required scanning tasks and inform the status of the tasks to the supervisory controllers. In short, the supervisory controller can be considered as high-level controller, whereas at the agent-level there can be low-level controller such as PID controller, LQG controller, and statistical controller.

7.3.1 Hybrid Automaton

The proposed hybrid hierarchical system includes both the continuous and discrete dynamics. The continuous dynamics work in the bottom tier, which include the joint control. In our system, statistical controllers are used for the joint control. On the other hand, the supervisory controller includes discrete dynamics. Because of the presence of both discrete and continuous dynamics, the system can be viewed as hybrid systems.

We use the definitions of hybrid automatons given in [128]. A hybrid automaton **H** can

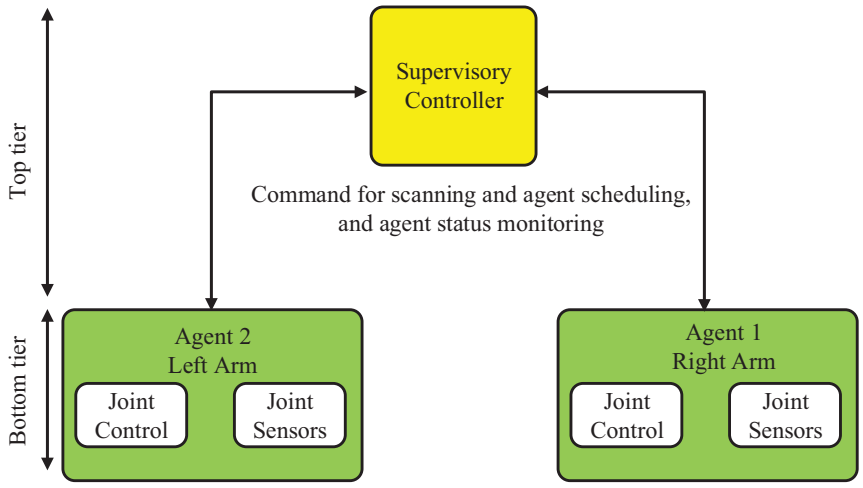

Figure 7.20: Hierarchical hybrid agent control system architecture for a dual arm robot assisted bimodal dynamic imaging system

be described mathematically as

$\mathbf{H} = (S, X, \Sigma_{in}, \Sigma_{out}, U, f, Init, D, E, G, R)$, where

S is the set of discrete states where the system is allowed to exist. X is the set that represents all of the continuous variables, possible in each of the states of S. The vector field, f, consists of time dependent functions such as differential equations that describe the time evolution of the variables in X. TX denotes the tangent bundle of X. The initial states are the initial values of the continuous variables. $\mathscr{D}$ contains the range where each continuous variable and discrete event that are allowed to exist. $P(X)$ denotes the set of all subsets of X. Σ_{in} and Σ_{out} denote the set of all discrete inputs and discrete outputs. The set of edges, $\mathscr{E}$, describe what transitions are allowed to occur between states. The guard conditions, G, describe the events that must occur for a transition to take place. Finally, the reset map, $\mathscr{R}$, is the set of conditions that cause the system to enter its initial state.

7.3.2 Supervisory Controller Model

The supervisory controller functions are as follows:

1. To generate and send commands to agents. In this case, the agents are the two robot arms or robot manipulators.

S	Finite set of discrete states of **H**,
X	Finite set of continuous variables,
Σ_{in}	Finite set of discrete input variables,
Σ_{out}	Finite set of discrete output variables,
U	Set of the continuous input variables,
$f : S \times X \rightarrow TX$	Continuous flow vector in discrete state,
$Init \subseteq S \times X$	Set of initial states
$\mathscr{D} : S \rightarrow P(X)$	Domain
$\mathscr{E} \subseteq S \times S$	Set of edges
$G : \mathscr{E} \subseteq P(X)$	Guard condition
$\mathscr{R} : \mathscr{E} \times S \times \Sigma_{in} \rightarrow P(X)$	Reset map

2. To schedule the scanning task command to control the agents.
3. To facilitate coordination between the agents so that they can act cooperatively.
4. To ensure safety in case of unexpected situations.

Supervisory controller automaton is modeled using discrete event systems. In our case, the supervisory controller is designed to execute its tasks sequentially. There are five discrete nodes, which constitute the discrete set $S = \{s_1, s_2, s_3, s_4, s_5\}$. Each nodes are defined as follows:

- **Idle Node** (s_1). In this node, the supervisory controller waits for the PowerON message from the operator. If the PowerON message is generated, the system jumps from node s_1 to node s_2. In the case, when the supervisory controller gets *UnexAg1Status = 1* or *UnexAg2Status = 1* message from node s_5 or *ScanCountFinish = 1* from node s_2, it sends the PowerOFF message to the operator.
- **Agent Scheduler Node** (s_2). In this node, the supervisory controller assigns the scanning task to Agent 1 and Agent 2 sequentially and checks for the scanning task status. If the scan count matches a pre-specified number, the system jumps from s_2 to s_1. Agent 1 sends back a scheduling success message via Ag1ScheduleFinish tag with 1 upon successful reception. Then the supervisory controller starts calculating task start and end time. The supervisory controller then jumps to s_3 to control Agent

1 to perform the task with a message tag *Ag1Active=1*. After a pre-specified time interval, the controller jumps back from s_3. The controller then jumps to s_4 with a message tag *Ag2Active=1*. The controller does the scheduling and time interval calculation for s_4. The scan count is incremented by 1 if Agent 2 sends back *AgTaskFinish = 1* tag. This sequence of jumping goes on until the scan is complete and s_2 generates a tag *ScanCountFinish = 1*.

- **AgentManeuver Node** (s_3 and s_4). In these nodes, the supervisory controller sends the control signal to permit pre-specified reference trajectory to the corresponding agent at the calculated task start time. The the supervisory controller will standby in s_3 or s_4 to wait for the task status feedback from Agent 1 or 2. After the supervisory controller receives the feedback, or if a TimeOut event is triggered, it will jump from s_3 to s_2 or from s_4 to s_2. The scanning task includes positioning of the robot arm joints at the desired position and capturing images. If the scheduled scanning task has been successfully performed by an agent, a feedback tag *AgTaskFinish = 1* is sent from the bottom tier to the top tier, and the supervisory controller jumps back to s_2.
- **UnexpectedStatusCheck Node** (s_5). In this node, the supervisory controller monitors for any unexpected situation. The unexpected situations can occur in different scenarios such as there is collision between the arms, there exist out of reach joint limit, or the operator is not satisfied with the scanning performance during the scanning. The generated message tag is *UnexAg1tatus* or *UnexAg2tatus*. If the tag is 1, the supervisory controller falls back to node s_1.

The finite set of continuous variable for the agent system is defined as $X = \{q_1, q_2, q_3, q_4, q_5, q_6, q_7\}$, where q_i, $i = 1, 2, \cdots, 7$ represents the joint angles of the robot arm. The continuous dynamics include the stochastic model of the robot arm with the state feedback statistical controller.

The finite set of discrete events has the input and output events. It can be represented as follows.

$$\Sigma_{in} = \{PowerON, AgkTaskStatus, ScanCountFinish, UnexAgkStatus\};$$

$$\Sigma_{out} = \{AgkTaskCMD\};$$

Note that Agk denote $Ag1$ and $Ag2$. The discrete transitions in the system are:

$$\mathscr{E} = \{(s_1,s_2),(s_2,s_1),(s_2,s_3),(s_3,s_2),(s_2,s_4),(s_4,s_2),(s_3,s_5),(s_4,s_5),(s_5,s_1)\}$$

The guard conditions are defined as:

$$\begin{bmatrix} G_1 \\ G_2 \\ G_3 \\ G4 \\ G5 \\ G6 \\ G7 \\ G8 \\ G9 \end{bmatrix} = \left\{ \begin{array}{l} (s_1,s_2) \Rightarrow \{PowerON \neq \varnothing\} \\ (s_2,s_1) \Rightarrow \{ScanCountFinish = 1\} \\ (s_2,s_3) \Rightarrow \{(Ag1Active = 1) \wedge (ScanCountFinish = 0)\} \\ (s_3,s_2) \Rightarrow \{Ag1TaskFinish = 1\} \\ (s_2,s_4) \Rightarrow \{(Ag2Active = 1) \wedge (ScanCountFinish = 0)\} \\ (s_4,s_2) \Rightarrow \{Ag2TaskFinish = 1\} \\ (s_3,s_5) \Rightarrow \{UnexAg1Status = 1\} \\ (s_4,s_5) \Rightarrow \{UnexAg2Status = 1\} \\ (s_5,s_1) \Rightarrow \{(UnexAg1Status = 1) \vee (UnexAg2Stat = 1)\} \end{array} \right\}$$

The state transition diagram for the supervisory controller (top tier) is given in Fig. 7.21.

7.3.3 Agent Model

The agent functions are as follows:

1. To receive reference trajectory commands from the supervisory controller.
2. To perform the joint maneuver so that the poses of the two end-effector are in line-of-sight.
3. To send the task status feedback to the supervisory controller to notify the task success.

- **Idle node** (s_1). In this node, the agent is at the initial position with the initial pose. The agent waits for the *AgentTaskCMD* from the supervisory controller to check if the joint maneuver is required. After receiving *AgentTaskCMD*, the agent jumps to node s_2.

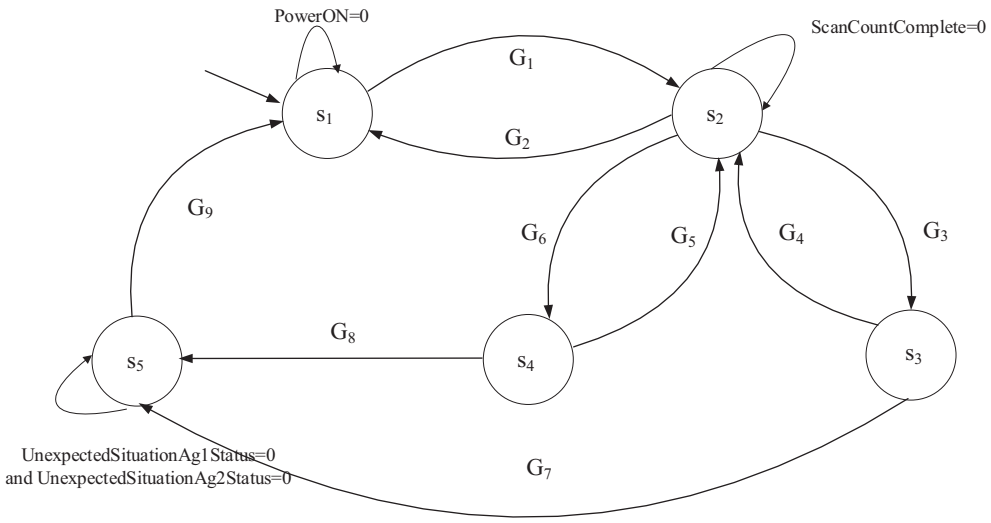

Figure 7.21: State transition diagram for supervisory controller

- **Joint maneuver node** (s_2). In this node, the agent changes its joint angles to the reference joint angles. If there are differences between the current and reference joint angles, then the agent adjusts its joint angles by applying required torque input. At this stage, a statistical controller is used to generate the required torque. If the differences between the current and reference joint angles are below certain thresholds, the agent jumps to node s_3.
- **Agent task status node** (s_3). In this node, the agent operates at the target joint angles with specified margins. The agent checks for the completion of the task assigned by the supervisory controller. The agent sends back a *AgentkTaskFinish* tag to the top tier to indicate that the joint maneuver is successful. If any unexpected situation occurs during the maneuver, the agent generates *UnexAgkStatus* tag to inform the top tier. Here k denotes 1 or 2.

The finite set of continuous variable for the agent system is defined as $X = \{q_1, q_2, q_3, q_4, q_5, q_6, q_7\}$, where q_i, $i = 1, 2, \cdots, 7$ represents the joint angles of the robot arm. The continuous dynamics include the stochastic model of the robot arm with the state feedback statistical controller.

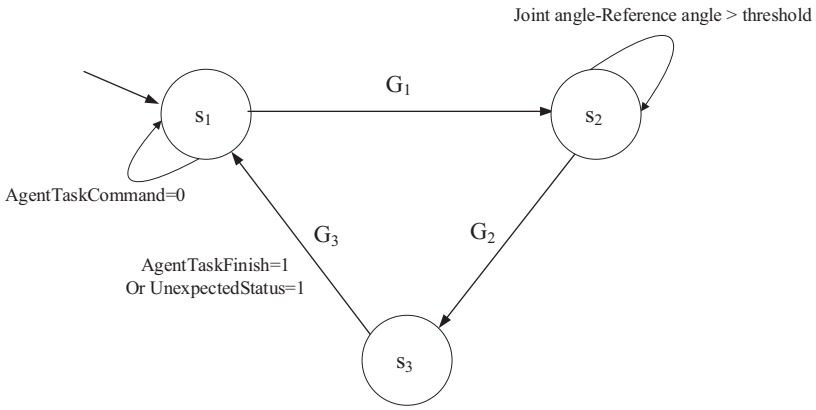

Figure 7.22: State transition diagram for agents

The finite set of discrete events has the input and output events. It can be represented as follows.

$$\Sigma_{in} = \{AgentkTaskCMD\};$$
$$\Sigma_{out} = \{AgkTaskFinish, UnexAgkStatus\};$$

Note that $Agentk$ denote $Agent1$ and $Agent2$, and Agk denote $Ag1$ and $Ag2$. Initial conditions enforced on the system are:

$$Init = \{q_i = q_{i0}\}; i = 1,2,\cdots,7$$

The discrete transitions in the system are:

$$\mathscr{E} = \{(s_1,s_2),(s_2,s_3),(s_3,s_1)\}$$

The guard conditions are defined as:

$$\begin{bmatrix} G_1 \\ G_2 \\ G_3 \end{bmatrix} = \left\{ \begin{array}{l} (s_1,s_2) \Rightarrow \{AgentkTaskCMD \neq \varnothing\} \\ (s_2,s_3) \Rightarrow \{Jointangle diff < threshold\} \\ (s_3,s_1) \Rightarrow \{(AgkTaskFinish=1) \vee (UnexAgkStatus=1)\} \end{array} \right\}.$$

The state transition diagram for the agents (bottom tier) is given in Fig. 7.22.

7.3.4 Hierarchical Hybrid System Simulation

We simulated a scenario of parallel scanning with the bimodal imaging system using the hybrid hierarchical system concept. In this scenario, Agent 1 is the right arm of Baxter

mounted with a laser. Agent 2 is the left arm of Baxter mounted with a tactile imaging system. In the hybrid hierarchical controller paradigm, Agent 1 should follow a reference trajectory required for a parallel scanning, and Agent 2 should follow the trajectory of Agent 1. Fig. 7.23 shows the proposed bimodal dynamic imaging system implemented with Baxter.

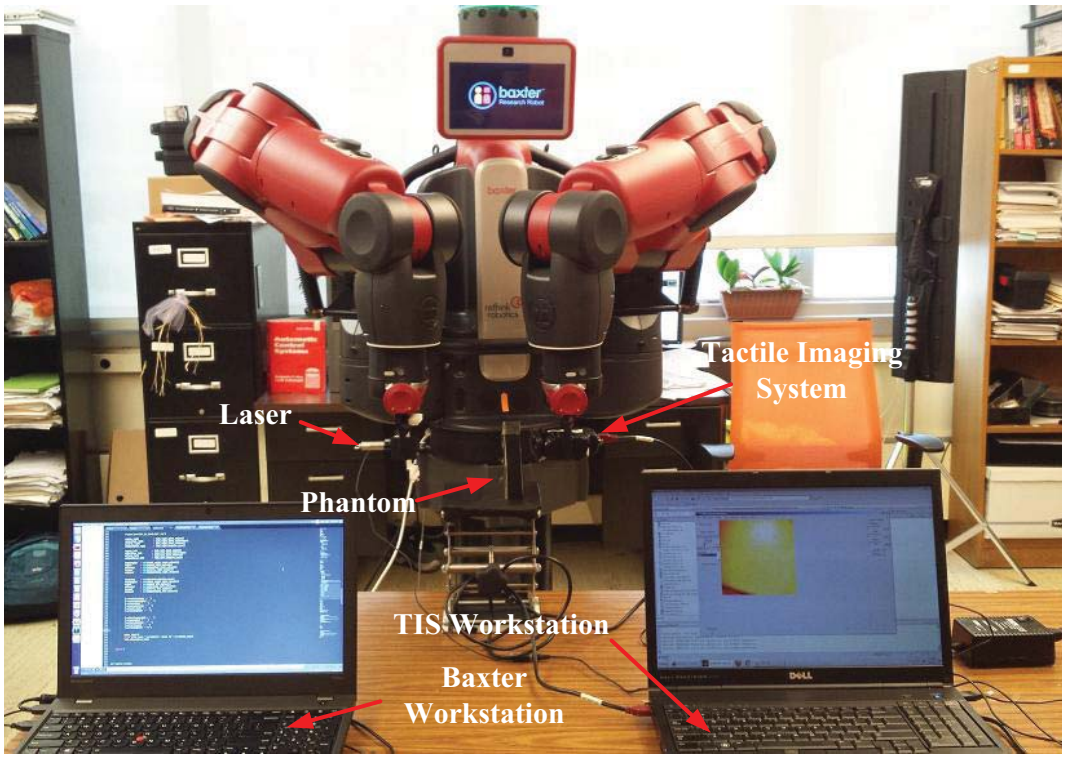

Figure 7.23: Bimodal dynamic imaging system implemented with the Baxter robot

Fig. 7.24 shows the simulation diagram for the hierarchical hybrid controller for the bimodal dynamic imaging system. In the top tier, a supervisory controller is in operation, while in the bottom tier, two statistical controllers are in operation for each robot arm.

Fig. 7.25 shows the block diagram for hybrid hierarchical statistical controller. In the top tier, a supervisory controller is in operation, while in the bottom tier, two feedback statistical controllers are in operation for each robot arm. Also, two feedforward controllers are used to follow the set-point tracking.

Fig. 7.26 shows a simplified diagram showing the positive x-, y-, and z-axes.

We built a testbed for the bimodal imaging system using Baxter with a laser and a

tactile imaging sensor mounted in the end-effector. Then, we maneuvered the end-effector along a linear trajectory and captured images at 15 positions. We collected the joint angles, velocities, torques, and end-effector pose. Then, we fed these reference joint trajectories for the simulation. This simulation was repeated 20 times with 20 different Gaussian white noise. The simulation was implemented using Matlab, Simulink, and Stateflow toolboxes.

Figs. 7.27 shows the trajectory tracking of Agent 1 and Agent 2. The initial position of Agent 1 was (554.80 mm, -84.80 mm, 100.40 mm), and Agent 2 had the initial position of (603.60 mm, 197.20 mm, 74.20 mm). At first, Agent 1 became active, and during initial transition period it reached a peak position of (827.10 mm, 8.56 mm, 296.50 mm) within t=1s. At t=2s, it reached a steady-state value of (669.8 mm, -77.30 mm, 171.10 mm). At t=8s, Agent 2 became active, and during initial transition period it reached a peak position of (939.90 mm, 1169.00 mm, 414.50 mm) within t=9s. At t=10s, Agent 2 reached a steady-state position of (655.30, 76.90, 155.10). When both the agents reached steady-state positions, the system started acquiring images. At t=16s, Agent 1 switched to a new position after being provided with the new reference position. This movement was repeated until 112s. The final positions of Agent 1 and Agent 2 were (618.80 mm, -78.30 mm, 150.20 mm) and (631.20 mm, 73.80 mm, 153.50 mm). Fig. 7.28 shows the trajectory tracking error of Agent 1 and Agent 2. We took a close-up look from t=17s to t=24s for all axes, and noticed that the tracking error did not settle to zero, rather oscillated around zero. This was because of the presence of the Gaussian white noise in the system. We observed the largest error for both agents when they became active initially. We measured the mean and standard deviation of the trajectory tracking error after both agents reached the steady-state values after t=10s until t=112s. Agent 1 tracking error (mean$\pm$standard deviation) was 1.49$\pm$ 0.86 mm, and Agent 2 tracking error was 1.50$\pm$ 0.86 mm.

Note that the experiment for collecting reference joint angles took 112 seconds. The images were taken at 15 positions. The length of the line being scanned was 30 mm. Therefore, for scanning a 30 mm $\times$ 30 mm area, it would take about 30-35 minutes. The robot arm travelling time between two adjacent positions was kept around 8 seconds considering the images would be captured manually. This time can be reduced if the image collection could be made automatic.

7.4 Discussion

This chapter presented a hybrid hierarchical statistical control architecture for the automatic sequential task execution for a bimodal dynamic imaging system, which is intended to be implemented on a dual-arm robot called 'Baxter'. A full-state feedback controller was designed to control each arm at the lower level with minimum position variation. At the higher level, a supervisory controller was used to coordinate the sequential task. These simulation results demonstrated that the developed hybrid hierarchical model can maintain the linear trajectories under a high-level supervisory controller and a low level statistical controller with about 2 mm tracking error variation. In the next chapter, we present the dissertation conclusions and future works.

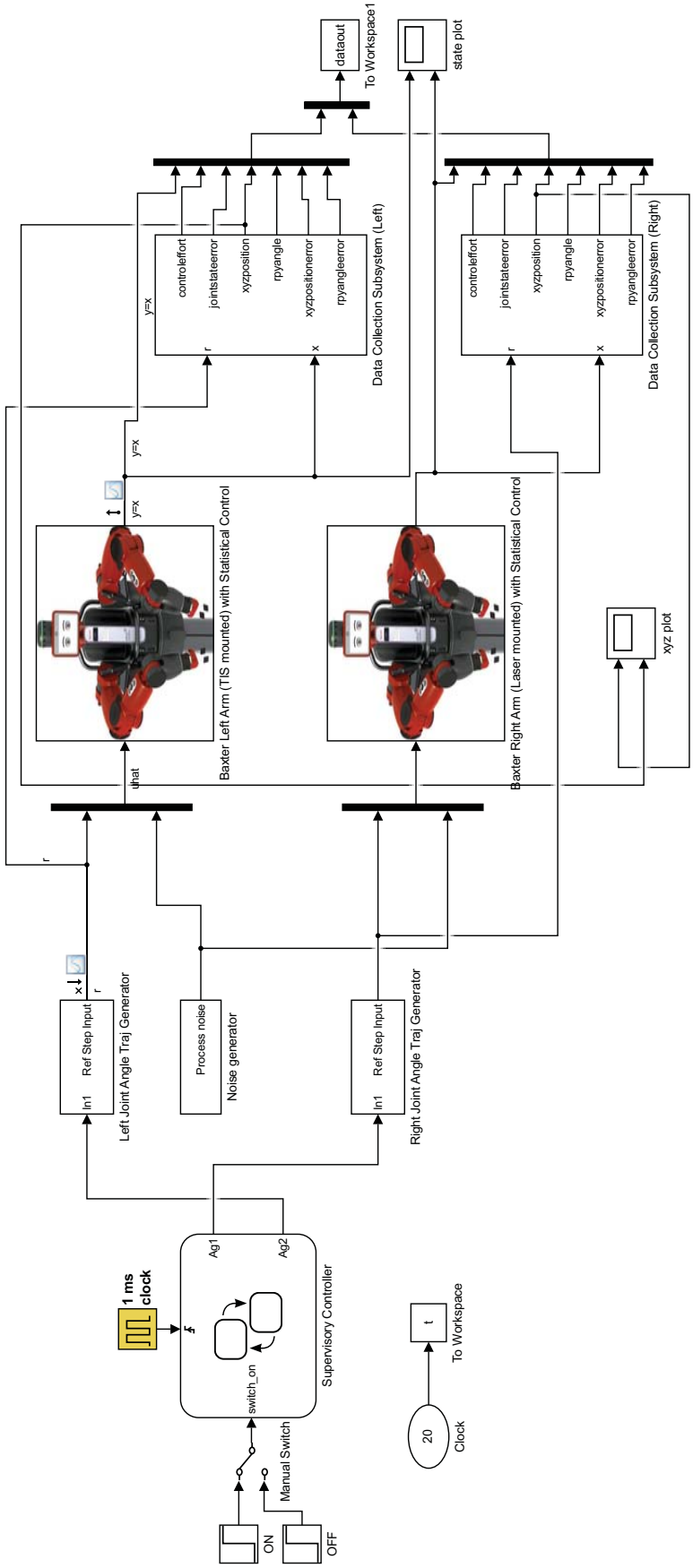

Figure 7.24: Simulink diagram for hierarchical hybrid controller

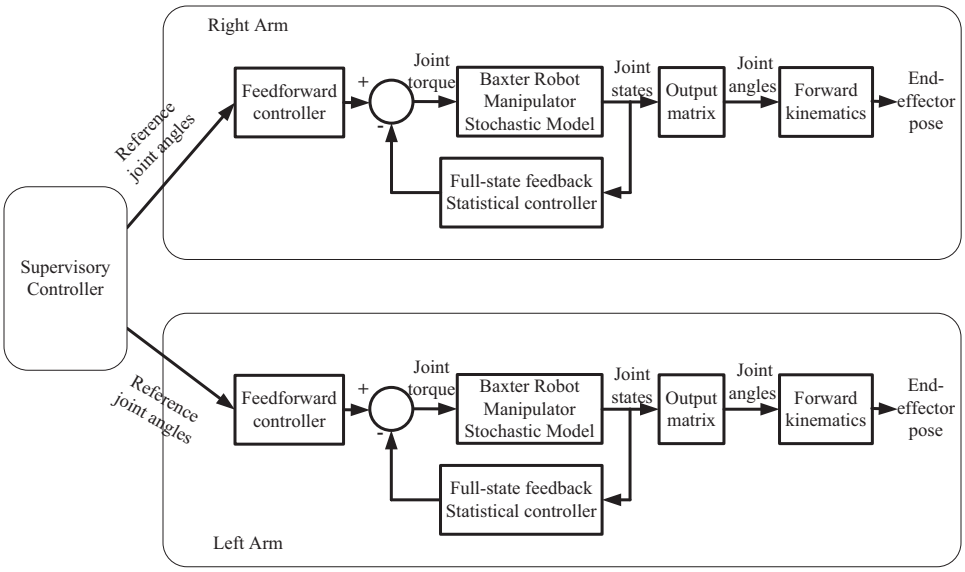

Figure 7.25: Hybrid hierarchical statistical control block diagram

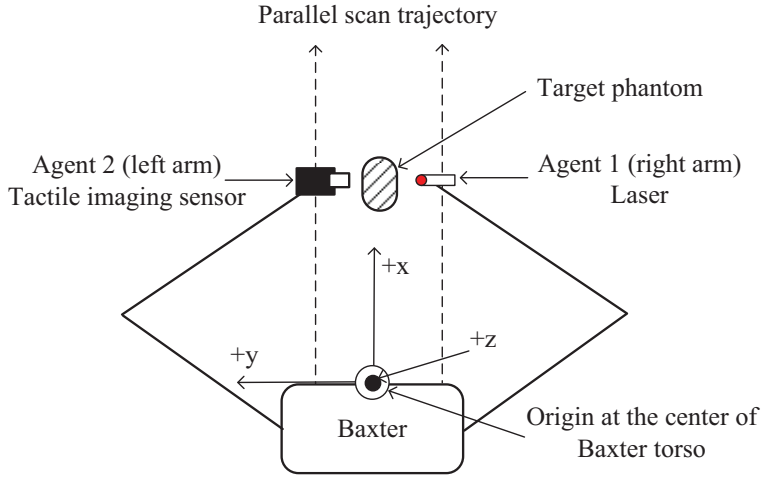

Figure 7.26: Simplified diagram of a bimodal dynamic imaging system (top view)

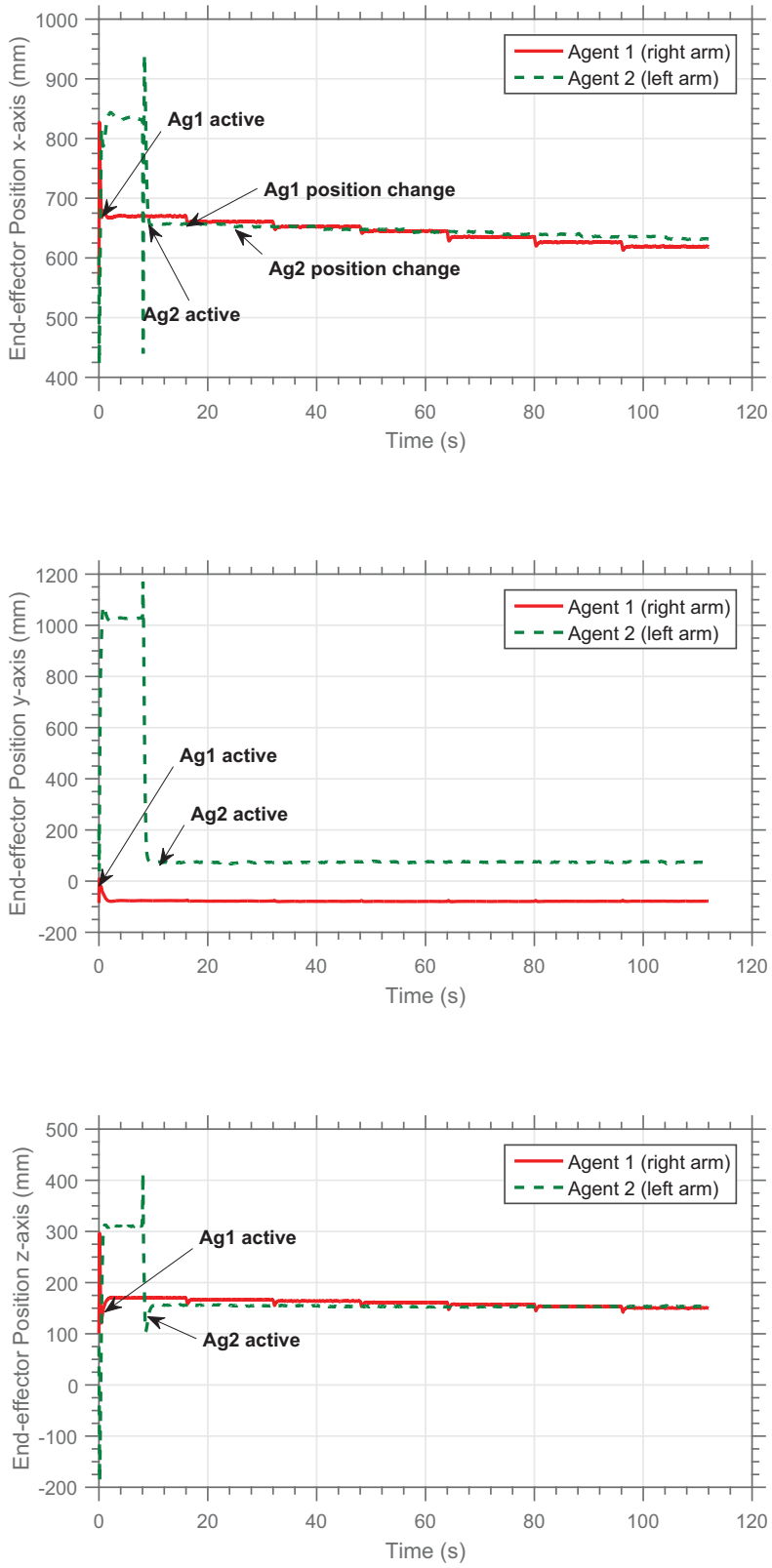

Figure 7.27: End-effector trajectory tracking with hybrid hierarchical statistical controller

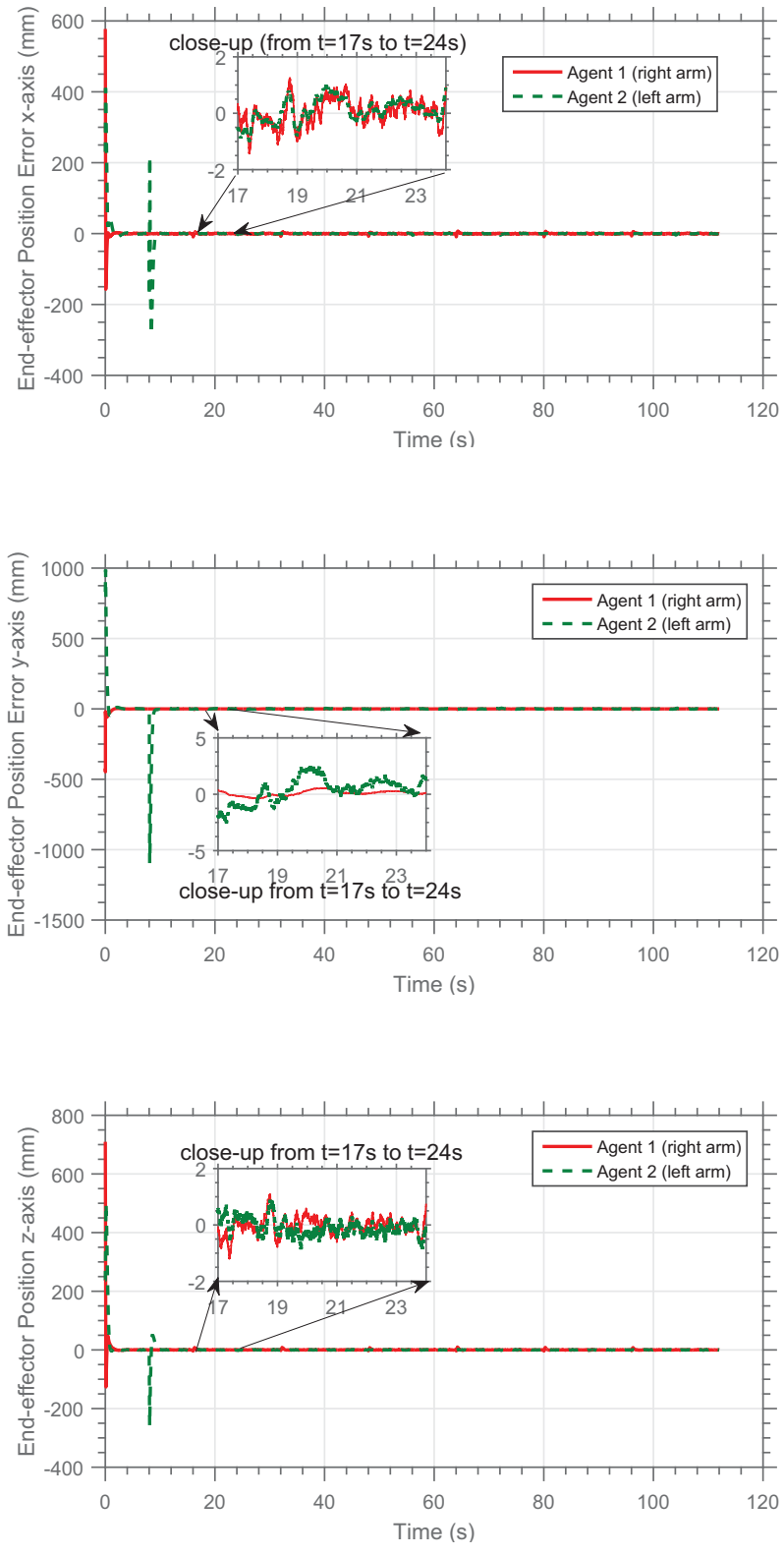

Figure 7.28: End-effector trajectory tracking error with hybrid hierarchical statistical controller

CHAPTER 8

CONCLUSIONS AND FUTURE WORKS

8.1 Conclusions

In this dissertation, a bimodal dynamic imaging system and associated hybrid statistical controller were designed and evaluated for estimating mechanical and spectral properties of the tumor. The main focus of this dissertation was on improving breast tumor characterization by taking advantage of multimodality and dynamic motion of the source and the detector. We consider on improving mechanical and spectral properties estimation, specifically the size, depth, elastic modulus, and absorption coefficients measurement of tumors.

In Chapter 1, we presented the background and literature review on imaging techniques used in breast cancer diagnosis, followed by the discussion on dynamic positioning of the source and detector. We discussed the statistical game control and hybrid hierarchical statistical control approaches for dynamic positioning of the source-detector. Then, we discussed the tactile sensing and diffuse optical imaging, which are the two modalities utilized in the bimodal dynamic imaging system. We stated the research goals of this dissertation, the proposed prototype overview, the contributions of the dissertation, and the outline of the dissertation.

In Chapter 2, we presented the wave-optics analysis and numerical simulation for the verification of the imaging principle used in building the tactile sensor. Then, a phantom experimental validation study is carried out for the mechanical properties estimation methods for measuring size, depth, and elastic modulus of an embedded inclusion. The chapter ends with the results from the phantom experiments. The experimental results showed size, depth, and elastic modulus estimation using tactile imaging system method with 7.23%, 41.83%, and 96.80% errors. This estimation performance can be improved using dynamic positioning of the source-detector setup.

In Chapter 3, we derived a spectral properties estimation method based on the diffuse optics theory. The method is specifically devised for estimating the coefficient from the

diffuse optics image collected by the CCD camera. The desired spectral property in this dissertation is absorption coefficient. The phantom experiment results for validating the spectral properties estimation method were presented. The results demonstrated the feasibility of using a CCD camera as a detector for measuring absorption coefficients of two phantoms with 68.75% and 26.37% errors.

Chapter 4, we presented the new bimodal dynamic imaging method. We validated the method by a bimodal tissue phantom with an embedded inclusion of known mechanical and spectral properties. The mechanical properties measured with the bimodal dynamic imaging method was compared to the TIS measurements. This new method improved the size, depth, and elastic modulus estimation errors by 6.43%, 21.83%, and 22.01%, compared to the TIS method. We demonstrated that the bimodal dynamic imaging method can be extended to determine chromophore concentrations using the lasers of multiple wavelengths.

In Chapter 5, we formulated an open-loop Stackelberg game control problem targeted to maneuver the source and the detector in the bimodal dynamic imaging system. Under two-player nonzero-sum game frame work, a solution is derived for the problem of minimizing the leader cost variance, while the follower cost mean is minimized. We simulated the open-loop Stackelberg minimal cost variance controller with a simple linear system model.

In Chapter 6, we derived a linearized model for a dual arm seven degree-of-freedom robot Baxter. This robot will be used as test-bed for the bimodal dynamic imaging method in conjunction of the hybrid statistical controller. We validated the linearized model with an experimental study. The validation study showed that the tracking performance of the linear model was as good as the Baxter robot.

Chapter 7 discussed a hybrid hierarchical statistical control approach for the bimodal dynamic imaging. We provided numerical simulations of a hybrid statistical controlled dual-arm robot used for bimodal dynamic imaging. The simulation studies showed about 2 mm tracking error margin for both robot arms under hybrid hierarchical statistical control framework.

8.2 Future Works

The works presented in this dissertation is the initial step towards developing a bimodal dynamic imaging for improved tumor characterization with the application of hybrid hierarchical statistical control. Here are some future works.

Our bimodal phantom is not biological, therefore, the accurate estimation of physiological parameters is out of scope of this paper. In order to obtain accurate physiological parameter measurements, the number of wavelengths should be increased, and the measurement should be performed on blood phantom and *in-vivo* patients.

The background light and drifting of light sources are two sources of spectral properties measurement error. We performed our bimodal dynamic imaging experiment in a relatively dark room to minimize the light disturbance. The drifting occurred when the camera captures unnecessary light. In order to prevent that the precise positioning of the laser source and detector is required. In the future, both the source and detector will be mounted on the mechanical scanning platform capable of precise positioning.

The feasibility of using the hybrid hierarchical statistical control for the automatic control of the bimodal dynamic imaging system requires experimental validation. The statistical controller has to be validated for each arm of the dual-arm Baxter robot. Next, the complete bimodal imaging process needs to be tested with the hybrid hierarchical statistical controller.

Another attractive control scheme for the automatic control of the bimodal dynamic imaging is open-loop Stackelberg minimal control variance control. This controller needs to be validated using simulation and experimental studies. However, the closed-loop Stackelberg statistical control is more appropriate for the bimodal dynamic imaging system. Extending the theory of Stackelberg statistical control for closed-loop systems is challenging and reserved for future works.

REFERENCES

[1] National Cancer Institute, "Nci dictionary of cancer terms," National Cancer Institute, Rockville, MD, USA, 2015, http://www.cancer.gov/publications/dictionaries/cancer-terms, Last accessed on 2015-11-19. [Online]. Available: http://www.cancer.gov/publications/dictionaries/cancer-terms

[2] Phillips Healthcare, "Mobile C-arms," http://www.healthcare.philips.com/main/products/xray/products/c_arms/, Phillips Healthcare, MA, USA, 2015, Online, Last accessed on 2015-11-20.

[3] B. RethinkRobotics, "Baxter research robot: Urdf," http://http://sdk.rethinkrobotics.com/wiki/URDF, 2016, online; accessed on 10/17/2016.

[4] H. G. Welch, "Responding to the challenge of overdiagnosis," *Academic Radiology*, vol. 22, no. 8, pp. 945–946, Dec. 2015. [Online]. Available: http://dx.doi.org/10.1016/j.acra.2014.08.019

[5] S. Jha, "Barriers to reducing overdiagnosis," *Academic Radiology*, vol. 22, no. 8, pp. 1048–1049, Dec. 2015. [Online]. Available: http://dx.doi.org/10.1016/j.acra.2015.06.007

[6] R. Moynihan, J. Doust, and D. Henry, "Preventing overdiagnosis: how to stop harming the healthy," *BMJ*, vol. 344, 2012. [Online]. Available: http://www.bmj.com/content/344/bmj.e3502

[7] C. Harding, F. Pompei, D. Burmistrov, H. Welch, R. Abebe, and R. Wilson, "Breast cancer screening, incidence, and mortality across us counties," *JAMA Internal Medicine*, vol. 175, no. 9, pp. 1483–1489, 2015. [Online]. Available: +http://dx.doi.org/10.1001/jamainternmed.2015.3043

[8] C. Biesheuvel, A. Barratt, K. Howard, N. Houssami, and L. Irwig, "Effects of study methods and biases on estimates of invasive breast cancer overdetection with mammography screening: a systematic review," *The Lancet Oncology*, vol. 8, no. 12, pp. 1129 – 1138, 2007. [Online]. Available: http://www.sciencedirect.com/science/article/pii/S1470204507703807

[9] S. Morrell, A. Barratt, L. Irwig, K. Howard, C. Biesheuvel, and B. Armstrong, "Estimates of overdiagnosis of invasive breast cancer associated with screening mammography," *Cancer Causes & Control*, vol. 21, no. 2, pp. 275–282, 2010. [Online]. Available: http://dx.doi.org/10.1007/s10552-009-9459-z

[10] K. M, A. H, B. M, and T. RM, "Overdiagnosis of invasive breast cancer due to mammography screening: Results from the norwegian screening program," *Annals of Internal Medicine*, vol. 156, no. 7, pp. 491–499, 2012. [Online]. Available: +http://dx.doi.org/10.7326/0003-4819-156-7-201204030-00005

[11] K. J. Jørgensen and P. C. Gøtzsche, "Overdiagnosis in publicly organised mammography screening programmes: systematic review of incidence trends," *BMJ*, vol. 339, 2009. [Online]. Available: http://www.bmj.com/content/339/bmj.b2587

[12] L. Esserman, I. Thompson, and B. Reid, "Overdiagnosis and overtreatment in cancer: An opportunity for improvement," *JAMA*, vol. 310, no. 8, pp. 797–798, 2013.

[13] L. J. Esserman, I. M. Thompson, B. Reid, P. Nelson, D. F. Ransohoff, H. G. Welch, S. Hwang, D. A. Berry, K. W. Kinzler, W. C. Black, M. Bissell, H. Parnes, and S. Srivastava, "Addressing overdiagnosis and overtreatment in cancer: a prescription for change," *The Lancet Oncology*, vol. 15, no. 6, pp. e234 – e242, 2014.

[14] P. Skaane, S. Hofvind, and A. Skjennald, "Randomized trial of screen-film versus full-field digital mammography with soft-copy reading in population-based screening program: Follow-up and final results of oslo ii study," *Radiology*, vol. 244, no. 3, pp. 708–717, 2007, pMID: 17709826. [Online]. Available: https://doi.org/10.1148/radiol.2443061478

[15] E. D. Pisano, C. Gatsonis, E. Hendrick, M. Yaffe, J. K. Baum, S. Acharyya, E. F. Conant, L. L. Fajardo, L. Bassett, C. D'Orsi, R. Jong, and M. Rebner, "Diagnostic performance of digital versus film mammography for breast-cancer screening," *New England Journal of Medicine*, vol. 353, no. 17, pp. 1773–1783, 2005, pMID: 16169887. [Online]. Available: http://dx.doi.org/10.1056/NEJMoa052911

[16] E. D. Pisano, E. R. Hendrick, M. J. Yaffe, J. K. Baum, S. Acharyya, J. B. Cormack, L. A. Hanna, E. F. Conant, L. L. Fajardo, L. W. Bassett, C. J. D'Orsi, R. A. Jong, M. Rebner, A. N. A. Tosteson, and C. A. Gatsonis, "Diagnostic accuracy of digital versus film mammography: Exploratory analysis of selected population subgroups in dmist," *Radiology*, vol. 246, no. 2, pp. 376–383, 2008, pMID: 18227537. [Online]. Available: https://doi.org/10.1148/radiol.2461070200

[17] K. K, G. D, B. J, S. EA, and E. V, "Effect of age, breast density, and family history on the sensitivity of first screening mammography," *JAMA*, vol. 276, no. 1, pp. 33–38, 1996. [Online]. Available: +http://dx.doi.org/10.1001/jama.1996.03540010035027

[18] K. E. Dee and E. A. Sickles, "Medical audit of diagnostic mammography examinations," *American Journal of Roentgenology*, vol. 176, no. 3, pp. 729–733, Mar 2001. [Online]. Available: https://doi.org/10.2214/ajr.176.3.1760729

[19] D. J. Hilleren, I. T. Andersson, K. Lindholm, and F. S. Linnell, "Invasive lobular carcinoma: mammographic findings in a 10-year experience." *Radiology*,

vol. 178, no. 1, pp. 149–154, 1991, pMID: 1984294. [Online]. Available: https://doi.org/10.1148/radiology.178.1.1984294

[20] K. N. Krecke and J. J. Gisvold, "Invasive lobular carcinoma of the breast: mammographic findings and extent of disease at diagnosis in 184 patients." *American Journal of Roentgenology*, vol. 161, no. 5, pp. 957–960, Nov 1993. [Online]. Available: https://doi.org/10.2214/ajr.161.5.8273634

[21] M. L. Gal, L. Ollivier, B. Asselain, M. Meunier, M. Laurent, P. Vielh, and S. Neuenschwander, "Mammographic features of 455 invasive lobular carcinomas." *Radiology*, vol. 185, no. 3, pp. 705–708, 1992, pMID: 1438749. [Online]. Available: https://doi.org/10.1148/radiology.185.3.1438749

[22] National Cancer Institute, "Mammograms," Rockville, MD, USA, Tech. Rep., 2015, http://www.cancer.gov/types/breast/mammograms-fact-sheet, Last accessed on 2015-11-19. [Online]. Available: http://www.cancer.gov/types/breast/mammograms-fact-sheet

[23] T. M. Kolb, J. Lichy, and J. H. Newhouse, "Comparison of the performance of screening mammography, physical examination, and breast us and evaluation of factors that influence them: An analysis of 27,825 patient evaluations," *Radiology*, vol. 225, no. 1, pp. 165–175, 2002, pMID: 12355001. [Online]. Available: https://doi.org/10.1148/radiol.2251011667

[24] M. T. Mandelson, N. Oestreicher, P. L. Porter, D. White, C. A. Finder, S. H. Taplin, and E. White, "Breast density as a predictor of mammographic detection: Comparison of interval- and screen-detected cancers," *JNCI: Journal of the National Cancer Institute*, vol. 92, no. 13, p. 1081, 2000. [Online]. Available: +http://dx.doi.org/10.1093/jnci/92.13.1081

[25] L. Fass, "Imaging and cancer: A review," *Molecular Oncology*, vol. 2, no. 2, pp. 115 – 152, 2008. [Online]. Available: http://www.sciencedirect.com/science/article/pii/S1574789108000598

[26] S. Pani, S. Saifuddin, F. Ferreira, N. Henthorn, P. Seller, P. Sellin, P. Stratmann, M. Veale, M. Wilson, and R. Cernik, "High energy resolution hyperspectral x-ray imaging for low-dose contrast-enhanced digital mammography," *IEEE Transactions on Medical Imaging*, vol. PP, no. 99, pp. 1–1, 2017.

[27] R. S. Butler, L. A. Venta, E. L. Wiley, R. L. Ellis, P. J. Dempsey, and E. Rubin, "Sonographic evaluation of infiltrating lobular carcinoma." *American Journal of Roentgenology*, vol. 172, no. 2, pp. 325–330, Feb 1999. [Online]. Available: https://doi.org/10.2214/ajr.172.2.9930776

[28] C. P. Paramagul, M. A. Helvie, and D. D. Adler, "Invasive lobular carcinoma: sonographic appearance and role of sonography in improving diagnostic sensitivity." *Radiology*, vol. 195, no. 1, pp. 231–234, 1995, pMID: 7892476. [Online]. Available: https://doi.org/10.1148/radiology.195.1.7892476

[29] V. L. Selinko, L. P. Middleton, and P. J. Dempsey, "Role of sonography in diagnosing and staging invasive lobular carcinoma," *Journal of Clinical Ultrasound*, vol. 32, no. 7, pp. 323–332, 2004. [Online]. Available: http://dx.doi.org/10.1002/jcu.20052

[30] L. C. Wang, "{MR} imaging: Future imaging techniques," *Radiologic Clinics of North America*, vol. 55, no. 3, pp. 553 – 577, 2017, breast Imaging. [Online]. Available: http://www.sciencedirect.com/science/article/pii/S0033838916302081

[31] L. Wang, P. Fallavollita, R. Zou, X. Chen, S. Weidert, and N. Navab, "Closed-form inverse kinematics for interventional c-arm x-ray imaging with six degrees of freedom: Modeling and application," *Medical Imaging, IEEE Transactions on*, vol. 31, no. 5, pp. 1086–1099, May 2012.

[32] M. Osborne and A. Rubinstein, *A Course in Game Theory*. Cambridge, MA: MIT Press, 1994. [Online]. Available: https://books.google.com/books?id=5ntdaYX4LPkC

[33] J. von Neumann and O. Morgenstern, *Theory of Games and Economic Behavior (Commemorative Edition)*, ser. Princeton Classic Editions. NJ, USA: Princeton University Press, 2007. [Online]. Available: https://books.google.com/books?id=_aIGYI-jGEcC

[34] R. Isaacs, *Differential Games: A Mathematical Theory with Applications to Warfare and Pursuit, Control and Optimization*. New York, NY: John Wiley & Sons, 1965.

[35] J. Nash, *Non-cooperative Games*. NJ,USA: Princeton University, 1950. [Online]. Available: https://books.google.com/books?id=zxtUHAAACAAJ

[36] T. Başar and G. J. Olsder, *Dynamic Noncooperative Game Theory*. Philadelphia, PA: SIAM, 1999.

[37] H. von Stackelberg, *The Theory of the Market Economy*. Oxford University Press, 1952. [Online]. Available: https://books.google.com/books?id=o3ceAAAAIAAJ

[38] M. K. Sain, "Control of Linear Systems According to the Minimal Variance Criterion—A New Approach to the Disturbance Problem," *IEEE Transactions on Automatic Control*, vol. AC-11, no. 1, pp. 118–122, Jan. 1966.

[39] M. K. Sain and S. R. Liberty, "Performance Measure Densities for a Class of LQG Control Systems," *IEEE Transactions on Automatic Control*, vol. AC-16, no. 5, pp. 431–439, Oct. 1971.

[40] M. K. Sain, C.-H. Won, B. F. Spencer, Jr., and S. R. Liberty, "Cumulants and risk-sensitive control: A cost mean and variance theory with application to seismic protection of structures," in *Advances in Dynamic Games and Applications*, ser. Annals of the International Society of Dynamic Games, J. Filar, V. Gaitsgory, and K. Mizukami, Eds. Birkhauser Boston, 2000, vol. 5, pp. 427–459. [Online]. Available: http://dx.doi.org/10.1007/978-1-4612-1336-9_23

[41] C.-H. Won, R. W. Diersing, and B. Kang, "Statistical Control of Control-Affine Nonlinear Systems with Nonquadratic Cost Function: HJB and Verification Theorems," *Automatica*, vol. 46, no. 10, pp. 1636–1645, 2010.

[42] C. N. Aduba and C.-H. Won, "Two-Player Cost Cumulant Game Control for Nonlinear Systems," in *Proc. of the American Control Conference*, Chicago, IL, Jun. 2015, p. Submitted.

[43] C. Chen and J. Cruz, J., "Stackelburg solution for two-person games with biased information patterns," *Automatic Control, IEEE Transactions on*, vol. 17, no. 6, pp. 791–798, Dec 1972.

[44] M. Simaan, J. B. Cruz, M. Si, and I. B. Cruz, "Additional aspects of the Stackelberg strategy in non-zero sum games," *Journal of Optimization Theory and Applications*, vol. 11, no. 6, pp. 613–626, 1973. [Online]. Available: http://www.springerlink.com/index/10.1007/BF00935561

[45] M. Simaan and J. B. Cruz, "On the Stackelberg strategy in nonzero-sum games," *Journal of Optimization Theory and Applications*, vol. 11, no. 5, pp. 533–555, 1973.

[46] A. Bagchi and T. Başar, "Stackelberg strategies in linear-quadratic stochastic differential games," *Journal of Optimization Theory and Applications*, vol. 35, no. 3, pp. 443–464, 1981.

[47] C. G. Cassandras and S. Lafortune, *Introduction to Discrete Event Systems*. Secaucus, NJ, USA: Springer-Verlag New York, Inc., 2006.

[48] M. Bjerkeng, P. Falco, C. Natale, and K. Y. Pettersen, "Stability analysis of a hierarchical architecture for discrete-time sensor-based control of robotic systems," *IEEE Transactions on Robotics*, vol. 30, no. 3, pp. 745–753, June 2014.

[49] R. Caccavale and A. Finzi, "Flexible task execution and attentional regulations in human-robot interaction," *IEEE Transactions on Cognitive and Developmental Systems*, vol. 9, no. 1, pp. 68–79, March 2017.

[50] M. Saen, K. Ito, and K. Osada, "Action-intention-based grasp control with fine finger-force adjustment using combined optical-mechanical tactile sensor," *IEEE Sensors Journal*, vol. 14, no. 11, pp. 4026–4033, Nov 2014.

[51] B. Kang, "Statistical control using neural network methods with hierarchical hybrid systems," Ph.D. dissertation, Temple University, 2011.

[52] C. G. Cassandras and W. Li, "Sensor networks and cooperative control," in *Proceedings of the 44th IEEE Conference on Decision and Control*, Dec 2005, pp. 4237–4238.

[53] Y. Fung, *Biomechanics: Mechanical Properties of Living Tissues*, ser. Biomechanics. Springer New York, 1993.

[54] T. A. Krouskop, T. M. Wheeler, F. Kallel, B. S. Garra, and T. Hall, "Elastic moduli of breast and prostate tissues under compression," *Ultrasonic Imaging*, vol. 20, no. 4, pp. 260–274, 1998. [Online]. Available: http://uix.sagepub.com/content/20/4/260.abstract

[55] V. Egorov, T. Kearney, S. Pollak, C. Rohatgi, N. Sarvazyan, S. B. S. Airapetian, and A. Sarvazyan, "Differentiation of benign and malignant breast lesions by mechanical imaging," *Medical Imaging, IEEE Transactions on*, vol. 118, no. 1, pp. 67–80, Nov 2009.

[56] American Cancer Society, "Breast cancer facts and figures 2015-2016," Atlanta, GA, USA, Tech. Rep., 2015, http://www.cancer.org/research cancerfactsstatistics/breast-cancer-facts-figures, Last accessed on 2015-11-18. [Online]. Available: http://www.cancer.org/researchcancerfactsstatistics/breast-cancer-facts-figures

[57] J. K. Bobo, N. C. Lee, and S. F. Thames, "Findings from 752 081 clinical breast examinations reported to a national screening program from 1995 through 1998," *Journal of the National Cancer Institute*, vol. 92, no. 12, pp. 971–976, 2000. [Online]. Available: http://jnci.oxfordjournals.org/content/92/12/971.abstract

[58] R. D. Howe, "Tactile sensing and control of robotic manipulation," *Journal of Advanced robotics*, vol. 8, no. 3, pp. 245–261, 1994.

[59] P. Wellman, "Tactile imaging," Ph.D. dissertation, Harvard University, Cambridge, MA, 1999.

[60] A. Galea, "Mapping tactile imaging information: Parameter estimation and deformable registration," Ph.D. dissertation, Harvard University, Cambridge, MA, 2004.

[61] V. Egorov and A. Sarvazyan, "Mechanical imaging of the breast," *Medical Imaging, IEEE Transactions on*, vol. 27, no. 9, pp. 1275–1287, Sept 2008.

[62] J.-H. Lee and C.-H. Won, "High-resolution tactile imaging sensor using total internal reflection and nonrigid pattern matching algorithm," *Sensors Journal, IEEE*, vol. 11, no. 9, pp. 2084–2093, Sept 2011.

[63] ——, "The tactile sensation imaging system for embedded lesion characterization," *Biomedical and Health Informatics, IEEE Journal of*, vol. 17, no. 2, pp. 452–458, March 2013.

[64] F. Saleheen, V. Oleksyuk, A. Sahu, and C.-H. Won, "Non-invasive mechanical properties estimation of embedded objects using tactile imaging sensor," in *Proc. SPIE 8719, Smart Biomedical and Physiological Sensor Technology X*, vol. 8719, Baltimore, USA, May 2013, pp. 1–11. [Online]. Available: http://dx.doi.org10.1117/12.2015803

[65] A. Yodh and B. Chance, "Spectroscopy and imaging with diffusing light," *Physics Today*, vol. 48, pp. 34–40, March 1995.

[66] A. G. Yodh and D. A. Boas, *Functional Imaging with Diffusing Light*. CRC Press, 2003. [Online]. Available: http://www.lrsm.upenn.edu/pmi/papers/AGYgroup/DavidBoas

[67] N. Weidner, J. Folkman, F. Pozza, P. Bevilacqua, E. N. Allred, D. H. Moore, S. Meli, and G. Gasparini, "Tumor angiogenesis: A new significant and independent prognostic indicator in early-stage breast carcinoma," *Journal of the National Cancer Institute*, vol. 84, no. 24, pp. 1875–1887, 1992. [Online]. Available: http://jnci.oxfordjournals.org/content/84/24/1875.abstract

[68] S. Thomsen and D. Tatman, "Physiological and pathological factors of human breast disease that can influence optical diagnosisa," *Annals of the New York Academy of Sciences*, vol. 838, no. 1, pp. 171–193, 1998. [Online]. Available: http://dx.doi.org/10.1111/j.1749-6632.1998.tb08197.x

[69] J. R. Mourant, J. P. Freyer, A. H. Hielscher, A. A. Eick, D. Shen, and T. M. Johnson, "Mechanisms of light scattering from biological cells relevant to noninvasive optical-tissue diagnostics," *Appl. Opt.*, vol. 37, no. 16, pp. 3586–3593, Jun 1998. [Online]. Available: http://ao.osa.org/abstract.cfm?URI=ao-37-16-3586

[70] V. Ntziachristos and B. Chance, "Breast imaging technology: Probing physiology and molecular function using optical imaging - applications to breast cancer," *Breast Cancer Res*, vol. 3, no. 1, 2000. [Online]. Available: http://dx.doi.org/10.1186/bcr269

[71] B. J. Tromberg, B. W. Pogue, K. D. Paulsen, A. G. Yodh, D. A. Boas, and A. E. Cerussi, "Assessing the future of diffuse optical imaging technologies for breast cancer management," *Medical Physics*, vol. 35, no. 6, pp. 2443–2451, 2008. [Online]. Available: http://scitation.aip.org/content/aapm/journal/medphys/35/6/10.1118/1.2919078

[72] T. Durduran, R. Choe, W. B. Baker, and A. G. Yodh, "Diffuse optics for tissue monitoring and tomography," *Reports on Progress in Physics*, vol. 73, no. 7, pp. 076 701+, Jul. 2010. [Online]. Available: http://dx.doi.org/10.1088/0034-4885/73/7/076701

[73] C. Kuhl, "The current status of breast mr imaging part i. choice of technique, image interpretation, diagnostic accuracy, and transfer to clinical practice," *Radiology*, vol. 244, no. 2, pp. 356–378, 2007, pMID: 17641361. [Online]. Available: http://dx.doi.org/10.1148/radiol.2442051620

[74] J. Chang, H. Graber, P. C. Koo, R. Aronson, S.-L. Barbour, and R. Barbour, "Optical imaging of anatomical maps derived from magnetic resonance images using time-independent optical sources," *Medical Imaging, IEEE Transactions on*, vol. 16, no. 1, pp. 68–77, Feb 1997.

[75] B. W. Pogue and K. D. Paulsen, "High-resolution near-infrared tomographic imaging simulations of the rat cranium by use of a priori magnetic resonance

imaging structural information," *Opt. Lett.*, vol. 23, no. 21, pp. 1716–1718, Nov 1998. [Online]. Available: http://ol.osa.org/abstract.cfm?URI=ol-23-21-1716

[76] V. Ntziachristos, A. G. Yodh, M. D. Schnall, and B. Chance, "Mri-guided diffuse optical spectroscopy of malignant and benign breast lesions," *Neoplasia*, vol. 4, pp. 347–354, 2002.

[77] B. Brooksby, H. Dehghani, B. Pogue, and K. Paulsen, "Near-infrared (nir) tomography breast image reconstruction with a priori structural information from mri: algorithm development for reconstructing heterogeneities," *Selected Topics in Quantum Electronics, IEEE Journal of*, vol. 9, no. 2, pp. 199–209, March 2003.

[78] B. Brooksby, S. Jiang, H. Dehghani, B. W. Pogue, K. D. Paulsen, J. Weaver, C. Kogel, and S. P. Poplack, "Combining near-infrared tomography and magnetic resonance imaging to study in vivo breast tissue: implementation of a laplacian-type regularization to incorporate magnetic resonance structure," *Journal of Biomedical Optics*, vol. 10, no. 5, pp. 051 504–051 504–10, 2005. [Online]. Available: http://dx.doi.org/10.1117/1.2098627

[79] A. Li, E. L. Miller, M. E. Kilmer, T. J. Brukilacchio, T. Chaves, J. Stott, Q. Zhang, T. Wu, M. Chorlton, R. H. Moore, D. B. Kopans, and D. A. Boas, "Tomographic optical breast imaging guided by three-dimensional mammography," *Appl. Opt.*, vol. 42, no. 25, pp. 5181–5190, Sep 2003. [Online]. Available: http://ao.osa.org/abstract.cfm?URI=ao-42-25-5181

[80] Q. Zhang, T. J. Brukilacchio, A. Li, J. J. Stott, T. Chaves, E. Hillman, T. Wu, M. Chorlton, E. Rafferty, R. H. Moore, D. B. Kopans, and D. A. Boas, "Coregistered tomographic x-ray and optical breast imaging: initial results," *Journal of Biomedical Optics*, vol. 10, no. 2, pp. 024 033–024 033–9, 2005. [Online]. Available: http://dx.doi.org/10.1117/1.1899183

[81] S. D. Konecky, R. Choe, A. Corlu, K. Lee, R. Wiener, S. M. Srinivas, J. R. Saffer, R. Freifelder, J. S. Karp, N. Hajjioui, F. Azar, and A. G. Yodh, "Comparison of diffuse optical tomography of human breast with whole-body and breast-only positron emission tomography." *Med Phys*, vol. 35, no. 2, pp. 446–455, Feb. 2008. [Online]. Available: http://dx.doi.org/10.1118/1.2826560

[82] Q. Zhu, T. Durduran, V. Ntziachristos, M. Holboke, and A. G. Yodh, "Imager that combines near-infrared diffusive light and ultrasound," *Optics Letters*, vol. 24, pp. 1050–1052, 1999. [Online]. Available: http://www.lrsm.upenn.edu/pmi/papers/AGYgroup/TurgutDurduran/QZhu1999OLv24i15.pdf

[83] Q. Zhu, N. Chen, and S. H. Kurtzman, "Imaging tumor angiogenesis by use of combined near-infrared diffusive light and ultrasound," *Opt. Lett.*, vol. 28, no. 5, pp. 337–339, Mar 2003. [Online]. Available: http://ol.osa.org/abstract.cfm?URI=ol-28-5-337

[84] Q. Zhu, S. H. Kurtzman, P. Hegde, S. Tannenbaum, M. Kane, M. Huang, N. G. Chen, B. Jagjivan, and K. Zarfos, "Utilizing optical tomography with ultrasound localization to image heterogeneous hemoglobin distribution in large breast cancers," *Neoplasia*, vol. 7, no. 3, pp. 263 – 270, 2005. [Online]. Available: http://www.sciencedirect.com/science/article/pii/S1476558605800272

[85] M. Katz, *Introduction to Geometrical Optics*. World Scientific, 2002. [Online]. Available: https://books.google.com/books?id=agsOmxYsyCIC

[86] B. Saleh and M. Teich, *Fundamentals of Photonics*, ser. Wiley Series in Pure and Applied Optics. Wiley, 2013. [Online]. Available: https://books.google.com/books?id=Qfeosgu08u8C

[87] T. Durduran, R. Choe, W. Baker, and A. G. Yodh, "Diffuse optics for tissue monitoring and tomography," *Rep. Prog. Phys.*, vol. 73, no. 7, pp. 1–43, 2010.

[88] R. Choe, S. D. Konecky, A. Corlu, K. Lee, T. Durduran, D. Busch, S. Pathak, B. Czerniecki, J. Tchou, D. Fraker, A. DeMichele, B. Chance, S. Arridge, M. Schweiger, J. Culver, M. Schnall, M. Putt, M. Rosen, and A. Yodh, "Differentiation of benign and malignant breast tumors by in-vivo three-dimensional parallel-plate diffuse optical tomography," *J Biomed Opt.*, vol. 14, no. 2, Mar-Apr 2009.

[89] R. C. Haskell, L. O. Svaasand, T.-T. Tsay, T.-C. Feng, B. J. Tromberg, and M. S. McAdams, "Boundary conditions for the diffusion equation in radiative transfer," *J. Opt. Soc. Am. A*, vol. 11, no. 10, pp. 2727–2741, Oct 1994. [Online]. Available: http://josaa.osa.org/abstract.cfm?URI=josaa-11-10-2727

[90] S. Taylor, "CCD and CMOS imaging array technologies: Technology review," Xerox Research Centre Europe, Tech. Rep., 1998.

[91] S. Arridge and W. Lionheart, "Nonuniqueness in diffusion-based optical tomography," *Opt. Lett.*, vol. 23, no. 11, p. 882, 1998. [Online]. Available: http://dx.doi.org/10.1364/OL.23.000882

[92] T. Minagawa, P. Zirak, U. M. Weigel, A. K. Kristoffersen, N. Mateos, A. Valencia, and T. Durduran, "Low-cost diffuse optical tomography for the classroom," *Am. J. of Phys.*, vol. 80, no. 10, pp. 876–881, 2012.

[93] S. Prahl, "Tabulated molar extinction coefficient for hemoglobin in water," http://omlc.org/spectra/hemoglobin/summary.html, Oregon Medical Laser Center, http://omlc.org/spectra/hemoglobin/summary.html, Last accessed on 2016-02-04.

[94] P. Vaupel, K. Schlenger, C. Knoop, and M. Hl, "Oxygenation of human tumors: Evaluation of tissue oxygen distribution in breast cancers by computerized o2 tension measurements," *Cancer Research*, vol. 51, no. 12, pp. 3316–3322, 1991.

[95] P. Vaupel, O. Thews, D. K. Kelleher, and M. Hoeckel, *Oxygen Transport to Tissue XX*. Boston, MA: Springer US, 1998, ch. Current Status of Knowledge

and Critical Issues in Tumor Oxygenation, pp. 591–602. [Online]. Available: http://dx.doi.org/10.1007/978-1-4615-4863-8_70

[96] S. Fantini and A. Sassaroli, "Near-infrared optical mammography for breast cancer detection with intrinsic contrast," *Ann Biomed Eng*, vol. 40, no. 2, pp. 398–407, Feb 2012, 21971964[pmid]. [Online]. Available: http://www.ncbi.nlm.nih.gov/pmc/articles/PMC3678374/

[97] R. Choe, "Diffuse optical tomography and spectroscopy of breast cancer and fetal brain," Ph.D. dissertation, University of Pennsylvania, Philadelphia, PA, 2005.

[98] B. J. Tromberg, N. Shah, R. Lanning, A. Cerussi, J. Espinoza, T. Pham, and J. Butler, "Non-invasive in vivo characterization of breast tumors using photon migration spectroscopy," *Neoplasia*, vol. 2, no. 1-2, p. 26?40., 2000.

[99] V. Ntziachristos, A. G. Yodh, M. Schnall, and B. Chance, "Concurrent mri and diffuse optical tomography of breast after indocyanine green enhancement," *Proceedings Of The National Academy Of Sciences Of The United States Of America*, vol. 97, pp. 2767–2772, 2000. [Online]. Available: http://www.lrsm.upenn.edu/pmi/papers/AGYgroup/VasilisNtziachristos/VNtziachristos2000PNASv97i6.pdf

[100] N. C. Biswal, Y. Xu, and Q. Zhu, "Imaging tumor oxyhemoglobin and deoxyhemoglobin concentrations with ultrasound-guided diffuse optical tomography," *Technol Cancer Res Treat*, vol. 10, no. 5, pp. 417–429, Oct 2011, 21895027[pmid]. [Online]. Available: http://www.ncbi.nlm.nih.gov/pmc/articles/PMC3546825/

[101] R. Choe, A. Corlu, K. Lee, T. Durduran, S. D. Konecky, M. Grosicka-Koptyra, S. R. Arridge, B. J. Czerniecki, D. L. Fraker, A. DeMichele, B. Chance, M. A. Rosen, and A. G. Yodh, "Diffuse optical tomography of breast cancer during neoadjuvant chemotherapy: A case study with comparison to mri," *Medical Physics*, vol. 32, no. 4, pp. 1128–1139, 2005. [Online]. Available: http://scitation.aip.org/content/aapm/journal/medphys/32/4/10.1118/1.1869612

[102] G. Chalkiadakis, E. Elkind, and M. Wooldridge, *Computational Aspects of Cooperative Game Theory*, ser. Synthesis lectures on artificial intelligence and machine learning. Morgan & Claypool Publishers, 2011. [Online]. Available: https://books.google.com/books?id=bN9aC0uabBAC

[103] A. Brandenburger, "Cooperative game theory," *Teaching Materials at New York University*, 2007.

[104] R. V. Ham, T. G. Sugar, B. Vanderborght, K. W. Hollander, and D. Lefeber, "Compliant actuator designs," *IEEE Robotics Automation Magazine*, vol. 16, no. 3, pp. 81–94, September 2009.

[105] G. A. Pratt and M. M. Williamson, "Series elastic actuators," in *Proceedings 1995 IEEE/RSJ International Conference on Intelligent Robots and Systems. Human Robot Interaction and Cooperative Robots*, vol. 1, Aug 1995, pp. 399–406 vol.1.

[106] M. Williamson, "Series Elastic Actuator," M. Eng. thesis, Massachusetts Institute of Technology, Cambridge, MA, Feb 1995.

[107] C. Fitzgerald, "Developing baxter," in *2013 IEEE Conference on Technologies for Practical Robot Applications (TePRA)*, April 2013, pp. 1–6.

[108] N. Roy, P. Newman, and S. Srinivasa, *CompAct x2122; Arm: a Compliant Manipulator with Intrinsic Variable Physical Damping*. MIT Press, 2013, pp. 504–. [Online]. Available: http://ieeexplore.ieee.org/xpl/articleDetails.jsp?arnumber=6577988

[109] B. RethinkRobotics, "Baxter research robot: Arms," http://sdk.rethinkrobotics.com/wiki/Arms, 2016, online; accessed on 10/17/2016.

[110] F. Saleheen, "Modeling and Statistical Control of a Gimbaled Laser Target System," M. S. Eng. thesis, Temple University, Philadelphia, PA, Nov 2013.

[111] A. Bagchi and T. Başar, "Team decision theory for linear continuous-time systems," Dep. Applied Math., Twente Univ. of Technol., Enschede, The Netherlands, Tech. Rep. Memo 274, 1979.

[112] L. Arnold, *Stochastic Differential Equations: Theory and Applications*. New York, NY: John Wiley & Sons Inc., 1974.

[113] W. H. Fleming and M. Nisio, "On the existence of optimal stochastic controls," *Journal of Mathematics and Mechanics*, vol. 15, pp. 777–794, 1966.

[114] W. H. Fleming and R. W. Rishel, *Deterministic and Stochastic Optimal Control*. New York, NY: Springer-Verlag, 1975.

[115] P. J. Smith, "A Recursive Formulation of the Old Problem of Obtaining Moments from Cumulants and Vice Versa," *The American Statistician*, vol. 49, no. 2, pp. 217–219, 1995.

[116] E. Stein and R. Shakarchi, *Real Analysis: Measure Theory, Integration, and Hilbert Spaces*. Princeton University Press, 2009. [Online]. Available: https://books.google.com/books?id=2Sg3Vug65AsC

[117] A. Bagchi and T. Başar, "Team decision theory for linear continuous-time systems," *Automatic Control, IEEE Transactions on*, vol. 25, no. 6, pp. 1154–1161, Dec 1980.

[118] A. Baggeroer, "A state-variable approach to the solution of fredholm integral equations," *IEEE Transactions on Information Theory*, vol. 15, no. 5, pp. 557–570, Sep 1969.

[119] T. Başar and G. J. Olsder, "Team-optimal closed-loop stackelberg strategies in hierarchical control problems," *Automatica*, vol. 16, no. 4, pp. 409–414, 1980. [Online]. Available: http://doc.utwente.nl/68707/

[120] A. Bensoussan, S. Chen, and S. P. Sethi, "The maximum principle for global solutions of stochastic stackelberg differential games," *SIAM Journal on Control and Optimization*, vol. 53, no. 4, pp. 1956–1981, 2015. [Online]. Available: http://dx.doi.org/10.1137/140958906

[121] G. Papavassilopoulos and J. Cruz, "Nonclassical control problems and stackelberg games," *IEEE Transactions on Automatic Control*, vol. 24, no. 2, pp. 155–166, Apr 1979.

[122] G. P. Papavassilopoulos and J. B. Cruz, "Sufficient conditions for stackelberg and nash strategies with memory," *Journal of Optimization Theory and Applications*, vol. 31, no. 2, pp. 233–260, 1980. [Online]. Available: http://dx.doi.org/10.1007/BF00934113

[123] F. Lewis, D. Dawson, and C. Abdallah, *Robot Manipulator Control: Theory and Practice*, ser. Automation and Control Engineering. CRC Press, 2003. [Online]. Available: https://books.google.com.au/books?id=8002tURlPP4C

[124] M. Spong, S. Hutchinson, and M. Vidyasagar, *Robot Modeling and Control*. Wiley, 2005. [Online]. Available: https://books.google.com.au/books?id=wGapQAAACAAJ

[125] K. Fu, R. González, and C. Lee, *Robotics: control, sensing, vision, and intelligence*, ser. McGraw-Hill series in CAD/CAM robotics and computer vision. McGraw-Hill, 1987. [Online]. Available: https://books.google.com/books?id=qUdSAAAAMAAJ

[126] P. Corke, *Robotics, Vision and Control: Fundamental Algorithms in MATLAB*, ser. Springer Tracts in Advanced Robotics. Springer Berlin Heidelberg, 2011. [Online]. Available: https://books.google.com.au/books?id=hdkytqtBcyQC

[127] B. Francis and W. Wonham, "The internal model principle of control theory," *Automatica*, vol. 12, no. 5, pp. 457 – 465, 1976. [Online]. Available: http://www.sciencedirect.com/science/article/pii/0005109876900066

[128] J. Lygeros, K. H. Johansson, S. N. Simic, J. Zhang, and S. S. Sastry, "Dynamical properties of hybrid automata," *IEEE Transactions on Automatic Control*, vol. 48, no. 1, pp. 2–17, Jan 2003.

APPENDIX A

OPERATING BAXTER

A.1 Baxter Hardware

Baxter Robot

Baxter is a dual arm robot. Each of its arms has seven degrees of freedom. At every joint, Baxter has force, position, and torque sensing capability. It has one camera on its head-mounted display, and two cameras on its arms.

Figs. A.1 and A.3 show the front and back views of Baxter. Fig. A.2 shows the condition rings status meaning. Fig. A.4 shows the connectivity of Baxter of hardware.

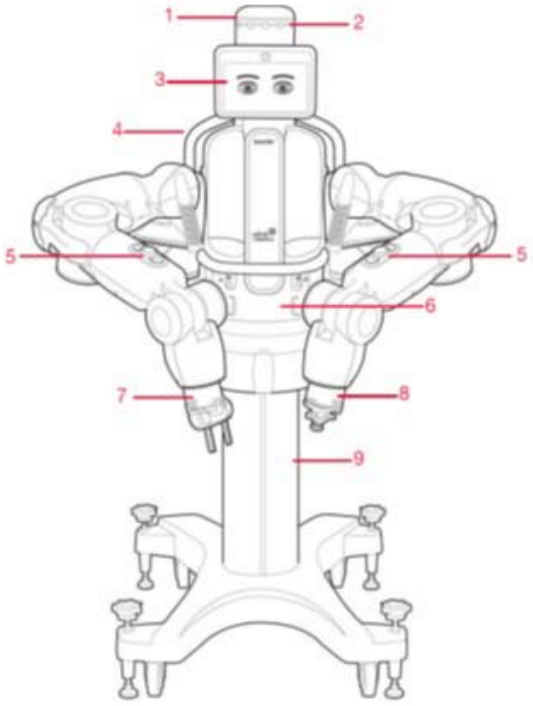

1. Condition ring
2. Attention ring
3. Display
4. Torso
5. Navigator (one on each forearm)
6. Lower front panel
7. Training cuff (shown with parallel gripper)
8. Training cuff (shown with vacuum gripper)
9. Pedestal

Figure A.1: Front view of Baxter

A.2 Specification of joint angles

Fig. A.5 shows the bend joints and Table A.1 their values.

Fig. A.6 shows the bend joints and Table A.2 their values.

Light Color and Pattern	What it Means
Solid green	Baxter is working
Slow pulsing green	User is interacting with Baxter
Solid yellow	Baxter is confused and needs user assistance
Slow blinking yellow	Baxter is sleeping
Fast blinking red	Baxter reports an error

Figure A.2: Baxter LED indicator meaning

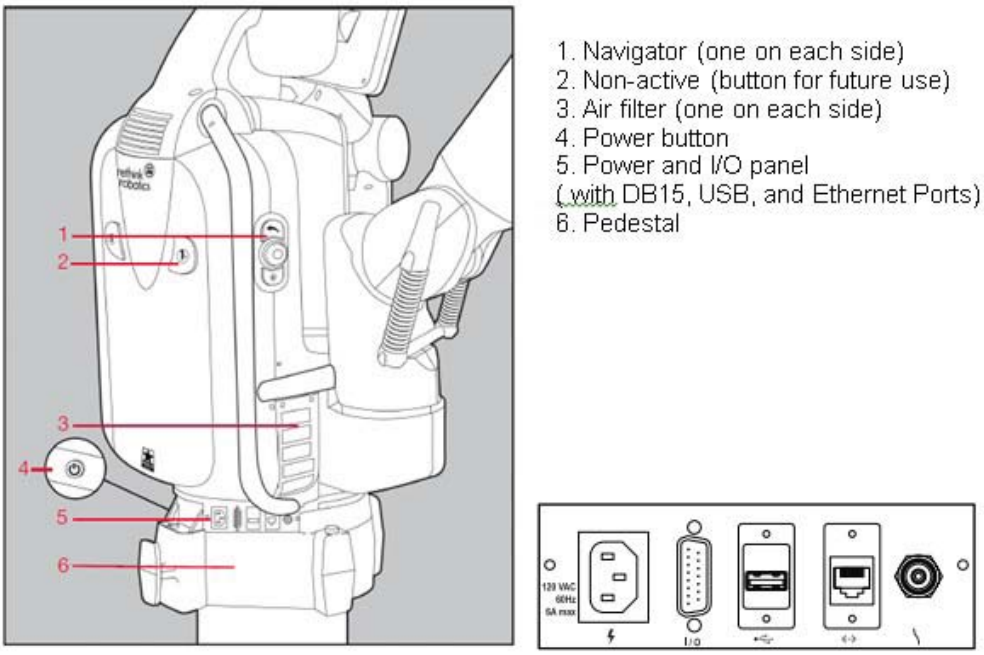

Figure A.3: Back view of Baxter

Table A.1: Bend joints range table

Joint	Min limit (°)	Max limit	Range	Min limit (rad)	Max limit	Range
S1	−123	+60	183	−2.147	+.047	3.194
E1	−2.864	+150	153	−0.05	+2.618	2.67
W1	−90	+120	210	−1.5707	+2.094	3.6647

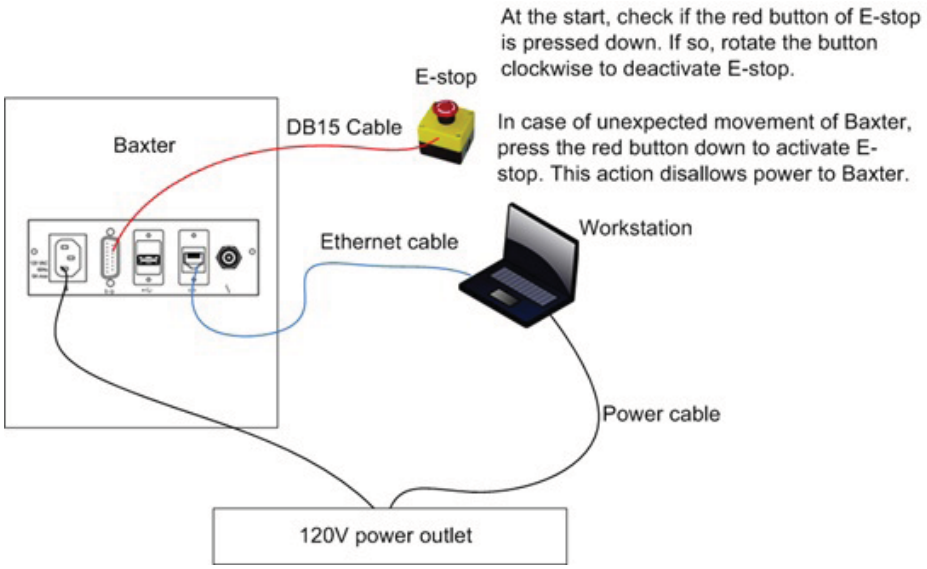

Figure A.4: Baxter connectivity

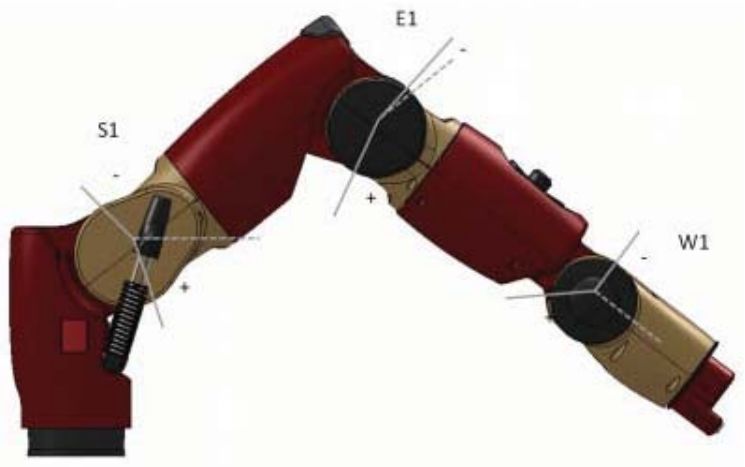

Figure A.5: Baxter range of motion - bend joints (left arm).

Table A.2: Twist joints range table

Joint	Min limit (°)	Max limit	Range	Min limit (rad)	Max limit	Range
S0	−97.494	+97.494	194.998	−1.7016	+1.7016	3.4033
E0	−174.987	+174.987	349.979	−3.0541	+3.0541	6.1083
W0	−175.25	+175.25	350.5	−3.059	+3.059	6.117
W2	−175.25	+175.25	350.5	−3.059	+3.059	6.117

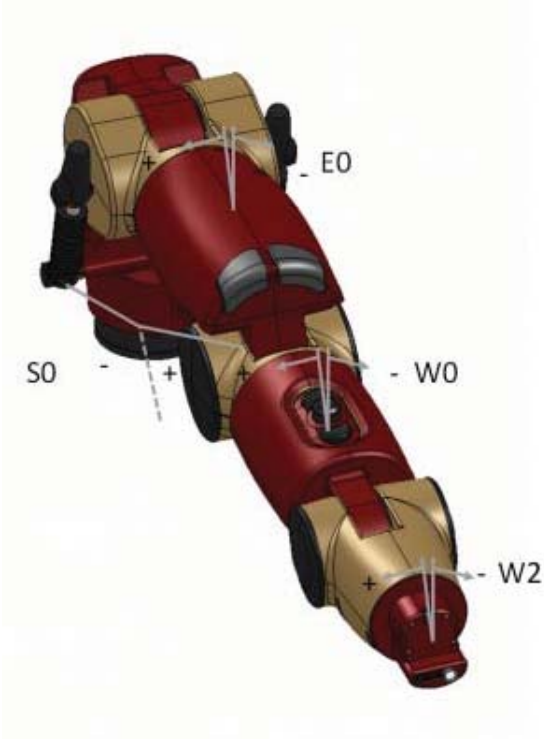

Figure A.6: Baxter range of motion - twist joints (left arm).

Working with Baxter

1. Make sure the following before powering up Baxter:
   a. the workstation is connected to Baxter with an Ethernet cable,
   b. the emergency stop button is connected to Baxter,
   c. Baxter and the workstation are connected to power outlet of 120V AC.
2. Run the workstation. Wait until Ubuntu login page comes and asks for password. The login password is ***. Ubuntu is installed in the workstation with ROS (robotic operating system) packages. To learn how the workstation setup is done, visit this page: `http://sdk.rethinkrobotics.com/wiki/Workstation_Setup` or, watch this tutorial video: `https://youtu.be/2QfP4qY_7_c`
3. Press the power button of Baxter located at the back. Wait until the condition ring in Baxter's head is green, the attention ring blinks orange, and the display shows "baxter Research Robot".
4. Currently, Baxter is connected directly to the workstation by an Ethernet cable. If the network configuration needs to be changed in future (example, Baxter can be connected to the workstation through a router), visit this page: `http://sdk.rethinkrobotics.com/wiki/Networking`. For current networking setup, complete the Avahi configuration steps:
   a. Disable Wi-fi and networking from the top-right of the desktop. Make sure Enable Wi-fi and Enable Networking are unchecked.
   b. Open a new terminal in the workstation by pressing Ctrl+Alt+T. The ethernet

connection to the robot is on eth0. Check the status of eth0

```
cwon@baxterws: ~$ ifconfig eth0
```

You should not see any IP addresses under inet.

c. Use Avahi to designate an IP address to eth0 (do not close the terminal after running avahi-autoipd):

```
cwon@baxterws: ~$ sudo avahi-autoipd eth0
```

You will be asked password for username: ****. Type the password: ****.

d. Make sure an IP address is successfully claimed.

```
cwon@baxterws: ~$
Found user 'avahi-autoipd' (UID 105) and group 'avahi-autoipd'
(GID 113).
    Successfully called chroot().
    Successfully dropped root privileges.
    Starting with address 169.254.10.30
    Callout BIND, address 169.254.10.30 on interface eth0
    Successfully claimed IP address 169.254.10.30
```

Keep this Terminal running in the background.

5. Open another terminal. Initialize by running baxter.sh script and verify SDK environment. The commands with the outputs are as follows:

```
cwon@baxterws:~$ cd ~/ros_ws
cwon@baxterws:~/ros_ws$ . baxter.sh
View and validate your ROS environment:
[baxter - http://011508P0028.local:11311]
cwon@baxterws:~/ros_ws$ env | grep ROS
ROS_ROOT=/opt/ros/indigo/share/ros
ROS_PACKAGE_PATH=/home/cwon/ros_ws/src:
/opt/ros/indigo/share:/opt/ros/indigo/stacks
ROS_MASTER_URI=http://011508P0028.local:11311
ROS_HOSTNAME=csnapbaxterworkstation.local
ROSLISP_PACKAGE_DIRECTORIES=/home/cwon/ros_ws/devel/share/common-lisp
__ROS_PROMPT=1
ROS_DISTRO=indigo
ROS_ETC_DIR=/opt/ros/indigo/etc/ros
```

6. Verify communication to and from Baxter and our development workstation. Find Baxter hostname and verify ROS master ping. at the start of every command to keep it simple.

```
$ env | grep ROS_MASTER_URI
ROS_MASTER_URI=http://011508P0028.local:11311

$ ping 011508P0028.local
PING 011508P0028.local (169.254.12.81) 56(84) bytes of data.
64 bytes from 011508P0028.local (169.254.12.81):
icmp_seq=1 ttl=64 time=0.369 ms
64 bytes from 011508P0028.local (169.254.12.81):
icmp_seq=2 ttl=64 time=0.176 ms
64 bytes from 011508P0028.local (169.254.12.81):
icmp_seq=3 ttl=64 time=0.305 ms
64 bytes from 011508P0028.local (169.254.12.81):
icmp_seq=4 ttl=64 time=0.173 ms
64 bytes from 011508P0028.local (169.254.12.81):
icmp_seq=5 ttl=64 time=0.167 ms
64 bytes from 011508P0028.local (169.254.12.81):
icmp_seq=6 ttl=64 time=0.184 ms
^C
--- 011508P0028.local ping statistics ---
6 packets transmitted, 6 received, 0% packet loss, time 4999ms
rtt min/avg/max/mdev = 0.167/0.229/0.369/0.078 ms
```

7. Verify workstation ping. Now we will SSH to Baxter and verify communication from Baxter to the workstation. The SSH password is rethink.

```
[baxter - http://011508P0028.local:11311]
cwon@baxterws:~/ros_ws$ env | grep ROS_HOSTNAME
ROS_HOSTNAME=csnapbaxterworkstation.local

ssh ruser@011508P0028.local
#Password: rethink
ruser@011508P0028 ~ $ ping csnapbaxterworkstation.local
PING csnapbaxterworkstation.local (169.254.10.130) 56(84)
bytes of data.
64 bytes from csnapbaxterworkstation.local (169.254.10.130):
icmp_seq=1 ttl=64 time=0.278 ms
64 bytes from csnapbaxterworkstation.local (169.254.10.130):
icmp_seq=2 ttl=64 time=0.213 ms
64 bytes from csnapbaxterworkstation.local (169.254.10.130):
icmp_seq=3 ttl=64 time=0.282 ms
64 bytes from csnapbaxterworkstation.local (169.254.10.130):
icmp_seq=4 ttl=64 time=0.284 ms
64 bytes from csnapbaxterworkstation.local (169.254.10.130):
icmp_seq=5 ttl=64 time=0.240 ms
64 bytes from csnapbaxterworkstation.local (169.254.10.130):
icmp_seq=6 ttl=64 time=0.248 ms
```

```
^C
--- csnapbaxterworkstation.local ping statistics ---
6 packets transmitted, 6 received, 0% packet loss, time 4999ms
rtt min/avg/max/mdev = 0.213/0.257/0.284/0.030 ms
ruser@011508P0028 ~ $ exit
Connection to 011508p0028.local closed.
```

8. Baxter must be enabled in order to actively command any of the motors. Enable the robot:

```
$ rosrun baxter_tools enable_robot.py -e
[INFO] [WallTime: 1459114148.773143] Robot Enabled
Remember the command to disable the robot (do not execute)

$ rosrun baxter_tools enable_robot.py -d
```

   Baxter will now be enabled. The joints will be powered, and Baxter will hold his current joint positions with in a position control loop.
9. Assuming the Baxter arms are tucked, we shall execute the command for untucking the arms:

```
$ rosrun baxter_tools tuck_arms.py -u
[INFO] [WallTime: 1459114811.052979] Untucking arms
[INFO] [WallTime: 1459114811.202719] Moving head to neutral position
[INFO] [WallTime: 1459114811.202930] Untucking: One or more arms
 Tucked; Disabling Collision Avoidance and untucking.
[INFO] [WallTime: 1459114819.040865] Finished tuck
```

10. Run an example program provided by Rethink Robotics.

```
$ rosrun baxter_examples joint_velocity_wobbler.py
Initializing node...
Getting robot state...
Enabling robot...
[INFO] [WallTime: 1459114651.749367] Robot Enabled
Moving to neutral pose...
Wobbling. Press Ctrl-C to stop...
```

    This example will move the arms to a neutral position, enter into velocity control mode, moving each joint through a random sinusoidal motion.
11. At the end of your experiment, tuck the arms of Baxter using this command:

```
[baxter - http://011508P0028.local:11311]
cwon@baxterws:~/ros_ws$ rosrun baxter_tools tuck_arms.py -t
```

12. Turn off the power of Baxter.

A.3 Parallel Scan Procedure

1. Power up Baxter and complete the steps 1-4 in "working with Baxter" section. This will establish the communication between the Baxter and the workstation.
2. Baxter must be enabled from another terminal in order to actively command any of the motors. Enable the robot:

```
$ rosrun baxter_tools enable_robot.py -e
[INFO] [WallTime: 1459114148.773143] Robot Enabled
```

3. For parallel scan procedure, two python scripts are necessary. `par2d_v2.py` and tf.py. Execute "python `par2d_v2.py`" in the terminal. The file "tf.py" should be in the same directory with "python `par2d_v2.py`". The "tf.py" is used for converting quaternion parameters to euler angles. The "tf.py" is written by people from ROS community. The python script "`par2d_v2.py`" is written by CSNAP researchers.
4. Following is the code inside `par2d_v2.py`. This script makes the arms do 15 line scan. In each scan line, the arm pauses at 15 positions for 6 seconds for capturing images. So this script is ready for taking 15x15=225 images from 225 points. In the script, inside `parallel_move` function, the arms are given initial positions (`left_point_x`, `left_point_y`, `left_point_z`, `right_point_x`, `right_point_y`, `right_point_z`), interval between each position (x0linc,y0linc,z0linc,x0rinc,y0rinc, z0rinc), and the number of line scan (zlooprange), the number of scan in each line scan (xloopscan).

```
#par2d_v2.py
#!/usr/bin/env python
from __future__ import division, print_function
import math
import datetime
import tf
import numpy
import time
import doctest
import random  # used in doctests
import argparse
import sys
import rospy
import baxter_interface
from geometry_msgs.msg import (
    PoseStamped,
```

```
    Pose,
    Point,
    Quaternion,
)
from std_msgs.msg import Header
from baxter_core_msgs.srv import (
    SolvePositionIK,
    SolvePositionIKRequest,
)
__version__ = '2015.07.18'
__docformat__ = 'restructuredtext en'
__all__ = ()

#from printstate2file import print_states
# create an instance of baxter_interface's Limb class
def get_joint_angles(limb,Px,Py,Pz,Qx,Qy,Qz,Qw):

    rospy.init_node("rsdk_ik_service_client")
    ns = "ExternalTools/"+limb+"/PositionKinematicsNode/IKService"
    iksvc = rospy.ServiceProxy(ns, SolvePositionIK)
    ikreq = SolvePositionIKRequest()
    hdr = Header(stamp=rospy.Time.now(), frame_id='base')
    poses = {
    'left': PoseStamped(
        header=hdr,
        pose=Pose(
            position=Point(
                x = Px,    #original val:  0.657579481614,
                y = Py,    #original val:  0.851981417433,
                z = Pz,    #original val:  0.0388352386502,
            ),
            orientation=Quaternion(
                x = Qx, #original val: -0.366894936773,
                y = Qy, #original val:  0.885980397775,
                z = Qz, #original val:  0.108155782462,
                w = Qw, #original val:  0.262162481772,
            ),
        ),
    ),
    'right': PoseStamped(
        header=hdr,
        pose=Pose(
            position=Point(
                x=Px, #original val:  0.656982770038,
                y=Py, #original val: -0.852598021641,
                z=Pz, #original val:  0.0388609422173,
```

```
                ),
                orientation=Quaternion(
                    x=Qx, #original val:  0.367048116303,
                    y=Qy, #original val:  0.885911751787,
                    z=Qz, #original val: -0.108908281936,
                    w=Qw, #original val:  0.261868353356,
                ),
            ),
        ),
        }

        #print (poses)
        ikreq.pose_stamp.append(poses[limb])


        try:
            rospy.wait_for_service(ns, 5.0)
            resp = iksvc(ikreq)
        except (rospy.ServiceException, rospy.ROSException), e:
            rospy.logerr("Service call failed: %s" % (e,))
            return 1
        if (resp.isValid[0]):
            print("SUCCESS - Valid Joint Solution Found:")
            # Format solution into Limb API-compatible dictionary
            limb_joints = dict(zip(resp.joints[0].name, \
            resp.joints[0].position))
            #print limb_joints
            #if limb == 'left':
            #    limb_left = baxter_interface.Limb('left')
            #    limb_left.move_to_joint_positions(limb_joints)
            #if limb == 'right':
            #   limb_right = baxter_interface.Limb('right')
            #     limb_right.move_to_joint_positions(limb_joints)
            return (limb_joints)
        else:
            print("INVALID POSE - No Valid Joint Solution Found.")
        return 0

    def parallel_move():
        # initialize laser (RIGHT) arm position at (xr0, yr0, zr0)
        # initialize TIS (LEFT) arm position at (xl0, yl0, zl0)

        # initial position adjustment parameters
        z0rinc = 0.000
        z0linc = 0.01
```

```
        x0rinc = -0.014
        x0linc = -0.0

        # specify step interval in meter
        zrinc = 0.002
        zlinc = 0.002

        xrinc = 0.002
        xlinc = 0.002

        # for laser 800nm
        right_point_x=0.657

        # for laser 600nm
        #right_point_x=0.657 + x0rinc
        right_point_y=-0.170
        right_point_z=0.038 + z0rinc

        left_point_x=0.657
        left_point_y=0.0685
        left_point_z=0.038 + z0linc


      # initialize right and left arm orientation
        right_yaw=-0.5*math.pi
        right_pitch=0
        right_roll=0

        left_yaw=0.5*math.pi
        left_pitch=0
        left_roll=0


        change_angle=0

        initial_xr=right_point_x
        initial_xl=left_point_x


    # increment in z-direction (away from the robot towards the viewer)
        zlooprange = 15
        xlooprange = 15

        for inter_z in range(zlooprange):
            right_point_x=initial_xr
            left_point_x=initial_xl
```

```
            right_point_z=right_point_z-zrinc
            left_point_z=left_point_z-zlinc


            print ("z level: "+str(inter_z))

            for inter_x in range(xlooprange):
                right_point_x=right_point_x-xrinc
                left_point_x=left_point_x-xlinc

                #left_pitch=left_pitch+0.1
                right_q=tf.quaternion_from_euler(right_yaw,right_pitch,\
                right_roll,'sxyz')
                left_q=tf.quaternion_from_euler(left_yaw,left_pitch,\
                left_roll,'sxyz')

                #print ('the rotation xyz is ')
                #print(left_q)


                right_x_rotation=right_q[0]
                right_y_rotation=right_q[1]
                right_z_rotation=right_q[2]
                right_w_rotation=right_q[3]


                left_x_rotation=left_q[0]
                left_y_rotation=left_q[1]
                left_z_rotation=left_q[2]
                left_w_rotation=left_q[3]



        # use inverse kinematics solver to obtain joint angles
        # given end-effector pose (quaternion)
                    joint_angler_input=get_joint_angles('right',\
                    right_point_x,right_point_y,right_point_z,\
                    right_x_rotation,right_y_rotation,\
                    right_z_rotation,right_w_rotation)
                    limb_right = baxter_interface.Limb('right')
                    limb_right.move_to_joint_positions(joint_angler_input)
                    print ("right_done: "+str(inter_x))

                    joint_anglel_input=get_joint_angles('left',\
                    left_point_x,left_point_y,left_point_z,left_x_rotation,\
                    left_y_rotation,left_z_rotation,left_w_rotation)
```

```
limb_left = baxter_interface.Limb('left')
limb_left.move_to_joint_positions(joint_anglel_input)
print ("left_done: "+str(inter_x))

# write joint parameter measurement into a file

f=open('parallel_2d_test12.txt','a+')

angles_right             = limb_right.joint_angles()
velocities_right         = limb_right.joint_velocities()
efforts_right            = limb_right.joint_efforts()
endpointpose_right       = limb_right.endpoint_pose()

angles_left             = limb_left.joint_angles()
velocities_left         = limb_left.joint_velocities()
efforts_left            = limb_left.joint_efforts()
endpointpose_left       = limb_left.endpoint_pose()

timestamp     = str(datetime.datetime.now())

inputangler   = str(joint_angler_input.values())
angler        = str(angles_right.values())
velocityr     = str(velocities_right.values())
torquer       = str(efforts_right.values())
endposer      = str(endpointpose_right.values())


inputanglel   = str(joint_anglel_input.values())
anglel        = str(angles_left.values())
velocityl     = str(velocities_left.values())
torquel       = str(efforts_left.values())
endposel      = str(endpointpose_left.values())

f.write(timestamp +'  ')
f.write(inputangler + '  ')
f.write(angler + '  ')
f.write(velocityr + '  ')
f.write(torquer + '  ')
f.write(endposer + '  ')


f.write(inputanglel + '  ')
f.write(anglel + '  ')
f.write(velocityl + '  ')
f.write(torquel + '  ')
f.write(endposel + '\n')
```

```
                pause_time=6
                print ("All_done: "+str(inter_x)+' pause for '\
                +str(pause_time))

                time.sleep(pause_time)


        return 0

    if __name__ == "__main__":
        parallel_move()
```

5. After finishing the scan, disable the robot, and shut the power down.

A.4 Angular Scan Procedure

1. Enable the robot as done in parallel scan procedure. Following is the `ang2d_v1.py` script for the moving the robot arms in an angular fashion. The increment of angle is 1 degree. The laser and the tactile imaging sensor should be in line of sight while scanning the target.

```
#ang2d_v1.py
#!/usr/bin/env python
from __future__ import division, print_function

import math
import datetime
import tf
import numpy
import time
import doctest
import random  # used in doctests
import argparse
import sys
import rospy
import baxter_interface
from geometry_msgs.msg import (
    PoseStamped,
    Pose,
    Point,
    Quaternion,
)
from std_msgs.msg import Header
```

```
from baxter_core_msgs.srv import (
    SolvePositionIK,
    SolvePositionIKRequest,
)
__version__ = '2015.07.18'
__docformat__ = 'restructuredtext en'
__all__ = ()
'''
limbs = ('left', 'right')
arms = {
            'left': baxter_interface.Limb('left'),
            'right': baxter_interface.Limb('right'),
            }

'''
#from printstate2file import print_states


# create an instance of baxter_interface's Limb class

def get_joint_angles(limb,Px,Py,Pz,Qx,Qy,Qz,Qw):

    rospy.init_node("rsdk_ik_service_client")
    ns = "ExternalTools/" + limb + \
    "/PositionKinematicsNode/IKService"
    iksvc = rospy.ServiceProxy(ns, SolvePositionIK)
    ikreq = SolvePositionIKRequest()
    hdr = Header(stamp=rospy.Time.now(), frame_id='base')
    poses = {
    'left': PoseStamped(
        header=hdr,
        pose=Pose(
            position=Point(
                x = Px,    #original val:  0.657579481614,
                y = Py,    #original val:  0.851981417433,
                z = Pz,    #original val:  0.0388352386502,
            ),
            orientation=Quaternion(
                x = Qx, #original val: -0.366894936773,
                y = Qy, #original val:  0.885980397775,
                z = Qz, #original val:  0.108155782462,
                w = Qw, #original val:  0.262162481772,
            ),
```

```
            ),
        ),
        'right': PoseStamped(
            header=hdr,
            pose=Pose(
                position=Point(
                    x=Px, #original val:  0.656982770038,
                    y=Py, #original val: -0.852598021641,
                    z=Pz, #original val:  0.0388609422173,
                ),
                orientation=Quaternion(
                    x=Qx, #original val:  0.367048116303,
                    y=Qy, #original val:  0.885911751787,
                    z=Qz, #original val: -0.108908281936,
                    w=Qw, #original val:  0.261868353356,
                ),
            ),
        ),
        }

        #print (poses)
        ikreq.pose_stamp.append(poses[limb])


        try:
            rospy.wait_for_service(ns, 5.0)
            resp = iksvc(ikreq)
        except (rospy.ServiceException, rospy.ROSException), e:
            rospy.logerr("Service call failed: %s" % (e,))
            return 1
        if (resp.isValid[0]):
            print("SUCCESS - Valid Joint Solution Found:")
            # Format solution into Limb API-compatible dictionary
            limb_joints = dict(zip(resp.joints[0].name, \
            resp.joints[0].position))
            #print limb_joints
            #if limb == 'left':
            #    limb_left = baxter_interface.Limb('left')
            #    limb_left.move_to_joint_positions(limb_joints)
            #if limb == 'right':
            #   limb_right = baxter_interface.Limb('right')
            #     limb_right.move_to_joint_positions(limb_joints)
            return (limb_joints)
```

```
        else:
            print("INVALID POSE - No Valid Joint Solution Found.")
        return 0




    def angular_move():



    # another way for initial angle
        left_yaw=0.5*math.pi
        left_pitch=0
        left_roll=0
        right_yaw=-0.5*math.pi
        right_pitch=0
        right_roll=0
        change_angle=0

        #
        intial_left_yaw=left_yaw
        intial_right_yaw=right_yaw
         #phantom width
        distance_a=0.27
        #distance from cam to edge of phantom
        distance_b=0.005
        #distance from laser to edge of phantom
        distance_c=0.081
            #position of left gripper
        distance_d=0.090
        #didnt use it
        distance_e=0.040
        # length of TIS camera
        distance_h=0.1
        # didnt use it
        distance_g=0.094
        #length of laser
        distance_l=0.150
        #distance from robot origin to nearest edge of phantom.
        distance_i=0.7
        R2=0.5*distance_l+distance_c+distance_a+distance_b \
        +0.5*distance_h
```

```
    #initial position5
        left_point_x=distance_i+0.5*distance_d
        left_point_y= distance_b+0.5*distance_a+0.5*distance_h
        left_point_z=0.01
        right_point_x=left_point_x
        right_point_z=left_point_z
        right_point_y=-(distance_c+0.5*distance_a+0.5*distance_l)




        for inter in range(10):

            left_q=tf.quaternion_from_euler(left_yaw,left_pitch,\
            left_roll,'sxyz')
            right_q=tf.quaternion_from_euler(right_yaw,right_pitch,\
            right_roll,'sxyz')

            left_x_rotation=left_q[0]
            left_y_rotation=left_q[1]
            left_z_rotation=left_q[2]
            left_w_rotation=left_q[3]
            joint_anglel_input=get_joint_angles('left',left_point_x,\
            left_point_y,left_point_z,left_x_rotation,\
            left_y_rotation,left_z_rotation,left_w_rotation)
            limb_left = baxter_interface.Limb('left')
            limb_left.move_to_joint_positions(joint_anglel_input)
            print ("left_done: "+str(inter))

            right_x_rotation=right_q[0]
            right_y_rotation=right_q[1]
            right_z_rotation=right_q[2]
            right_w_rotation=right_q[3]
            joint_angler_input=get_joint_angles('right',right_point_x,\
            right_point_y,right_point_z,right_x_rotation, \
            right_y_rotation,right_z_rotation,right_w_rotation)
            limb_right = baxter_interface.Limb('right')
            limb_right.move_to_joint_positions(joint_angler_input)
            print ("right_done: "+str(inter))



            pause_time=5
```

```
            print("All_done:"+str(inter)+' pause for '+str(pause_time))
            time.sleep(pause_time)

            angleinc=1
            change_angle+=math.radians(angleinc)
            left_yaw=change_angle+intial_left_yaw
            right_yaw=change_angle+intial_right_yaw

            left_point_x=left_point_x-R2*math.sin(change_angle)
            left_point_y=R2*math.cos(change_angle)\
            -(distance_c+0.5*distance_a+0.5*distance_l)


        return 0


    if __name__ == "__main__":

        angular_move()
```

2. After finishing the scan, disable the robot, and shut the power down.

A.5 Baxter support

Join the google group of Baxter Research Robot Community `https://groups.google.com/a/rethinkrobotics.com/forum/#!forum/brr-users` In order to join you can send request to `imcmahon@rethinkrobotics.com` introducing yourself. You can discuss your issue in this group.

A.6 Useful Suggestions from Baxter Community

Baxter wiki: `Baxterwiki:sdk.rethinkrobotics.com/wiki/Getting_Started`.

You should understand how to write a ROS publisher and subscriber, what those are, and how they relate to the robot. You should also learn what a topic is and how to figure out which ROS topics are being published. `http://wiki.ros.org/ROS/Tutorials`

If you do not know much about Git, you may also want to learn the basics (not necessary, but helpful for understanding what's going on): `https://try.github.io/levels/1/challenges/1`

There is also documentation for Gazebo simulator available on the Gazebo website, though you probably do not need this information. `http://gazebosim.org/tutorials` Some (non-robotics) Python tutorials that may be helpful in getting you started (Baxter currently use Python version 2.7): `http://hetland.org/writing/instant-hacking.html` `http://www.alan-g.me.uk/tutor/index.htm` `http://thepythonguru.com/`

The Baxter SDK uses ROS and Python for communication with the robot. While knowing ROS is not strictly necessary for using Baxter, having a basic understanding of the Publisher/Subscriber message passing framework it uses is certainly helpful. Check out this high level explanation from robohub:
http://robohub.org/ros-101-intro-to-the-robot-operating-system/
and creating a simple ROS-python Publisher and Subscriber: click here.
For a more advanced understanding of ROS and python (rospy) see these explanations: http://wiki.ros.org/rospy/Overview

Take a read through the Baxter SDK Examples section of the wiki: http://sdk.rethinkrobotics.com/wiki/Examples You can then click through each of the examples there, and then proceed to the Code Walkthroughs section in each. For instance, here's the Wobbler Code Walkthrough: http://sdk.rethinkrobotics.com/wiki/Wobbler_-_Code_Walkthrough.

There you will find what is happening inside the code to cause the arms to move. As for a direct answer to your question about which files to change to modify the behavior of Baxter, see this directory structure of the baxter_ examples git repository:
https://github.com/RethinkRobotics/baxter_examples/blob/master/README.rst

The file you will need to modify to change the Velocity Wobbler example is:

```
$ gedit ~/ros_ws/src/baxter_examples/scripts/joint_velocity_wobbler.py
```

APPENDIX B

BIMODAL OPTO-MECHANICAL PHANTOM PREPARATION PROCEDURE

This chapter describes the procedure for preparing a bimodal opto-mechanical phantom.

B.1 Materials

Table B.1 lists the tools required for the phantom preparation.

Table B.1: List of required tools

Item	Operating range	Quantity
Precise scale	0.0001 g	1
Bath sonicator with a clamp	n/a	1
Vacuum desiccator	65 liters in volume	1
Heat plate	50-100∘C	1
Phantom mold (Pyrex glass storage container with a lid)	11 cup	3
Sample mold (plastic box)	10×10× 14 cm	3
Measurement containers	n/a	6
Vial or plastic container with cap (sonication)	500 ml	3
Glass beaker	500 ml	2
Glass beaker	40 ml	1
Glass mixing rod	n/a	1
Plastic bowl	5 L	1
Spatula or plastic spoon	n/a	2
Paper towels	n/a	1
Isopropyl Alcohol (for cleanup)	200 ml	1

The phantom mold is a pyrex container with an 11-cup rectangle unit with plastic cover. The dimension is $26.5 \times 21.5 \times 16.5$ cm^3.

B.2 Target Mechanical and Optical Properties

Table B.2 lists the target mechanical and optical properties of the phantom. Polydimethylsiloxane (PDMS) was used for phantom preparation. PDMS is prepared from component materials RTV 6136-D1. For the target elastic modulus values of 23 kPa and 355 kPa, the base (agent A) and curing agents (agent B) were mixed in the ratio of 1:1.3 and 1:10.

Table B.2: Target mechanical and optical properties of the phantom

Phantom region	Dimension (mm^3)	l_d (mm)	h (mm)	E (kPa)	μ_a (cm^{-1})	μ_s' (cm^{-1})
Tissue	90×90×17	-	-	23.00	0.05	8.0
Tumor	10×10×10	11.90	6.00	355.00	0.20	8.0

Optical properties were varied by adding scattering and absorbing components to PDMS mixture (to curing agent B). Table B.3 lists the amount of components for the required optical properties of the phantom.

Table B.3: Amount of the components for the required optical properties of the phantom

μ_a, cm^{-1}	μ_s', cm^{-1}	Total volume, ml	Carbon black, mg (approximate)	TiO_2, g
0.05	8	2400	0.034	5.585
0.20	8	2500	0.140	5.818

B.3 Instructions for Tumor Phantom Preparation Procedure

1. Mark the Pyrex mold with a horizontal line 6 cm from the bottom (take into consideration the thickness of the glass).
2. Mark a plastic container (10×10×14 cm^3) with a horizontal line 2 cm from the bottom.
3. Mark a tumor mold (50 ml beaker) with 1cm horizontal line form the bottom.
4. In a 500 ml vial, put 300 ml of RTV6136-D1 curing agent B.
5. Measure 0.140 g of carbon black using a precise weight.
6. Measure 5.818 g of TiO_2 using a precise weight.
7. Add measured quantities of carbon black and TiO2 to the vial with RTV6136-D1 curing agent B
8. Mix thoroughly for 5 min.
9. Pour mixture to the plastic vial (500 ml). Do not close the cap very tightly.
10. Ice bath sonicate the vial with mixture for 1 hour. For the ice bath, put ice cubes in the sonicator because RTV6136-D1 has flash point at 177 °C (351 °F). Sonication will break lumped together particles. Mix the mixture several times during sonication.
11. Add sonicated mixture from the vial to 5 L bowl.
12. In a 5 l bowl measure ((2500ml/11*10) - 300 ml) = 1972.7ml of RTV6136-D1 agent B
13. Mix thoroughly for 5 min. Do not do it fast to prevent extra bubbles.
14. Sequentially add (2500ml/11*1) = 227.3 ml of RTV6136-D1 base agent A.
15. Mix thoroughly the mixture in the beaker (200-300 strokes). Do not mix it fast to prevent extra bubbles.
16. Pour into a phantom mold up to a mark of 6 cm.

17. Pour into a sample mold up to a mark of 2 cm.
18. Pour into a tumor mold up to 1 cm mark.
19. Place molds into a vacuum desiccator to pump out the bubbles. Use medium vacuum pressure until no bubbles formed.
20. Place a small tumor mold (glass) on a heat plate (setting 2 (80 °C) for 370 Hotplate/Stirrer from VWR Scientific Products) for 30 min. Remove it.
21. Place the glass mold on a heat plate (setting 2 (80 °C) for 370 Hotplate/Stirrer from VWR Scientific Products) for 1 hr. Remove it.
22. Meanwhile clean used bowl and beakers with paper towels and alcohol spray.
23. PDMS will be completely ready in 1 day.

B.4 Instructions for Tissue with Tumor Phantom Preparation Procedure

1. Mark a plastic container (10×10×14 cm3) with a horizontal line 2cm from the bottom.
2. Mark the Pyrex mold with horizontal lines 2.5 and 6 cm from the bottom (take into consideration the thickness of the glass).
3. In a 500 ml vial, put 300 ml of RTV6136-D1 curing agent B.
4. Measure 0.034 g of carbon black using a precise weight.
5. Measure 5.585 g of TiO_2 using a precise weight.
6. Add measured quantities of carbon black and TiO_2 to the vial with RTV6136-D1 curing agent B.
7. Mix thoroughly for 5 min.
8. Pour mixture to the plastic vial (500 ml). Do not close the cap very tightly.
9. Ice bath sonicate the vial with mixture for 1 hour. For the ice bath, put ice cubes in the sonicator because RTV6136-D1 has flash point at 177 °C (351 °F). Sonication will break lumped together particles. Mix the mixture several times during sonication. Bottom layer (42% of 2250ml = 945ml)
10. In a 5 l bowl measure (300*.42) = 126 ml from sonicated vial.
11. ((945*1.3/2.3)-126 = 534.13-126) = 408.13 ml of RTV6136-D1 agent B.
12. Add sonicated mixture from the vial.
13. Sequentially add 410.87 ml of RTV6136-D1 base agent A.
14. Mix thoroughly the mixture in the beaker (approximately 200 strokes). Do not mix it fast to prevent extra bubbles.
15. Pour into a phantom mold up to 2.5 cm mark.
16. Place molds into a vacuum desiccator to pump out the bubbles. Use medium vacuum pressure until no bubbles formed.
17. Place the glass mold on a heat plate (setting 2 (80°C) for 370 Hotplate/Stirrer from VWR Scientific Products) for 30 min.
18. Meanwhile clean used bowl and beakers with paper towels and alcohol spray.
19. When bottom layer is semi-cured, place a $1cm^3$ tumor. Then, the top layer (rest of 2400 ml = 1455 ml) is prepared.
20. In a 5 l bowl measure (300*.58) = 174 ml from sonicated vial.
21. ((1455*1.3/2.3)-174 = 822.4-174) = 648.4 ml of RTV6136-D1 agent B.
22. Sequentially add 632.61 ml of RTV6136-D1 base agent A.
23. Mix thoroughly the mixture in the beaker (approximately 200 strokes). Do not mix it fast to prevent extra bubbles.
24. Pour into the phantom mold up to a mark of 6 cm.

25. Place molds into a vacuum desiccator to pump out the bubbles. Use medium vacuum pressure until no bubbles formed.
26. Place the glass mold on a heat plate (setting 2 (80°C) for 370 Hotplate/Stirrer from VWR Scientific Products) for 45 min.
27. Meanwhile clean used bowl and beakers with paper towels and alcohol spray.
28. PDMS will be completely ready in 1 day.

After preparing the phantom, we measured the elastic moduli using Instron and the absorption and reduced scattering coefficients using diffuse optical spectroscopy instrument. Table B.4 lists the measured mechanical and optical properties of the phantom.

Table B.4: Measured mechanical and optical properties of the phantom

Phantom region	Dimension (mm^3)	l_d (mm)	h (mm)	E (kPa)	μ_a (cm^{-1})	μ_s' (cm^{-1})
Tissue	90×90×17	-	-	45.00	0.082	6.8
Tumor	10×10×10	11.90	6.00	355.00	0.30	6.8